Fine-grained pyrite within the Mount Isa (Enterprise) copper system, NW Queensland; geological relationships, modelled distribution and links to reactive ground

Thesis submitted in accordance with the requirements of the University of Adelaide for an Honours Degree in Geology

Samuel John Connell

October 2016

THE UNIVERSITY of ADELAIDE

Fine-grained pyrite within the Mount Isa (Enterprise) copper system, NW Queensland; geological relationships, modelled distribution and links to reactive ground.

Analysis of fine-grained pyrite at Mount Isa

Abstract

The Mount Isa Cu and Pb-Zn-Ag deposits are located in North-West Queensland within the Western Fold Belt of the Mount Isa Inlier. The genesis of these deposits has been debated since mining began in the 1920s. The most abundant sulphide within the host unit is fine-grained pyrite, which is present in high concentrations within the mining area. There is debate on the origin and timing of fine-grained pyrite, and how it relates to the silica-dolomite alteration halo, and copper mineralisation.

This thesis is presented as a broad multi-focussed project, with the overarching aim to characterise the fine-grained pyrite mineralisation at Mount Isa. The relationship of fine-grained pyrite to the ore system and to reactive ground is also investigated. In this thesis, hand sample observation, petrographic analysis, SEM analysis and MLA analysis are used to interpret the geology of pyritic shales. Additionally, Leapfrog geological modelling of diamond drill-hole data was used to visualise the large-scale distribution of fine-grained pyrite. In order to test the relationship between fine-grained pyrite and reactive ground, 63 pyritic shale samples from underground were tested for reactivity with explosive products.

Results indicate that fine-grained pyrite has been deposited over a protracted period, spanning over deformation periods, and its formation is related to the early stages of the main hydrothermal system. Fine-grained pyrite appears to act as a rheological inhibitor to hydrothermal fluids on both the micro and macro scales, affecting the distribution of subsequent alteration, brecciation, and location of Cu mineralisation. Rare magnetite mineralisation has been observed and is interpreted to have formed at a later stage to fine-grained pyrite. Ore textures within pyritic shales often show economic base metal sulphides (Cu, Pb and Zn) with paragenetic relationships indicating co-precipitation. Reactive ground testing provided evidence that the concentration of fine-grained pyrite alone does not directly control reactivity. Samples rich in fine-grained pyrite hence do not necessarily pose a direct risk to drilling and blasting.

Within the context of the deposit, fine-grained pyrite was an important pre-ore mineralisation component of the Urquhart shale which has influenced the location of the later copper orebodies. The rheological variations of the variably pyritic sedimentary layers, distribution of silica/dolomite alteration and orientation of the Paroo Fault were also significant factors enabling the unique circumstances for the deposition of the Cu-Pb-Zn ore system at Mount Isa.

Key Words

Fine-grained pyrite (Pyrite 1), Coarse-grained pyrite (Pyrite 2), Brassy pyrite, Mount Isa Timing, Structure, Distribution, Reactive ground, Magnetite

Table of Contents

List of Figures and Tables

Figures

Tables

Appendices

1. Introduction

Stratiform fine-grained pyrite (FeS_2) is a common accessory mineral in sedimentary base-metal deposits and constitutes a significant portion of the sulphide mineralisation within the mineral deposits of North-West Queensland (Mount Isa, George Fisher/Hilton, Century, McArthur River and Lady Loretta) (Perkins, 1998). The host rock unit to the Mount Isa copper deposit contains abundant fine-grained pyrite mineralisation (Pyrite 1), which forms large bedding parallel lobes, commonly enveloping the copper orebodies and silica-dolomite alteration halo (Perkins, 1998). On the micro-scale, fine-grained pyrite is observed to be bedding-parallel and is controlled by carbonaceous seams within the finely bedded Urquhart Shale (Painter *et al*., 1999). A paragnetically later coarser-grained pyrite (Pyrite 2) stage is related to the chalcopyrite mineralising system (Painter *et al*., 1999; Perkins, 1998, Taylor & Lilly 2016).

The fine-grained pyrite mineralisation is of interest as it only occurs within the Urquhart shale host unit, has strongest concentrations within the centre of the mining area, and is often located directly adjacent to high grade copper ore (Perkins, 1998). Furthermore, between the Mount Isa mine and Hilton mine (20km North of Mount Isa along strike), fine-grained pyrite is lacking or absent within the Urquhart Shale (Waring, 1990). Because of this association, there has been debate over the timing of the fine-grained pyrite and whether the pre-ore pyrite had any geochemical or structural role in the formation of the breccia-hosted copper orebodies and juxtaposed stratiform Pb-Zn deposits. According to Wilde *et al*., (2005), the Urquhart shale is chemically similar to other sedimentary units of the Mount Isa group. Therefore, the reason for the Urquhart shale to behave uniquely during deformation, allowing the generation of permeability for ore-bearing hydrothermal fluids, is an important issue (Gessner *et al*., 2006). With on-going debate on the origin of the copper deposit, the prominence of the abundant fine-grained pyrite mineralisation is re-addressed in this thesis.

Large concentrations of fine-grained pyrite can also cause safety concerns for mining operations through reactive ground. Reactive ground is an important safety issue in many locations around Australia, where mining is conducted within sedimentary black shale (Bellairs, 1997). Reactive ground refers to sedimentary rock (shale or coal) containing abundant iron-sulphide minerals which have the potential to undergo heat releasing, exothermic reactions after coming into contact with a reactant (water, air, or nitrates contained in explosives) (AEISG, 2012; Kennedy and Tyson, 2001). Because of the potential for excessive heat release, it is an important safety concern for underground mining operations (including at Mount Isa) that use drilling and explosive blasting for ore extraction. Establishing geological constraints on reactivity is important for identifying risk levels, and for the implementation of cost-effective safety management practices.

This thesis is written as a multi-facet project containing several sections, each with a different focus relating to fine-grained pyrite. Using samples primarily from the Enterprise ore body, this work aims to constrain the timing of fine-grained pyrite mineralisation, characterise the textural variety and investigate its influence on the ore system using hand samples, petrology, SEM, Mineral Liberation Analysis (MLA) and LA-ICP-MS. In addition, having identified rare magnetite mineralisation within pyritic shale, the mineral relationships of magnetite are also investigated using these methods. The deposit-scale distribution of fine-grained pyrite is visualised using drill-hole data and Leapfrog geological modelling software. The relationship between fine-grained pyrite and reactive ground was tested by using pyritic shale samples collected underground and tested through the Mount Isa Mines reactivity testing procedure.

.

The hypotheses tested in this project are:

1. Fine-grained pyrite formed prior to all deformation and was not part of the economic base metal mineralising system.

2. Fine-grained pyrite and ‘brassy pyrite’ are the same generation of pyrite mineralisation.

3. The distribution of fine-grained pyrite had no influence on the location of copper ore deposition, or silica-dolomite alteration.

4. The concentration of fine-grained pyrite within shale is directly related to the risk of a rock mass becoming reactive.

2. Background Geology

2.1 Regional geology – Mount Isa Inlier and the Western Succession

The Mount Isa copper deposit is located within the Mount Isa Inlier, North-West Queensland, Australia. The Palaeo-proterozoic to Mesoproterozoic terrain is divided into the Eastern Fold Belt, Western Fold Belt, and (central) Kalkadoon-Leichhardt Belt (Figure 1). The Mount Isa deposit lies within the Leichhardt River Fault Trough of the Western Fold Belt (Figure 1) (Blake *et al.*, 1998). Within the Western Fold Belt, an early tectonic cycle involved the deformation, and metamorphism of 1900 – 1870 Ma basement rocks during the Barramundi Orogeny. A younger tectonic cycle involved three cover sequences between 1870 – 1625 Ma. Cover sequence 3 (1680 – 1625 Ma) includes the Mount Isa Group, which hosts the Mount Isa deposit, predominantly consisting of fine-grained carbonate and siliciclastic rocks. The Isan Orogeny (1590 – 1500 Ma) terminated sediment deposition within this cycle (Betts and Lister, 2002). The Mount Isa group is comprised of carbonaceous shales and siltstones deposited within an intra-continental basin (Neudert, 1983). At Mount Isa, the sediments dip approximately west at 60-70°, and form the western limb of a regional anti-form. The underlying basement is composed of meta-greenstone altered mafic volcanics and interbedded siliciclastic quartzite sediments of the Eastern Creek Volcanics (Conaghan *et al.*, 2003).

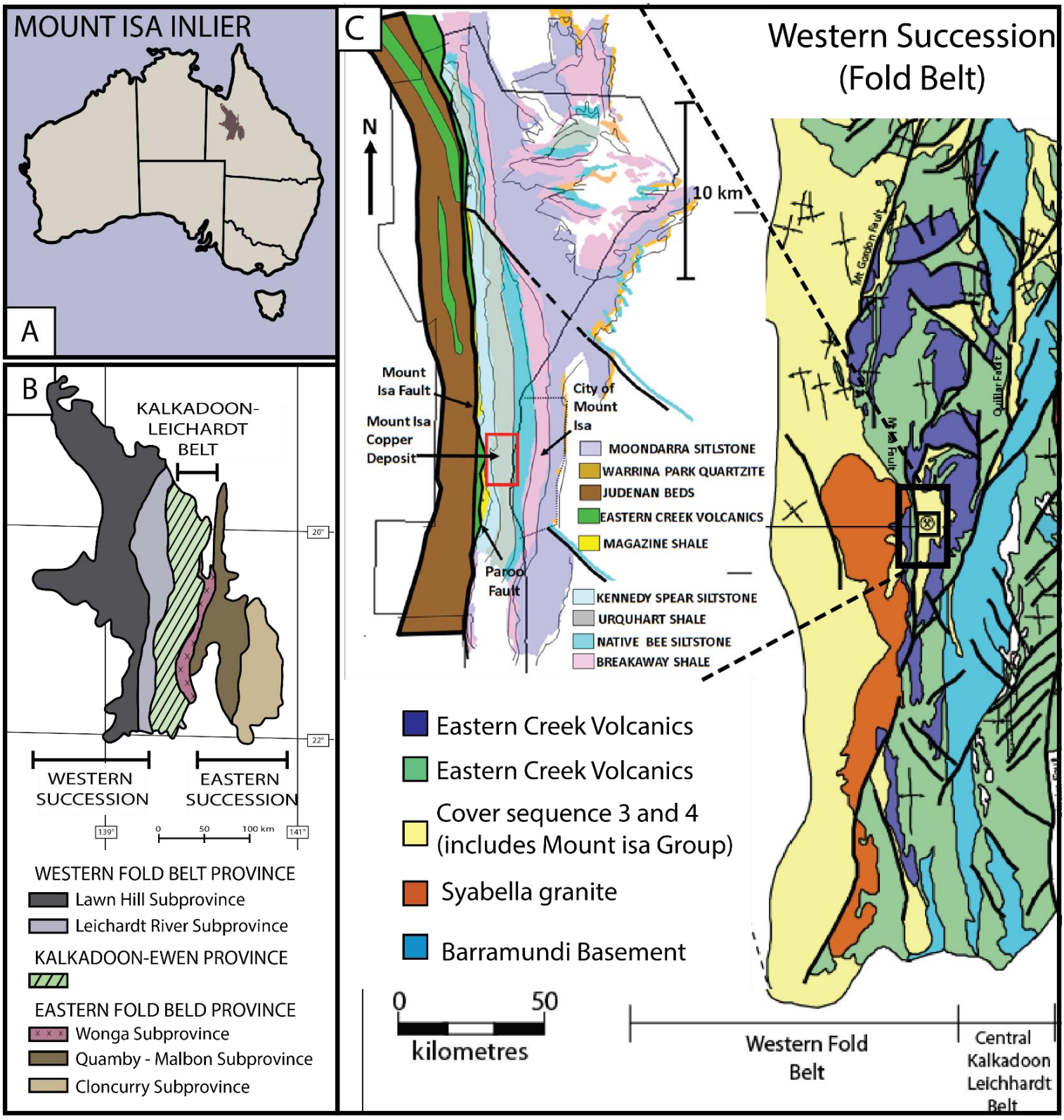

Figure 1: Map showing the regional location of the Mount Isa Inlier (A), the division of the Inlier into Western Succession, Kalkadoon Leichardt Belt, and Eastern Successions (B). Image C shows the Western Succession in more detail, with an inset of the Mount Isa region and stratigraphy after Miller, 2006 and Bullock, 2009.

2.2 Deformation history of the region

There are three main deformation events known to have occurred within the Mount Isa Group. D_1 was a North-South directed thrust system which created the contact between the Mount Isa group and the underlying basement, and created folds with East-West orientated hinges. D_2 was an East-West directed thrust event and formed folds striking North-South. This event created the sigmoidal shape of the basement contact, and folded the Mount Isa group sediments. D_3 was an ENE - WSW directed thrust event. Copper mineralisation has originally been thought to have been introduced throughout this event, although late D_2 has also been postulated (Long, 2010). Post D_3 events include late faulting, which strike NE and SW, and a relatively minor D_4 event evidenced by crenulations and kink folds in the basement contact (Gessner *et al.,* 2006; Bell *et al.,* 1988; Hinde, 1994).

2.3 Local geology – Urquhart Shale Host Unit

Economic Cu-Pb-Zn and all fine-grained pyrite mineralisation are strictly confined to within the Urquhart Shale unit. The Urquhart shale is a ~1000m thick sequence of thinly-laminated, carbonaceous, pyritic siltstones containing alternating beds of dolomitic siltstone, and mudstone (see Figure 2). The unit is in contact with a major shear zone known as the Paroo Fault, which marks the boundary between the Mount Isa sediments and underlying basement (Conaghan *et al.,* 2003). The Paroo Fault has an unusual shape in that it changes dip from steep westerly dipping close to the surface, before becoming sub-horizontal directly below the copper orebodies, then steeply East at depth (Figure 3). The copper orebodies occur either directly adjacent to the Paroo Fault, or perched above it (Figure 4), and are surrounded by a silica-dolomite alteration halo. Siliceous alteration containing the highest ore grades occurs closest to the basement contact, and progressively grades into dolomitic alteration (Perkins, 1990; Gessner *et al.,* 2006).

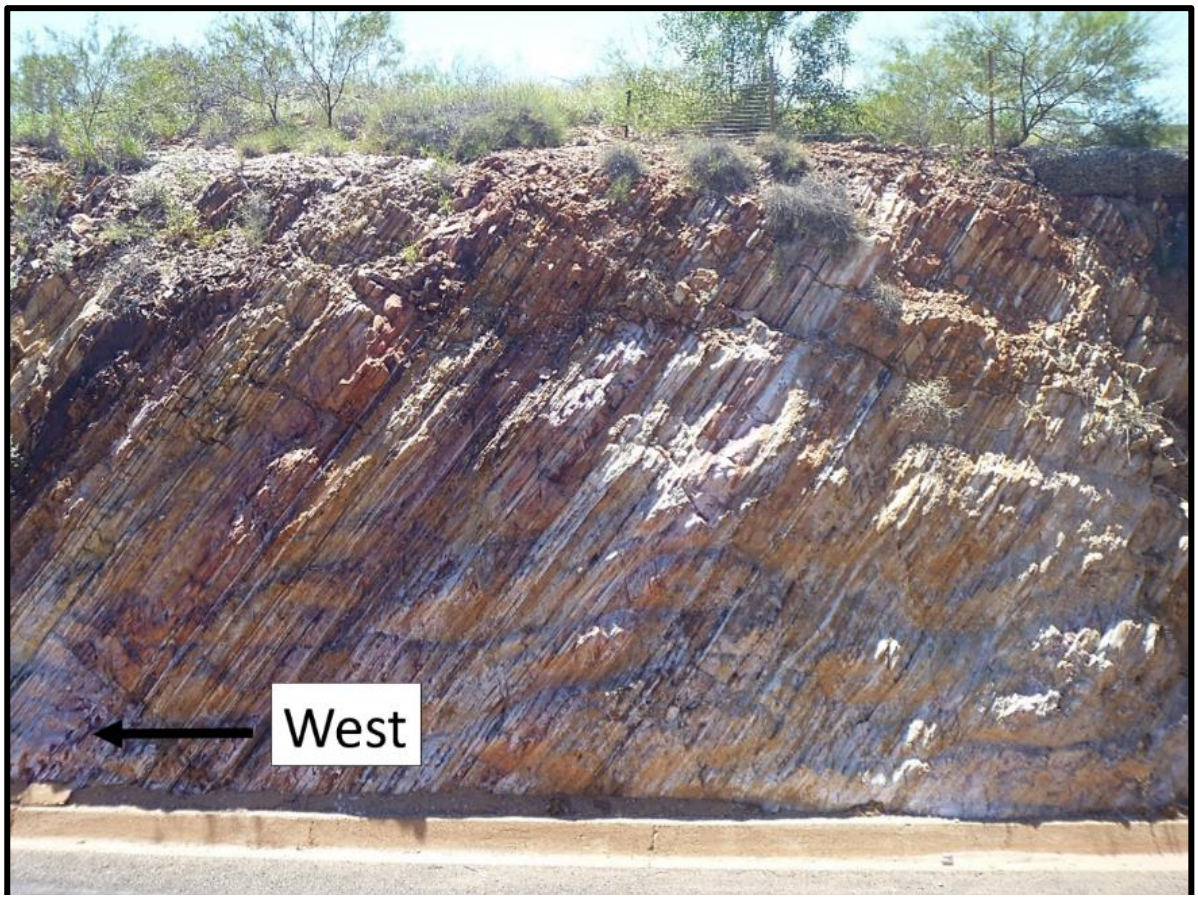

Figure 2: Photo of the Urquhart Shale, host rock to the Mount Isa Copper Deposit, as it appears in surface outcrop, North-East of the mine. Note the steeply dipping bedding (60-65 degrees) towards the West. Here, the pyritic shales and siltstones are severely leached and oxidised. Note the very fine laminations and heterogeneity between beds.

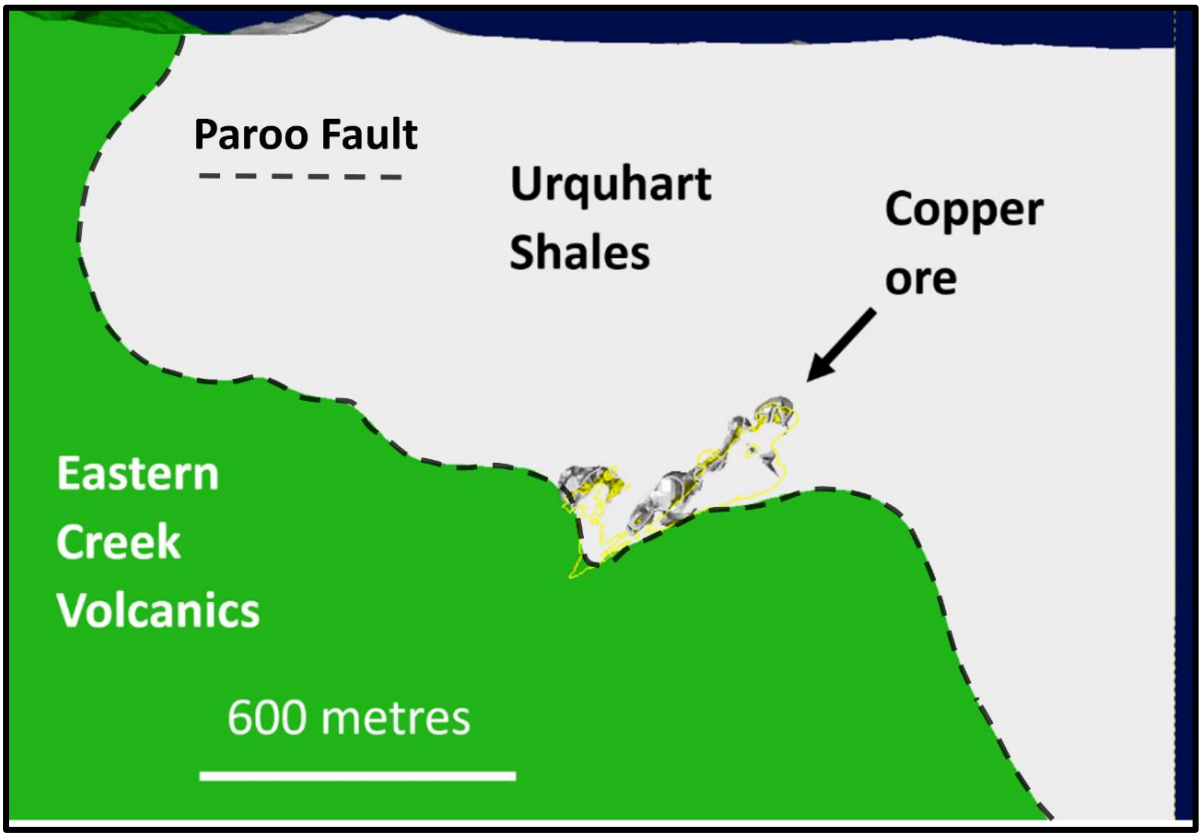

Figure 3: Schematic model of the Mount Isa deposit setting, showing the typical sigmoidal shape of the Paroo Fault, marking the contact between the Mount Isa Group sediments (grey) and Eastern Creek Volcanics (green). Model is shown in cross-section view, looking directly North. The yellow outline represents copper ore (1.5% grade shell) originating from the 'kink' in the fault zone.

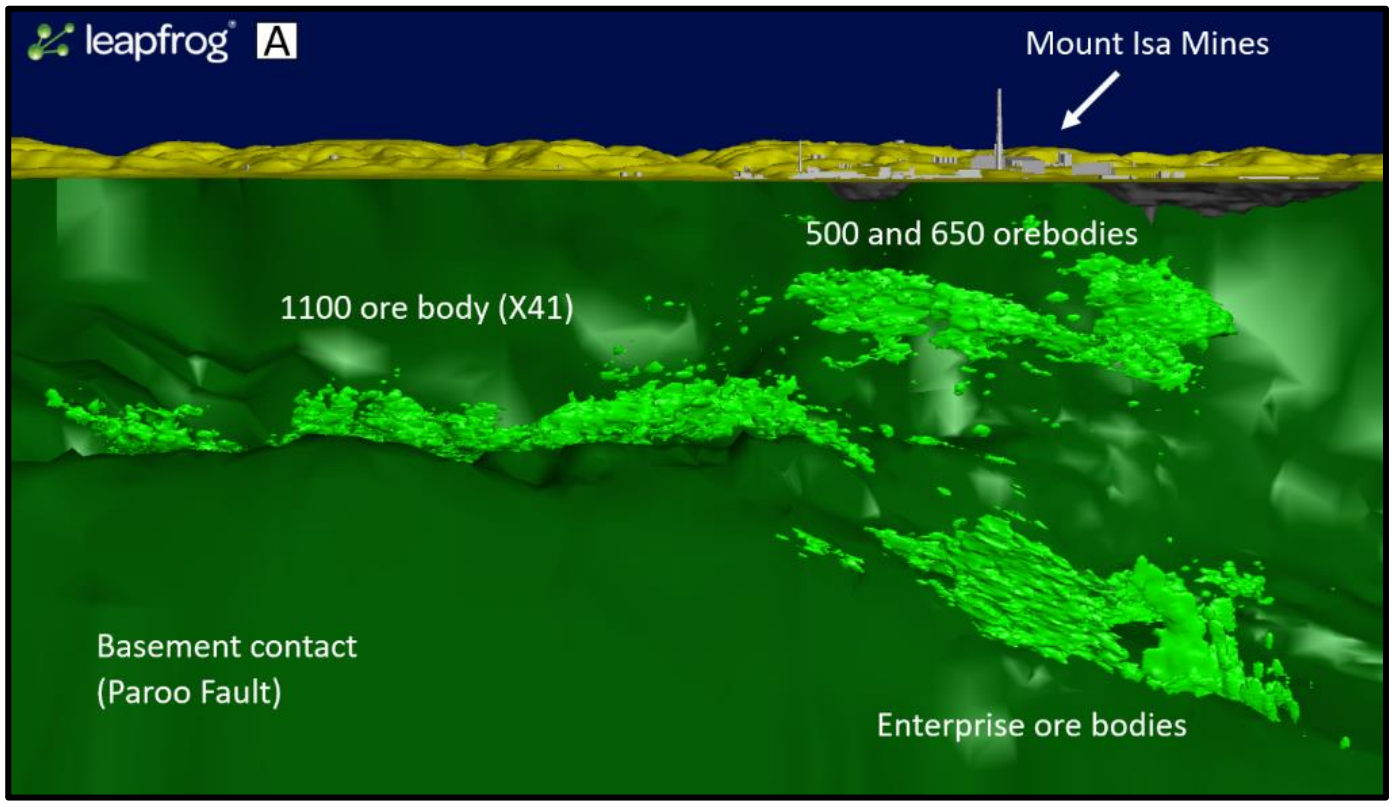

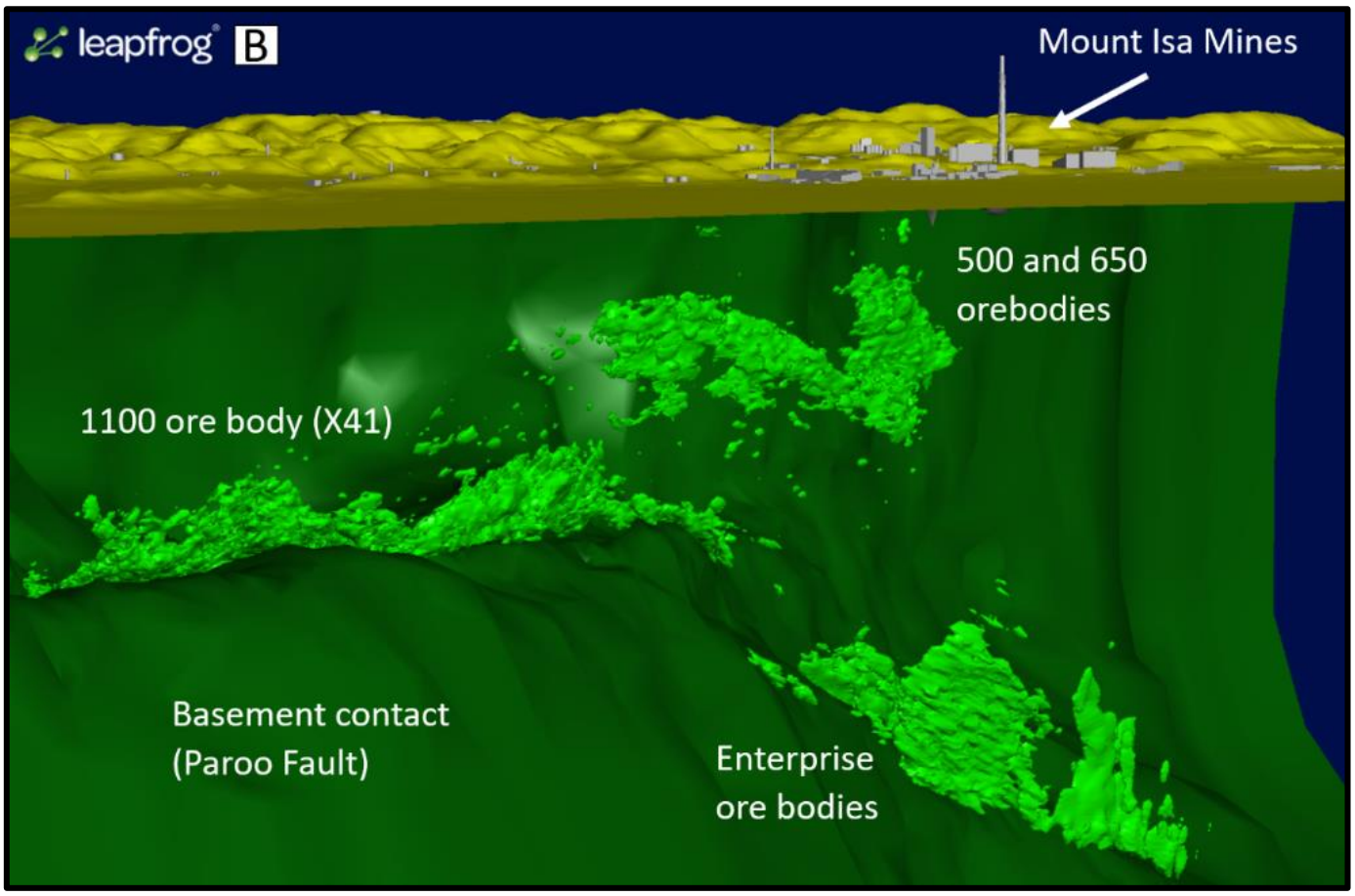

Figure 4: Image A - Long section of the Mount Isa Copper deposit, looking directly West. Copper grade shells are 3% Cu. Image B – Long section of the Mount Isa Copper Deposit looking directly North-West. The 1100 and Enterprise orebodies occur directly adjacent to the basement contact (dark green). The 500 and 650 orebodies occur perched above the basement contact.

2.4 Ore genesis

The genesis of the copper and lead-zinc orebodies has been continuously debated since the discovery of the deposit (see Table 1). Explanations range from syn-genetic, remobilised syn-genetic, and epigenetic. Most recently, Taylor and Lilly (2016), have reviewed the work on Mount Isa, and have supported the epigenetic model for all mineralisation, consistent with Perkins (1997).

According to Taylor and Lilly (2016), movement along the Paroo Fault during deformation created a linked fracture zone, which developed along a bend in the Paroo Fault. Structural controls on copper mineralisation were influenced by bedding plane shear and rheological differences (presence of pre-existing fine-grained pyrite).

Syngenetic Pb-Zn-Ag, syngenetic Cu	Syngenetic Pb-Zn-Ag and epigenetic Cu from the same ore fluid	Syngenetic Pb-Zn-Ag, epigenetic Cu	Epigenetic Pb-Zn-Ag, epigenetic Cu
			Grondijs and Schouten (1937)
Mathias and Clark (1975)			
	Finlow-Bates and Stumpfl (1979)		
		Perkins (1984) Swager (1985) Heinrich et al. (1989)	
		Waring (1990) Heinrich et al. (1995)	
			Perkins (1997) Davis (2004)
		Wilde et al. (2006)	Taylor and Lilly (2016)

Table 1: History of genetic models by different authors, used to explain the genesis for the Mount Isa Deposit. The variety of models demonstrate the complexity and unique circumstances of the deposit. Syngenetic Pb-Zn, and epigenetic Cu has been accepted in the modern day. However, most recent interpretations suggest all mineralisation to be epigenetic.

Taylor and Lilly (2016), have reviewed the para-genesis of the deposit. This is supported within this thesis and is presented as follows:

1. Chlorite (dominantly in basement)
2. Quartz : Minute infill style veinlets
3. Pyrite 1
4. Carbonate-1 ± quartz ± pyrite 2 ± cobaltite.
5. Carbonate-2 ± minor sericite.
6. Chalcopyrite, sphalerite ± galena ± pyrrhotite ± minor carbonate ± arsenopyrite ± tetrahedrite

According to Perkins (1997), economic sulphides were deposited successively from a fluid containing reduced sulphur, with an increasing influence from bedding structures during lead-zinc deposition. The zonation may have been temperature controlled, resulting in chalcopyrite depositing as the youngest sulphide (Perkins, 1997). This was consistent with Bullock (2001), who noted from trace element data (Co/Ni ratios) that there is an inner zone of hydrothermal chalcopyrite, and an outer zone with a more sedimentary-influenced signature, suggesting a temperature controlled system.

There are multiple opinions on the role of pre-ore sulphide mineralisation in aiding the formation of the copper orebodies. Gessner *et al.,* (2006), consistent with Bell (1988), suggested the rheology of the Urquhart Shale allowed the generation of permeability and fluid pathways. They emphasise the importance of anisotropic contrasts between shale and siltstone beds, which led to dilation and fracturing of layers during deformation.

Robertson (1982), suggested all chalcopyrite mineralisation utilised the iron and sulphur consumed from fine-grained pyrite during formation. Alternatively, Wilde *et al.,* (2006), suggests from textural observation, that the source of iron-sulphide for chalcopyrite was obtained from outside the host unit. Bullock (2001), noted that S and Cu cannot be transported together at high temperatures. The S source for chalcopyrite must have been separate from the Cu source in order to produce large ore bodies.

2.5 Background on fine-grained pyrite

Fine-grained pyrite mineralisation at Mount Isa has been previously studied in an attempt to describe its origin, timing, and relationship to base-metal deposits (Painter, 2003; Perkins, 1998; Robertson, 1982; Grondis and Schouten, 1937). According to Painter (2003), consistent with Grondis and Schouten (1937), there are three species of pyrite in the Mount Isa system. These are fine-grained pyrite (Pyrite 1), brassy pyrite and coarse-grained pyrite (Pyrite 2). Due to the similarity of textures, the discrepancy between varieties is unclear creating confusion on the timing, and geological relationships of pyrite to the ore system.

Fine-grained pyrite (Pyrite 1) includes rounded spherules and euhedral shaped crystallites, which strictly occur in strati-form, bedding-parallel, carbonaceous-rich seams which often irregularly link around dolomitic shale. The grain size ranges from 0.005 to 0.025 mm (5-20 μm). A second species labelled 'brassy pyrite', is coarser grained (20-200um), euhedral and has a more reflective, golden appearance (Painter *et al*., 2003). It has been suggested as representing metamorphic recrystallization of fine-grained pyrite (Waring, 1990). Perkins (1997), suggested brassy pyrite to be an independent mineralising event to fine-grained pyrite. True coarse-grained pyrite (Pyrite 2) (>250um) is known to occur as part of the same mineralising system as the chalcopyrite, and is found as isolated porphyroblastic, cubic crystals, or masses of smaller euhedral crystals (Painter, 2003; Waring, 1990).

3. Methods

3.1 Reactive ground sampling

It is not physically possible, or economically viable to take enough samples to characterise the reactivity, or geology within the Mount Isa Mine. Results from this project serve as an indication of the geology of pyritic shales, and the response to reactivity testing. All samples used for research of fine-grained pyrite were selected from the larger range of samples collected for reactive ground testing. The methodology of this sample collection is presented below. In-depth methodology of reactivity sampling and testing can be found in Appendix 6.

This study collected 63 fresh pyritic shale rock samples (1-10kg) taken from *in-situ* locations on the walls of mine drives, based on a detailed review of available mine data. Drill-core data, geological mapping, development inspections, and underground knowledge from Mount Isa geologists were utilised to plan sampling locations. Sampling was focussed within the Enterprise system, in areas of current mine development. Approximate sampling locations, are shown in Figures 5 and 6. (Specific coordinates, and maps of sampling locations can be found in Appendix 5)

Sample locations were recorded using prepared maps of the mine drives and a disto-metre to measure sampling points from known survey locations. Each sample was categorised into percentage based increments based on fine-grained pyrite concentration and labelled accordingly. Samples were split for the purpose of assaying, reactivity testing and thin section preparation.

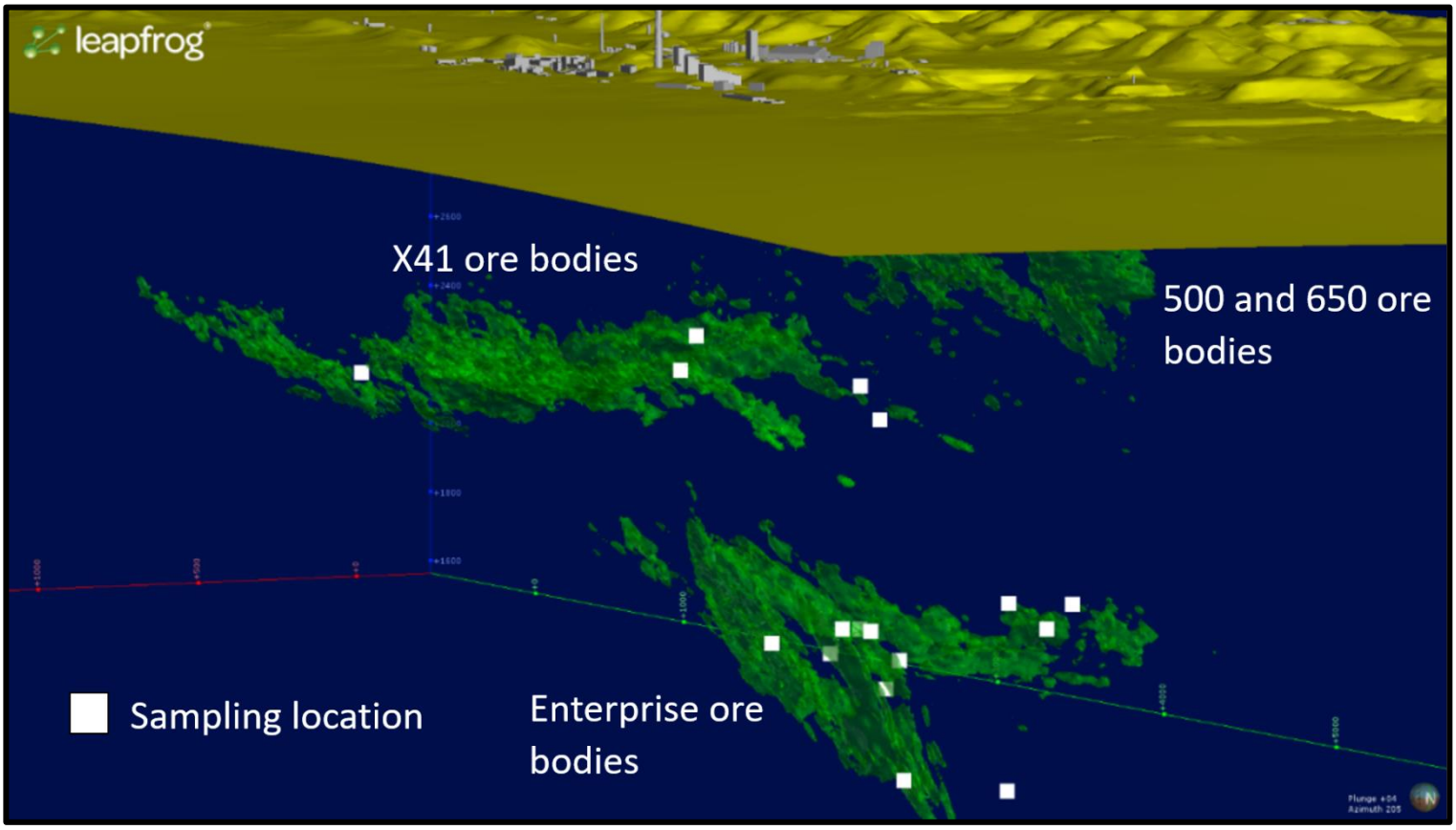

Figure 5: Approximate locations of reactive ground sampling underground, with reference to the copper orebodies (3% Cu). Note the majority of samples were taken in the Enterprise system. These samples were used for both reactive ground testing, and for further research on fine-grained pyrite, using various research techniques. Image taken in section view, looking South-West.

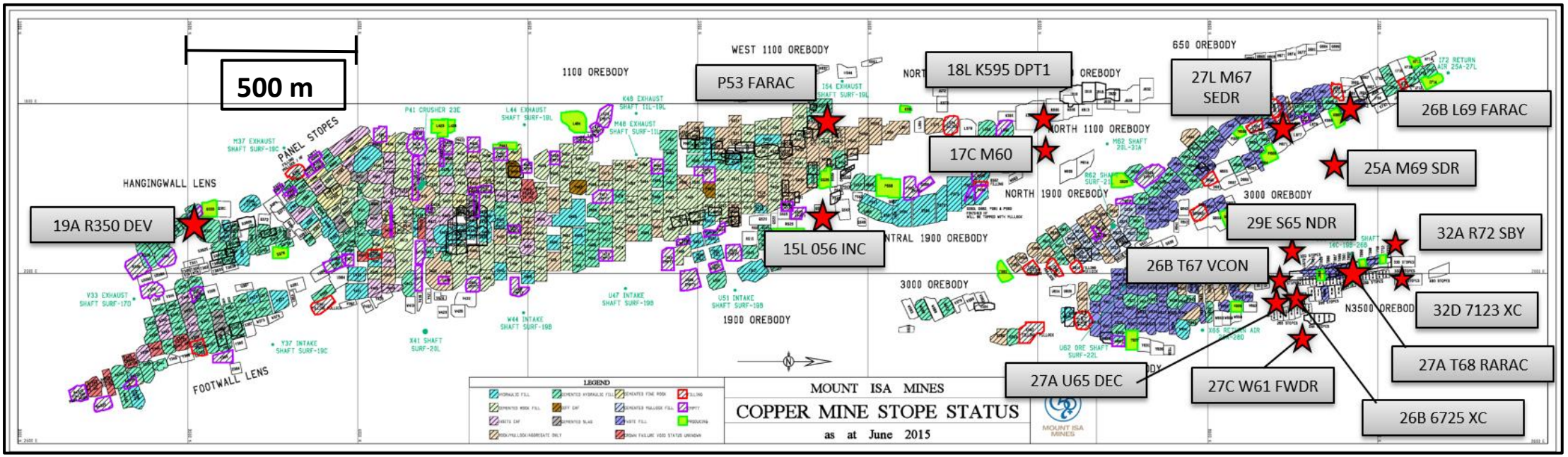

Figure 6: Map of the Mount Isa underground mining stopes, showing the approximate locations of where sampling was conducted. The majority of sampling was completed in the Enterprise system; namely the 3000 and 3500 ore bodies.

3.2 Hand samples and thin section analysis

In order to characterise fine-grained pyrite and analyse its relationship with the ore system, the pyritic shale hand samples were visually examined. In-depth core logging was conducted on O406 ED2 (a hole drilled from the surface through the halo of the X41 1100 ore body), to determine the mineralogical relationships of fine-grained pyrite. Rock samples chosen from each reactive ground location were selected for in-depth analysis of geological relationships. Rocks were cut with a diamond saw perpendicular to bedding. Rocks were described and photographed, identifying specific areas of interest and made into petrographic thin sections. Petrography work was conducted using an Olympus polarising optical microscope.

3.3 SEM

The FEI Quanta 600 MLA Scanning Electron Microscope (SEM) was used for textural and mineralogical analysis of the pyritic shale, and to generate high quality images. The SEM was equipped with a tungsten filament electron source and was used for imaging the sample surface. The energy-dispersive X-ray spectrometer was used to identify mineralogy within each sample. Back-scattered electron (BSE) imaging was also used to show broader scale relationships at a high resolution.

3.4 MLA

Mineral liberation analysis (MLA) was undertaken on the FEI Quanta 600 to assist in the identification of sample mineralogy. It was further used to produce detailed, high-resolution mineralogical maps within areas where mineral relationships were complex on a macro-scale.

3.5 LA-ICP-MS

Laser Ablation Inductively Coupled Plasma Mass Spectrometry (LA-ICP-MS) was used to identify chemical differences between pyrite varieties. Data was collected using the laser at a specified resolution over a small area (1cmx1.5cm) containing different pyrite varieties.

3.6 Leapfrog modelling

Modelling used underground drill-hole data logged by Mount Isa geologists for the duration of its mine life. The 'Leapfrog Geo' geological modelling software was used to model the data. After errors and duplicates were corrected for, geological information in the drill-holes was simplified by grouping lithologies into broad, overarching units. Units within the shale were then modelled and refined. Cross-sections of models were produced to interpret relationships and are discussed below. For a video on how modelling was conducted, see Appendix 1.Examples of final models produced are shown in Figure 7.

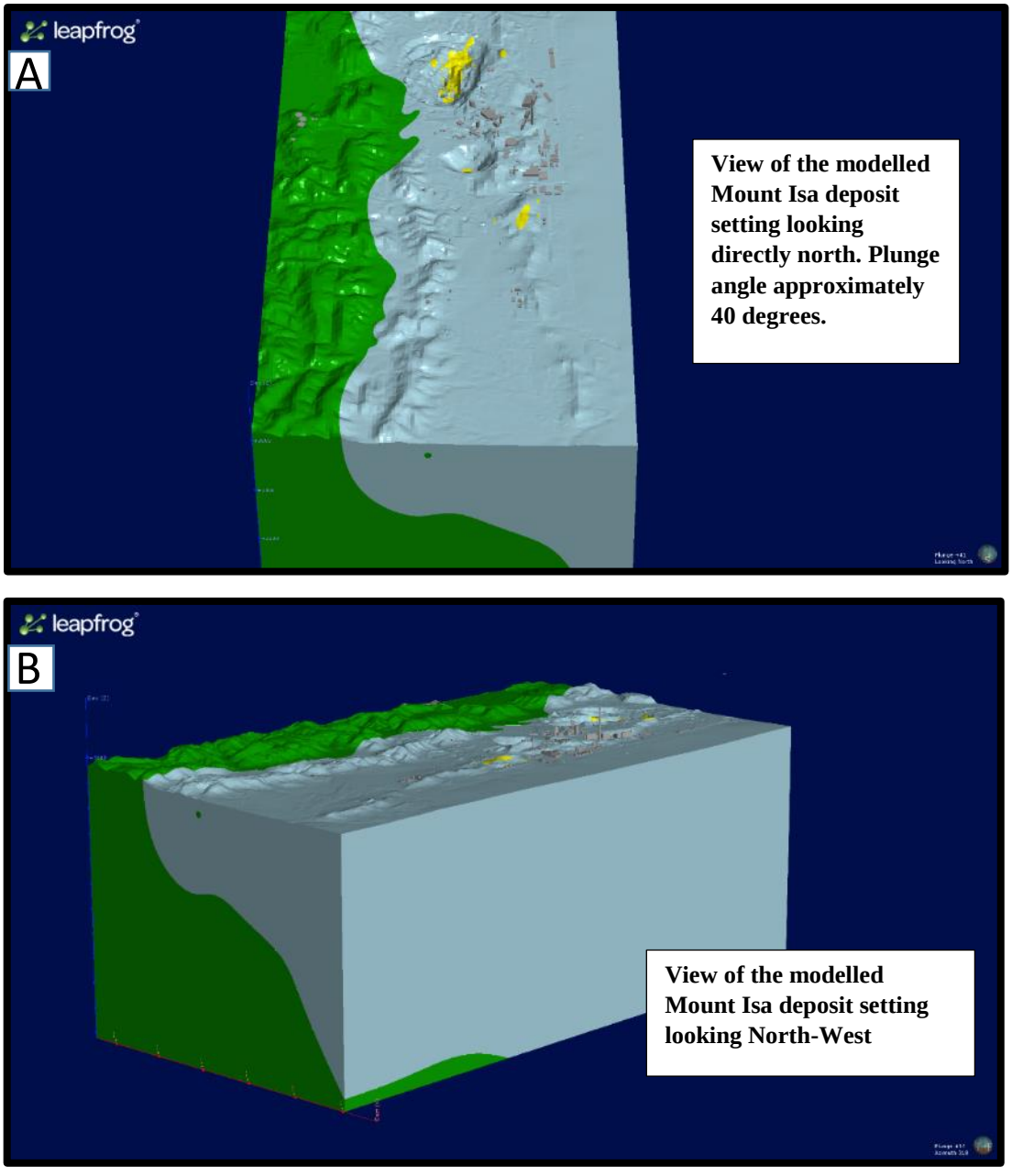

Figure 7: Examples of completed Leapfrog models of the Mount Isa deposit. Blue represents bedded shale units (Urquhart Shale), while green represents basement (Eastern Creek Volcanics). Other lithological units are modelled inside the shale unit.

4. Observations and Results

4.1 Hand samples and drill core

Textures of fine-grained pyrite

In its original form, fine-grained pyrite is recognised by a characteristic dull, earthy, non-reflective, bronze colour. It occurs in strati-form bands, often taking up the majority of mineralogy within a bed. Its relative concentration within a bed can vary considerably between <10% up to ~100%. It has a strong preference to occur within carbonaceous-rich beds within shale, as opposed to dolomitic siltstone. In contrast, ore minerals and coarse-grained pyrite (Pyrite 2) occur within the dolomitic siltstone layers, which have acted as the major alteration zones and (permeable) fluid pathways.

Multiple varieties of fine-grained pyrite were observed within samples. A coarser grained, crystalline pyrite (‘brassy pyrite’), occurs amongst fine-grained pyrite bands, or within adjacent strati-form layers (Figure 9. A,B,E,F and Figure 11. B,D). Brassy pyrite has a golden colour, and is more reflective than fine-grained pyrite. This variety is common within strongly altered samples (Figure 10).

Mineral relationships

Observations on alteration and ore fluid pathways showed progression between beds of fine-grained pyrite, with the pyrite acting as a barrier to alteration. High grade chalcopyrite is rare amongst fine-grained pyrite, and preferentially occurs in adjacent beds. Within strongly brecciated/altered units, remnant fine-grained pyrite is commonly retained within fractures, or is mineralised within fault zones and veins.

True porphyroblastic coarse-grained pyrite (Pyrite 2) is not usually associated with fine-grained pyrite. Instead, it forms isolated crystals within silica/dolomite alteration zones, ore veins, or amongst chalcopyrite mineralisation. Some samples show coarse-grained pyrite as strati-form, tabular, continuous blocks parallel to bedding (Figure 11.C). These may represent re-crystallisation of pyrite 1 as a result of intense alteration. The textures indicate that pyrite 2

has crystallised prior to periods of deformation (folding). This also constrains pyrite 1 to have deposited prior to periods of deformation.

When present, magnetite mineralisation was observed to be euhedral, coarse-grained and appeared to be restricted to formation within pyritic shale bearing beds (Figure 12.D).

Structure

When fine-grained pyrite forms dense clusters it exhibits a ductile nature, often showing well preserved folding. This commonly results in dilation and brittle failure of adjacent units, and the localisation of alteration and ore fluids to specific zones, with fine-grained pyrite acting as a potential barrier to hydrothermal fluids (Figure 10.A). Additionally, dense fine-grained pyrite beds are observed to be impenetrable by ore veins without a pre-existing weakness point (Figure 12.C).

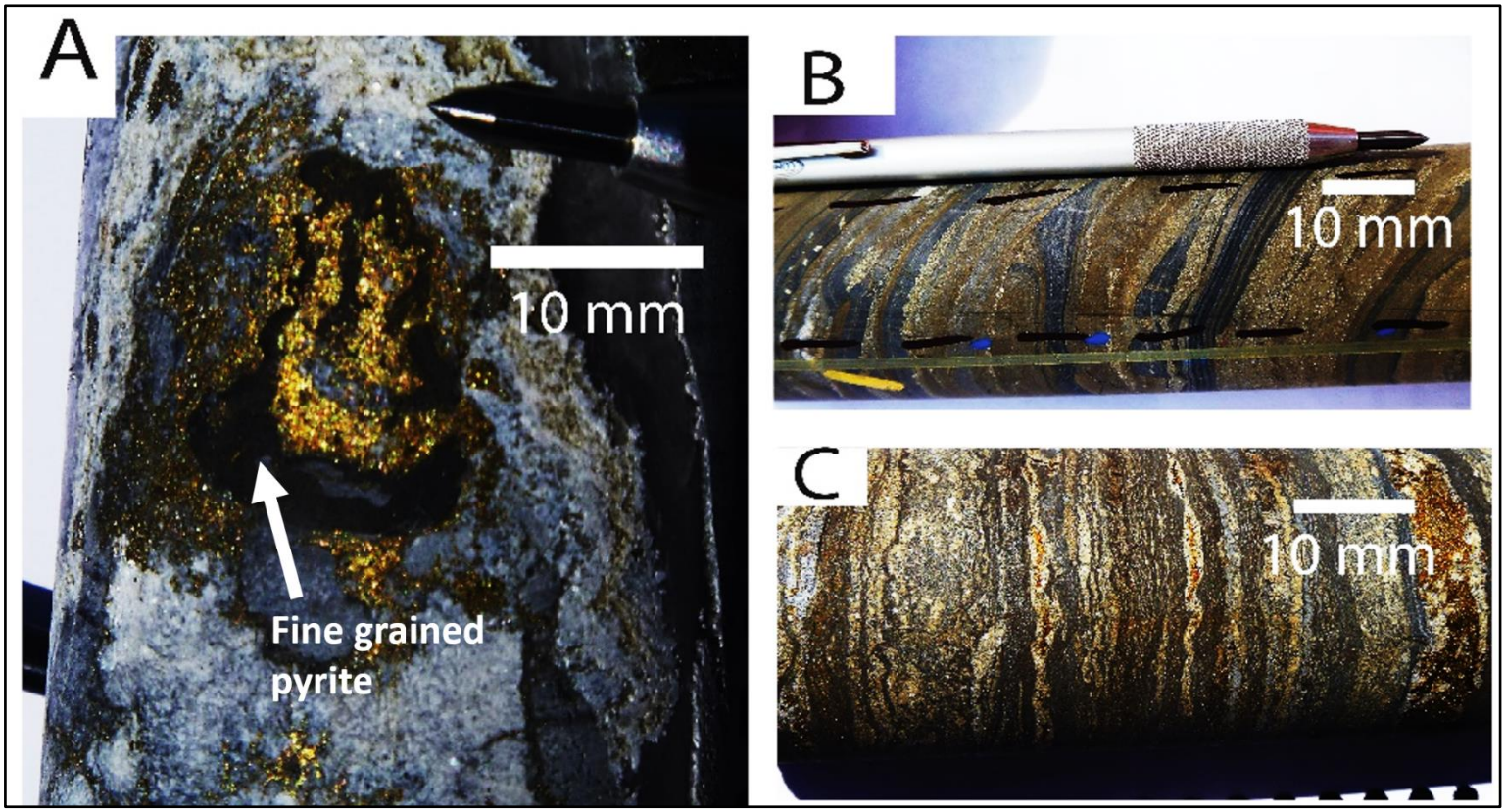

Figure 8: Photos of drill core containing fine-grained pyrite. Photos taken from drill hole 0406 ED2 above the 1100 orebody. Image A is a dolomitic breccia with remnant, deformed fine-grained pyrite surrounded by chalcopyrite. Image B is siliceous shale containing alternating bands of fine-grained pyrite and brassy pyrite. Image C shows fine-grained pyrite present in a dolomitic altered sample, within alternating beds of recrystallised dolomite. Note chalcopyrite only occurs within dolomitic alteration zones, as opposed to pyritic shale.

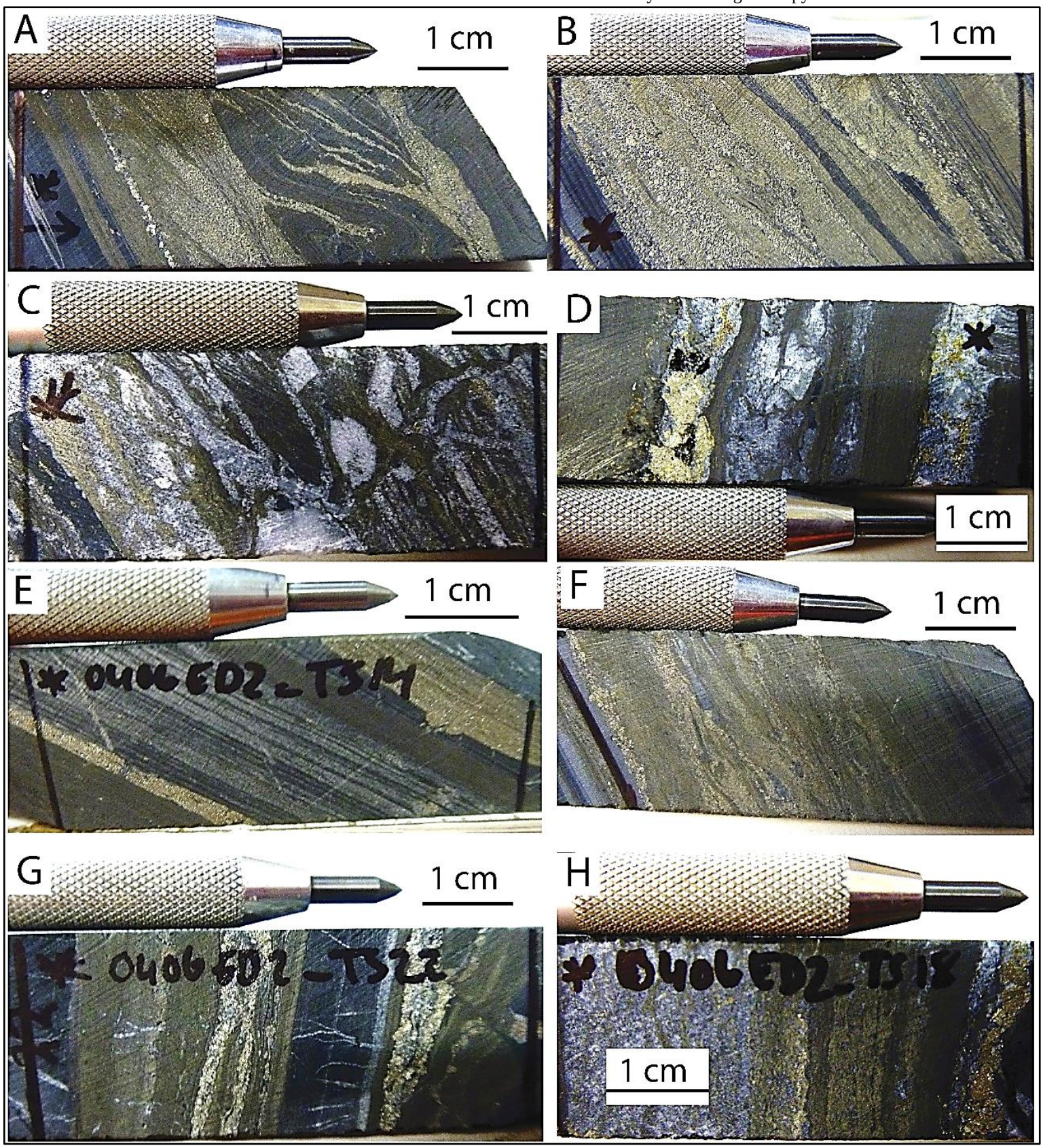

Figure 9: Photos of drill core containing fine-grained pyrite. Photos taken from drill hole 0406 ED2 above the 1100 orebody. Photos C, D and H are from altered/brecciated locations. Note ore minerals and alteration occur in between fine-grained pyrite beds in these samples. Photos A,B,E,F,G show the variety of pyrite textures in black shale. Note the occurrence of both brassy pyrite and fine-grained pyrite are evident. Brassy pyrite occurs in alternating beds, and is more crystalline and reflective. Fine-grained pyrite is orientated non-parallel to bedding in photo A.

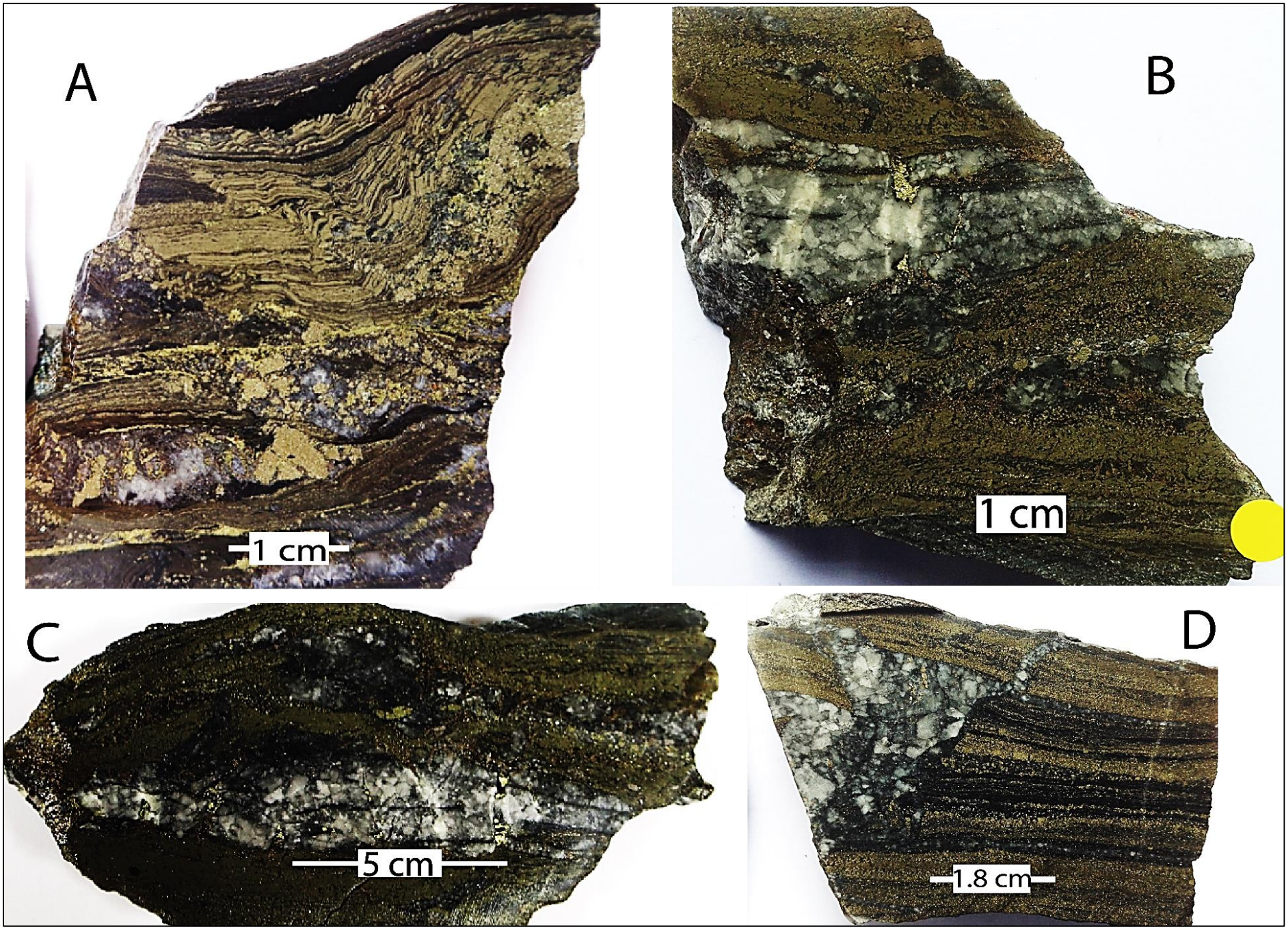

Figure 10: Representative pyritic shale samples from the Enterprise system, which display silica/dolomite alteration in combination with significant fine-grained pyrite mineralisation. Note that fine-grained pyrite is relatively un-affected by alteration, however it may appear more crystalline in altered samples. Economic sulphide minerals occur within dolomitic alteration zones, or at the boundary between fine-grained pyrite and shale. Image B shows the extremely ductile behaviour of dense fine-grained pyrite beds under deformation. Pyrrhotite is also seen to occur amongst fine-grained pyrite.

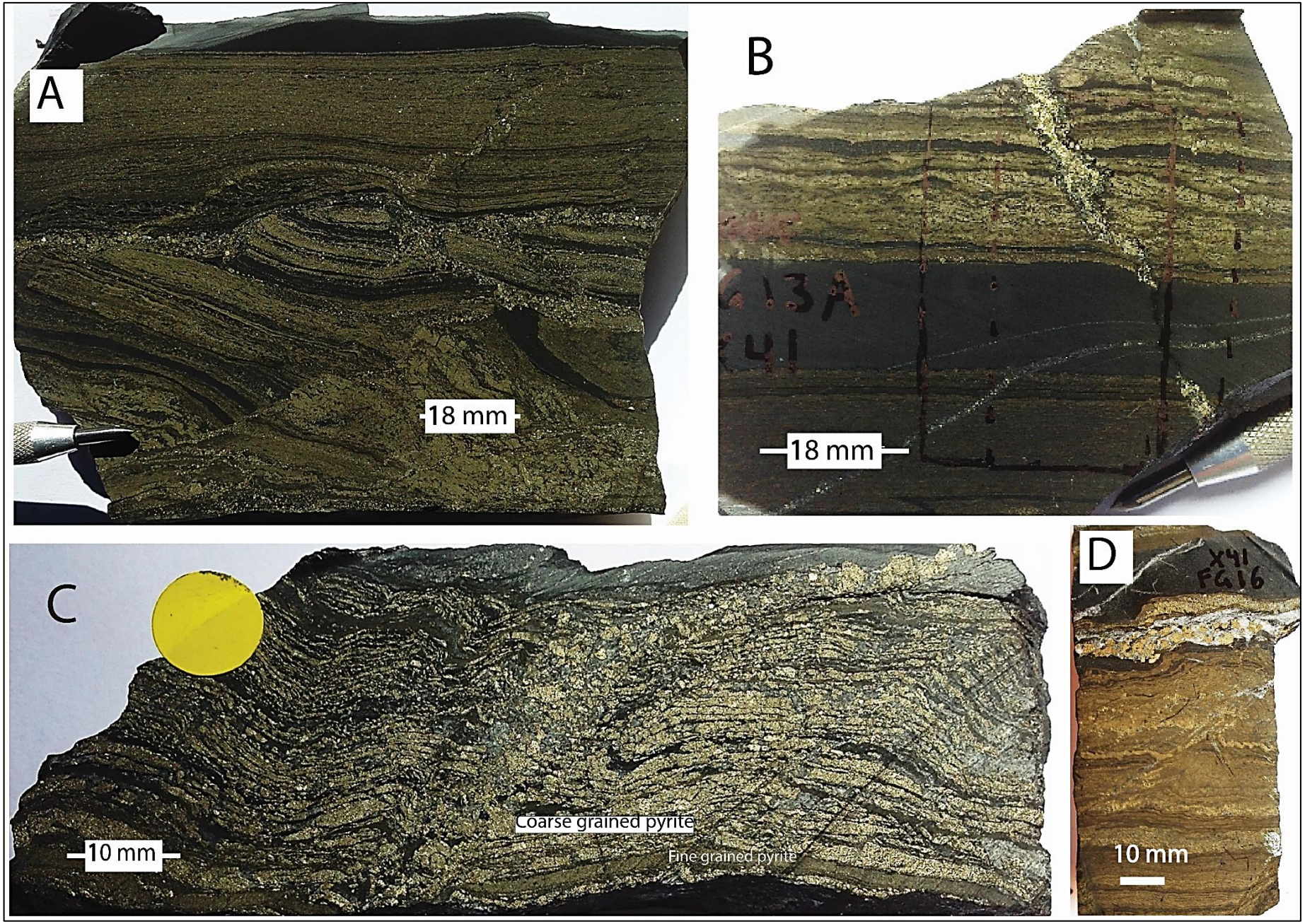

Figure 11: Representative pyritic samples from the Mount Isa mine. These samples demonstrate the variability in pyrite textures, and the difficulty in discriminating them. Image A shows a variety of fine-grained pyrite textures, within a deformed sample. Image B shows alternating layers of 'brassy pyrite' and fine-grained pyrite. An ore vein crosscuts both types of pyrite mineralisation. Image C shows coarse-grained pyrite occurring as tabular, crystalline blocks, surrounded by intense silica alteration. Coarse-grained pyrite may have entirely replaced fine-grained pyrite in this situation. Image D shows alternating fine-grained pyrite and brassy pyrite within shale. Dolomitic alteration vein containing coarse-grained pyrite occurs at the boundary between shale and fine-grained pyrite.

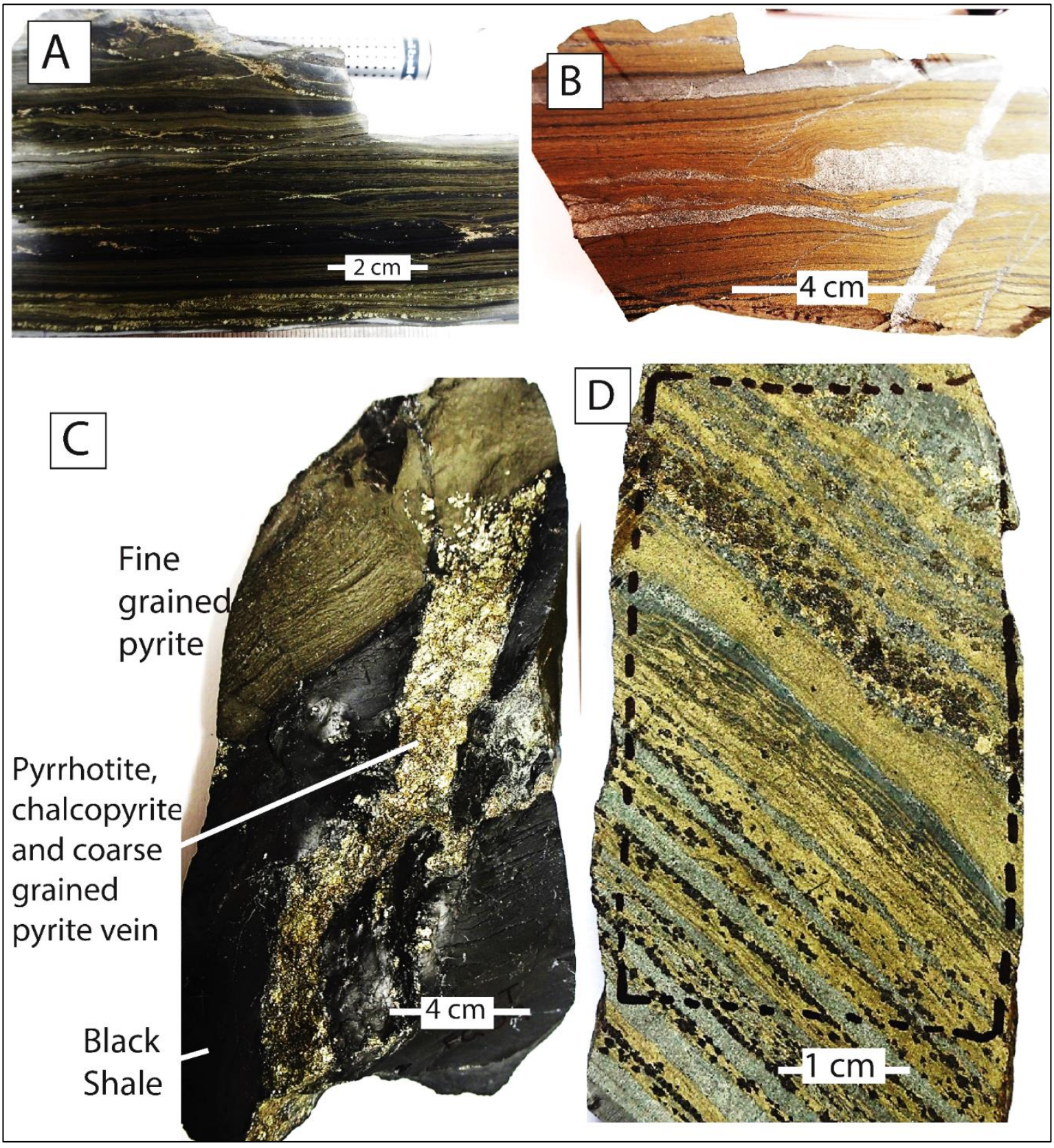

Figure 12: Representative pyritic samples from the Mount Isa mine. Images A and C show typical fine-grained pyrite textures in relatively unaltered rock samples. Image A is from a siliceous black shale, and image B is from a dolomitic zone. Image C shows the interaction between fine-grained pyrite, black shale and an ore vein containing chalcopyrite, coarse-grained pyrite and pyrrhotite. Note the vein does not penetrate the dense fine-grained pyrite bed. Image D shows prominent magnetite mineralisation within a fine-grained pyrite sample. Magnetite mineralisation is restricted to pyritic shale layers.

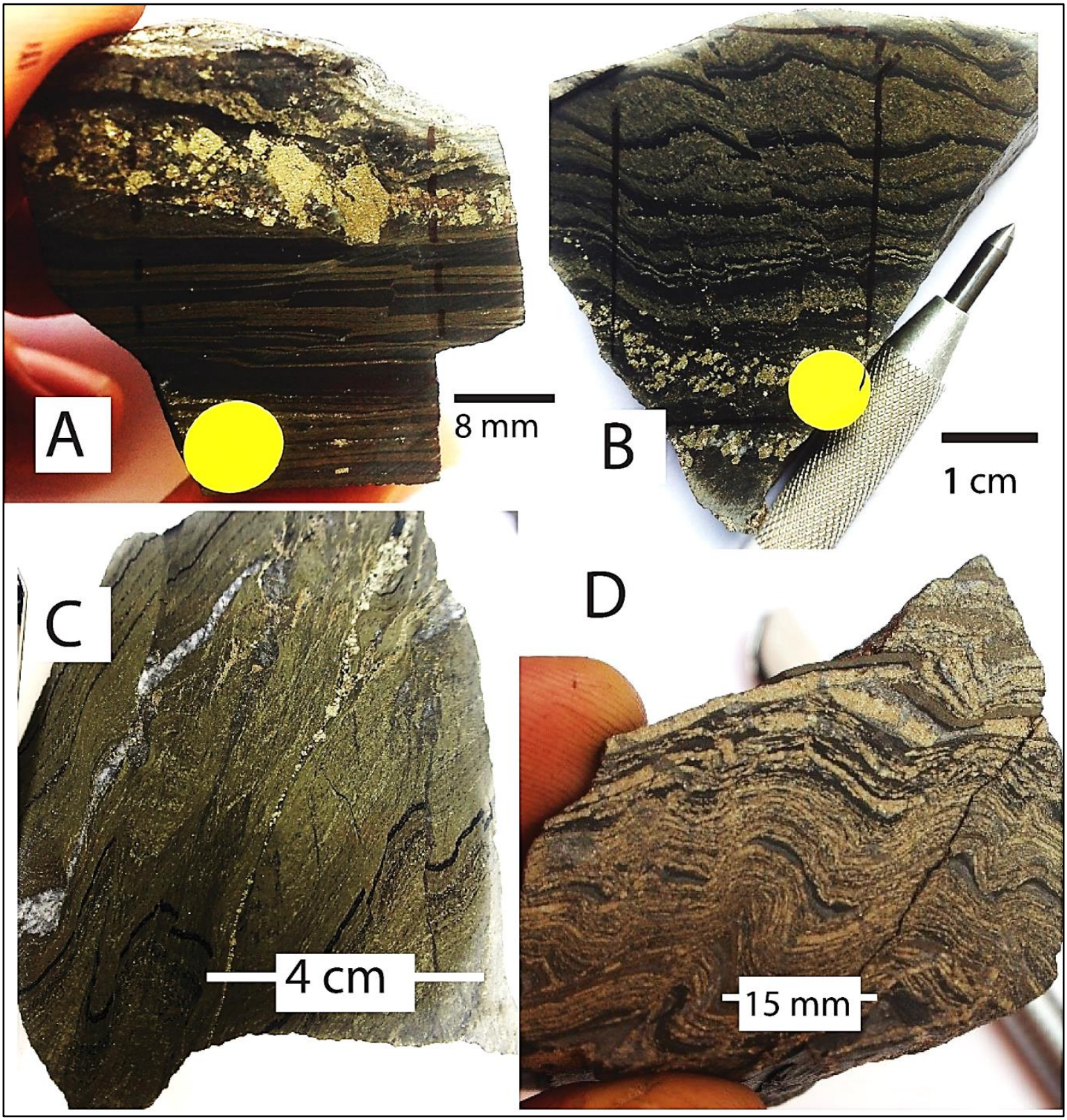

Figure 13: Representative deformed pyritic samples from the Mount Isa mine. These samples show the structures fine-grained pyrite commonly exhibits when folded or faulted. Image A shows a faulted pyritic shale, with fine-grained pyrite mineralisation overprinting the fault zone. Image B and C show folded pyritic shales with a strong cleavage development parallel to the strike of the micro-folds. Image D shows folded pyritic shales in an altered sample.

4.2 Petrography

For a detailed petrography report and analysis of pyritic shales, see Appendix 3. Petrographic results proved that there are many textural varieties of pyrite, making grouping into categories difficult. Nevertheless, dominant textures of pyrite observed are as follows:

- 'True' fine-grained pyrite (Pyrite 1) (variety of densities, dull, earthy, bronze colour)
  - Euhedral grains (crystallites)
  - Circular grains (spherules)
- Extremely dense mats of fine-grained pyrite (Pyrite 1) (appearance of brassy pyrite)
- Brassy pyrite (coarser grained, euhedral, crystalline, reflective)
  - Groups of isolated euhedral crystals
  - Further outward growth of fine-grained pyrite ± intergrowth of chalcopyrite ± sphalerite ± galena.
- Isolated, porphyroblastic, strongly euhedral, coarse-grained pyrite (Pyrite 2) grains
- Coarse-grained pyrite (Pyrite 2) occurring as hydrothermal grains clustered together.
  - Veins, alteration zones, or bedding parallel replacement

Textural characteristics

Fine-grained pyrite forms either as spherical grains (Figure 14.C) or as euhedral grains of similar size (Figure 15.A). The pyrite forms with variable concentrations within a bed, as shown in Figure 15.A-C. Grains of sphalerite and galena are common amongst fine-grained pyrite (Figure 15.D). Additionally, at high magnifications, chalcopyrite was commonly found to directly replace and pseudo-morph fine-grained pyrite (Figure 15.E,F). A variety of 'atoll' textures were observed, with fine-grained pyrite often displaying an inner core of varying composition, surrounded by an outer shell of pyrite. Different parts of the atoll grains are replaced by economic sulphides (galena, chalcopyrite, sphalerite) consistent with Grondis and Shoulten, (1937) (Figure 14.A,B). Fine-grained pyrite also regularly forms dense 'matted' clusters, giving it a massive, crystalline appearance. On close inspection, original fine-grained pyrite grains and central cores are still distinguishable, although grains are aggregated (Figure 14.D-F).

Within deformed samples fine-grained pyrite displays a highly ductile nature as opposed to other bedded units, displaying tight to isoclinal folding (Figure 19.E,F). This is especially true when in high concentrations.

Variety

Brassy pyrite is distinguished from fine-grained pyrite by a coarser grain size, euhedral texture, dense aggregation and close resemblance in colour and texture to coarse-grained pyrite (Figure 16 and 17). Brassy pyrite often forms adjacent to, or within fine-grained pyrite as discontinuous zones (Figures 16 and 17.C). It is present as groups of euhedral, hydrothermal crystals independent of fine-grained pyrite (Figure 17.A,B), or forms as continued growth of fine-grained pyrite (Figure 16). In these circumstances, further growth of pyrite ± chalcopyrite ± galena ± sphalerite have been observed inter-growing amongst fine-grained pyrite, forming a crystalline texture (Figure 14.D,E).

Coarse-grained pyrite and brassy pyrite have a different colour to fine-grained pyrite, representing a chemical difference (Figures 16, 17.H and 20.D). Coarse-grained pyrite (Pyrite 2) is also characterised by a typically continuous, unbroken, smooth crystal structure (Figures 17.A,D). Pyrite 2 is observed growing adjacent to fine-grained pyrite within alteration zones (silica or dolomite) and occurs with chalcopyrite and pyrrhotite (Figure 17.E,H, and 20.D,F).

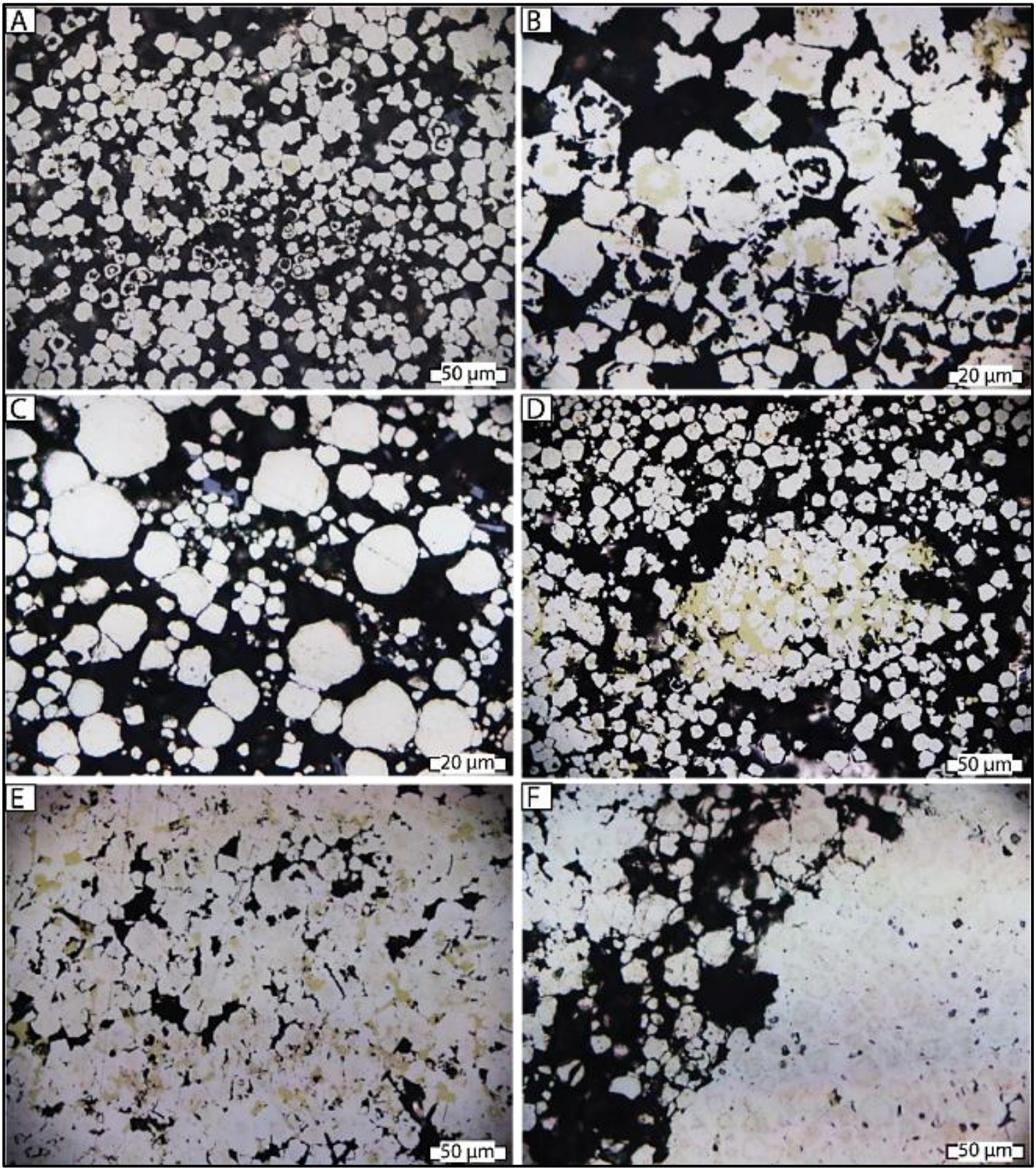

Figure 14: Petrographic images of fine-grained pyrite. Images A and B show typical atoll textures, which are often filled with chalcopyrite, galena or sphalerite. Image C shows fine-grained pyrite present mainly as rounded spherules. Images D, E and F show further growth of original fine-grained pyrite, supporting the hypothesis that brassy pyrite forms when additional pyrite, chalcopyrite or other sulphide infills and inter-grows with fine-grained pyrite.

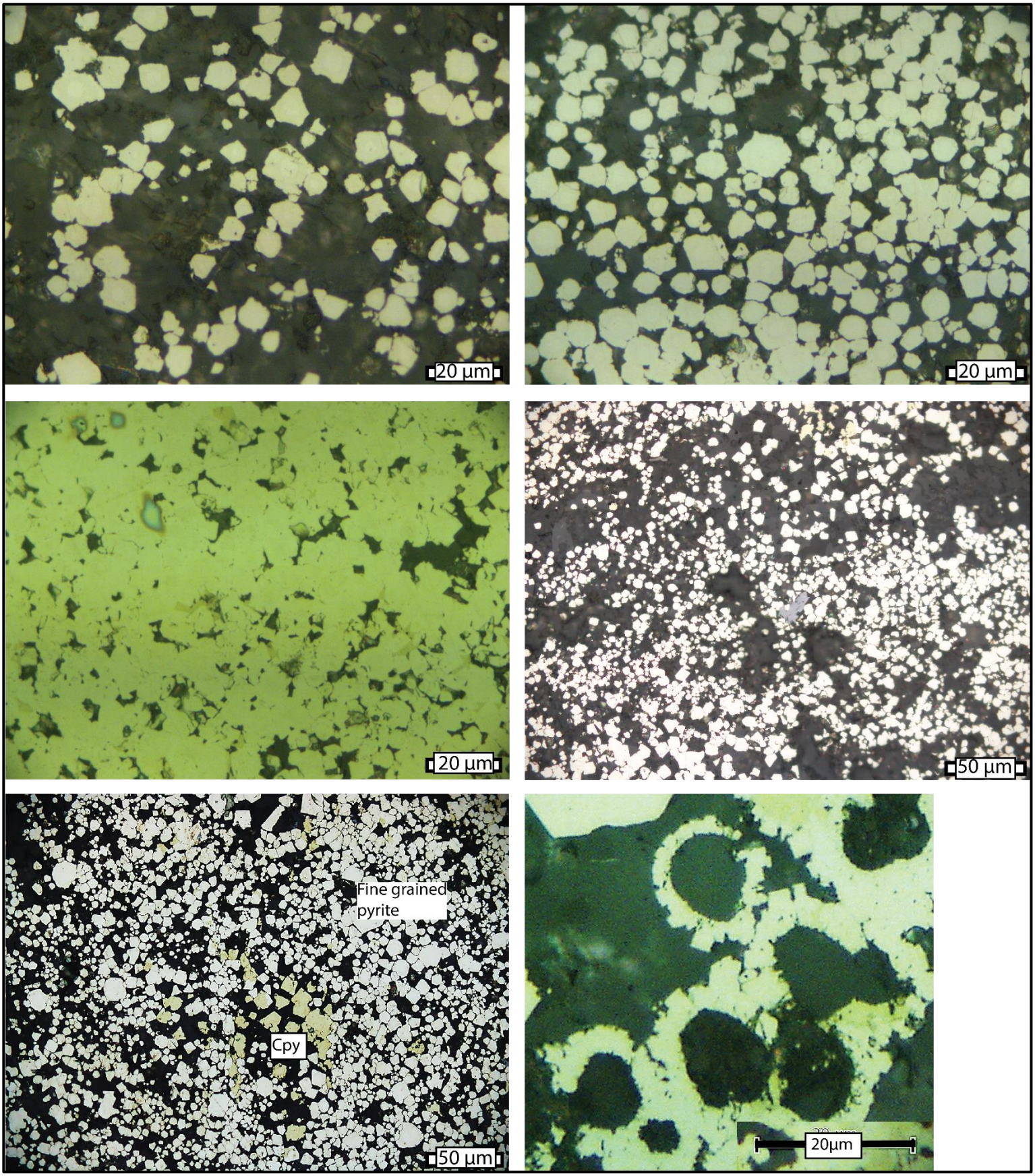

Figure 15: Typical petrographic images of fine-grained pyrite. Images A – C show the variable density of fine-grained pyrite (A- low density, B- medium density, C – high density) Image A displays typical euhedral 'crystallite' textures. Image D shows fine-grained pyrite surrounding a grain of galena. Image E shows chalcopyrite directly replacing fine-grained pyrite at high magnifications. Image F shows atoll textures of fine-grained pyrite, with parts of the atoll being replaced by chalcopyrite.

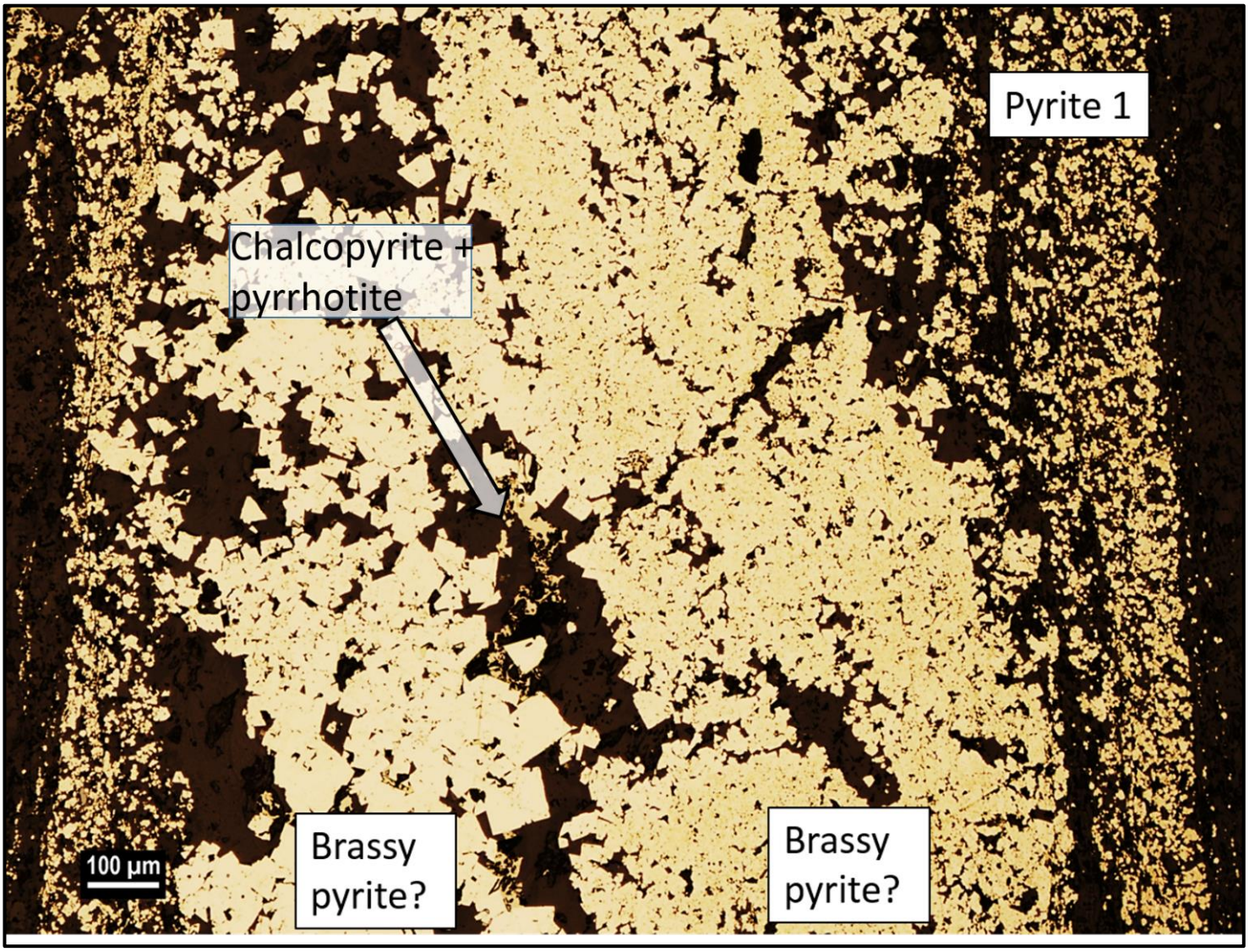

Figure 16: Image of pyritic shale showing three different textural varieties of fine-grained pyrite. Brassy pyrite is present as both light coloured euhedral crystals, associated with chalcopyrite and pyrrhotite (middle left), and additionally as over-growth of original fine-grained pyrite (middle-right). Original fine-grained pyrite is present as darker coloured, finer, irregular grains (far left and far right).

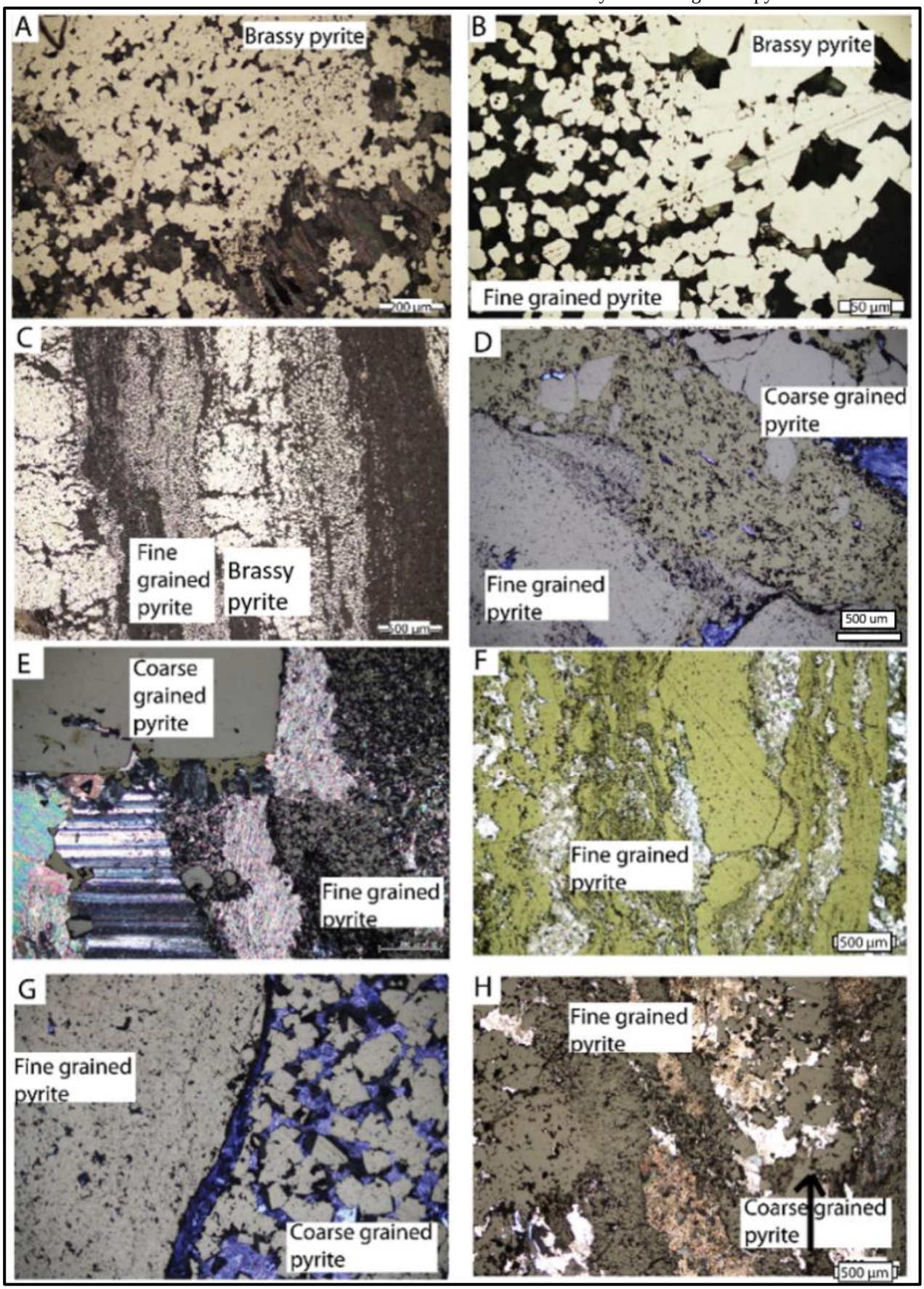

Figure 17: Typical petrographic images of fine-grained pyrite textural variety in Enterprise. Images A and B show the appearance of brassy pyrite in thin section. Image C shows clear alternating beds of 'brassy pyrite' and fine-grained pyrite. Image D shows dense matted fine-grained pyrite alongside coarse-grained pyrite and chalcopyrite. Image E shows true coarse-grained pyrite (continuous unbroken texture) alongside fine-grained pyrite. Image F shows fine-grained pyrite forming dense 'matted' textures, often difficult to discern from brassy pyrite. Images G and H show the crystallisation of coarse-grained pyrite in altered zones, occurring alongside fine-grained pyrite.

Control on deposition

Fine-grained pyrite was observed to display a linking pattern, concentrating within stratiform carbonaceous-rich cleavage seams rather than shale beds specifically (Figure 18 A-D). These cleavage seams are dominantly sub-parallel to bedding (S_2 cleavage), but are also observed to be parallel to an interpreted S_3 cleavage, parallel to the axial plane of micro-folds. Fine-grained pyrite is observed to overprint both generations of this cleavage (Figure 19.A-D), consistent with Perkins (1998). Additionally, fault zones rich in carbonaceous material are commonly crystallised by fine-grained pyrite (Figure 18.D).

Relationship to ore/alteration

Alteration and ore fluid pathways commonly form between fine-grained pyrite beds, or alternatively at the boundary of fine-grained pyrite beds. In this situation fine-grained pyrite can be interpreted to have acted as a barrier to fluid migration (Figure 20.A-D,F). In the rare cases that economic sulphide minerals were observed within pyritic shales, economic sulphides (Cu,Zn,Pb) formed with paragenetic relationships indicative of co-precipitation (Figure 21.A-F). Arsenopyrite was also observed in pyritic shales with the same para-genetic timing to coarse-grained pyrite (Figure 21.E).

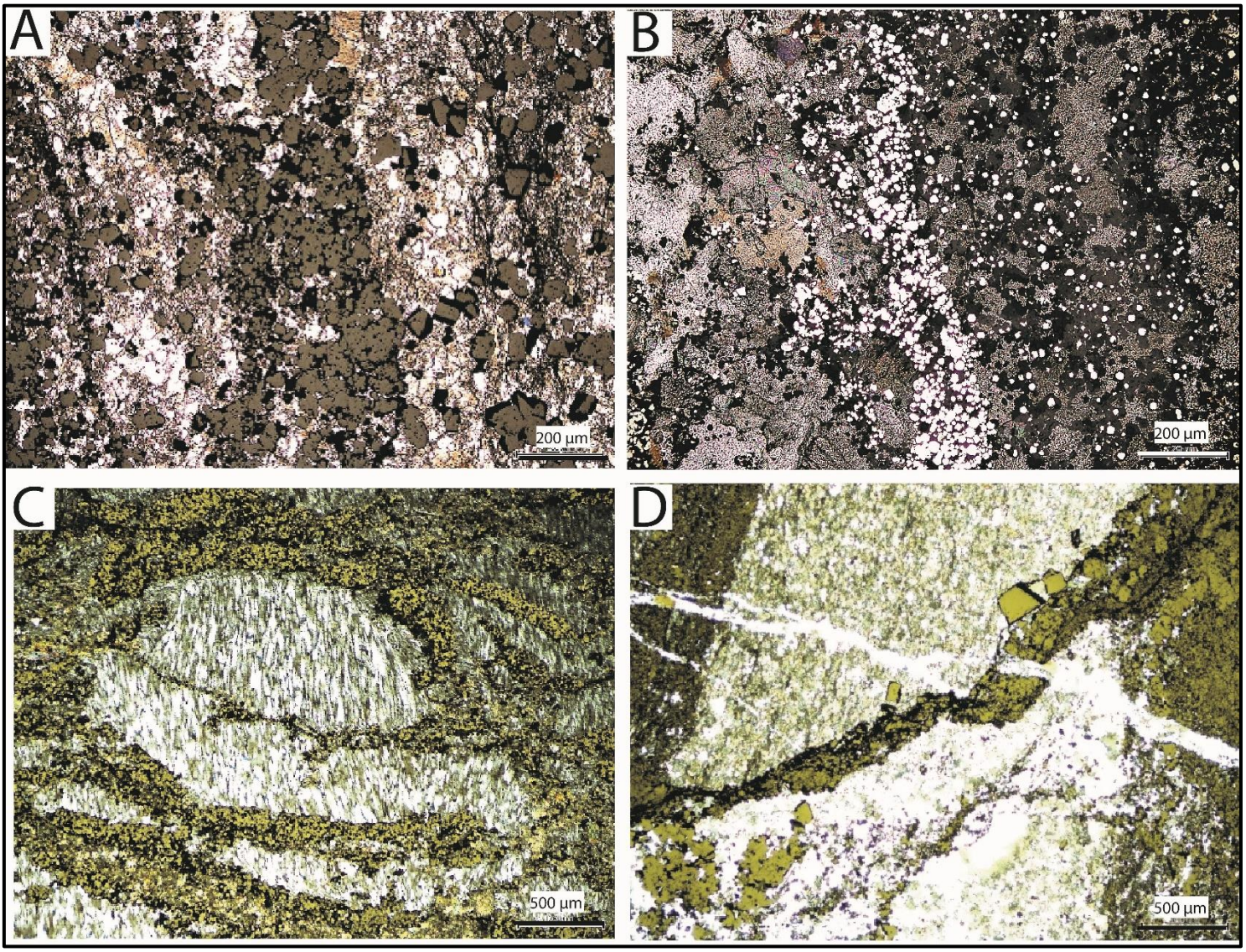

Figure 18: Typical petrographic images which demonstrate fine-grained pyrite being strongly controlled by carbonaceous rich seams or cleavages. Images A,B show fine-grained pyrite within linked carbonaceous seams, around dolomitic shale. Image C, shows fine-grained pyrite within seams surrounded by silica alteration. Image D shows fine-grained pyrite crystallisation within a carbonaceous rich fault zone, which cross-cuts bedding.

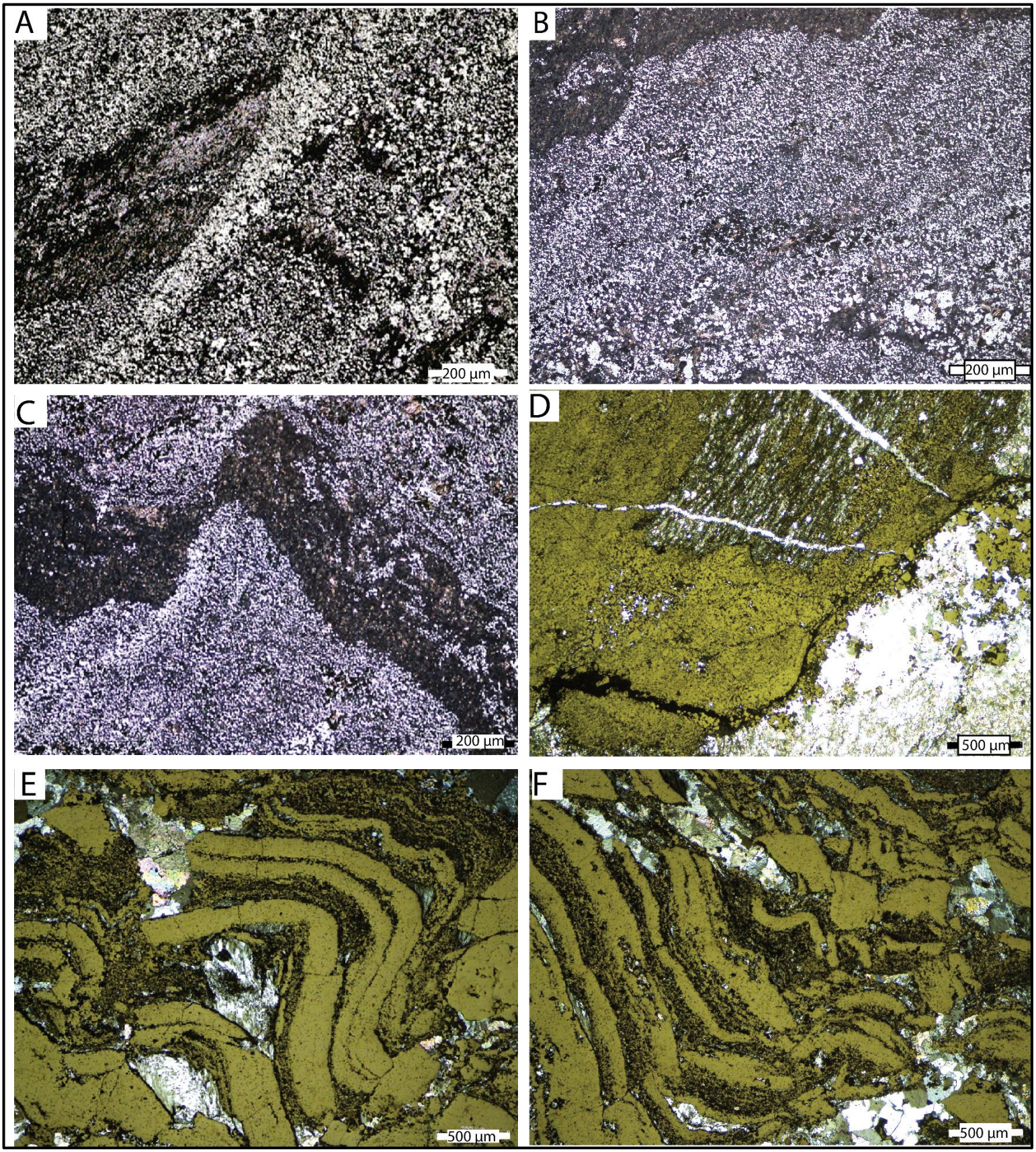

Figure 19: Typical petrographic images which show micro-scale structures of fine-grained pyrite. Images A, B and C show the orientation of fine-grained pyrite, non-parallel to bedding, and parallel to the axial plane of micro-folds. FigureD shows the irregular distribution of pyrite crystallisation, not always parallel to bedding. Images E and F demonstrate the ductile nature of fine-grained pyrite, and its ability to fold under stress, rather than fracture. Note that silica/dolomite alteration migrates in between fine-grained pyrite, with the pyrite acting as traps for alteration zones.

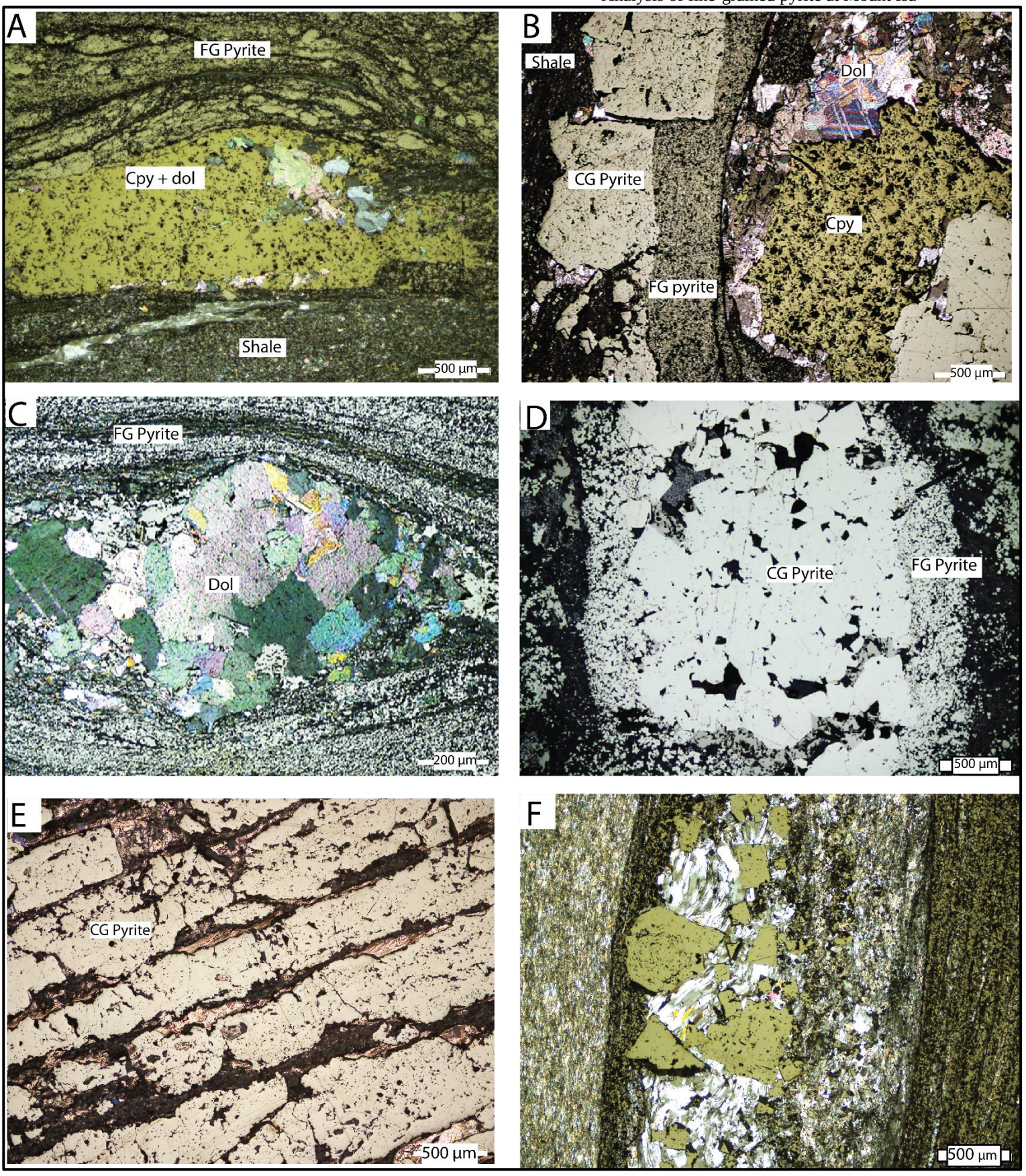

Figure 20: Typical petrographic images which show the relationship between fine-grained pyrite, ore minerals, and alteration. Images A, B and C show alteration pathways and chalcopyrite mineralisation occurring on the border of fine-grained pyrite beds, or in-between fine-grained pyrite beds. Image D shows coarse-grained pyrite mineralisation within an alteration zone, and is distinct from fine-grained pyrite. Image E shows stratiform, tabular blocks of coarse-grained pyrite in between silica alteration. Image F shows the ability of fine-grained pyrite to restrict alteration to specific zones. Note the unaltered shale to the far left, and silica alteration (middle).

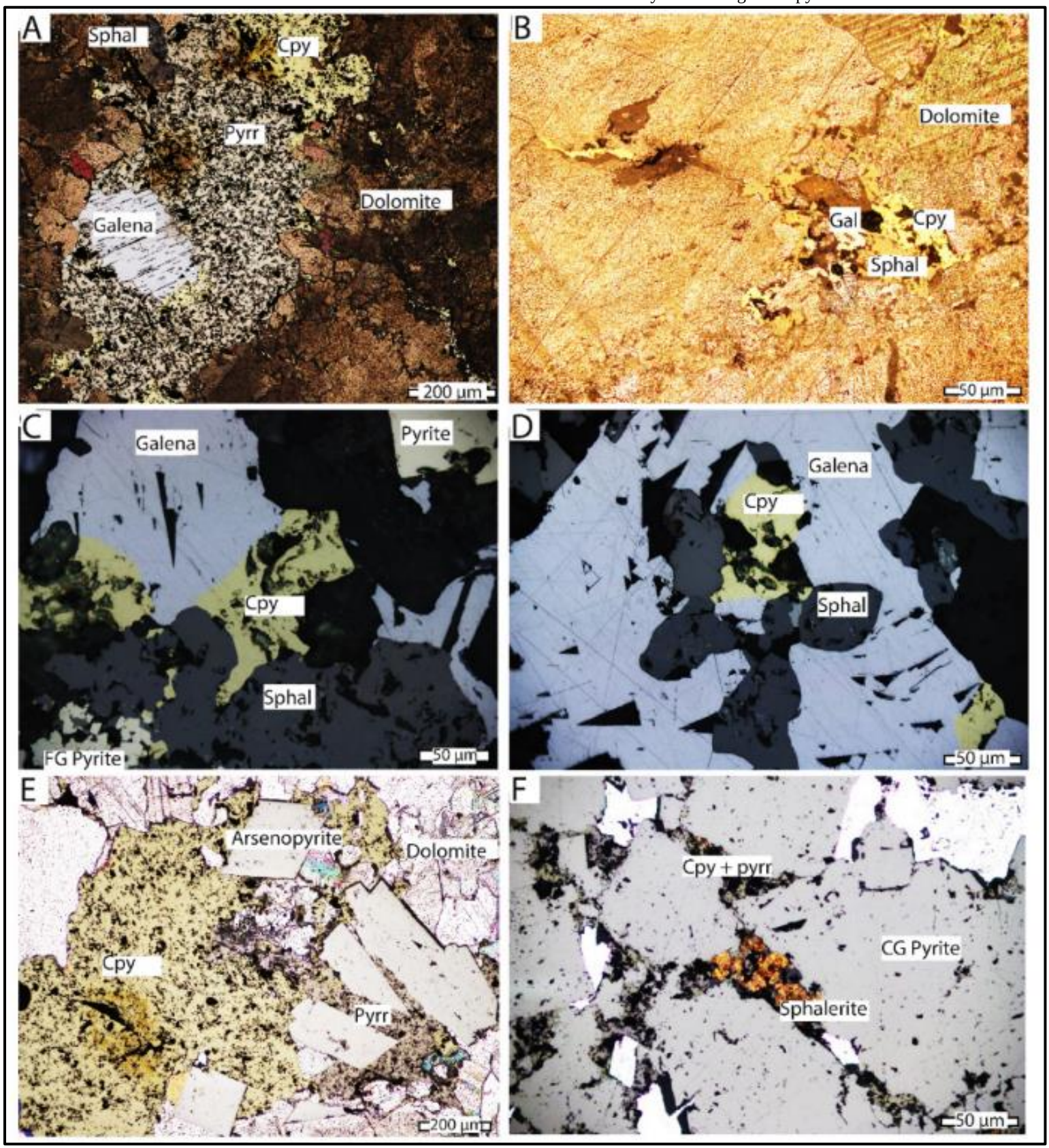

Figure 21: Typical petrographic images of ore minerals within pyritic shales in the enterprise system. Images A shows pyrrhotite, chalcopyrite, galena and sphalerite within the same sulphide grain. Image B shows galena, sphalerite and chalcopyrite infilling cracks within dolomite.-Images C and D show co-precipitation of galena, sphalerite and chalcopyrite. Image E shows crystallisation of arsenopyrite amongst chalcopyrite and pyrrhotite. Image F shows chalcopyrite, pyrrhotite ad sphalerite infilling amongst coarse-grained pyrite. These images suggest that in these cases, economic sulphides were part of the same system.

4.3 SEM

Textures

SEM analysis of pyritic shales confirmed that fine-grained pyrite consistently displays ‘atoll’ textures, growth zoning and cores of galena and chalcopyrite (Figure 22) consistent with the work of Grondis and Shoulten, (1937). The fine-grained pyrite atolls display a distinct dark coloured central zone and a lighter coloured rim, with both these zones often altered by later stage ore fluids. There are multiple generations of pyrite growth observed, demonstrated by different textural varieties occuring in adjacent layers within the same sample (Figures 24 A,B,D-F and 25.B,D).

Pyrite variety

Enterprise samples clearly contained alternating layers of brassy pyrite and fine-grained pyrite, with a clear mineralising fluid boundary between the two varieties (Figures 23, 24 and 25). The brassy pyrite mineralising event was overprinted by silica-dolomite veins containing Pyrite 2 and chalcopyrite (Figure 23). Brassy pyrite contains trace amounts of other sulphides including chalcopyrite, pyrrhotite, galena, and sphalerite (Figure 25.A,B). The pyrite varieties have notebly different colour shades, possibly reflecting different chemical compositions (Figure 24. E,F).

Structure and timing

In strongly deformed samples (Figure 26), the rock displays a cleavage orientatated parallel to the strike of micro-folds within the sample. The cleavage is defined by carbonaceous rich seams, with fine-grained pyrite crystallised within these seams (Figure 26). Veins of coarse-grained pyrite also follow the same trend in these samples. The individual pyrite grains do not appear strained, or preferentially orientated (Figure 26). Fine-grained pyrite that is crystallised parallel to the S3 cleavage, is almost identical in textural characteristics to the pyrite crystallised sub-parallel to bedding (Figure 26).

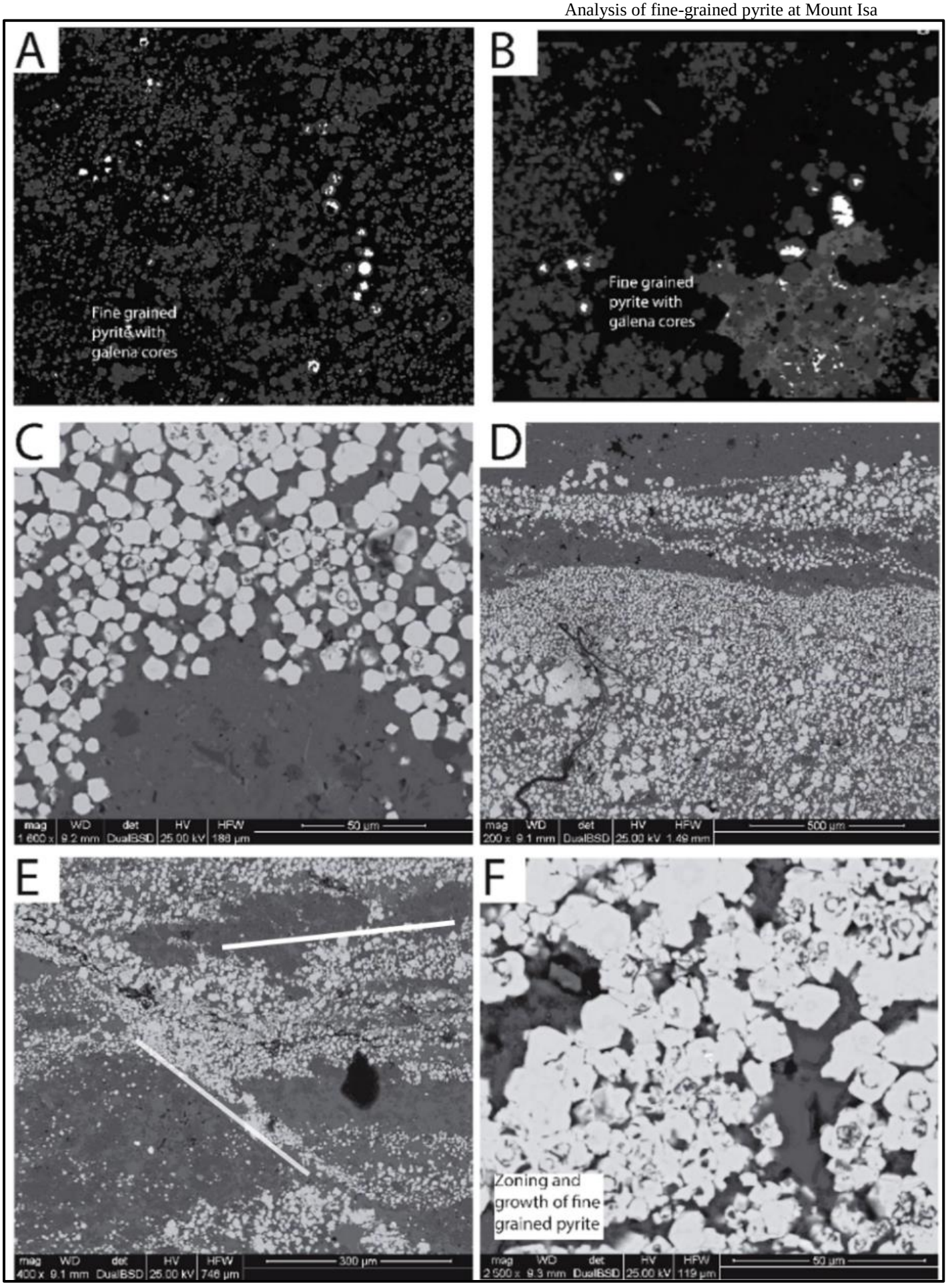

Figure 22: Scanning electron microscope images of typical fine-grained pyrite in the Enterprise system. Images A and B show galena replacing the cores of fine-grained pyrite. Images C and F show fine-grained pyrite with distinguishable cores, and growth zoning. Image E shows fine-grained pyrite non parallel to bedding, mineralising within a fault zone.

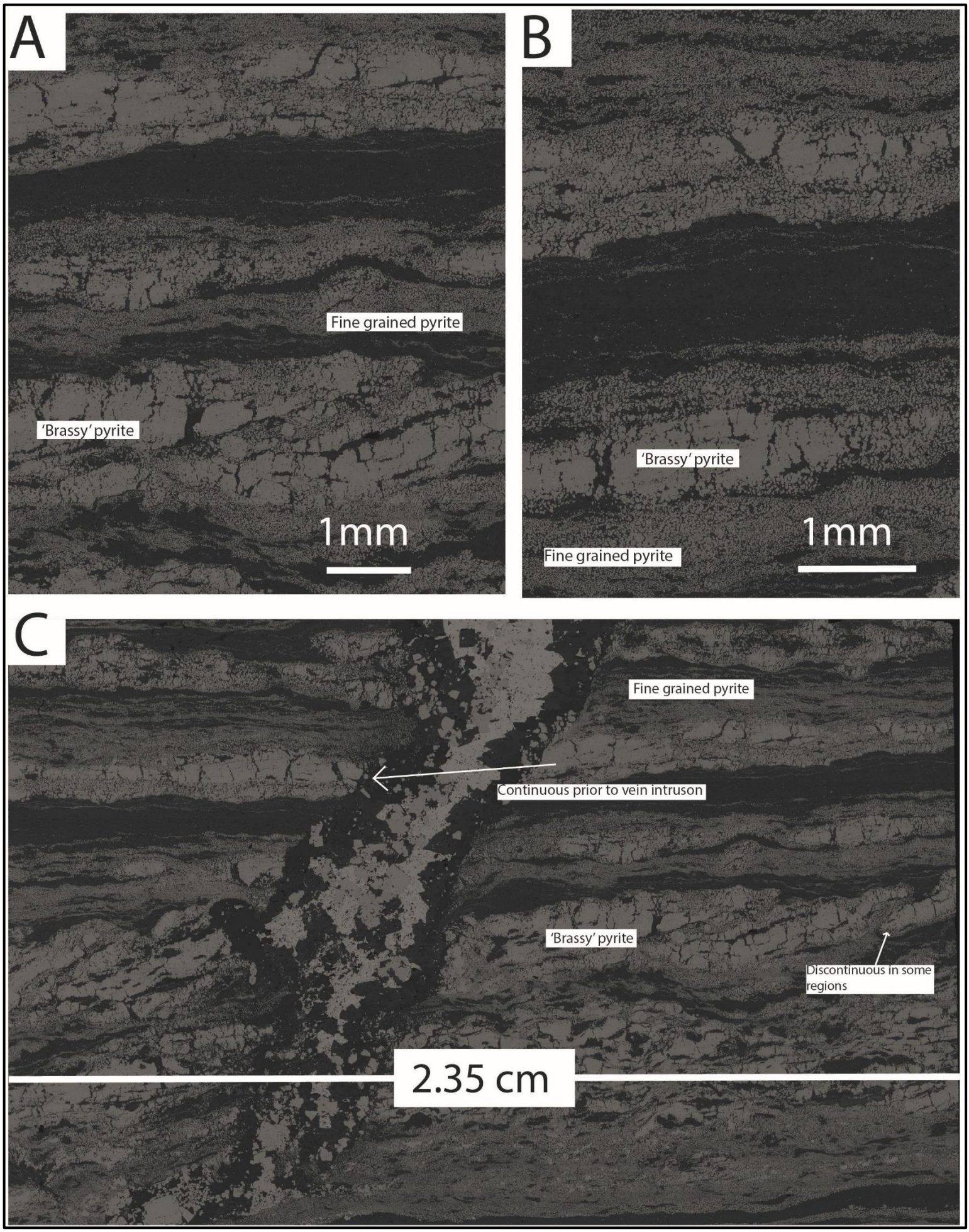

Figure 23: Scanning electron microscope images of fine-grained pyrite within the ENTFG13A sample. These images demonstrate the occurrence of both 'brassy pyrite' and fine-grained pyrite within the same sample. Brassy pyrite has as a massive, crystalline appearance due to further outward growth and infill of secondary pyrite, and economic sulphides. They occur in alternating layers and were present prior to intrusion of an ore vein (image C).

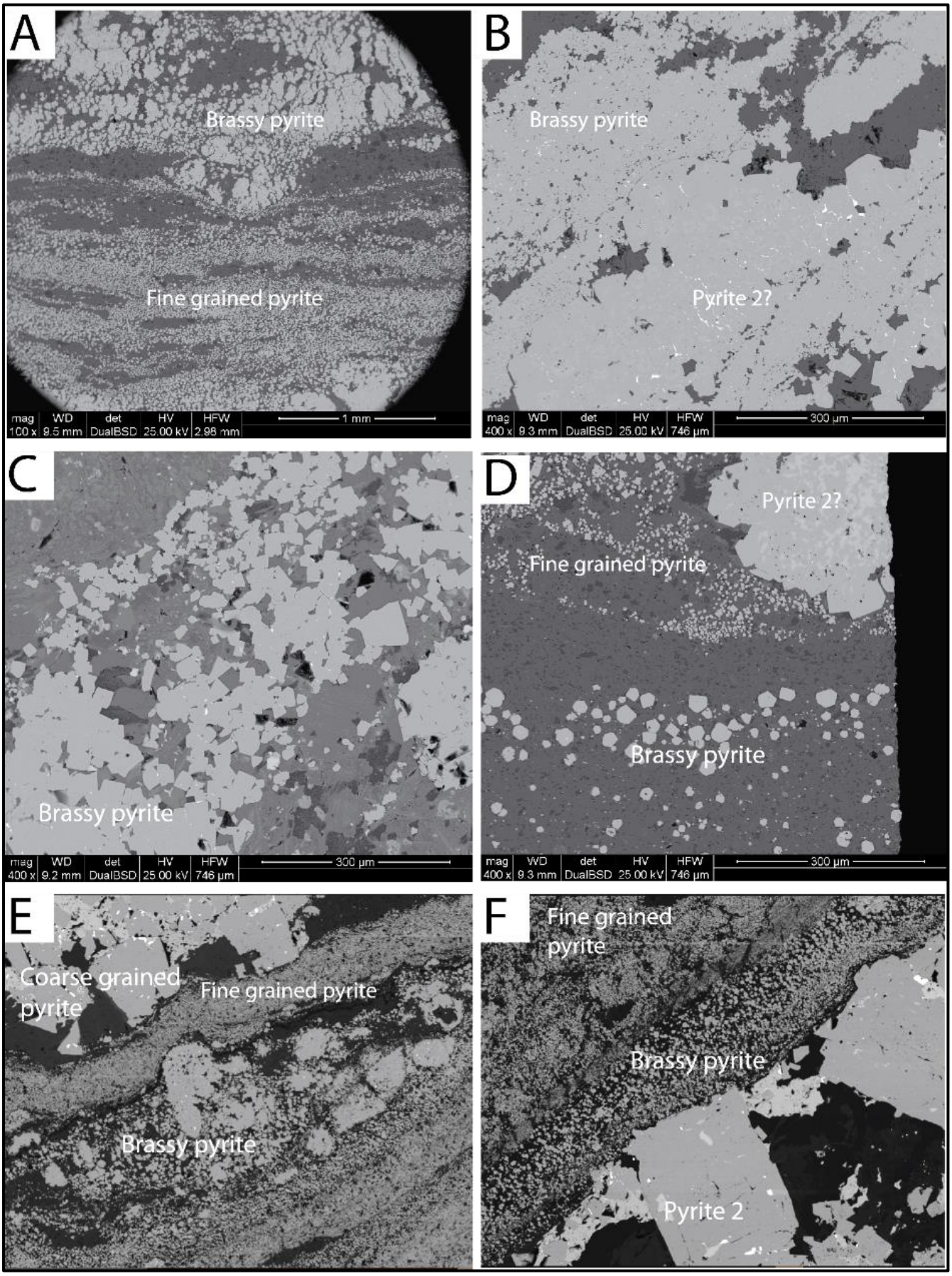

Figure 24: Scanning electron microscope images of pyrite variety within the Enterprise system. These images demonstrate the variety of textures observed between fine-grained pyrite, brassy pyrite and coarse-grained pyrite (pyrite 2). Note brassy pyrite and coarse-grained pyrite are associated with trace amounts of economic ore minerals. Image A – Brassy pyrite (above), and fine-grained pyrite (below). Image B, two different generations of pyrite (brassy pyrite or coarse-grained pyrite) which have overprinted fine-grained pyrite. Image C – typical 'brassy pyrite' textures. Image D,E,F – occurrence of both fine-grained pyrite, 'brassy pyrite' and coarse-grained pyrite adjacent to each other.

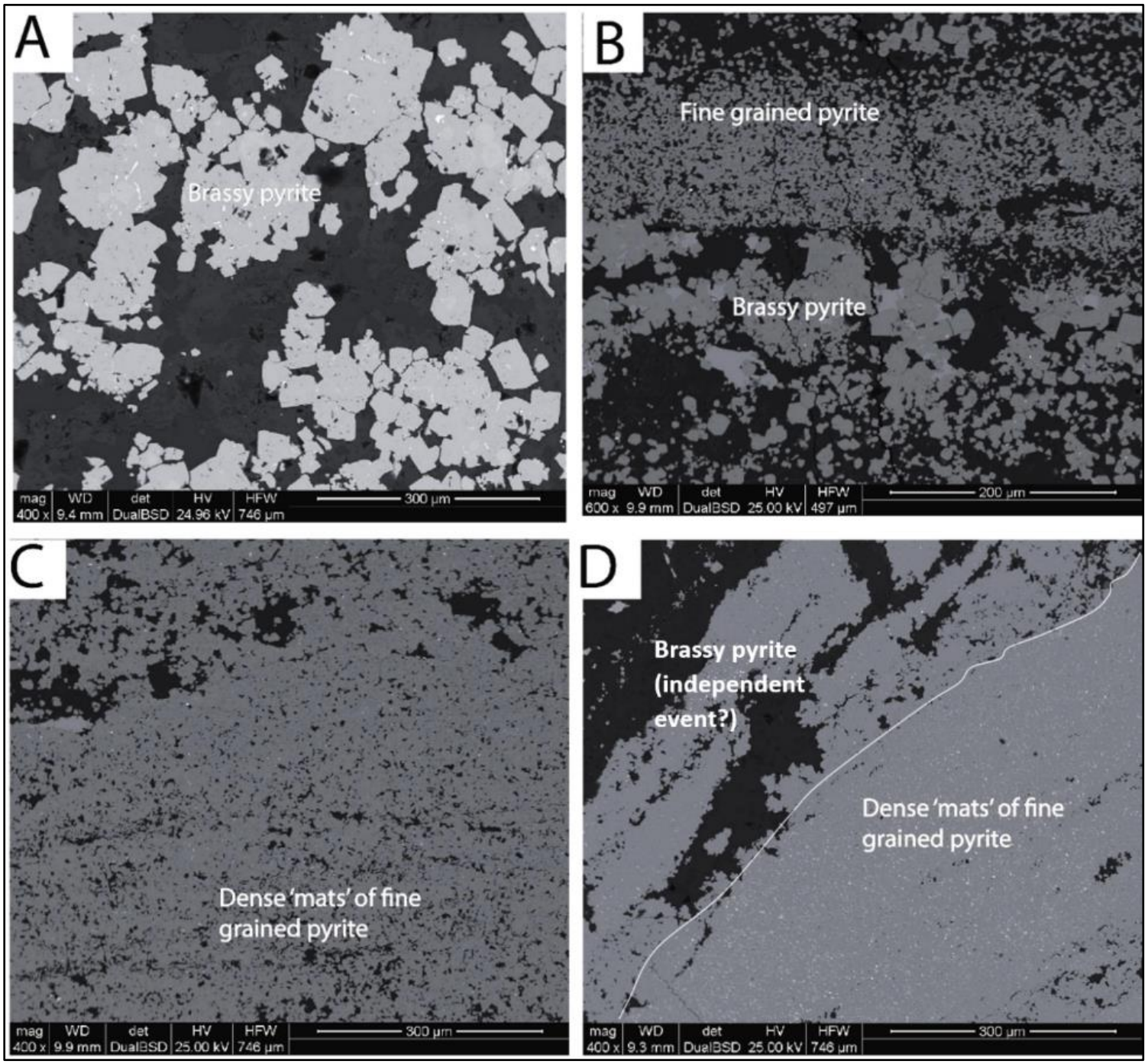

Figure 25: Scanning electron microscope images of pyrite variety within enterprise samples. These images demonstrate the variety of textures observed in different pyrite varieties. Image A shows brassy pyrite occuring on its own. Image B shows the contrast between brassy pyrite and fine-grained pyrite in adjacent layers. Image C and D show matted textures of fine-grained pyrite and 'brassy pyrite'.

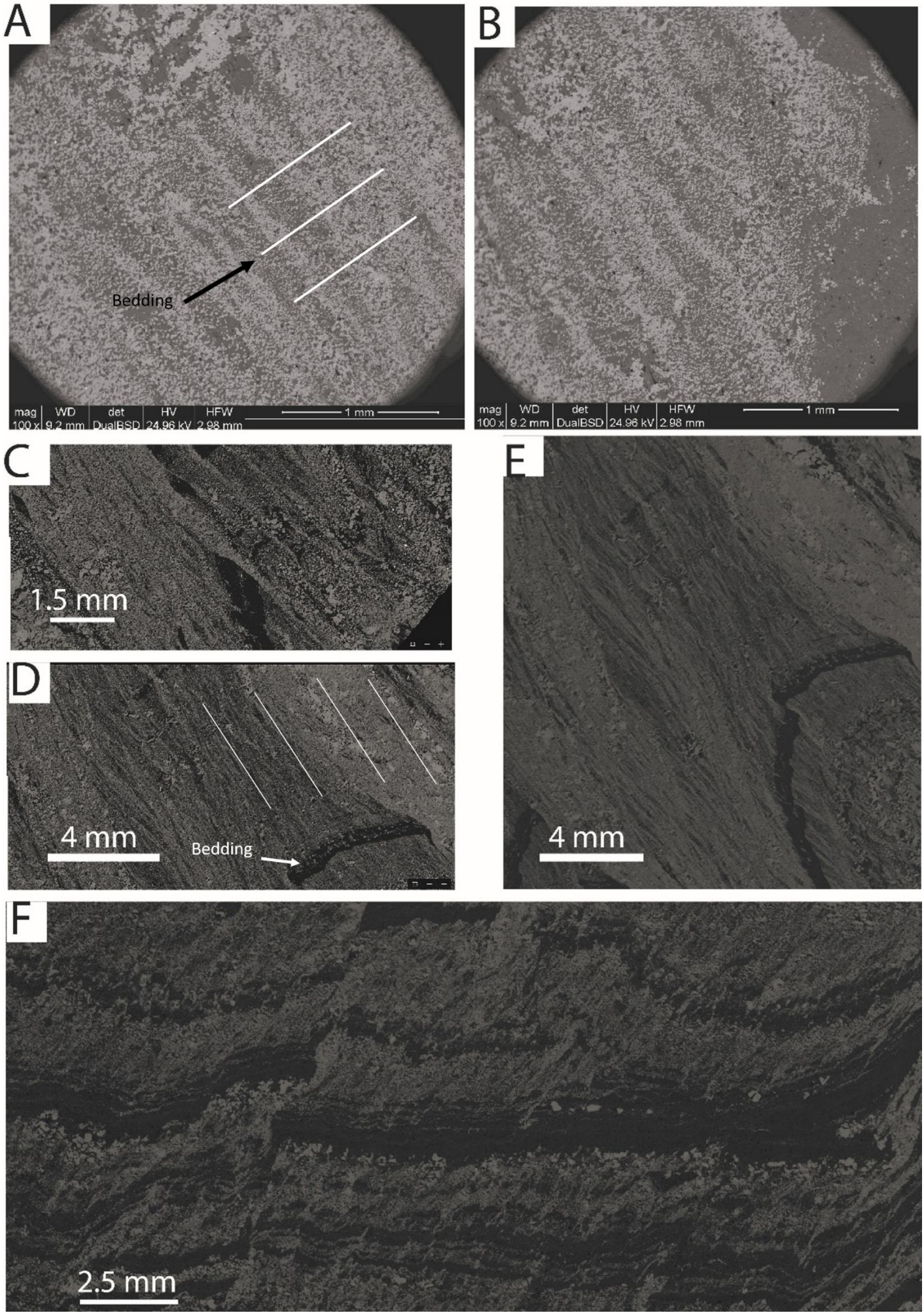

Figure 26: SEM images showing the crystallisation of pyrite parallel to the S_3 carbonaceous cleavage, parallel to axial plane of folds. Image A,B – fine-grained pyrite crystallising in a strong orientation non-parallel to bedding. Images C,D,E – folded samples with a strong cleavage development. Fine-grained pyrite is crystallised parallel to this cleavage and overprints the deformation in the sample. There is also pyrite sub-parallel to bedding in these samples. The characterisitics between these pyrite generations are almost identical. Image E shows pyrite both parallel to bedding, and orientated parallel to the S_3 cleavage.

4.4 LA- ICP - MS

Laser results show that ‘brassy pyrite’ is geochemically distinct from fine-grained pyrite and un-mineralised shale, with enriched concentrations of cobalt and copper (Figure 27).

Brassy pyrite has cobalt concentrations between 600 and 700 ppm, whereas fine-grained pyrite has cobalt concentrations of approximately 100 ppm. Likewise, brassy pyrite has copper concentrations over 4000 ppm, whereas fine-grained pyrite has copper concentrations between 0 and 100 ppm.

The Co/Fe ratios of brassy pyrite are between 0.4 and 0.6. Fine-grained pyrite has a Co/Fe ratio around 0.1. Therefore, when results are normalised to iron content there is enriched cobalt concentration evident in brassy pyrite. The brassy pyrite Cu/Fe ratio ranges from 0.2 to more than 1. The fine-grained pyrite and shale has a Cu/Fe ratio between 0 and 0.05. This implies copper is relatively absent within the fine-grained pyrite bearing shale. However, brassy pyrite contains copper concentrations equal to the concentration of iron in the layer.

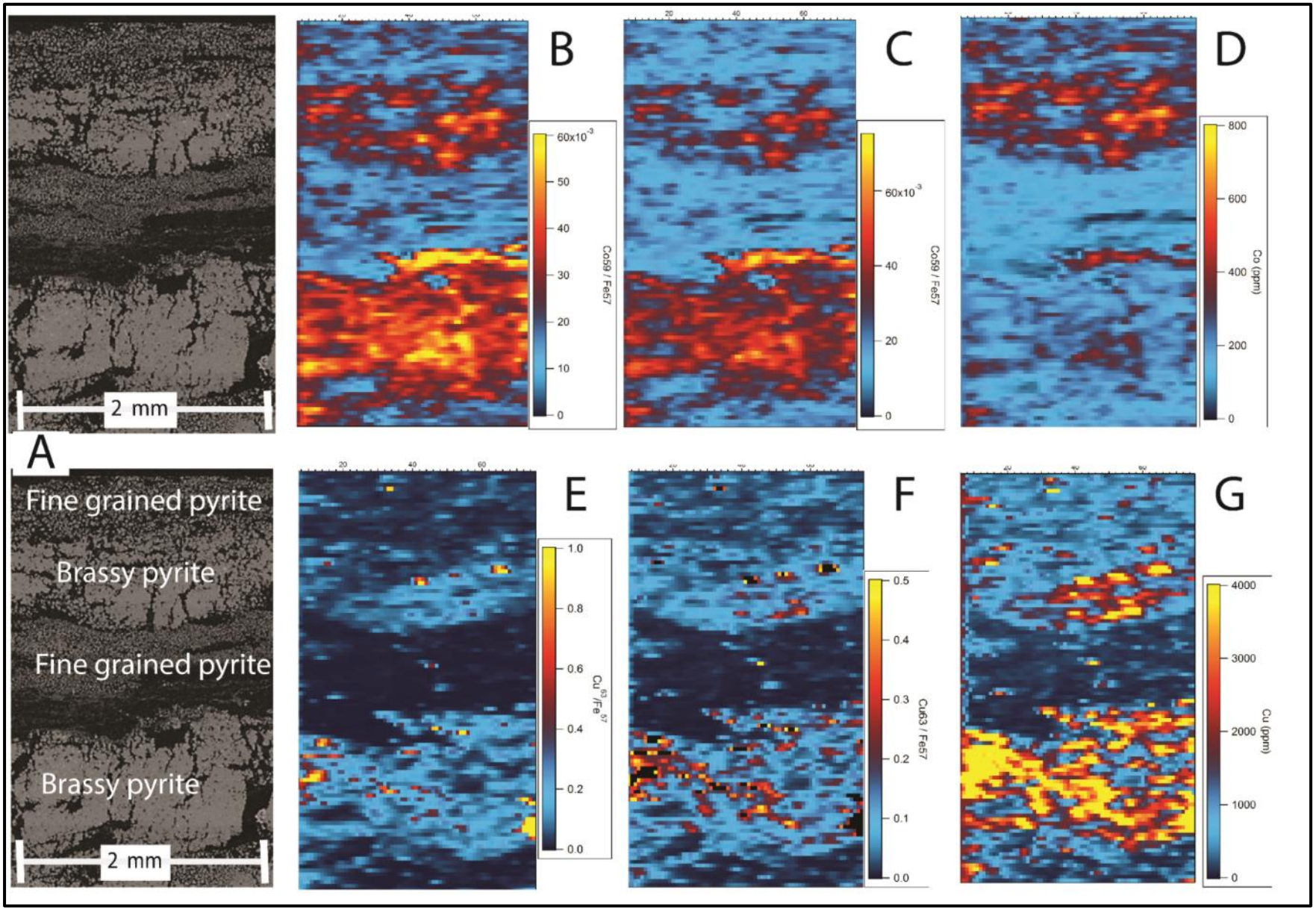

Figure 27: Images generated from data acquired through LA-ICP-MS. Note: The X axis on some images in Figure29, shows 'Co / Fe' or 'Cu / Fe'. This refers to the ratio of Co or Cu relative to Fe. This was done due to the pyritic shales generally being rich in Fe. It serves as an indication of Co or Cu abundance relative to Fe content. Observations show that brassy pyrite can be chemically distinguished from fine-grained pyrite. The symbol Cu / Fe and Co / Fe refers to the ratio of the element compared to Fe abundance. The original fine-grained pyrite (middle) appears chemically distinct from the brassy pyrite (upper and lower).

4.5 Magnetite - petrography, SEM and MLA

Magnetite was observed within pyritic shale samples from the W61 FWDR location (Figure 12.D). Magnetite is rare in the Mount Isa system, and the geological relationships are presented here.

Textural characteristics

Magnetite is observed as large, euhedral, porphyroblastic (0.1 – 3mm) crystals (Figure 28.F). Magnetite crystals have formed (aggregated) in groups, parallel to the direction of bedding (Figure 12.D). This is consistent with the interpretation that there has been a lithological, or bedding control on its formation. Crystals are observed growing amongst, or directly adjacent to fine-grained pyrite layers (Figure 28.F). Furthermore, most magnetite crystals contain inclusions of spherical, very fine-grained pyrite (Figure 28.A-D). Outside the magnetite crystal, fine-grained pyrite is coarser grained, euhedral and has a denser texture. The distribution of pyrite completely occupies all remaining space surrounding magnetite grains imparting a tightly packed appearance against the magnetite (Figure 28).

Mineral assemblages

Iron-carbonate, chlorite, and iron-rich phyllosilicate alteration are observed within the magnetite-bearing samples. The interpreted alteration originates from intruding veins, before utilising bedding parallel pathways amongst fine-grained pyrite (Figures 29 and 30). Fine-grained pyrite appears to localise alteration amongst pyritic bands. The veins contain altered carbonate minerals including siderite (FeC03) and ankerite ($Ca(Fe,Mg,Mn)(CO_3)_2$). Iron-rich phyllosilicates such as Stilpnomelane ($K(Fe^{2+},Mg,Fe^{3+})_8(Si,Al)_{12}(O,OH)_{27}n(H_2O)$), Fe-rich chlorite and biotite, also are present within the veins (Figures 29 and 30. Stilpnomelane grows within alteration zones as clusters of fibrous needle-textured grains and replaces shale minerals (Figures 30 and 31). Barium-rich dolomite is also abundant amongst the altered shale (Figure 30.D). Additionally, magnetite crystals form in conjunction with well-formed stilpnomelane and siderite crystals (Figure 29.A-D, Figure 30.D-G and Figure 31).

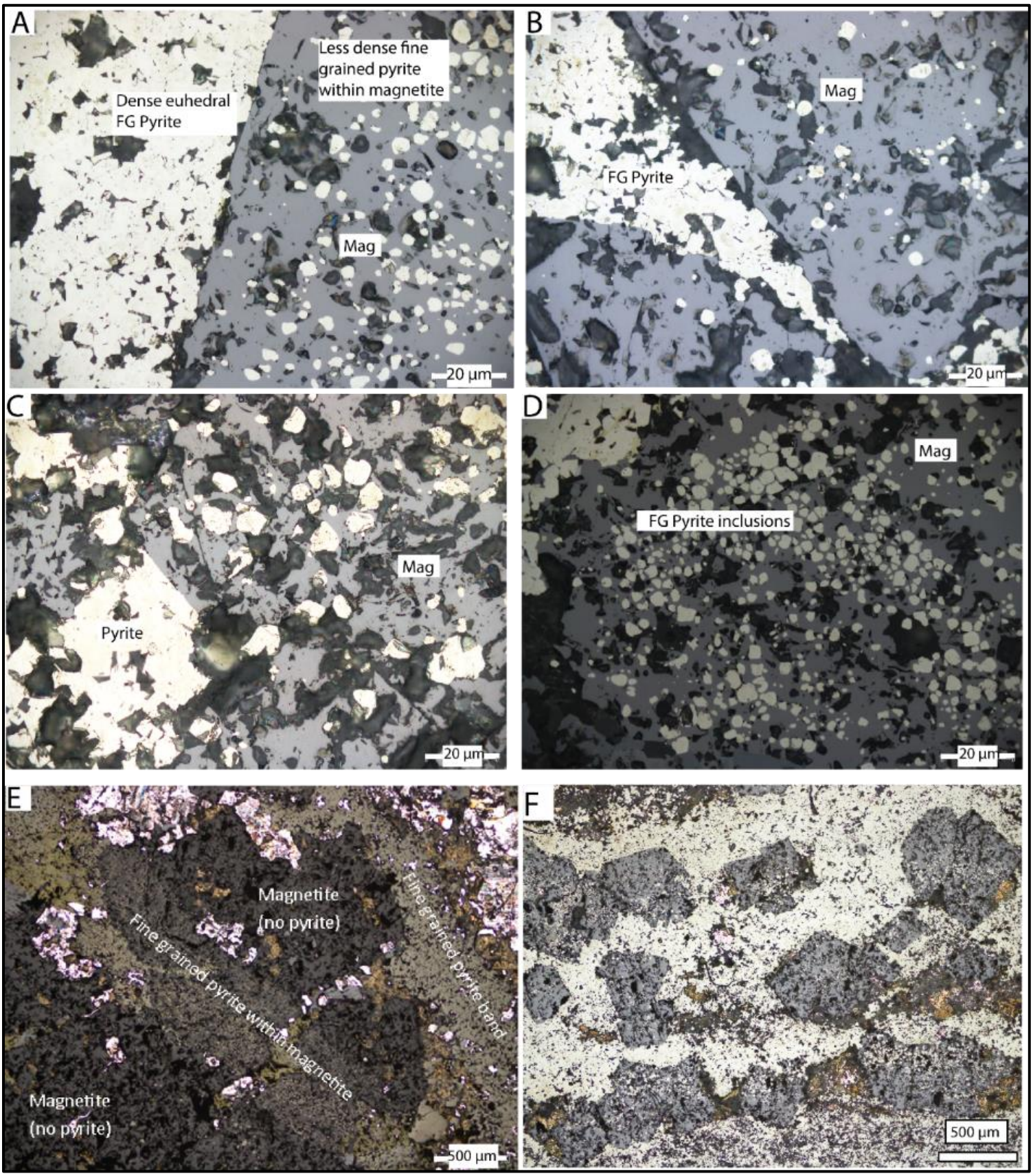

Figure 28: Petrographic images of fine-grained pyrite and magnetite. The fine-grained pyrite within magnetite is much less dense and is spherical shaped, whereas the fine-grained pyrite outside magnetite is dense, and has euhedral textures. Magnetite is seen to replace fine-grained pyrite, but does not require fine-grained pyrite to form (see Image E).

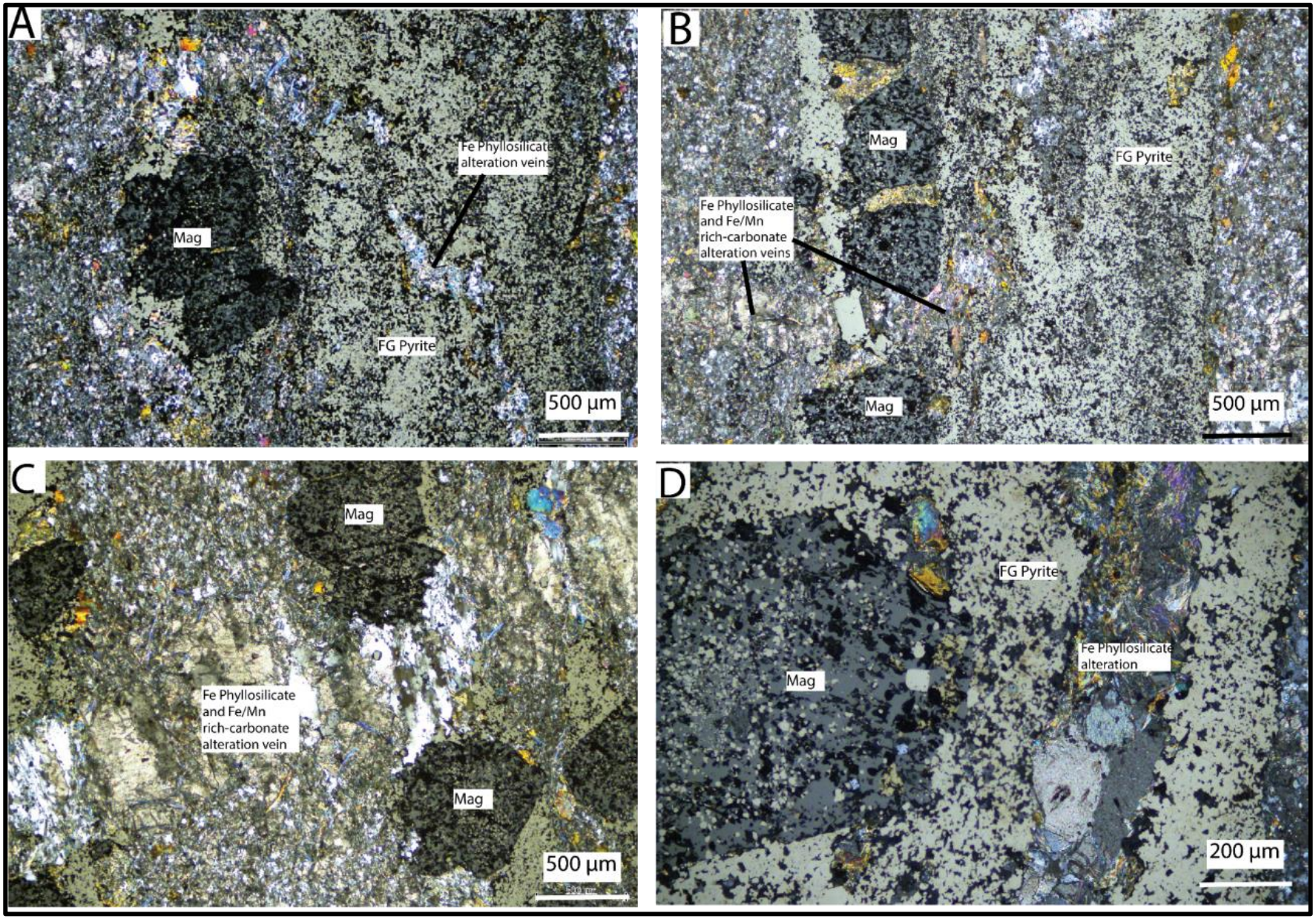

Figure 29: Magnetite petrographic samples depicting iron alteration through intruding veins. Resulting assemblages include magnetite, siderite, stilpnomelane and fine-grained pyrite. This alteration overprints fine-grained pyrite.

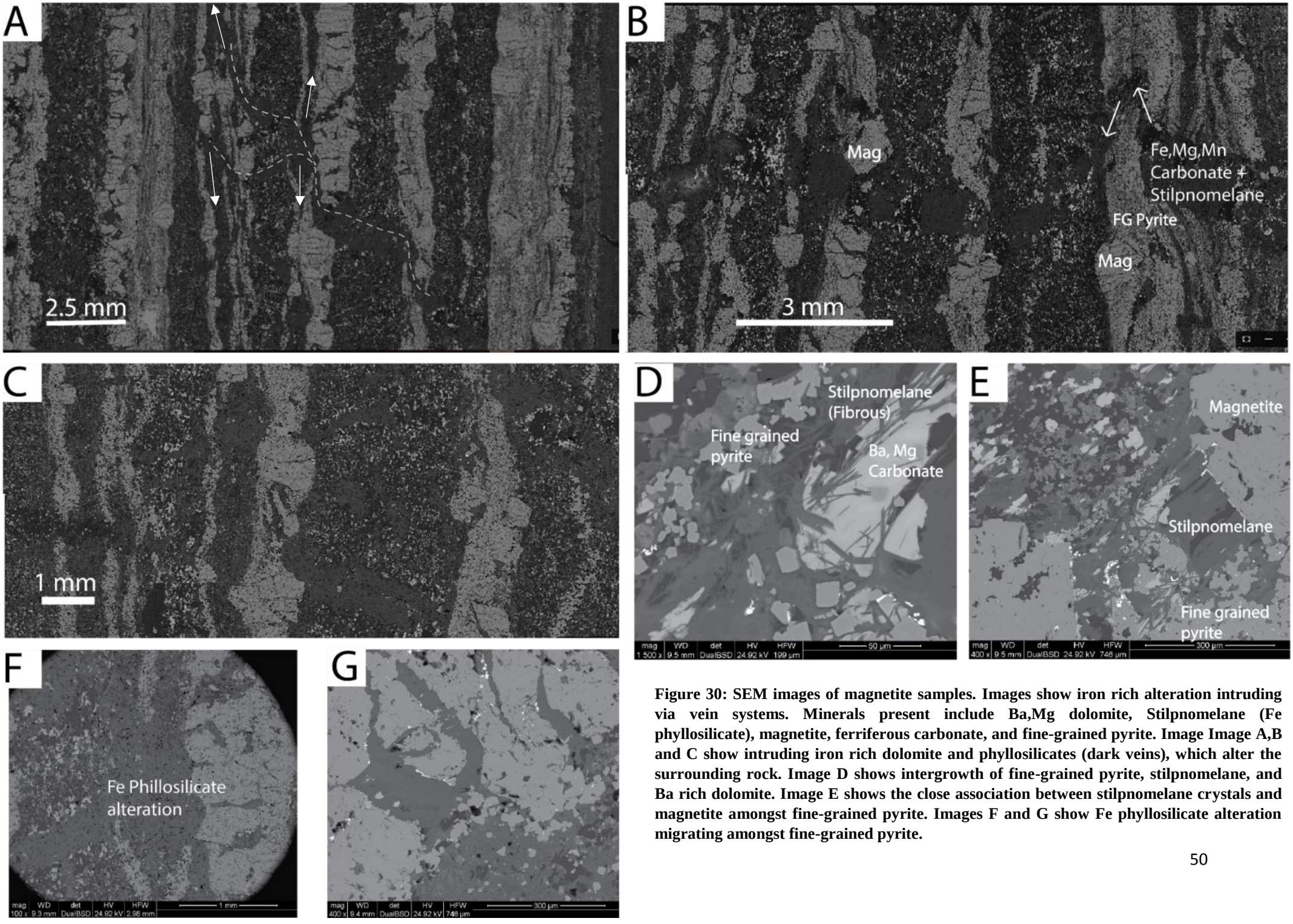

Figure 30: SEM images of magnetite samples. Images show iron rich alteration intruding via vein systems. Minerals present include Ba,Mg dolomite, Stilpnomelane (Fe phyllosilicate), magnetite, ferriferous carbonate, and fine-grained pyrite. Image Image A,B and C show intruding iron rich dolomite and phyllosilicates (dark veins), which alter the surrounding rock. Image D shows intergrowth of fine-grained pyrite, stilpnomelane, and Ba rich dolomite. Image E shows the close association between stilpnomelane crystals and magnetite amongst fine-grained pyrite. Images F and G show Fe phyllosilicate alteration migrating amongst fine-grained pyrite.

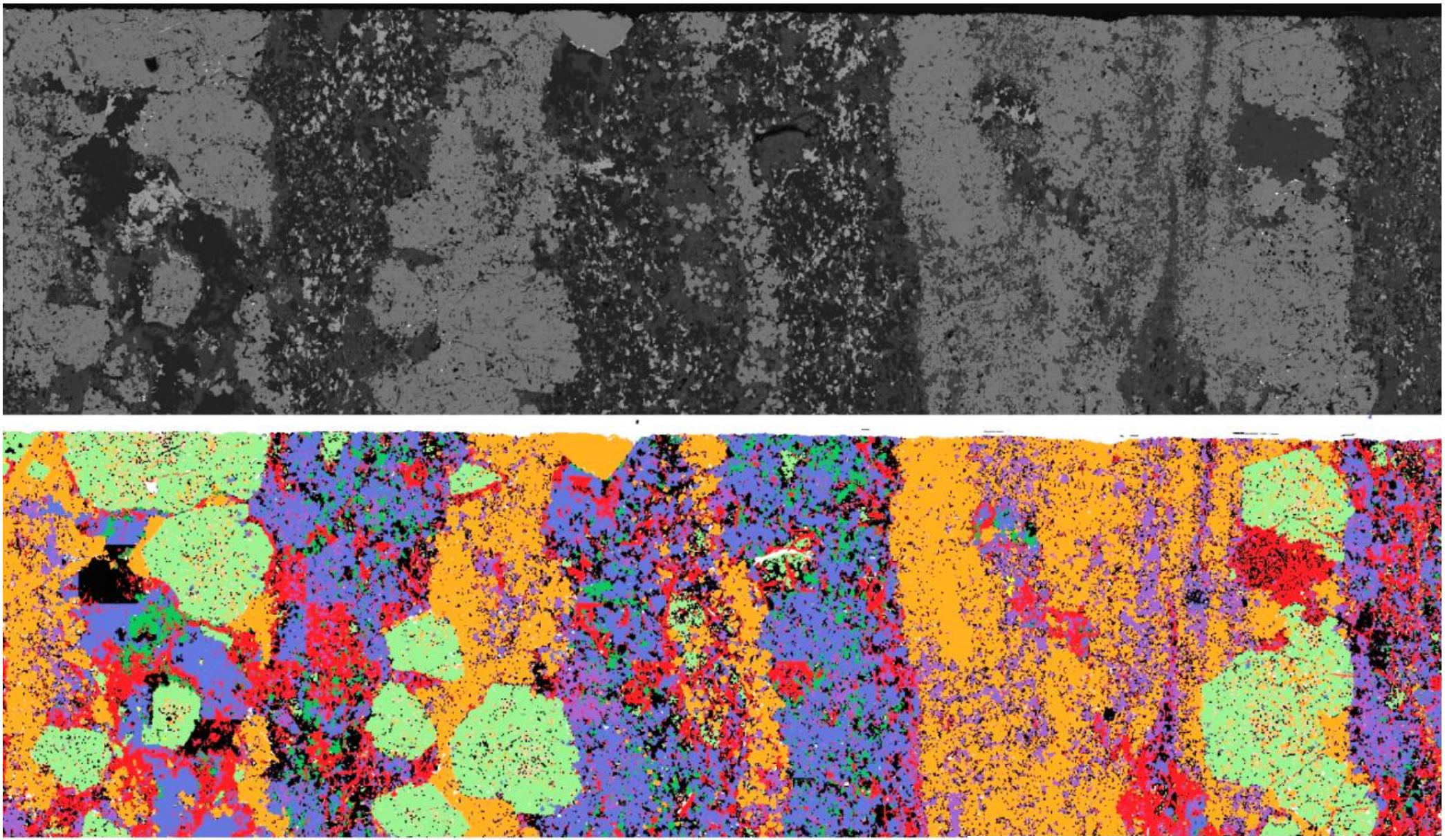

Figure 31: Mineral liberation analysis image within the magnetite sample. This image shows the alteration of shale by Fe rich phyllosilicate minerals (Stilpnomelane), and also the presence of Barium dolomite amongst shale. Note that Stilpnomelane is strongly correlated with magnetite (lower image upper right).

Relationship to ore minerals

Within a strata-bound zone, magnetite has grown to a coarser grain size. Within this bed, iron-rich sphalerite has entirely replaced the original rock surrounding magnetite, and fills the majority of the layer (Figure 32.E,G,H, and Figure 33). There is also abundant chalcopyrite and galena with concurrent timing (Figure 32.C,D,F). Small amounts of fine-grained pyrite are dispersed around the magnetite, and included within it.

The MLA map (Figure 36) revealed an altered zone containing barium-rich dolomite and iron carbonate on either side of the magnetite mineralisation. Iron-rich carbonate is present surrounding magnetite. The concurrent timing of sulphides and replacement of fine-grained pyrite by magnetite and economic sulphides, is also evident.

The samples containing magnetite (located within the N3500 Enterprise orebody) were assayed with results presented below. Grades up to 7% Zn, 5% Pb, 210 ppm Ag and 0.5% Cu were found within the same rock hand sample (table 2).

SAMPLE	Ag	Pb	Zn	S	Fe	Mg	Mn	Ba	Cu	Co
DESCRIPTION	ppm	%	%	%	%	%	ppm	ppm	ppm	ppm
RG27CW61FWDR002	100	2.5	2.09	16.4	22.8	2.89	3950	310	3290	68
RG27CW61FWDR003	210	5.67	7.06	16.65	18.25	1.26	4890	530	4450	90
RG27CW61FWDR004	51.2	1.485	2.73	16.25	25.7	1.96	8170	370	887	66

Table 2: Table showing the abundance of important elements within the W61 FWDR samples (containing magnetite). Assay results confirm the samples contain high amounts of silver, lead, zinc and copper within the same sample.

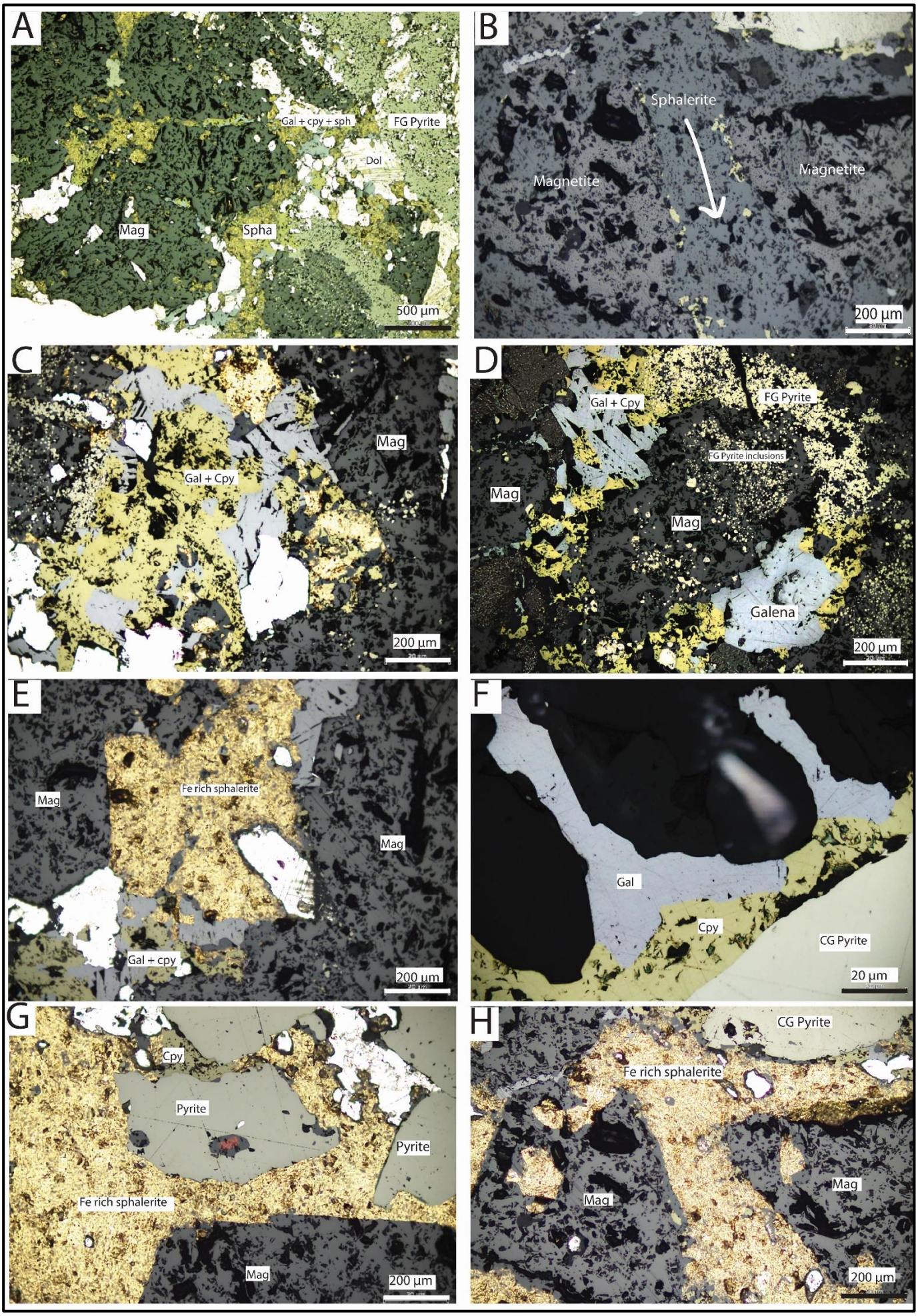

Figure 32: Petrographic images of magnetite and associated ore minerals. Iron-rich sphalerite occurs in high abundance surrounding magnetite, and included within coarse-grained pyrite. Chalcopyrite and galena occur with the same timing relationships. Magnetite and economic sulphides are observed to replace fine-grained pyrite and some dolomite.

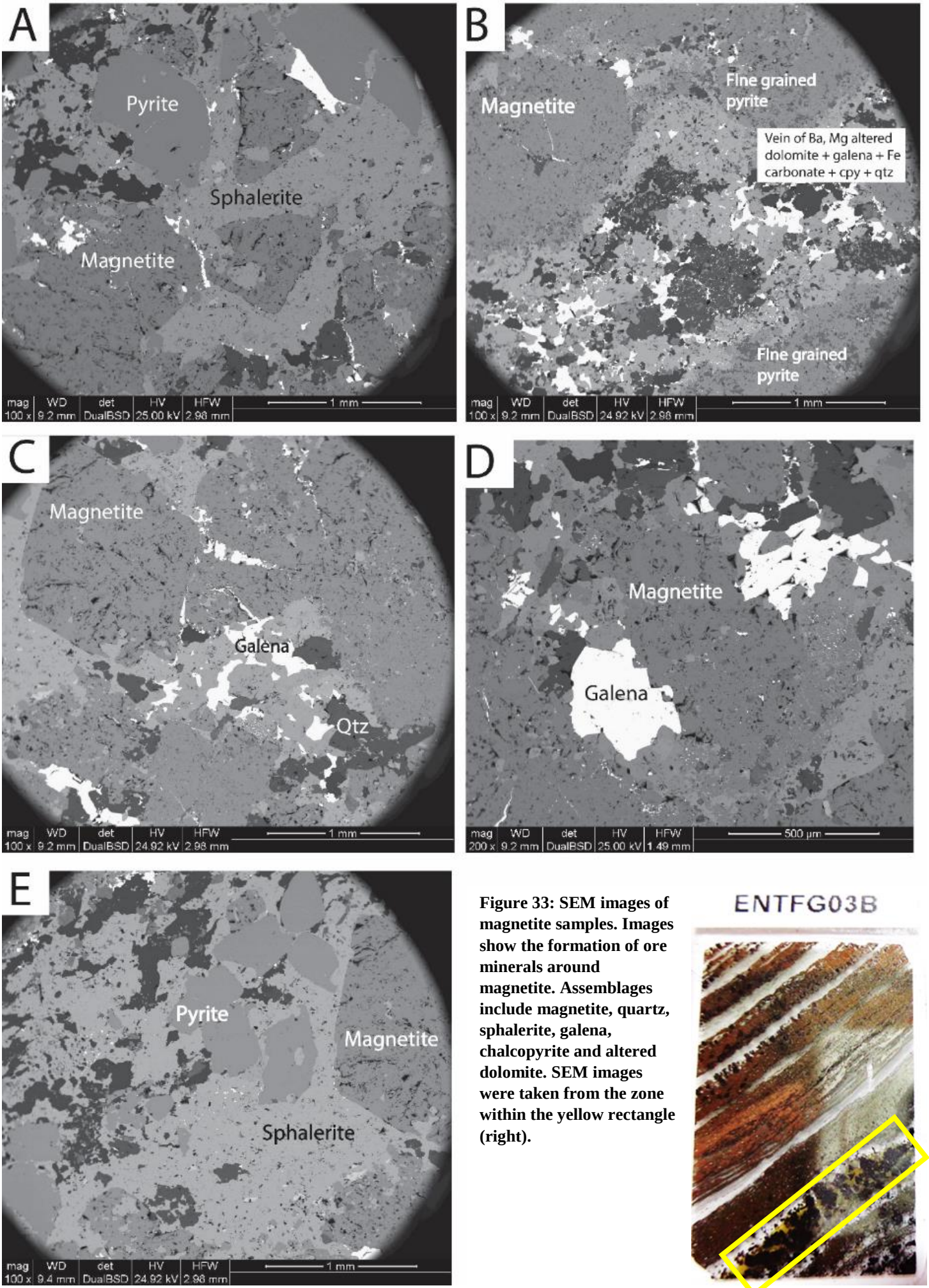

Figure 33: SEM images of magnetite samples. Images show the formation of ore minerals around magnetite. Assemblages include magnetite, quartz, sphalerite, galena, chalcopyrite and altered dolomite. SEM images were taken from the zone within the yellow rectangle (right).

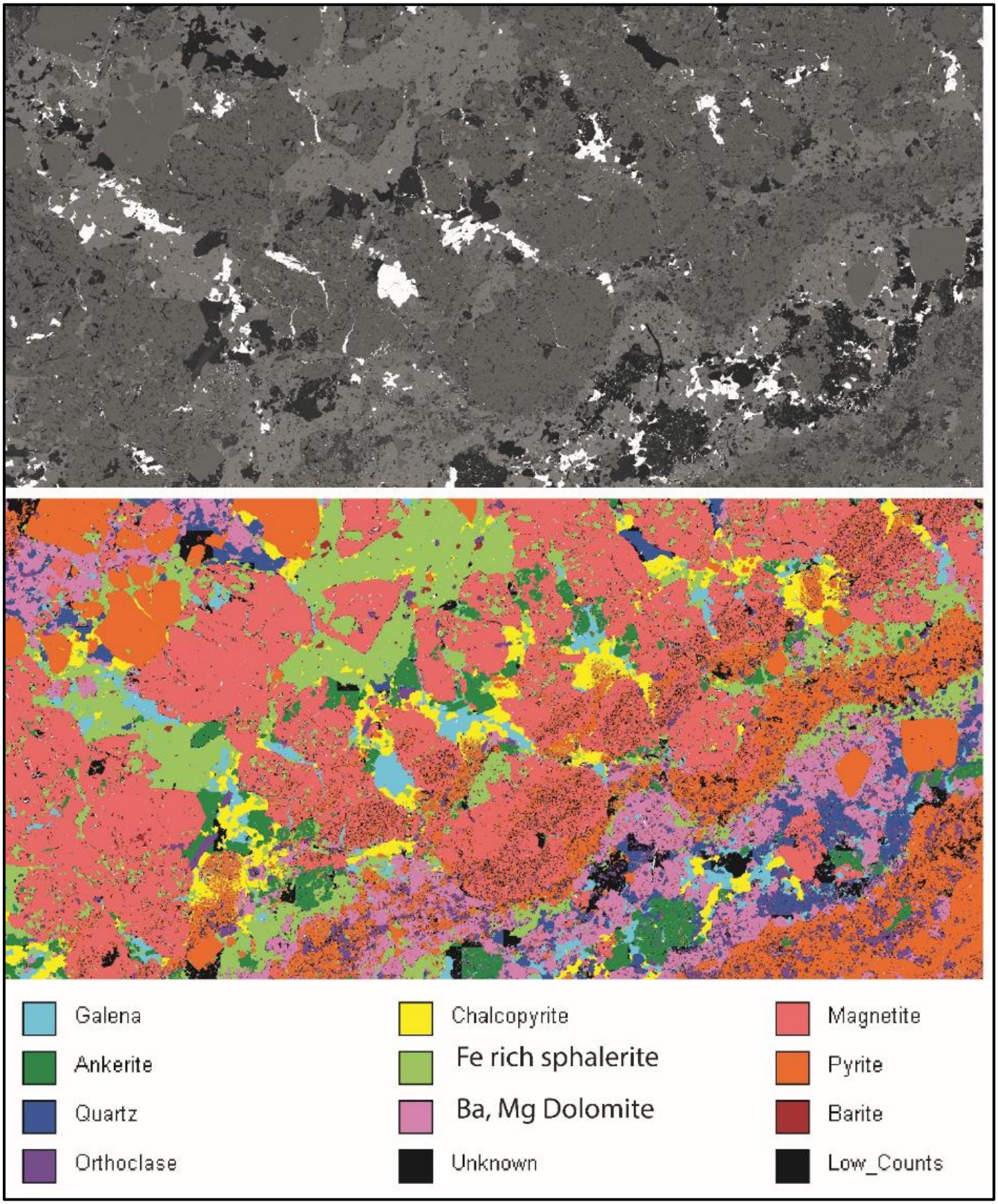

Figure 34: Mineral liberation analysis map of an ore zone within a magnetite sample, showing the formation of ore minerals around magnetite. Assemblages include magnetite, quartz, sphalerite, galena, chalcopyrite and dolomite. Sphalerite is dominant within the magnetite zone. Barium rich dolomite exists in an alteration vein (bottom right).

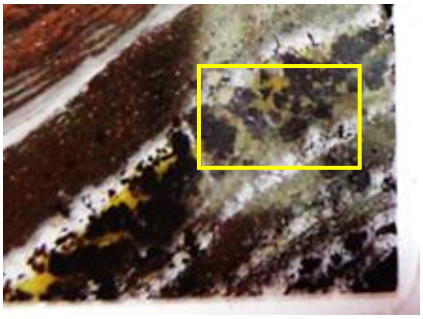

4.6 Leapfrog modelling

Leapfrog modelling tests whether fine-grained pyrite had any influence on the location of copper orebodies, brecciation or associated alteration halo. Modelling results are based on up-to-date drill-hole data, logged by Mount Isa geologists. All leapfrog cross sections produced from modelling are included as Appendix 2.

Distribution of Fine-grained Pyrite

On a deposit scale, modelling has confirmed that fine-grained pyrite is concentrated into several large bedding-parallel lobes, present from the current land surface towards the basement contact (Figure 35). It is evident that the pyrite lobes do cross-cut stratigraphy at various locations (particularly between 5230 mN and 5700mN). However, this could simply be due to folding or faulting, which is beyond the capabilities of leapfrog software. There is a general trend of increasing fine-grained pyrite abundance towards the NNW of the deposit. This is similar to the distribution of the copper orebodies and associated silica-dolomite alteration. There is a continuous lobe of highly concentrated fine-grained pyrite, extending from the 1100 orebody in the South, to lower Enterprise in the North, following the shape of the Basement Contact (Figure 35).

Relationship to alteration and ore

Fine-grained pyrite occurs within the same stratigraphic zones as high grade ore, consistent with Robertson (1982), and is particularly evident in the 1100 orebody (Figures 37-39). If fine-grained pyrite is modelled as veins (despite unrealistic geological shapes), it was evident that high grade ore, and siliceous breccia occurred between masses of fine-grained pyrite (Figures 36 and 42). The results show that large-scale brecciation and Cu deposition has taken place in areas with the lowest abundances of fine-grained pyrite. This is especially evident proximal to the 500 and 650 orebodies (Figures 45 and 46). Dolomitic and siliceous alteration appear to overlap with fine-grained pyrite. Rock containing high concentrations of fine-grained pyrite have not brecciated.

Within the Enterprise system, brecciated rock is located directly adjacent to fine-grained pyrite lobes, especially in the N3500 ore body. This ore body has a strong association with the Enterprise Footwall Fault, and the dense fine-grained pyrite lobe directly to the East. The Footwall Fault has formed between fine-grained pyrite and high grade copper ore. No copper ore is observed on the Eastern side of the Footwall Fault (Figures 41 and 44), consistent with results of Miller (2006).

On the deposit scale, modelling shows that copper-ore pathways are breccia controlled close to the basement contact, with bedding constrained pathways dominant distal to the contact. Bedding-parallel fluid pathways are often located at the contact between lobes of fine-grained pyrite and shale (Figures 39 and 43). This is consistent with petrography results indicating a fractal relationship on these apparent controls on mineralisation. High-grade copper and brecciated rock are consistently located directly adjacent to concentrated lobes of fine-grained pyrite (Figure 40).

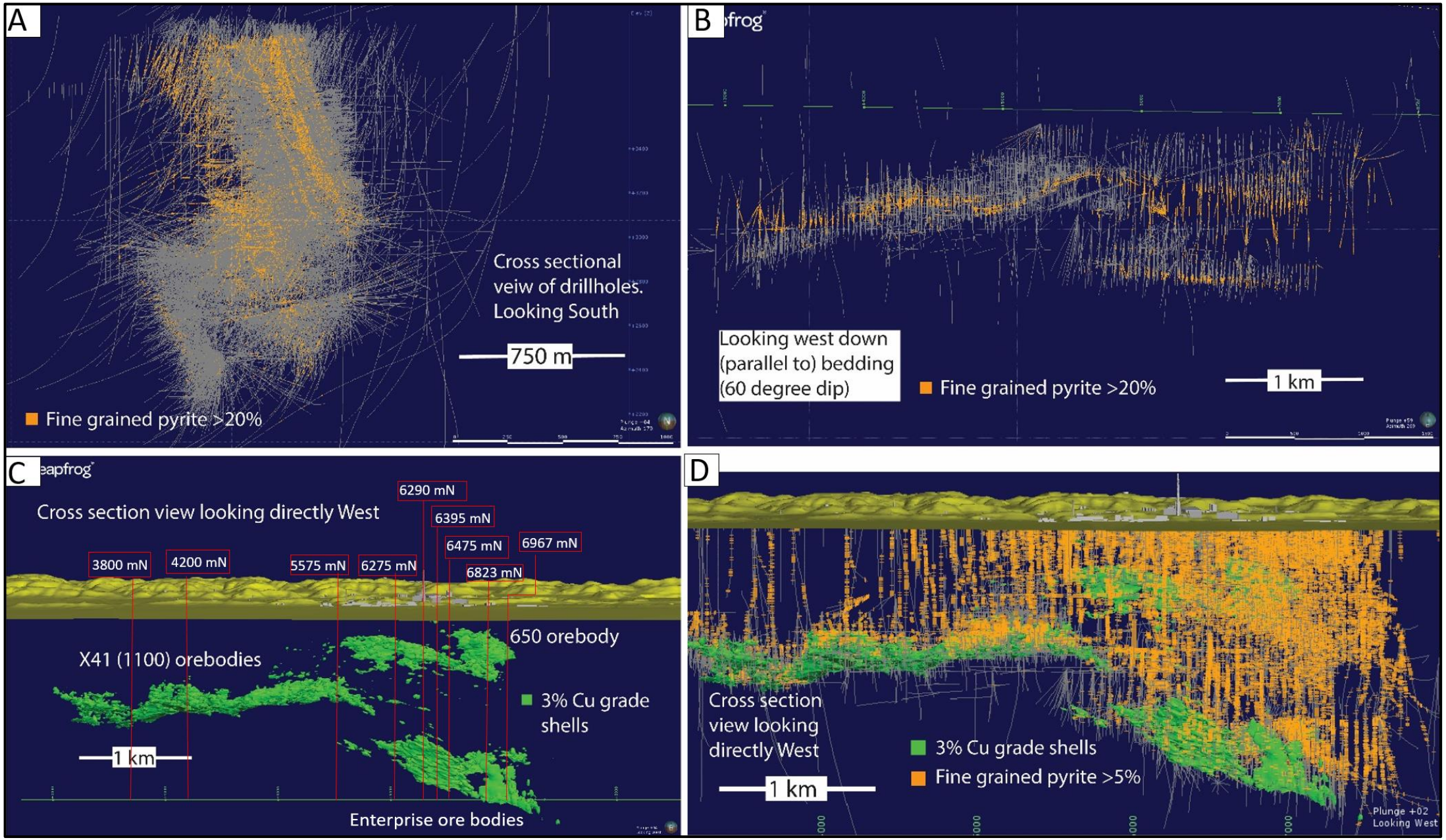

Figure 35: Leapfrog modelling images showing the structural distribution of fine-grained pyrite. Image A shows pyrite concentrated within bedding parallel lobes. Image B shows pyrite forming continuous lobes that extend the entire length of the deposit. Images C shows the location of copper orebodies relative to cross-sections included in this thesis (bottom-left). Image D shows the abundance of fine-grained pyrite in drill core relative to the copper orebodies (bottom-right).

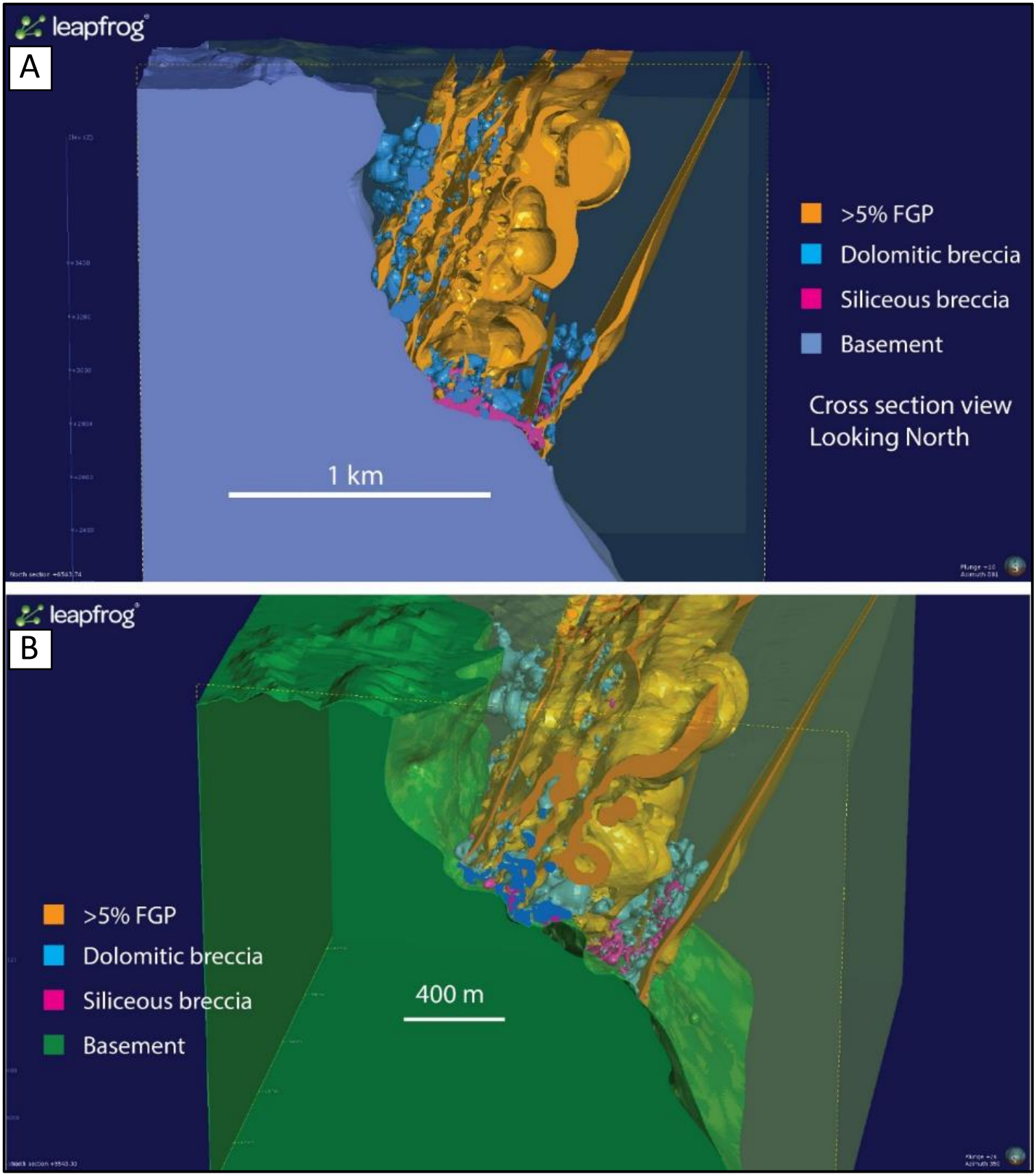

Figure 36: Simplistic conceptual model showing the distribution of fine-grained pyrite, and brecciated rock types. Pyrite was modelled as a vein system. Brecciated rock units occur between fine-grained pyrite lobes or in space where fine-grained pyrite does not occur in high concentrations.

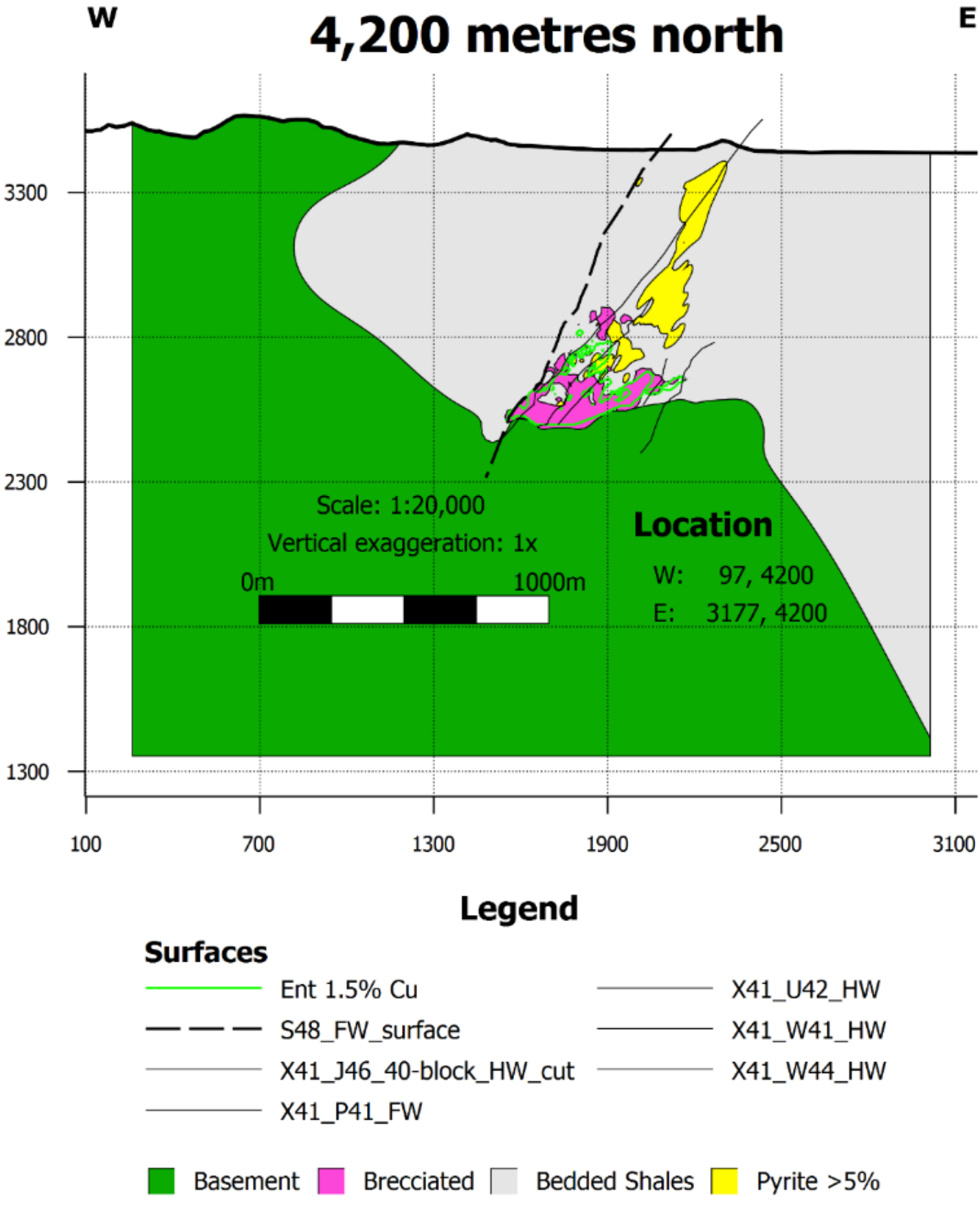

Figure 37: Leapfrog cross section of the Mount Isa deposit at 4200 Metres North. This image demonstrates the relationship between brecciated rock, copper ore, and fine-grained pyrite. Fine-grained pyrite and brecciated rock occur within the same stratigraphic interval, and have the same trend as major faults.

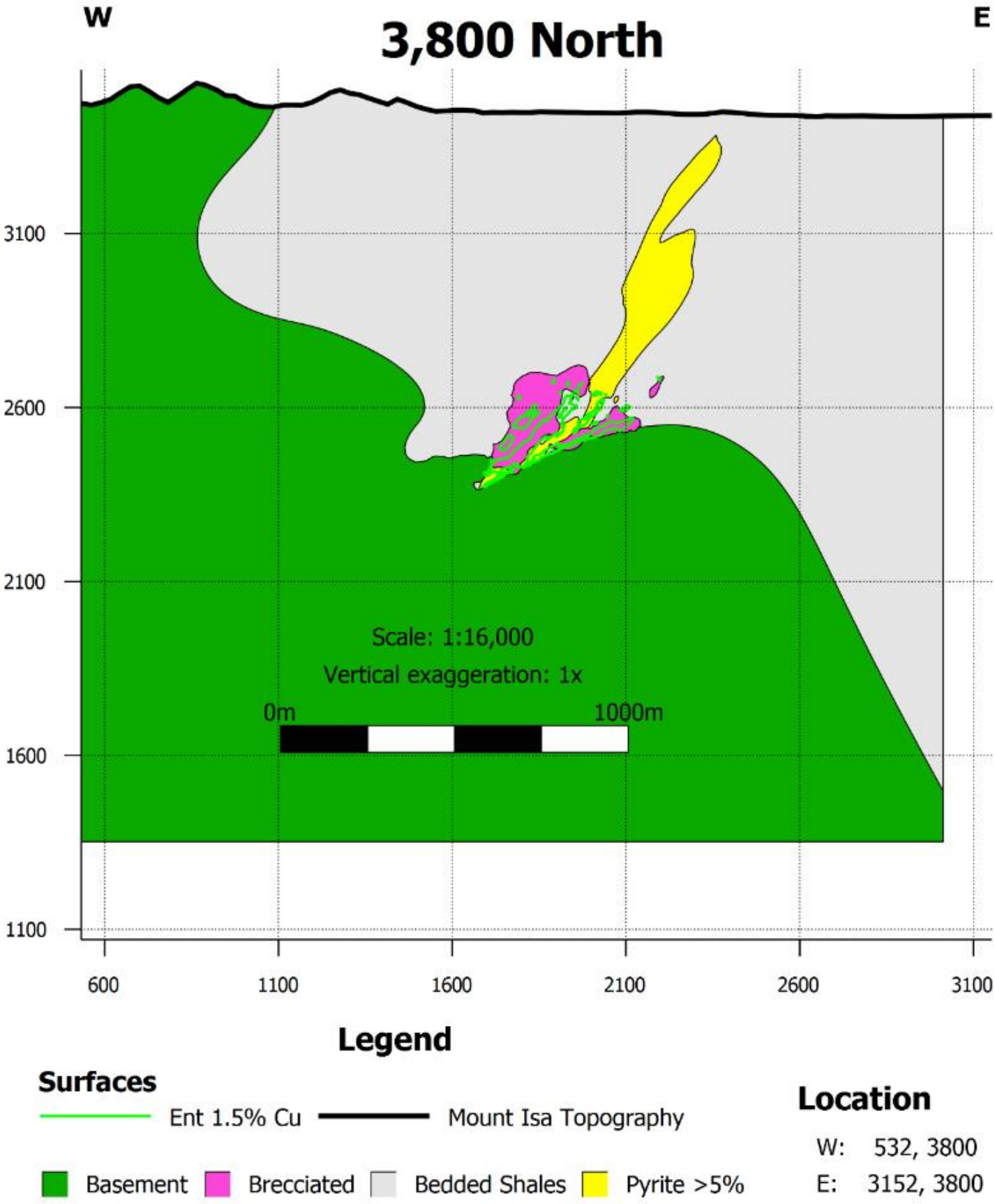

Figure 38: Cross section of the Mount Isa Deposit at 3800 metres north. This image demonstrates how fine-grained pyrite and copper ore both originate within the 'kink' in the Paroo Fault contact. Fine-grained pyrite and brecciated rock types often occur directly adjacent to each other but remain spatially distinct.

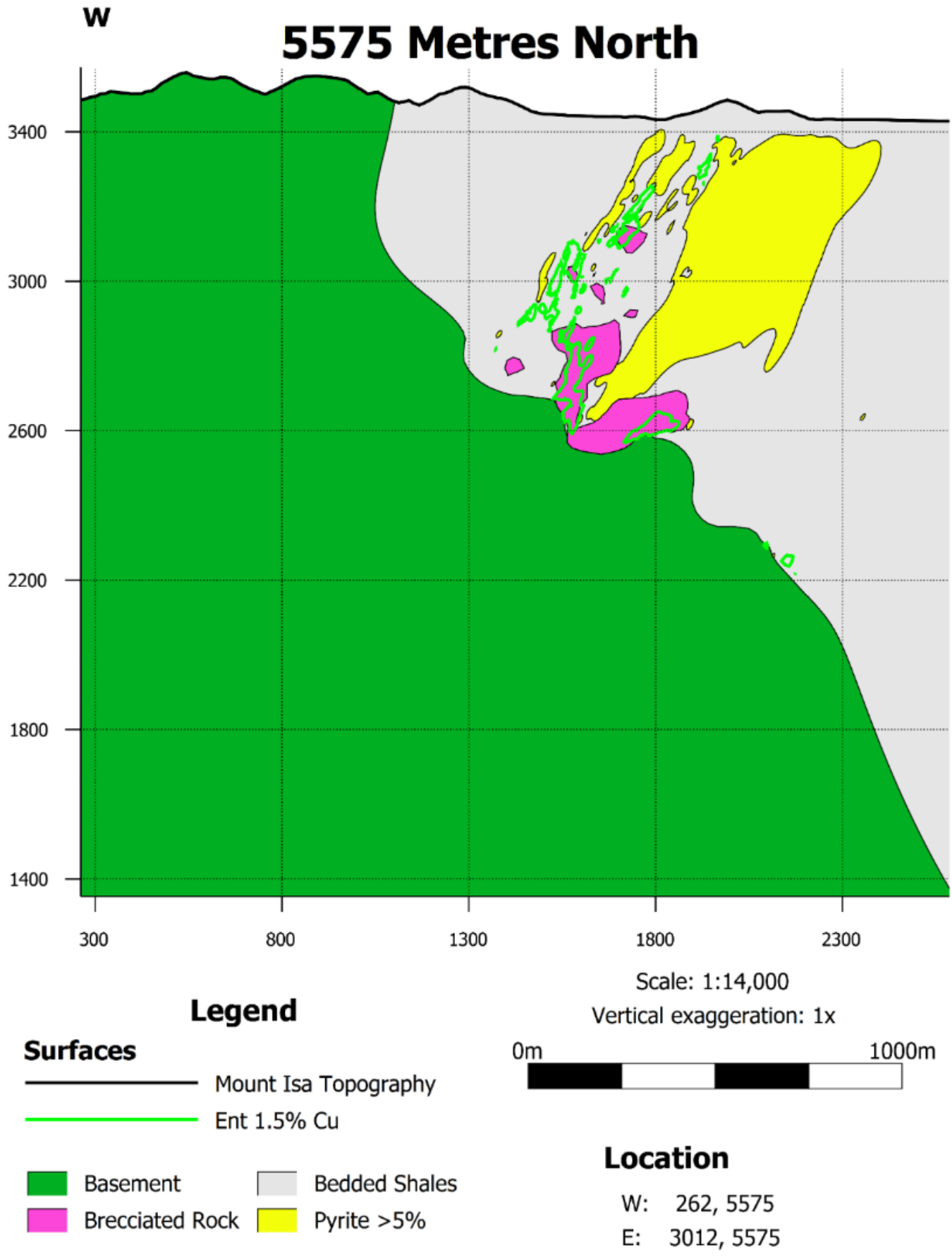

Figure 39: Leapfrog cross section of >5% fine-grained pyrite and brecciated rock at 5575 mN. The model shows the split style of the 1100 orebody. Brecciation wraps around the areas with abundant fine-grained pyrite.

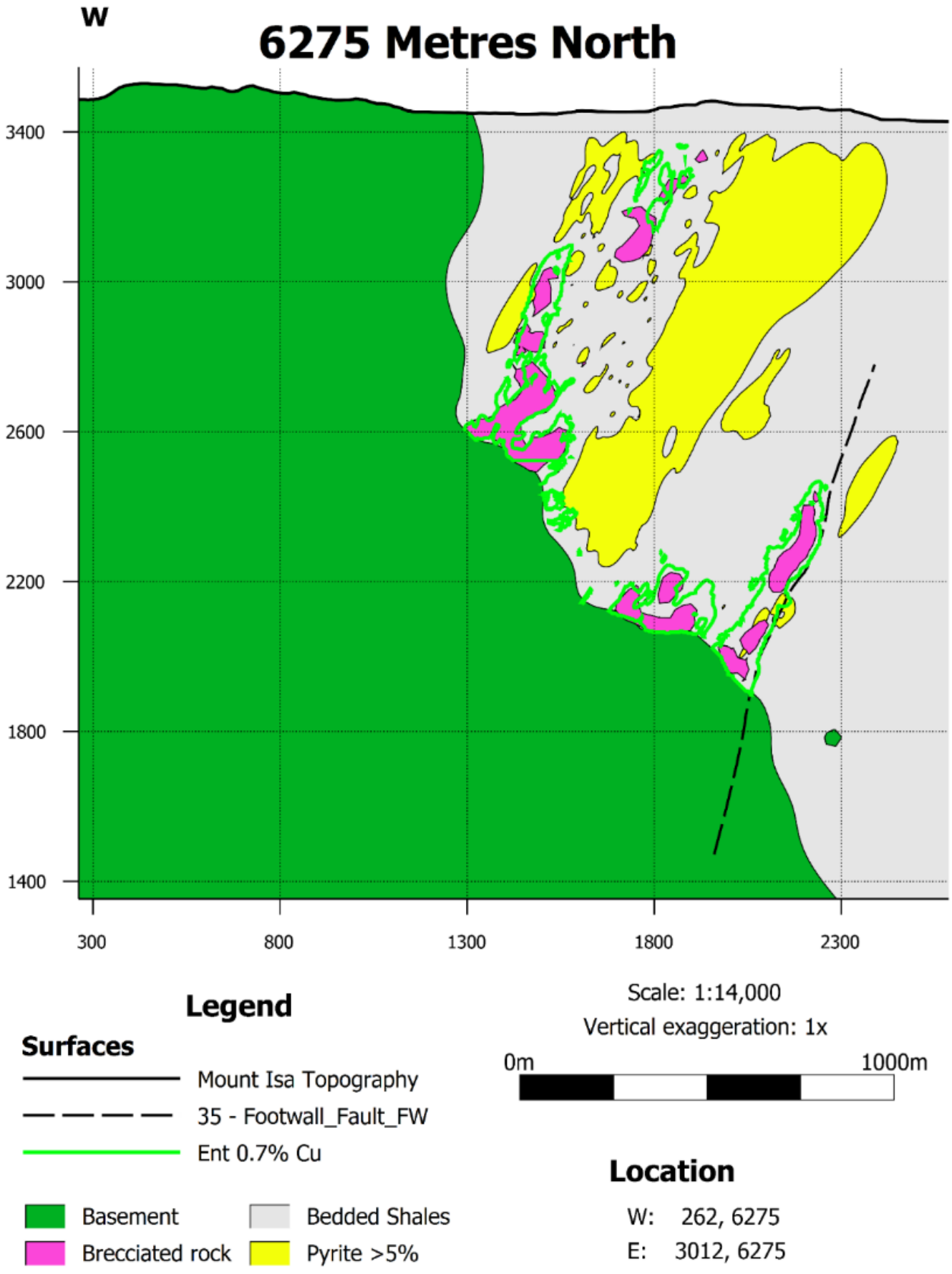

Figure 40: Leapfrog cross section of >5% pyrite and brecciated rock at 6275 metres north. This model shows the 650 and 500 orebodies (uppermost orebodies) occurring directly adjacent to fine-grained pyrite lobes.

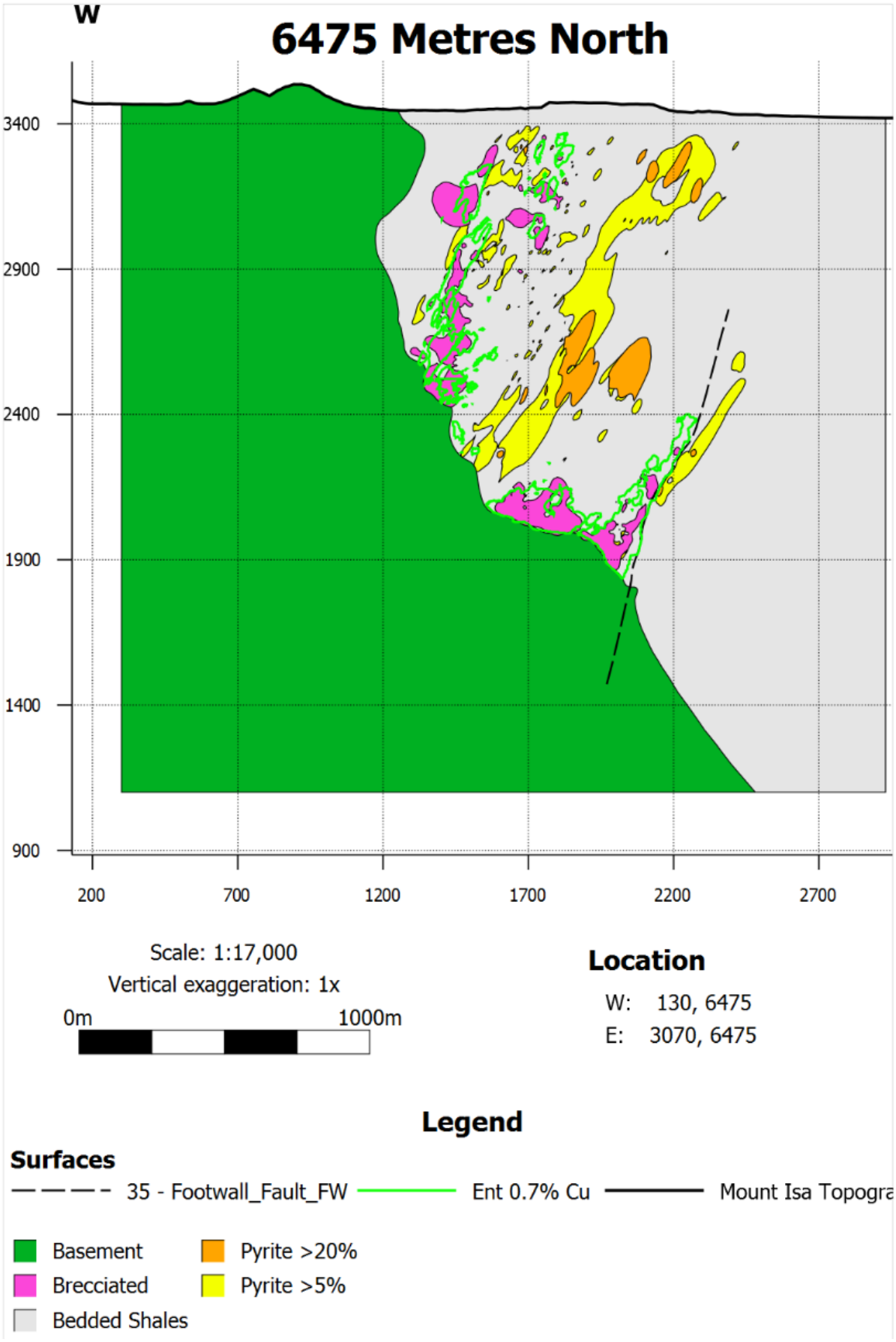

Figure 41: Leapfrog cross section at 6475 mN showing grade shells of >5% and >20 % fine-grained pyrite. The relationship between the 3500 orebody, footwall fault and lobe of fine-grained pyrite west of the footwall fault is well exemplified. High grade copper and fine-grained pyrite occur directly adjacent to each other, with the footwall fault occurring between these units.

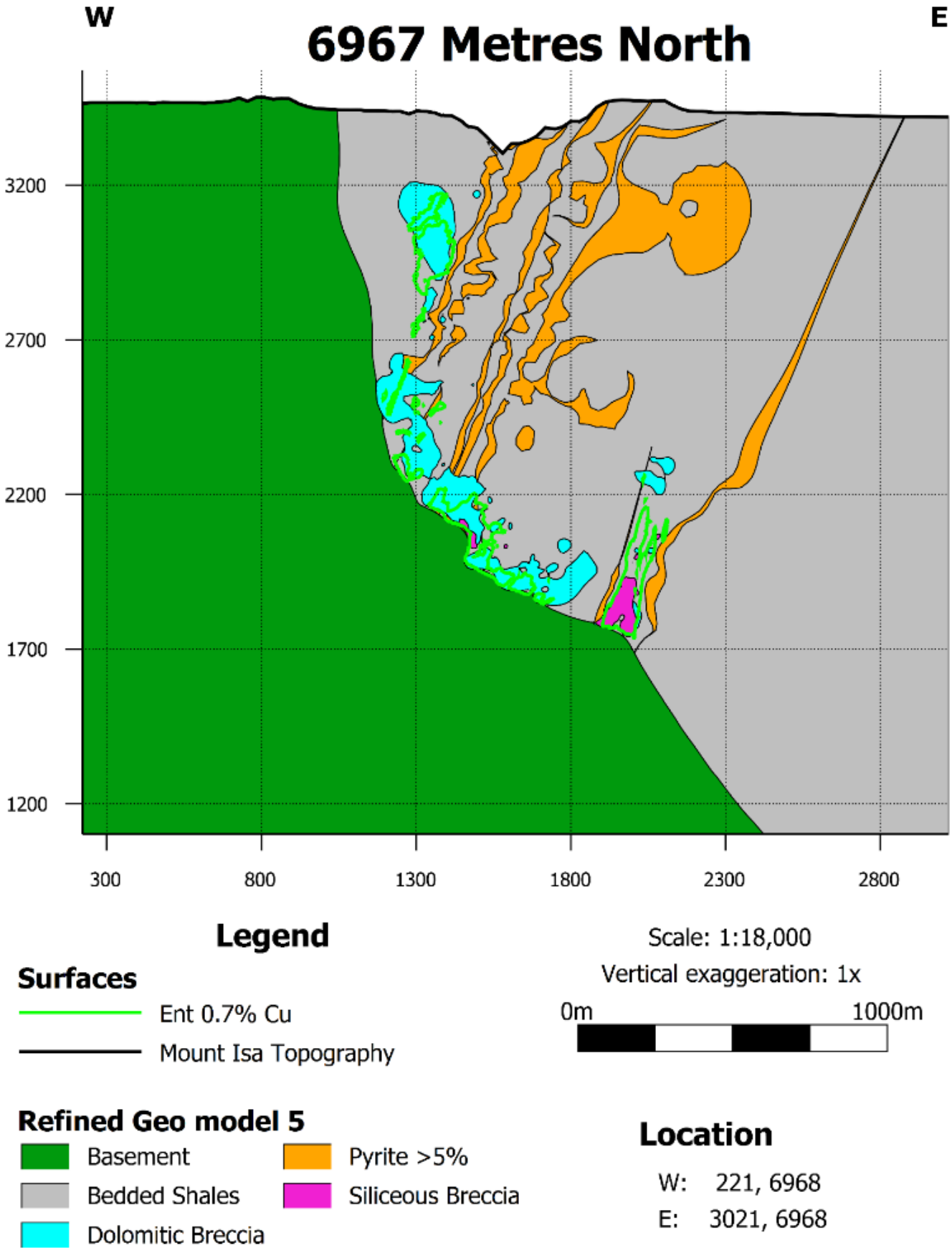

Figure 42: Leapfrog cross section at 6967 mN with pyritic shale (>5%) modelled as veins. Siliceous and dolomitic breccia's are also modelled. The main feature of this image is that it shows the high grade siliceous breccia of the 3500 orebody, occurring between two concentrated lobes of fine-grained pyrite

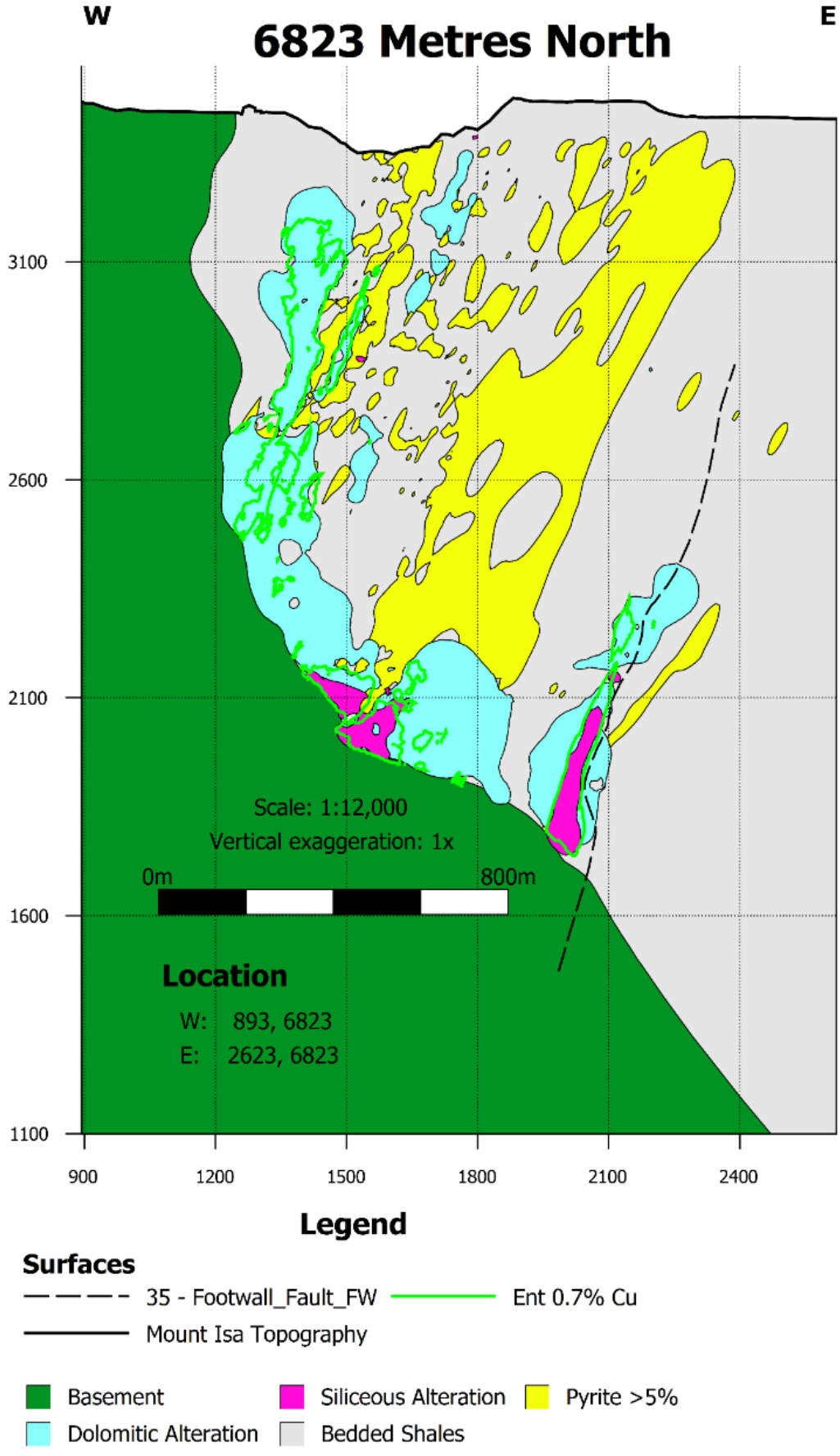

Figure 43: Leapfrog cross section at 6823 metres north. This model shows both the breccia and bedding control on ore and alteration pathways. Bedding parallel pathways are often between beds of fine-grained pyrite. Fine-grained pyrite also extends to the basement contact, adjacent to the high grade siliceous core.

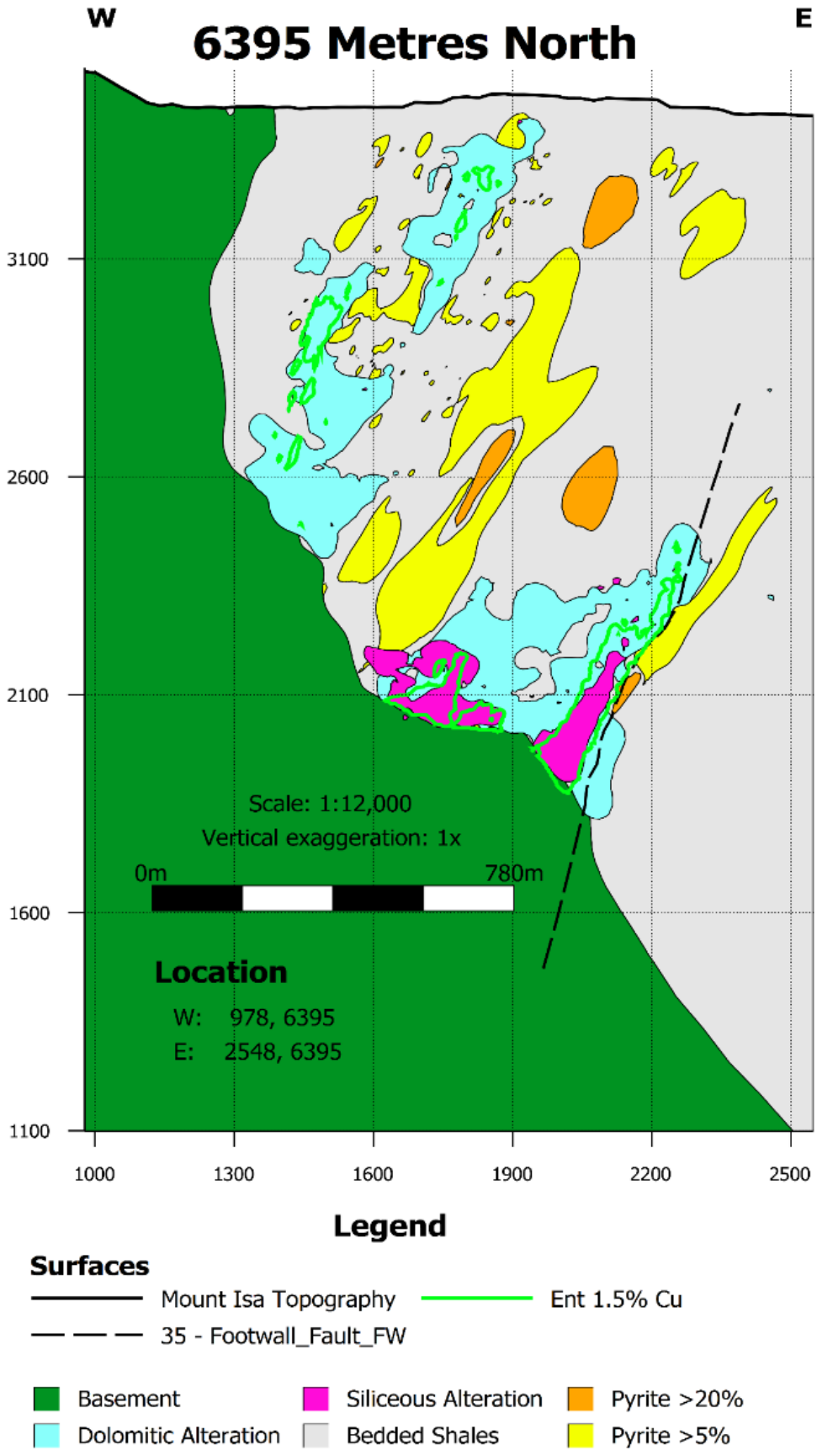

Figure 44: Leapfrog cross section at 6396 metres north. This model shows the relationship between high grade ore, and concentrated fine-grained pyrite in the footwall of the N3500 orebody. There is a sharp contrast between fine-grained pyrite and high grade ore, with the footwall fault forming directly between these units.

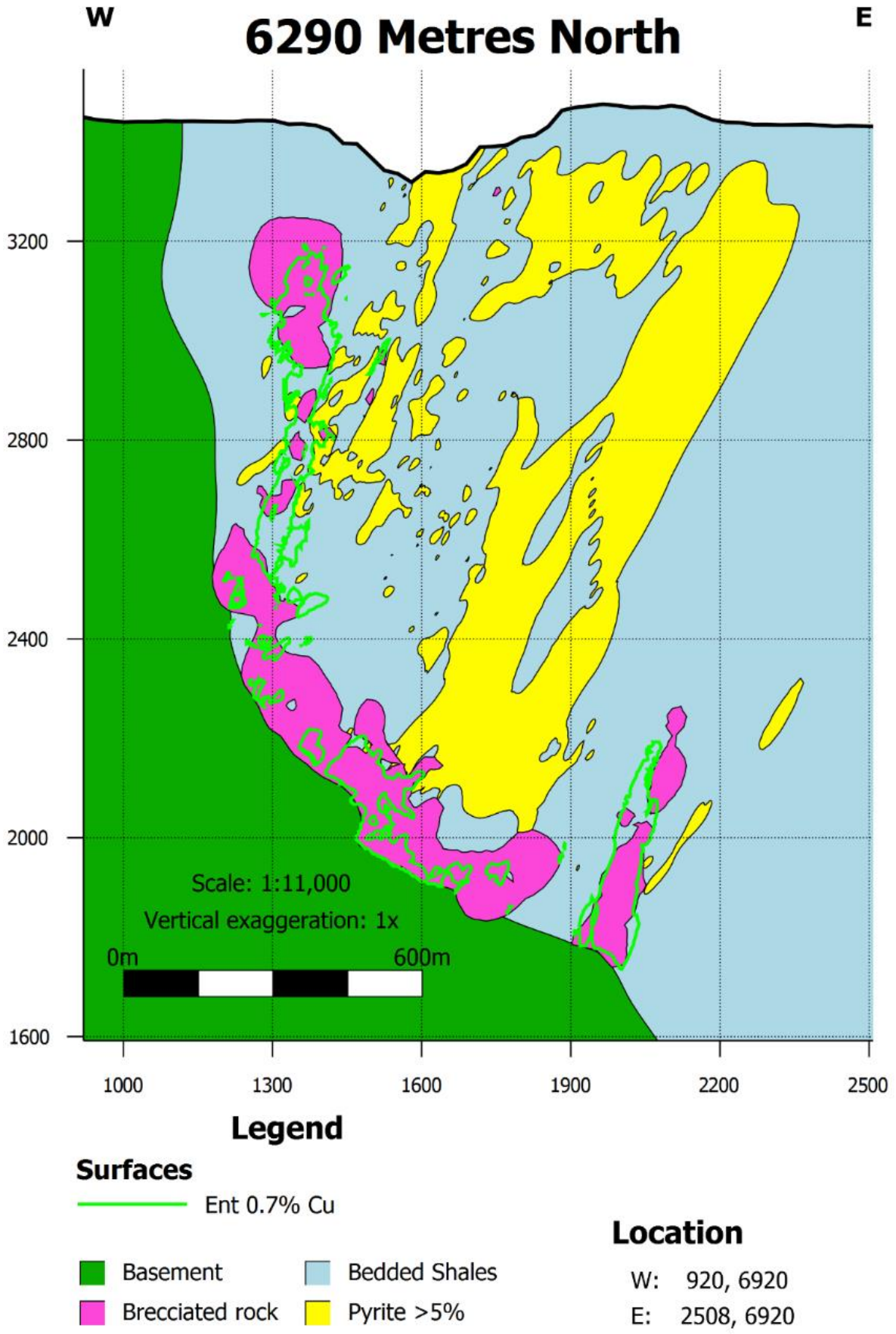

Figure 45: Leapfrog cross section of Mount Isa Mine at 6290 metres north. The image demonstrates fine-grained pyrite controlling the location of the 650 orebody (upper left). Changes in dip in the fine-grained pyrite lobe, are interpreted to create the pathway for the 650 and 500 orebodies. Brecciated pathways occur in-between fine-grained pyrite lobes. Chalcopyrite deposition occurred in the permeability created by this brecciation.

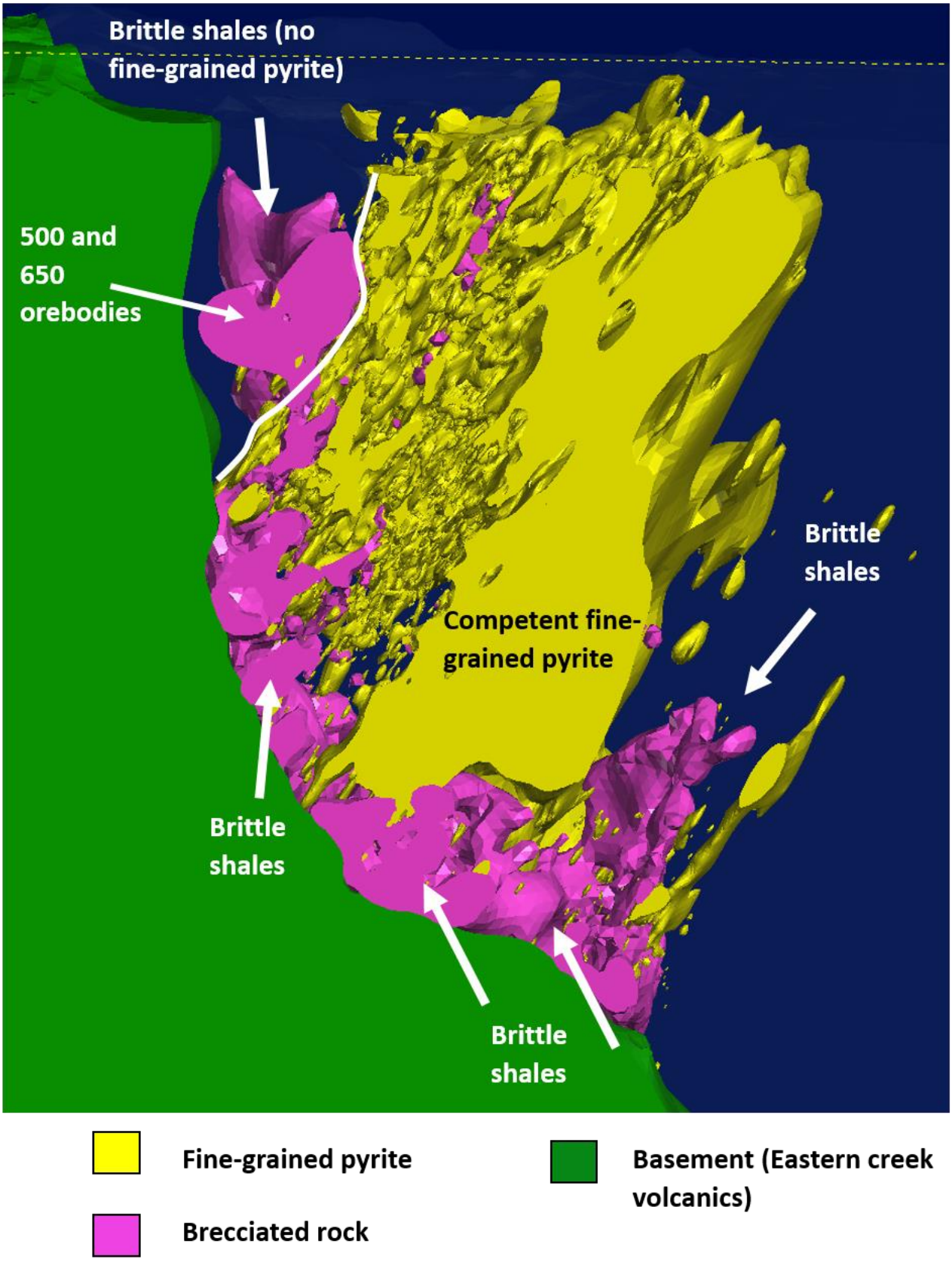

Figure 46: Leapfrog cross section demonstrating fine-grained pyrite controlling the location of the 650 orebody (upper left). Large-scale brecciation occurs where there are low concentrations of fine-grained pyrite. The shales accommodated stress by fracturing, generating permeability for Cu deposition.

5. Discussion

5.1 Fine-grained pyrite

Fine-grained pyrite has traditionally been considered as an early diagenetic mineral, with little relevance to the copper mineralisation. Authors have proposed pyritic shale as being the major sulphur source for chalcopyrite mineralisation (Robertson, 1982), or as acting as a reductant to precipitate Cu rich fluids (Wilde *et al.,* 2000; Heinrich *et al.,* 1993). However, its timing of formation relative to diagenesis, deformation events and deposition of base metals remains enigmatic. Painter *et al.,* (2003) argues that fine-grained pyrite formed through diagenetic, thermo-chemical sulphate reduction processes. He suggests sulphur sources originated from sulphate evaporate deposits and iron was sourced from ferroan dolomite. This interpretation relies on the assumption that there were high concentrations of readily available sulphur among the Urquhart shale sediments. This is consistent with Wilkin and Barnes (1997), who suggested bacterial sulphate reduction in organic/carbonaceous matter as a common method for fine-grained pyrite formation during diagenesis. Once formed, pyrite framboids can act as sites for secondary pyrite growth which can infill, or cause continued outward growth (Wilkin and Barnes, 1997).

Alternatively, Perkins (1998) suggested fine-grained pyrite formed through inorganic sulphate reduction within carbonaceous zones late in the deformation history. He suggested all sulphide mineralisation was a late stage hydrothermal system, concurrent with the D_3 deformation event. Grondis and Shouten, (1937), were also confident that their detailed petrology work provided evidence that the fine-grained pyrite mineralisation in Mount Isa occurred through replacement, concurrent with deformation. They stated fine-grained pyrite formed through the same mineralising agents, and through the same structural controls (shearing, faulting, crushing) responsible for the younger (economic) sulphides.

The observed atoll textures are consistent with the interpretation that some fine-grained pyrite did form through complex iron sulphide conversion processes, as opposed to hydrothermal activity. The timing of the true fine-grained framboidal pyrite is difficult to determine from presented data, however this thesis does present evidence for continuous growth of fine-grained pyrite over a spanned interval throughout deformation, rather than a single short-term event. Additionally, original fine-grained pyrite has been the focus for growth of paragenetically later hydrothermal-related pyrite during additional hydrothermal stages. Where fine-grained pyrite forms dense aggregations creating a massive crystalline appearance, the original pyrite grains can still be recognised because of different colour shades. Fine-grained pyrite also consistently displays growth zoning, showing that original fine-grained pyrite has acted as locations for further growth. It is interpreted that there has been continuous growth of fine-grained pyrite as iron and sulphur were introduced to the system. Subsequently, as base metals were introduced, base metal (Cu, Pb, Zn) sulphides became dominant.

Timing and structure

The primary structural control on the original fine-grained pyrite mineralisation is interpreted to be carbonaceous rich seams or laminae, with fine-grained pyrite overprinting this laminae (Perkins, 1997; Painter *et al* 2003). Painter *et al.*, (2003), suggests the S_3 cleavage overprints fine-grained pyrite, demonstrated by the absence of fine-grained pyrite within a strong structural foliation, but mineralised parallel to in the same sample. This places constraints on fine-grained pyrite as pre-D_3 and probably pre-D_2. Alternatively, Perkins suggests fine-grained pyrite post-dates folding within the mine, demonstrated by mineralisation of both the S_2 cleavage (parallel to bedding), and the S_3 cleavage (parallel to axial plane of folds), suggesting deposition during D_3. Others (Neudert, 1983;Wilkin and Barnes 1997), favour that all fine-grained pyrite formed during diagenetic processes.

From petrographic observations in the above works, the carbonaceous control on fine-grained pyrite is evident. As the carbonaceous laminae require significant burial to form, fine-grained pyrite mineralisation can be constrained to have occurred following laminae formation. The carbonaceous laminae are interpreted as forming parallel to a cleavage, which occurs both sub-parallel to bedding and parallel to the axial plane of folds. Evidence from petrography and hand sample observations has been presented, and confirmed that in some locations fine-grained pyrite has post-dated faulting and deformation. This is evident through fault fill, mineralisation of an S_3 cleavage parallel to the axial plane of folds, and overprinting of faults (see Appendix 3). The fine-grained pyrite that has mineralised parallel to bedding has the same textural characteristics as that which is mineralised parallel to cleavage suggesting they are the same generation of pyrite.

The above works provide evidence that pyrite has formed over a prolonged period, both prior to and during deformation. Paragenetically, fine-grained pyrite was introduced prior to silica/dolomite alteration and base-metal mineralisation. Brassy pyrite and Pyrite 2 have occurred as part of the base-metal mineralising system. Petrological and LA-ICP-MS data display evidence for the presence of economic sulphides within brassy pyrite mineralisation, which overprints fine-grained pyrite. LA-ICP-MS results are limited by the resolution of the spot analysis method of data collection.

Whether fine-grained pyrite formed during deep-burial diagenetic processes is beyond the scope of this project, however it is likely some pyrite did form during this time. Due to a lack of evidence for the dissolution of ferroan dolomite and large sulphur evaporate deposits, it is apparent that the majority formed in carbonaceous seams from an additional source of iron and sulphur. Consequently, on a deposit scale, deposition of fine-grained pyrite may have been controlled by similar structures that controlled the introduction of economic sulphide minerals. Based on in-depth observations of fault zones Miller (2006), suggested that copper mineralisation was a protracted process spanning both the D_2 & D_3 events of the Isan Orogeny, rather than a single brittle event, consistent with Long (2010). The contemporary interpretation that economic mineralisation can span over prolonged periods, rather than as a single instantaneous event, may also apply for the fine-grained pyrite mineralisation. Further study of the geochemical variation between pyrite species may provide additional evidence for this process.

Textural variety

Textural and geochemical evidence is consistent with the interpretation that brassy pyrite is related to the hydrothermal event which precipitated coarse-grained pyrite (Pyrite 2). Evidence for this interpretation is present as two main textural forms. Firstly, small euhedral hydrothermal crystals are present in specific zones, independent to fine-grained pyrite. Secondly, brassy pyrite overgrows and infills areas of fine-grained pyrite. Brassy pyrite also contains trace amounts of chalcopyrite, galena and sphalerite, which is consistent with the interpretation that the system has evolved with time and that economic sulphides became dominant late in the formation history. These observations are supported by LA-ICP-MS data, which show a distinct geo-chemical difference between fine-grained pyrite and brassy pyrite (see also Maguire, 2016).

Relationship to ore and alteration

In the rare cases where ore minerals are located within pyritic shales, fine-grained pyrite seems to act as a rheological inhibitor, localising alteration and ore veins. Fine-grained pyrite has a competent nature, displaying ductile behaviour under deformation, allowing space or traps to form for ore deposition. At high magnifications chalcopyrite commonly replaces and pseudo-morphs fine-grained pyrite grains, but the copper-ore system is dominantly contained within breccia zones. Hence, the majority of the copper observed in thin section is spatially discrete from fine-grained pyrite. Leapfrog modelling indicates that there was not enough fine-grained pyrite consumed to form the entirety of the very large copper orebodies. However the iron and sulphur may have been derived from the same source.

The spatial separation between the Cu and Pb-Zn deposits has historically been used as evidence to suggest the systems are unrelated. However, this is to be expected from an evolving fluid system. There should be a gradual change as low-grade Cu transitions into low-grade Pb-Zn. This thesis provides some evidence that pyritic shale samples contain low-grade Pb-Zn-Cu crystallised from the same fluid.

5.2 Timing of Magnetite Formation

Perkins (1997) proposed that magnetite occurred within a metasomatic replacement front, within a progressive alteration system, where magnetite was observed at variable locations forming a distribution parallel to the basement contact (Figure 46). However, the timing of magnetite growth in relation to other minerals was unclear at that time (Perkins, 1997). In this thesis paragenetic relationships of magnetite are complex, however based on observations a hypothesis is put forward.

Data from this study indicate that fine-grained pyrite was deposited first within carbonaceous rich seams within shale. At some stage, further growth of pyrite occured forming brassy pyrite. An iron-rich alteration system evolved from vein systems, utilising bedding parallel pathways, and overprinting both fine-grained pyrite events. The resulting assemblage includes siderite, ankerite, magnetite, Fe rich phyllosilicates (stilpnomelane, chlorite +- biotite) and also barium rich carbonate. Magnetite and stilpnomelane growth amongst pyritic shale, both replaced and included fine-grained pyrite grains. There is also evidence for replacement of dolomite. This formed strongly euhedral magnetite crystals, within areas of abundant fine-grained pyrite mineralisation. The magnetite, and other iron rich minerals, appear to have been introduced contemporaneously with the silica-dolomite alteration event, and prior to the introduction of economic base metals.

Relationship to ore minerals

It is interpreted that there has been additional magnetite growth during the deposition of economic metals. Sphalerite, galena and chalcopyrite are interpreted to have co-precipitated from the same fluid indicated by assay results of magnetite samples (Table 2), and confirmed through the use of petrography and MLA. Sphalerite displays the earliest paragenetic timing, while chalcopyrite and galena display concurrent relationships. It is interpreted that magnetite may act as a reductant in the Mount Isa system, facilitating the co-precipitation of base-metal sulphides.

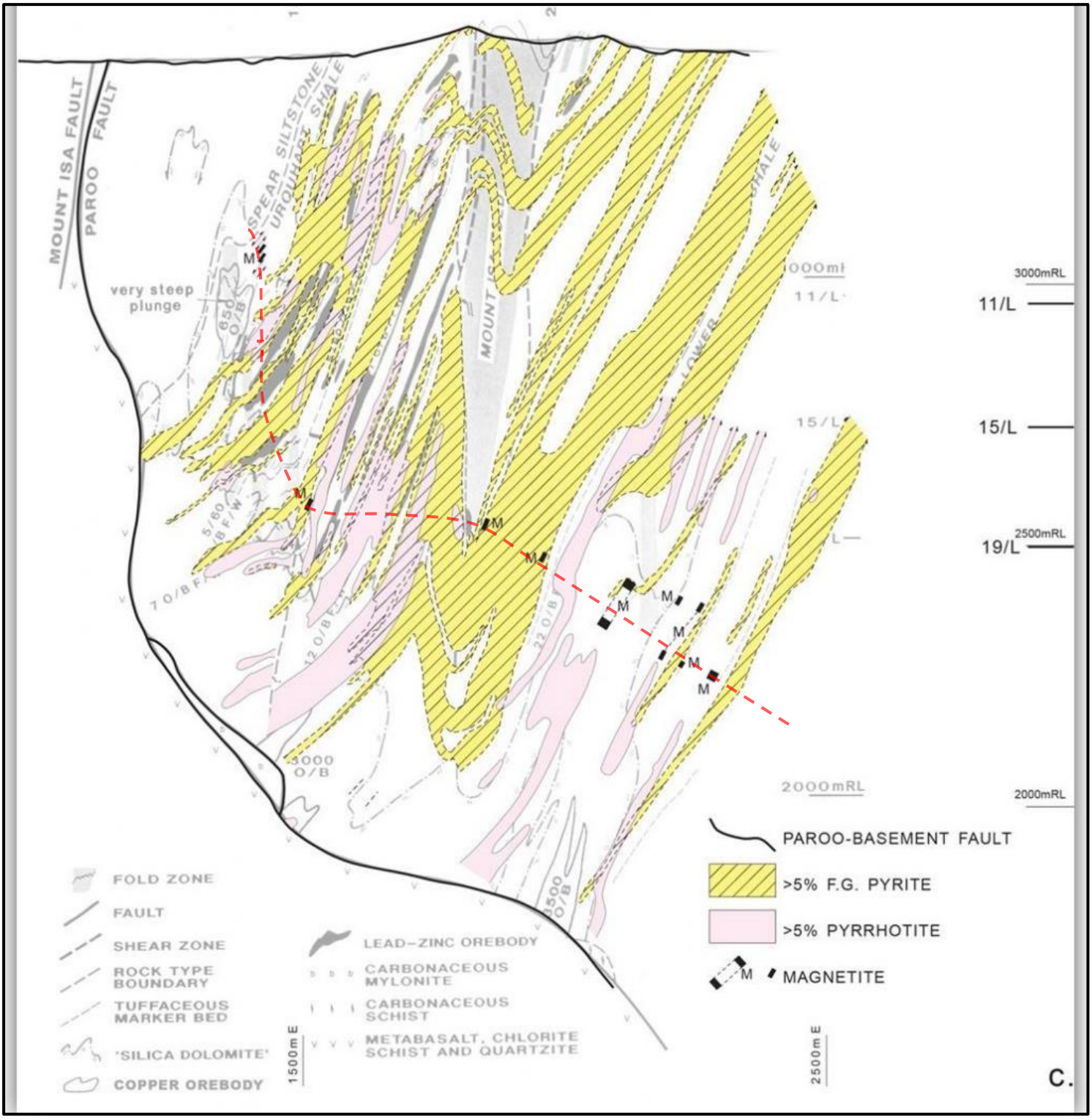

Figure 47: Figure adapted from Perkins (1997) (page 82), showing known locations of magnetite mineralisation. The locations occur in a zone parallel to the basement contact, suggesting it may be part of an alteration front.

5.3 Leapfrog Modelling

Distribution

Modelling results demonstrate that fine-grained pyrite is strongly concentrated within deposit-scale, bedding-parallel zones (consistent with bedding on the micro-scale). This is consistent with the interpretation that fine-grained pyrite precipitation has been influenced by large-scale carbonaceous rich zones within the Urquhart shale, which were originally controlled by sedimentary depositional processes. The X41 orebody has a single distinct lobe of fine-grained pyrite mineralisation. Associated with this is a single distinct copper orebody (1100). Within the Enterprise system (after 4800mN), there are several substantial pyrite lobes distinguishable. Consequently, there are also multiple copper orebodies (3000, 3500, 500/650) within this system. This provides initial indications for a link between fine-grained pyrite and copper ore deposition.

Relationship to ore and alteration

It is observed that the distribution of fine-grained pyrite and copper ore show a correlatable relationship. In the 1100 orebody, fine-grained pyrite occurs in similar stratigraphic locations to copper ore. Robertson (1982), uses this observation to argue that the consumption of fine-grained pyrite resulted in the formation of chalcopyrite ore. This study does not provide evidence to suggest that enough pyrite was consumed to form the orebodies of the Enterprise system.

Pyrite is also shown to consistently originate within the ‘kink’ in the Paroo Fault, similar to the copper mineralisation (Figure 41), providing evidence that the pyrite distribution may have been controlled by the same structures as the copper mineralisation. In the Enterprise system, major pyrite lobes extend from near the surface to the Paroo Fault basement contact. Here, copper ore and pyrite remain spatially distinct from each other, with copper ore occurring directly adjacent to lobes of fine-grained pyrite.

In the 1100 orebody, fine-grained pyrite only exists surrounding brecciated rock and copper ore, with no pyrite modelled elsewhere. Further North, the 500 and 650 orebodies are located closer to the surface, and are coincidentally surrounded by significant fine-grained pyrite lobes. A major lobe of pyrite is directly adjacent to the 3000 orebody, with the same applying for the N3500 orebody on the footwall side (Figure 43 and 44). This work is consistent with that of Waring (1990) who noticed a major lobe separating the 1100 orebody from the 1900 orebody. It is interpreted that the location of pyritic shales had a significant role in structurally controlling the deposition of the copper ore bodies. An explanation for this to take place is that slip (movement) became focussed on the margins between fine-grained pyrite and shale, and that maximum dilation occurred in these areas during shearing (consistent with Keys, 2007).

The overlap between dolomitic/siliceous alteration and fine-grained pyrite implies that on the macro-scale, fine-grained pyrite had little influence on the extent, and progression of silica/dolomite alteration within bedded rock units. However, fine-grained pyrite is interpreted to have a significant influence on the location of brecciation (brittle failure). This consequently controlled the generation of permeability and hence the location for deposition of high-grade ore. Permeability also controlled bedding-parallel alteration pathways, explaining why some alteration is confined by fine-grained pyrite lobes (Figure 43).

Control on orebody style

Both the 1100 and 3000 orebodies display a split ore body style (Figures 40 and 42). This may be due to the large fine-grained pyrite lobe that is present through the middle of the ore deposit. Elsewhere, the 3000 and 3500 orebodies form adjacent to the major fine-grained pyrite lobes, rather than in similar stratigraphic zones (Figure 43).

This is interpreted as fine-grained pyrite acting as a rheological inhibitor, influencing the location of brecciation. The 3500 ore body is seen to continue to high elevations from the

basement contact, in a thin zone of high-grade ore. Directly to the East of the 3500 orebody, there is a lobe of concentrated (>20%) fine-grained pyrite. The major footwall fault forms directly between this pyrite lobe and the 3500 copper orebody. The fault may have originated because of the anisotropic contrast between shale, and fine-grained pyrite bearing shales (Figures 44, 47). Results from Miller (2006) confirmed the fault to be a likely fluid conduit resulting in the N3500 orebody. Both the Footwall Fault and the fine-grained pyrite lobe on the eastern side of the fault may have acted as a barrier to mineralisation and contributed to the unusual up-dip extent and high ore grade of the 3500 orebody.

Summary

The distribution of brecciation, and consequently copper ore were influenced by the locations of pre-ore fine-grained pyrite mineralisation. Fine-grained pyrite appears to have been a significant rheological factor in the localisation of high-grade Cu ore. This rheological behaviour is observed on the micro to macro-scale (fractal relationship). Observations suggest Cu ore did not form from consumption of fine-grained pyrite. Instead, both stages of mineralisation are interrelated, and may share a common fluid source and structural control mechanisms. Evidence for these interpretations is based on the following.

- Brecciation ‘wrapping around’ fine-grained pyrite.
- Copper ore and fine-grained pyrite both appear to originate from the ‘kink’ in the Paroo Fault implying a common structural control on formation.
- Bedding controls on Cu fluid pathways are observed to be influenced by the presence of fine-grained pyrite.
- The proximity of fine-grained pyrite to high grade ore (implying a structural control).
- Fine-grained pyrite exhibits a control on orebody style and extent including the perched 500/650 orebodies, the up-dip extent of 3500 orebody, and the split 1100 orebody (after Keys 2007).
- Location of brecciation (areas of brittle shale, as opposed to relatively competent fine-grained pyrite). Especially applicable to the 500 and 650 orebodies.
- Alteration pathways often confined by fine-grained pyrite lobes.

5.4 Reactive ground

Background information, methodology, results and detailed discussion for reactive ground testing can be found in the technical report included in Appendix 6. Full results for reactive ground testing can be found in Appendix 7.

Coupled with the base of moderate leaching zone (BOML), fine-grained pyrite concentration has been used as an indicator for reactive ground risk within the Mount Isa Mine. The hypothesis for reactive ground testing was that fine-grained pyrite concentration was directly related to the reactivity of a rock mass.

Results found that using the Mount Isa Mines testing procedure, there was no statistical relationship between iron sulphide concentration and reactivity to ammonium nitrate. The same range of reactivity temperatures were observed throughout highly variable iron or sulphur concentrations (Figure 8, Appendix 7). Additionally, samples with >50% fine-grained pyrite did not produce any reaction. Out of 63 samples containing variable fine-grained pyrite concentrations, only 5 samples (estimated to have less than 10% fine-grained pyrite) were reactive (Table 1, Appendix 7).

The reactive ground data is consistent with the interpretation that reactive ground risk is a location specific phenomenon and is not directly related to the abundance of fine-grained pyrite in the local area. Iron-sulphide mineralogy is known to be a primary ingredient (Kennedy and Tyson, 2001), but the concentration of fine-grained pyrite in the rock does not seem to increase the likelihood of reactive ground. There is some evidence to suggest carbonate minerals may counteract the reactivity of the rock mass, but this was outside the scope for this thesis (for results relating trace element geochemistry to reactive ground, see Appendix 9). Factors that may also influence ground reactivity include (but not limited to); rock within the BOML, the presence of sulphate reducing bacteria, lithology and other chemical factors effecting the weathering of sulphides.

6. Conclusions

- There is evidence for a prolonged period of fine-grained pyrite deposition. (Hypothesis 1).
- Fine-grained pyrite pre-dates the deposition of brassy pyrite and Pyrite 2.
- 'Brassy pyrite' is a finer grained equivalent of Pyrite 2 and forms as coarse hydrothermal euhedral crystals, or as overgrowths of fine-grained pyrite (Pyrite 1). (Hypothesis 2).
- All pyrite species pre-date the introduction of the economic sulphides.
- The carbonaceous fine-grained pyrite has influenced the location of economic sulphide deposition through acting as an inhibitor of hydrothermal fluids.
- The presence of fine-grained pyrite affects the rheological behaviour of rock during deformation.
- The majority of copper ore did not form from consumption of fine-grained pyrite,
- The majority of fine-grained pyrite was deposited within the same overall mineralising system as economic sulphides.
- The hydrothermal system evolved with time such that economic sulphides became dominant after formation of fine-grained pyrite. (Hypothesis 1).
- Chalcopyrite, galena and sphalerite are observed replacing and inter-growing amongst fine-grained pyrite.
- Magnetite is associated with iron-rich phylllosilicates and ferroan dolomite, and appears to form an iron-rich alteration front sub-parallel to the basement contact.
- Magnetite is paragenetically earlier than the economic sulphide minerals.
- In locations where magnetite, sphalerite, galena, and fine-grained pyrite interact, magnetite, sphalerite and chalcopyrite replace fine-grained pyrite. However, these minerals do not appear to require the presence of fine-grained pyrite to form.
- The distribution of fine-grained pyrite appears to be controlled by similar structures to those that controlled later base-metal mineralisation.

- Fine-grained pyrite influenced the location of copper orebodies and had a structural role in localising deformation to specific areas resulting in high grade ore. (Hypothesis 3).
- Rheological differences, which often result from the presence of fine-grained pyrite, were important factors in the formation of the Mount Isa deposit.
- All sulphide mineralisation is synchronous over the Isan orogeny deformation periods, and are part of a related mineralising system controlled by similar structures including the Paroo fault, bedding parallel shear and cleavage.
- The concentration of fine-grained pyrite is not a significant factor in assessing the risk of reactive ground. (Hypothesis 4).

7. Recommendations for further study

Despite progress made in constraining the complex relationships of the pyrite mineralisation at Mount Isa, additional study and geochemical analysis are recommended in order to further understand the significance of fine-grained pyrite and its role in the formation of the deposit. Fine-grained pyrite within other mineral systems in the Mount Isa Inlier and surrounds (McArthur River, Hilton-George Fisher, Century and Lady Loretta) should be cross-examined to further constrain the formation of fine-grained pyrite, and ascertain whether there is a regional relationship between fine-grained pyrite and economic mineral deposits.

Further in-depth petrographic studies of pyritic shales are recommended to fully constrain the timing of fine-grained mineralisation relative to deformation events. Additionally, further in-depth petrographic studies of shale in areas within the transition zone from Cu mineralisation to Pb-Zn, may help confirm the relationship between lead-zinc and copper ore formation.

In order to fully comprehend reactive ground at Mount Isa Mines, further work in correlating known reactive ground locations to existing data such as lithological rock types, distance from the leaching zone and the assessment of the presence of bacteria is required. It is also recommended that the validity of the Mount Isa Mines reactive ground testing method is reviewed to assure it accurately replicates underground chemical processes and reactions. This is particularly true if the control on reactivity is found to be other contributing factors.

8. Acknowledgements

My supervisor Dr Richard Lilly for his academic advice and support for the entire year. His dedication to his work and passion for economic geology has kept me inspired in this field.

The Mount Isa Copper Operations technical services geology department for all their help and support during my vacation placement, and throughout this project. Special thanks to Daniel Taylor for his much needed advice and mentoring throughout this year and for finding time to help with the project.

Michael Fuss, Patricia Ila'ava, Lee Hutchins and Rhonda O'Sullivan who have also sacrificed much of their time to help me in this project.

Acknowledgements to Mount Isa Mines, and MICO for the use of the geological data base for modelling purposes including diamond drill-hole data and resource data.

Mount Isa Mines for providing funding to undertake research in this area of study. Funding covered research equipment costs, fieldwork costs and generation of thin sections.

The staff at Adelaide Microscopy for their time and effort in training myself on equipment, and for providing general advice.

To my family for their encouragement, support and helping me to relax throughout the year. Especially Mum, Dad and siblings.

Fellow honours students that are part of the A.W.E.S.O.M.E.S research unit at the University of Adelaide. They have been a big support, and have provided advice throughout the year.

Glencore scholarship program which has provided much needed economic support and funding for activities relating to my studies this year. Without this, studying honours in 2016 would not have been possible.

9. References

AEISG (Australian Explosives industry and Safety Group), 2012, 'Code of practice: Elevated temperature and reactive ground', Edition 3

BELL, TH, PERKINS, WG, SWAGER, CP (1988),'Structural controls on the development and localisation of syntectonic copper mineralisation at Mount Isa, Queensland', *Economic Geology*, Vol. 83, pp. 69-85

BELLAIRS, P (1997), 'Explosive ground reactivity indicators and strategies to overcome this phenomenon', International society of explosives engineers, MSc, Dyno Wesfarmers, Singleton Australia

BETTS, PG & LISTER, GS (2002), Geo-dynamically indicated targeting strategy for shale-hosted massive sulfide Pb–Zn–Ag mineralisation in the Western Fold Belt, Mt Isa terrane, Australian Journal of Earth Sciences, 49:6, 985-1010

BLAKE, DH, ETHERIDGE, MA, PAGE, RW, STEWART, AJ, WILLIAMS, PR, WYBORN, LA (1990), 'Mount Isa Inlier – Regional geology and mineralisation',*Geology of the mineral deposits of Australia and Papua New Guinea*, pp. 915-925

BULLOCK, N (2001),'Trace element geochemistry of sulphide phases: Copper mineralisation in the 3000- orebody at Mount Isa, Honours Thesis (Unpublished)

BULLOCK, N (2009), 'An overview of the Mount Isa Copper Mine', Presentation by MICO geology (unpublished)

CONAGHAN, EL, HANNAN, KW, TOLMAN, J (2003),'Mount Isa Cu and Pb-Zn-Ag deposits, NW Queensland Australia', *CRC LEME,*

GESSNER, K, JONES, PA, WILDE, AR, KUHN, M (2006), 'Significance of strain localization and fracturing in relation to hydrothermal mineralization at Mount Isa, Australia', *Journal of Geochemical Exploration* Vol. 89, pp. 129–132

GRONDIJS, HF & SCHOUTEN, C (1937), 'A study of the Mount Isa ores', *Economic Geology,* Vol. 32, No. 4, pp. 407-450

HINDE, JS (1994),'A summary of the geology and genesis of the Mount Isa Copper Orebodies',

HEINRICH, CA, BAIN, JHC, FARDY, JJ, WARING, CL (1993),'Br/Cl geochemistry of hydrothermal brines associated with Proterozoic metasediment-hosted copper mineralisation at Mount Isa, northern Australia', *Geochimica et Cosmochimica Acta*, Vol. 57, pp. 2991-3000

KENNEDY, J & TYSON, N (2001), 'Blasting in Reactive Ground', *EXPLO,*

KEYS, D (2007), 'Mount Isa Copper – Further Insights', presentation, *predictive mineral discovery: cooperative research centre,* (Unpublished presentation)

LONG, RD (2010), 'The Paroo Fault and the Mount Isa Orebodies; a revised structural and evolutionary model, Mt Isa, Qld, Australia, PhD thesis, James Cook University

MAGUIRE, (2016), 'Trace element variation of Pyrite 2 in the Mount Isa Copper System', University of Adelaide, Honours Thesis (unpublished)

MILLER, B (2006),'Characterisation and timing of faults with respect to copper mineralisation and talc alteration in the Northern 3500 orebody, Mount Isa, Northwest Queensland',

MILLER, J (2007), 'Project report: Structural Controls on the Mount Isa Copper Deposit, Qld', *Predictive Mineral Discovery, Cooperative Research Centre,* Project 17, pp. 1-60

NEUDERT, M (1983), 'A depositional model for the upper Mount Isa group and implications for ore formation', PhD Thesis, Australian National University

PAINTER, M (2003), 'Geochemical and Mineralogical haloes around the Mount Isa base metal orebodies', PhD Thesis,

PAINTER, M, GOLDING, SD, HANNAN, KW, NEUDERT, MK (1999),'Sedimentologic, petrographic, and sulphur isotope constraints on fine-grained pyrite formation at Mount Isa mine and environs, Northwest Queensland, Australia', Economic Geology, Vol. 94, pp. 883-912

PERKINS WG (1984),'Mount Isa Silica Dolomite and Copper Orebodies: The result of a syn-tectonic Hydrothermal Alteration System', *Economic Geology,* Vol. 79, pp. 601-637

PERKINS WG (1990),'Mount Isa Copper Orebodies', *Geology of the mineral deposits of Australia and Papua New Guinea,* pp. 935-

PERKINS WG (1997),'Mount Isa lead-zinc orebodies: Replacement lodes in a zoned syn-deformational copper-lead-zinc system?', *Ore Geology Reviews*, Vol. 12, pp 61-110

PERKINS WG (1998),'Timing of formation of Proterozoic strati-form fine-grained pyrite: post-diagenetic cleavage replacement at Mount Isa?', *Economic Geology*, Vol. 93, pp. 1153 – 1164

ROBERTSON, CW (1982), 'The role of pre-existing sulphides in copper-ore formation at Mount Isa, Queensland', *Journal of Australian Geology and Geophysics,* Vol. 7, pp 119-124

SWAGER,CP (1983),'Microstructural development of the silica dolomite and copper mineralisation at Mount Isa NW Qld, with special emphasis on the timing and mechanism of mineralisation', PhD Thesis, Vol. 1

TAYLOR, R & LILLY, R (2016), 'Is Mount Isa a zoned carbonate replacement system?' (Unpublished)

WARING, C (1990), 'Genesis of the Mount Isa ore System', BSc Hons Thesis,

WILDE, AR, JONES, PA, GESSNER, K, AILLERES, L, GREGORY, MJ, DUNCAN, RJ (2006),'A geochemical process model for the Mount Isa copper orebodies', Economic Geology, Vol. 101, pp. 1547-1567

WILKIN, RT AND BARNES, HL (1997),' Formation processes of framboidal pyrite', *Geochimica et Cosmochimica Acta,* Vol. 61, No.2, pp. 323-339

Appendix 1

Video demonstrating how leapfrog modelling was conducted

Please find below a link to you-tube or a drop-box folder containing a video on how leapfrog modelling was conducted for the Honours Thesis:

Fine-grained pyrite within the Mount Isa (Enterprise) Copper System, NW Queensland; geological relationships, modelled distribution and links to reactive ground

Samuel John Connell

University of Adelaide

October 2016

Please copy and paste these links into a web browser to receive access to the video.

https://www.youtube.com/watch?v=ol6ZO_8BQ7U

https://www.dropbox.com/sh/8rchb0l7oh9yyj2/AABQow3xHka3FxL3gFuLRrMFa?dl=0

THE UNIVERSITY of ADELAIDE

Appendix 2

Cross sections produced from leapfrog modelling

Please find below a link to a drop-box folder containing a PDF portfolio containing all cross sections produced from leapfrog modelling as part of the Honours Thesis:

Fine-grained pyrite within the Mount Isa (Enterprise) Copper System, NW Queensland; geological relationships, modelled distribution and links to reactive ground

Samuel John Connell
University of Adelaide
October 2016

Please copy and paste these links into a web browser to receive access to the PDF

https://www.dropbox.com/sh/mqek3u3c6lyuxf7/AACJy2Zmi-XmbdC3bvyOchZna?dl=0

THE UNIVERSITY of ADELAIDE

Appendix 3

Petrography report on pyritic shales at Mount Isa

Please find below a link to a drop-box folder containing the report submitted as part of the Honours Thesis:

Fine-grained pyrite within the Mount Isa (Enterprise) Copper System, NW Queensland; geological relationships, modelled distribution and links to reactive ground

Samuel John Connell

University of Adelaide

October 2016

Please copy and paste these links into a web browser to receive access to the PDF

https://www.dropbox.com/sh/8gkwaykbz9n06te/AAAUeIZsKQ6gXkSwUdZ4lscwa?dl=0

THE UNIVERSITY of ADELAIDE

Appendix 4.

Maps, coordinates and elevation data for underground sampling locations

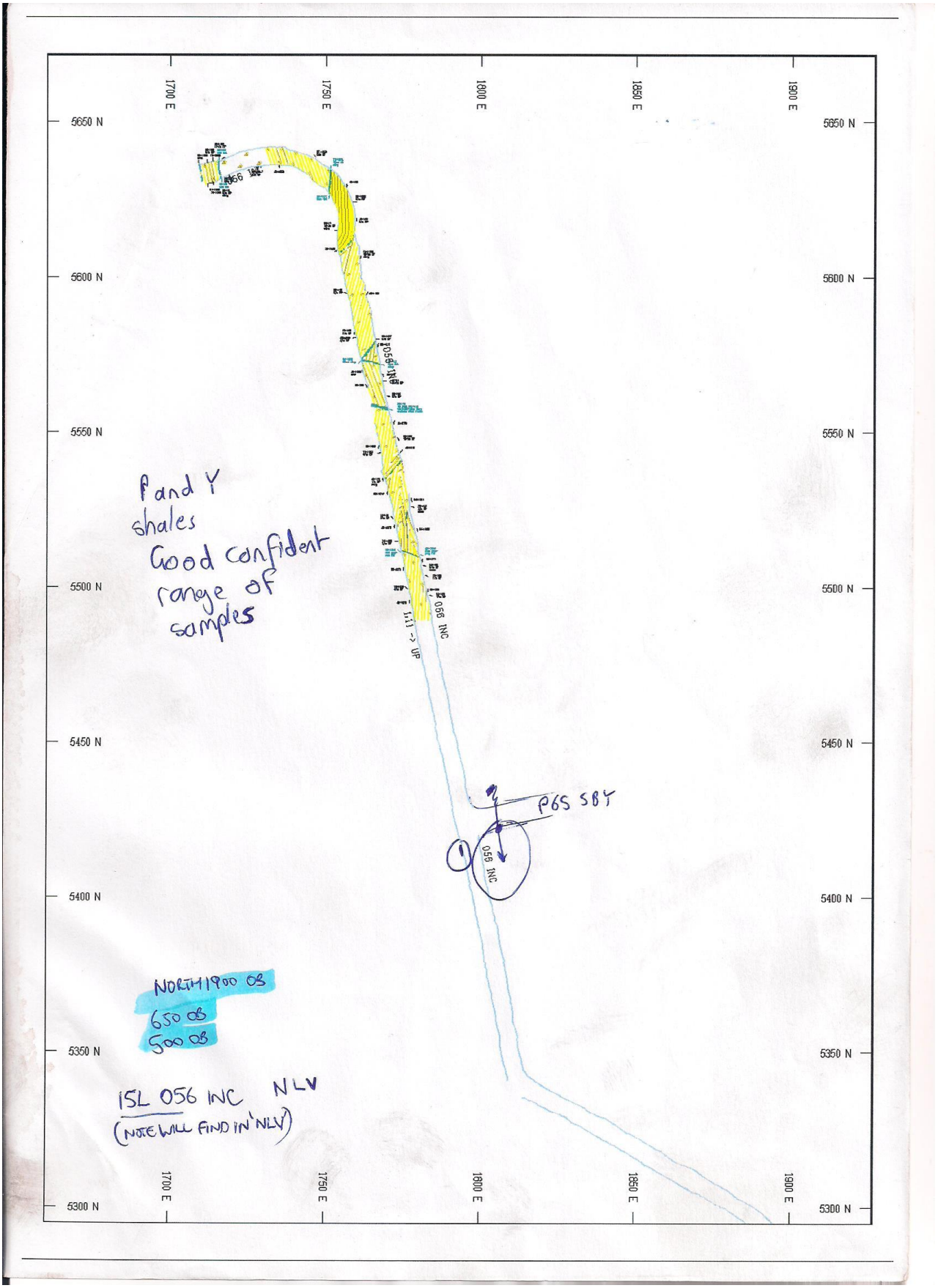
1700 E
1750 E
1800 E
1850 E
1900 E
5650 N
5600 N
5550 N
5500 N
5450 N
5400 N
5350 N
5300 N
P and Y shales
Good confident range of samples
056 INC
P65 SBY
NORTH 1900 OS
650 OS
500 OS
ISL 056 INC NLV
(NOTE WILL FIND IN NLV)

P53 FARAC

1760 E
1780 E
1800 E
1820 E
1840 E
1860 E
5460 N
5440 N
5420 N
5400 N
5380 N
5360 N
P547 DRT
Q542 CO
P52 NDR
P53 FARAC
NWDR
STG in backs
10cm shr+dol
talcose
Siliceous patches
Flt @ 28.5m
5cm Dol & Qtz
REM bdg starts
@ 10m
2cm QTZ & RUB
5cm QTZ & DOL
1m qtz dol brecc
sep. Major Fault
1m fault zone
shrg 5cm quartz
Kspar c dol tmb?
80 Gyp
80 Gyp & calc fill
Pk calc
Stg dol vng

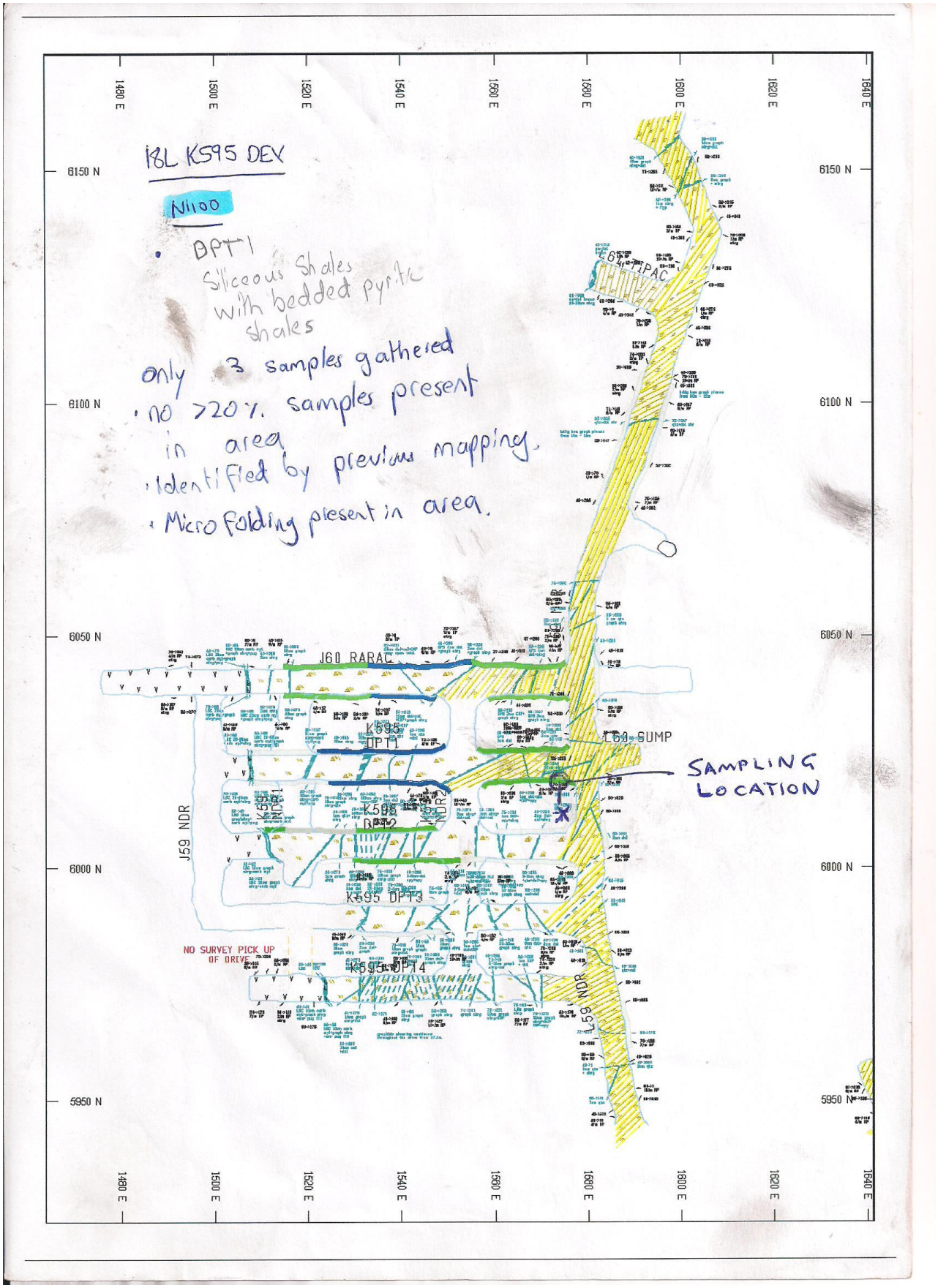
1480 E
1500 E
1520 E
1540 E
1560 E
1580 E
1600 E
1620 E
1640 E
6150 N
6100 N
6050 N
6000 N
5950 N
K595 DEV
N1100
DPT1
Siliceous Shales with bedded pyritic shales
Only 3 samples gathered
• no >20%. samples present in area
• Identified by previous mapping.
• Micro folding present in area.
J60 RARAC
K595 DPT1
J60 SUMP
SAMPLING LOCATION
J59 NDR
K595 DPT2
K595 DPT3
NO SURVEY PICK UP OF DRIVE
K595 DPT4
J57 NDR

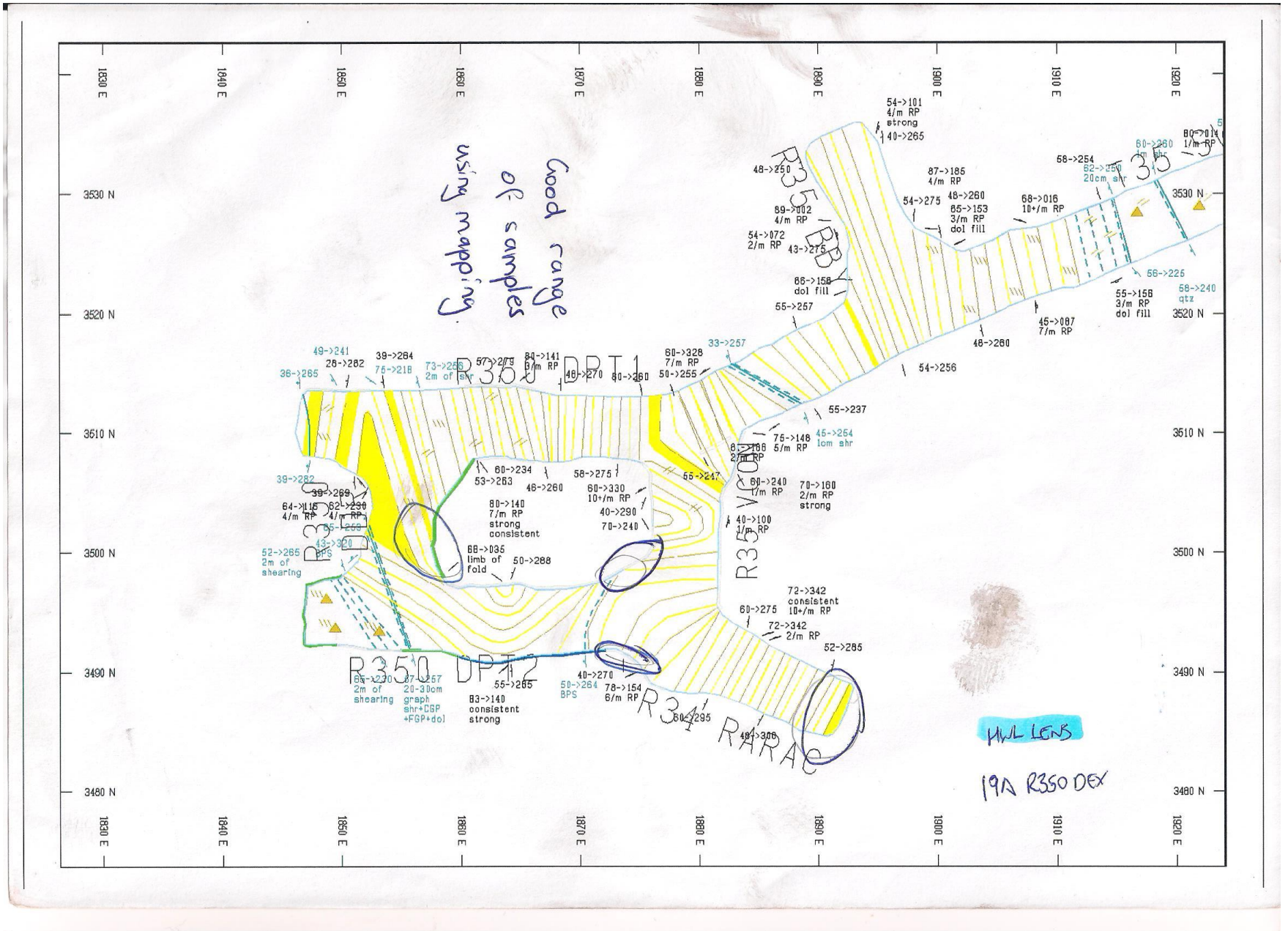
Guiding mapping using samples of good range
R350 DPT1
R350 DPT2
R350 VEIN
R350 RARAC
HWL LENS
19A R350 DEX
1830 E
1840 E
1850 E
1860 E
1870 E
1880 E
1890 E
1900 E
1910 E
1920 E
3530 N
3520 N
3510 N
3500 N
3490 N
3480 N

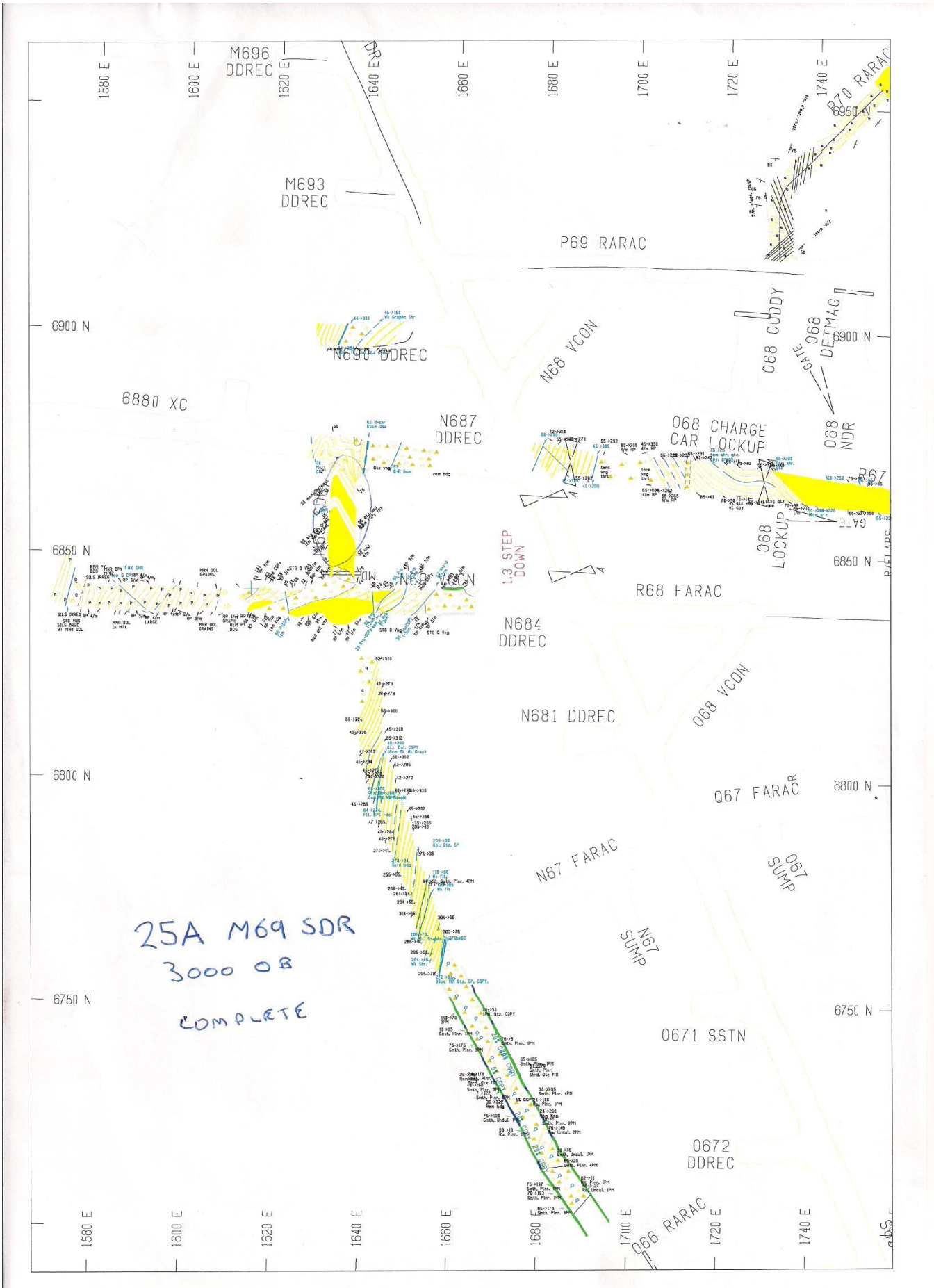
1580 E
1600 E
1620 E
1640 E
1660 E
1680 E
1700 E
1720 E
1740 E
6950 N
6900 N
6850 N
6800 N
6750 N
M696 DDREC
M693 DDREC
P69 RARAC
P70 RARAC
N690 DDREC
6880 XC
N687 DDREC
N68 VCON
068 CUDDY
068 DEIMAG
GATE
068 NDR
068 CHARGE CAR LOCKUP
P67
GATE
068 LOCKUP
1.3 STEP DOWN
R68 FARAC
N684 DDREC
N681 DDREC
068 VCON
067 FARAC
N67 FARAC
067 SUMP
N67 SUMP
0671 SSTN
0672 DDREC
066 RARAC
25A M69 SDR
3000 OB
COMPLETE

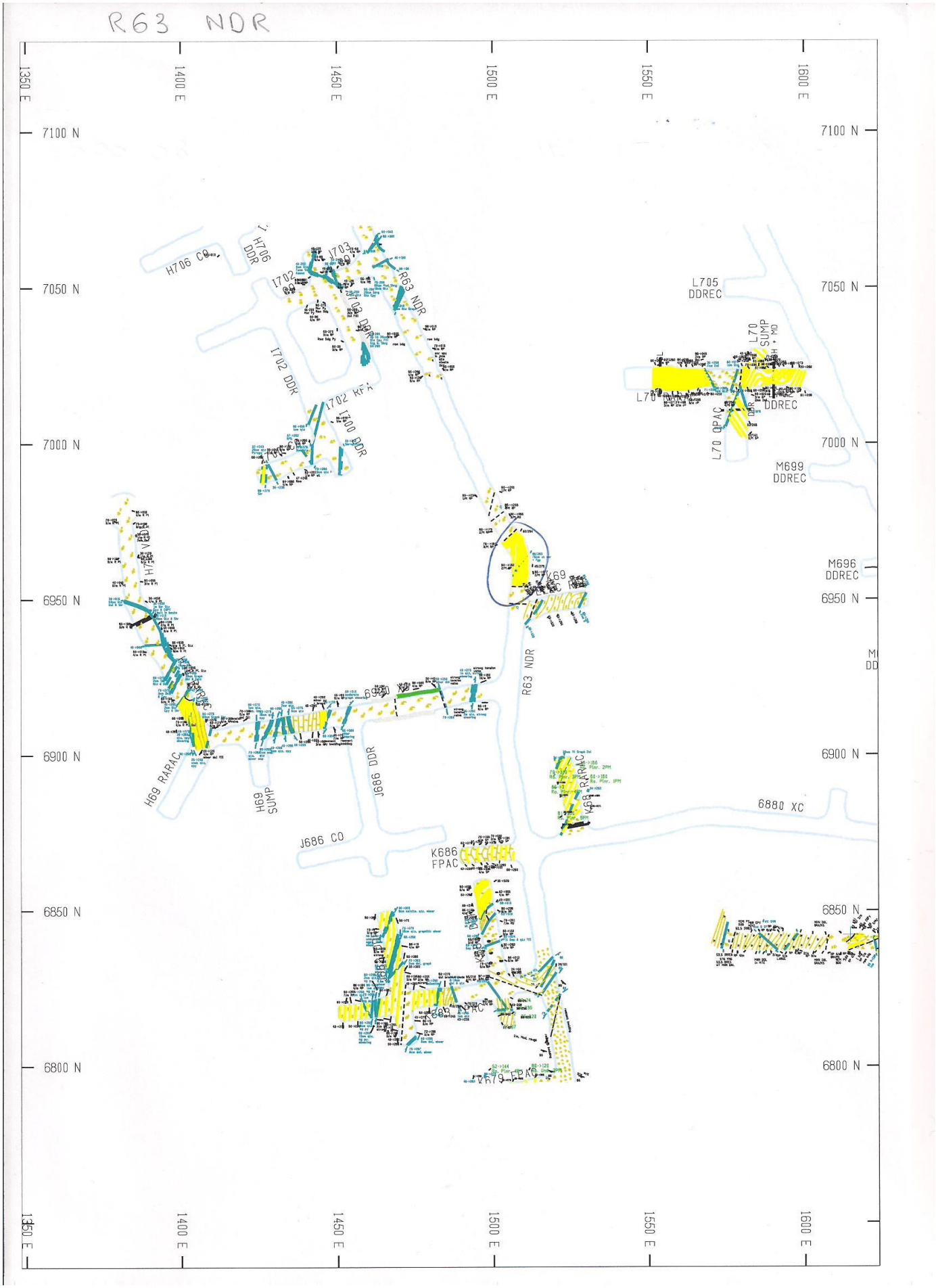
R63 NDR
1350 E
1400 E
1450 E
1500 E
1550 E
1600 E
7100 N
7050 N
7000 N
6950 N
6900 N
6850 N
6800 N
H706 CO
H706 DDR
I702
I703
I702 DDR
I702 HFA
I700 DDR
L705
DDREC
L70
SUMP
L70 QPAC
M699
DDREC
M696
DDREC
H69 RARAC
H69
SUMP
J686 DDR
J686 CO
K686
FPAC
6880 XC

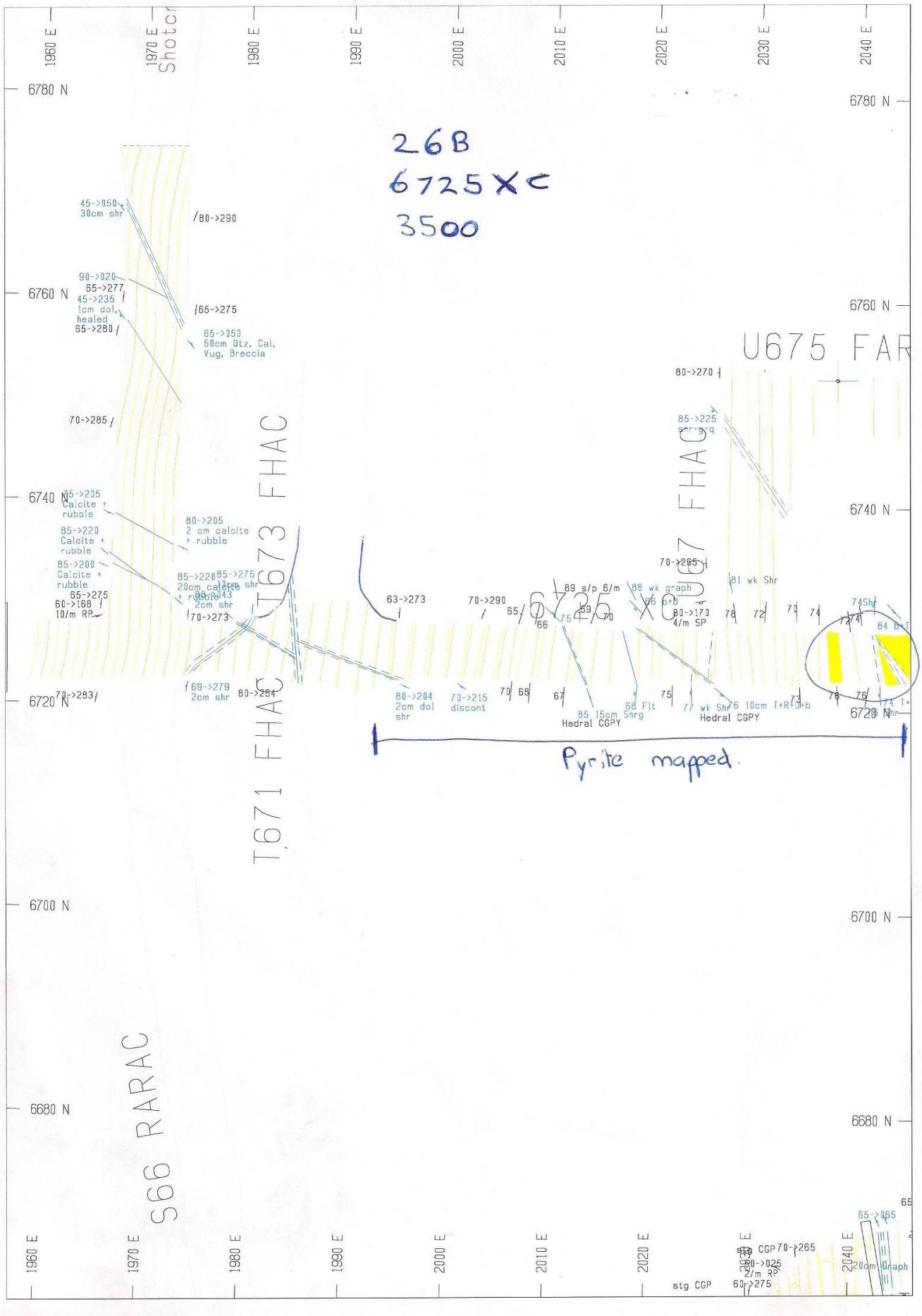
26B
6725XC
3500
1960 E
1970 E
1980 E
1990 E
2000 E
2010 E
2020 E
2030 E
2040 E
6780 N
6760 N
6740 N
6720 N
6700 N
6680 N
T671 FHAC
T673 FHAC
U675 FAR
S66 RARAC
45->050
30cm shr
/80->290
90->020
65->277
45->235
1cm dol,
healed
65->280
65->275
65->050
50cm Qtz, Cal,
Vug, Breccia
70->285
75->205
Calcite +
rubble
80->205
2 cm calcite
+ rubble
85->220
Calcite +
rubble
85->200
Calcite +
rubble
65->275
60->168
10/m RP
85->220
20cm calcite
+ rubble
85->275
15cm shr
88->043
2cm shr
70->273
69->279
2cm shr
80->284
70->283
63->273
70->290
89 s/p 6/m
88 wk graph
80->170
4/m SP
81 wk Shr
74Shr
84 D+T
70->265
80->270
85->225
80->204
2cm dol
shr
70->215
discont
85 15cm Shrg
Hedral CGPY
68 Flt
77 wk Shr
76 10cm T+R+D+b
Hedral CGPY
Pyrite mapped
65->165
20cm Graph
CGP 70->265
80->025
2/m RP
stg CGP
60->275

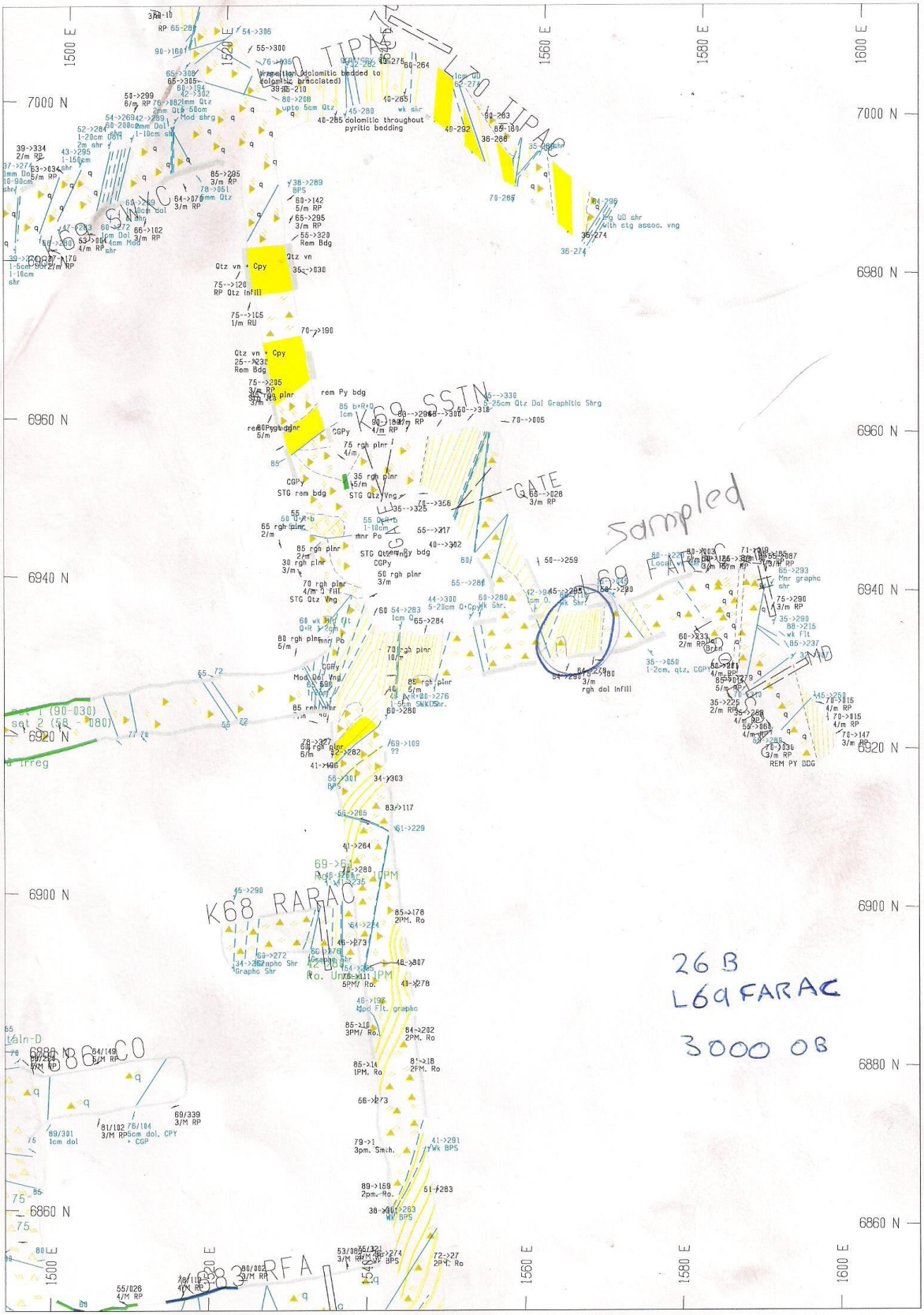
1500 E
1520 E
1560 E
1580 E
1600 E
7000 N
6980 N
6960 N
6940 N
6920 N
6900 N
6880 N
6860 N
L70 TIPAC
K68 SSTN
L69 FARAC
K68 RAPAC
K68 RFA
sampled
26 B
L69 FARAC
3000 OB

T67 VCON


6950 N
6900 N
6850 N
6800 N
6750 N
6700 N
6650 N
1900 E
1950 E
2000 E
2050 E
2100 E
26 B
T67 VCON
3500 OB
SL
S68 RARAC
S68 VCON
S69 SHACC
T67 VCON
V67 SKBY
U675 FARAC
T673 FHAC
T671 FHAC
V67 FHAC
W67 RARAC
S66 RARAC
6667 XC
S66 OPAC
W66 FARAC

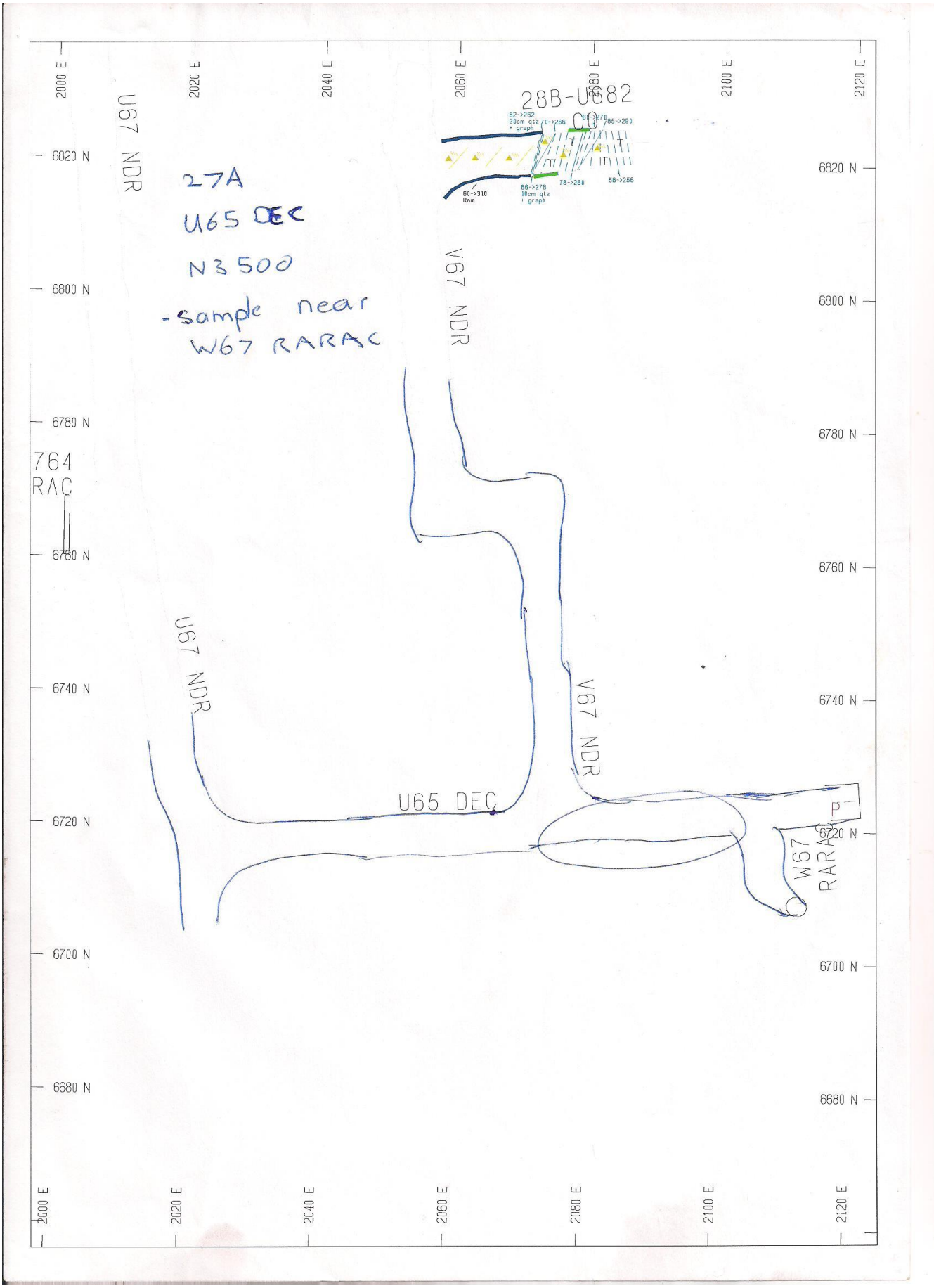
2000 E
2020 E
2040 E
2060 E
2080 E
2100 E
2120 E
6820 N
6800 N
6780 N
6760 N
6740 N
6720 N
6700 N
6680 N
U67 NDR
V67 NDR
U67 NDR
V67 NDR
U65 DEC
764
RAC
W67
RARAC
P
28B-U682
27A
U65 DEC
N3500
-sample near
W67 RARAC

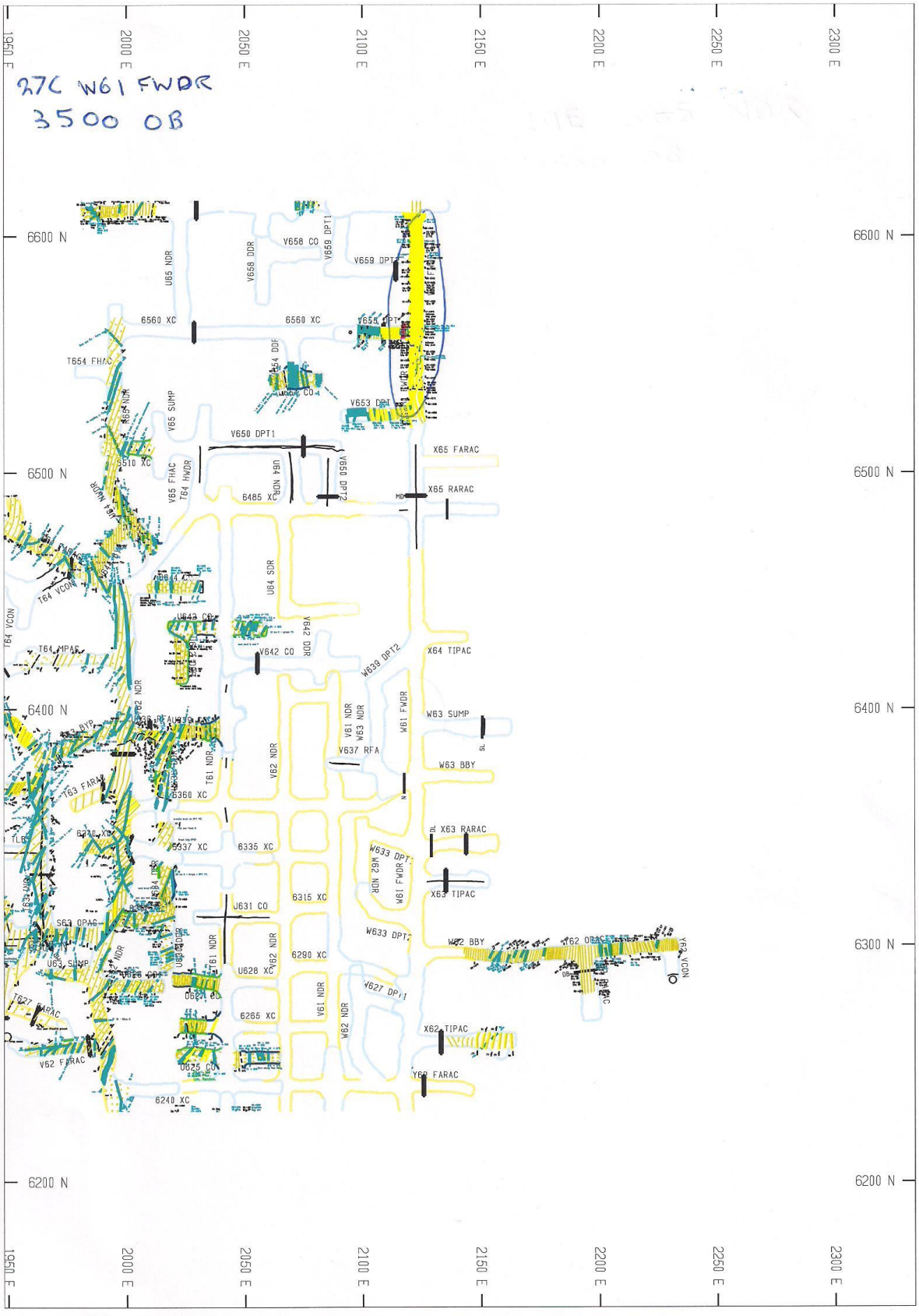
27C W61 FWDR
3500 OB
1950 E
2000 E
2050 E
2100 E
2150 E
2200 E
2250 E
2300 E
6600 N
6500 N
6400 N
6300 N
6200 N
V658 CO
V659 DPT1
V659 DPT2
U65 NDR
V658 DDR
6560 XC
T654 FHAC
V654 DDF
V653 DPT
V65 SUMP
V650 DPT1
X65 FARAC
X65 RARAC
6510 XC
V65 FHAC
T64 FWDR
U64 NDR
V650 DPT2
6485 XC
T64 VCON
U64 SDR
V642 CO
V642 DDR
T64 MPAC
W639 DPT2
X64 TIPAC
W63 SUMP
V637 RFA
V61 NDR
W63 NDR
W61 FWDR
W63 BBY
T63 FARAC
6360 XC
V62 NDR
T61 NDR
X63 RARAC
6335 XC
W633 DPT1
W62 NDR
W61 FWDR
X63 TIPAC
U631 CO
6315 XC
S63 OPAC
W633 DPT2
W62 BBY
V62 OPAC
T63 VCON
U63 SUMP
U628 XC
6290 XC
T627 MPAC
V627 DPT1
6265 XC
X62 TIPAC
V62 FARAC
U625 CO
Y62 FARAC
6240 XC

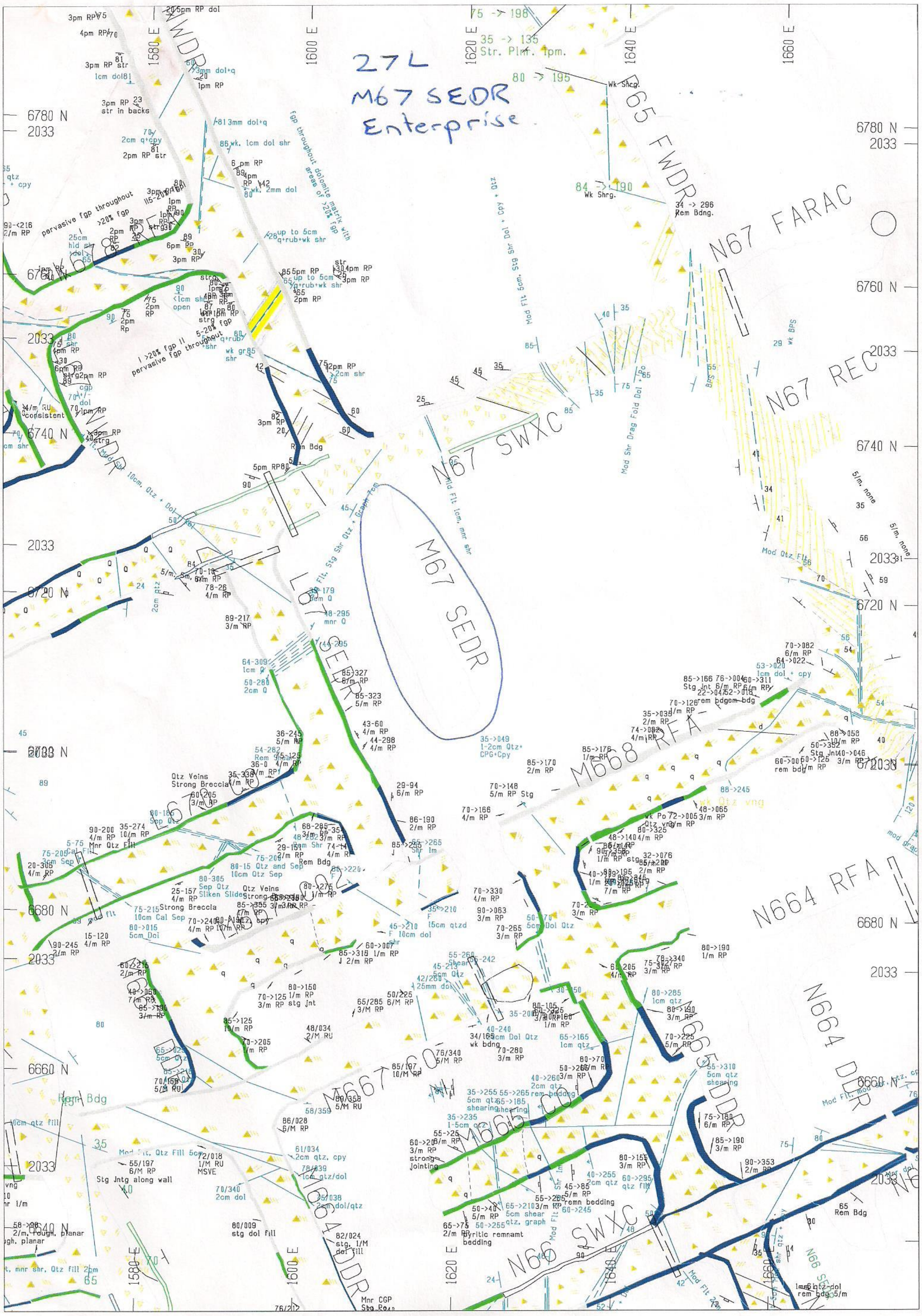
27L
M67 SEDR
Enterprise
N67 FARAC
N67 REC
N67 SWXC
M67 SEDR
P65 FWDR
M668 RFA
N664 RFA
N664 DDR
N66 SWXC
6780 N
6760 N
6740 N
6720 N
6680 N
6660 N
2033
1580 E
1600 E
1620 E
1640 E
1660 E

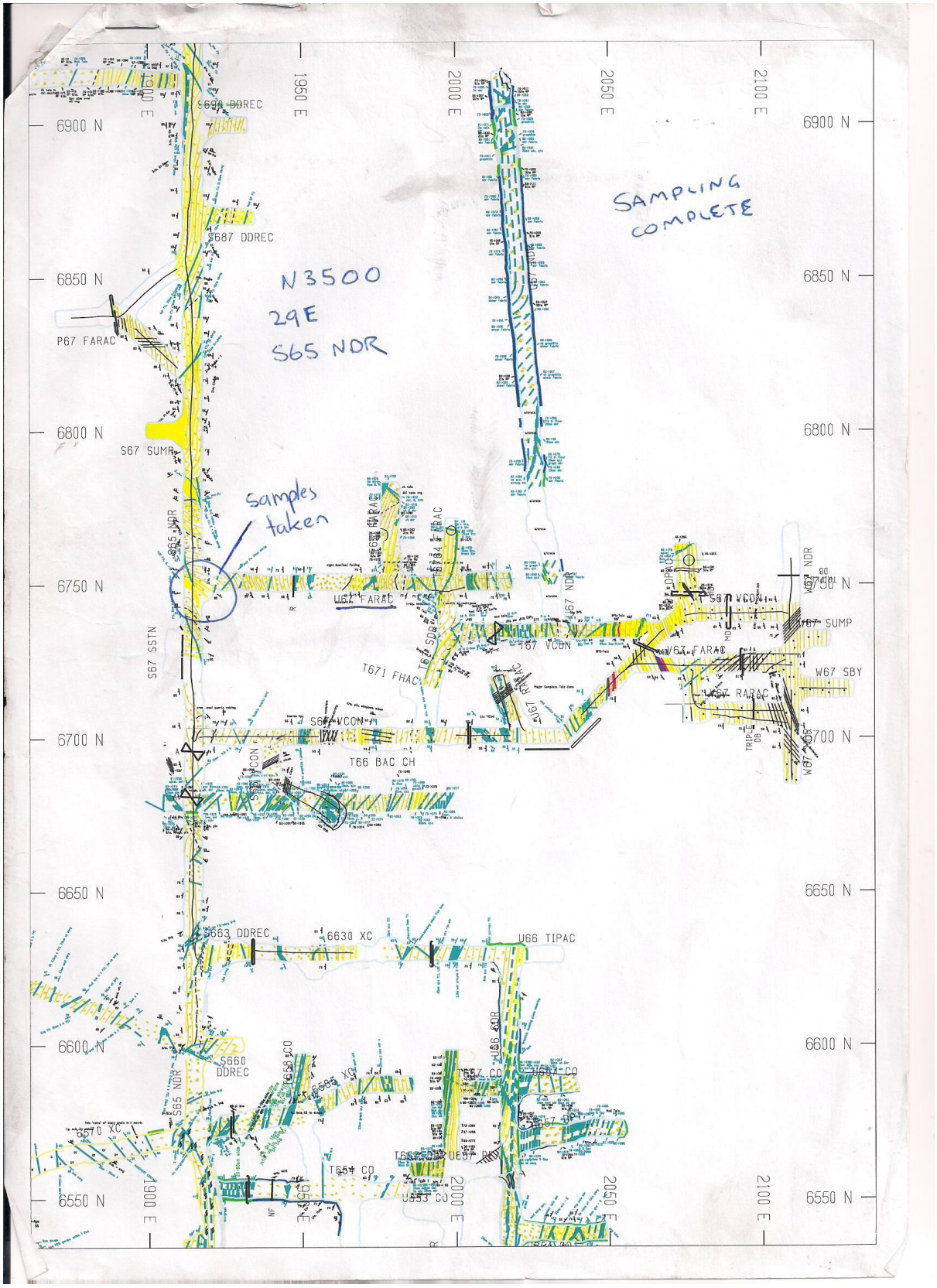
SAMPLING COMPLETE
N3500
29E
S65 NDR
samples taken
1900 E
1950 E
2000 E
2050 E
2100 E
6900 N
6850 N
6800 N
6750 N
6700 N
6650 N
6600 N
6550 N
S699 DDREC
S687 DDREC
P67 FARAC
S67 SUMP
S67 SSTN
S65 NDR
W67 FARAC
T67 VCON
T671 FHAC
S66 VCON
T66 BAC CH
S663 DDREC
6630 XC
U66 TIPAC
S660 DDREC
6570 XC
T654 CO
U653 CO
T667 CO
U667 CO
W67 SUMP
W67 SBY
W67 RARAC

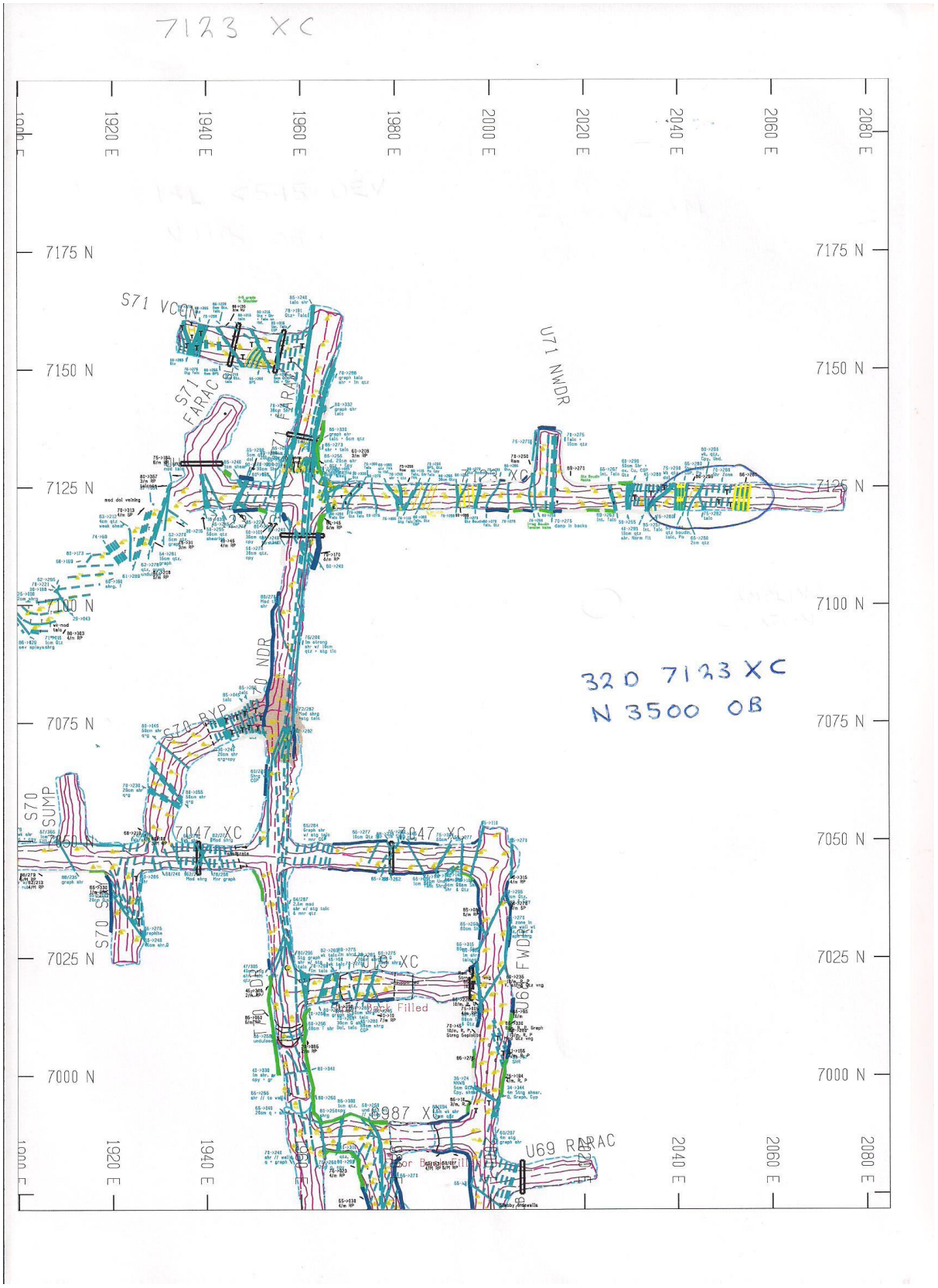
7123 XC
1900 E
1920 E
1940 E
1960 E
1980 E
2000 E
2020 E
2040 E
2060 E
2080 E
7175 N
7150 N
7125 N
7100 N
7075 N
7050 N
7025 N
7000 N
S71 VCON
S71 FARAC
U71 NWDR
U71 XC
S70 RVD
S70 NDR
S70 SUMP
S70 SWDR
7047 XC
7047 XC
7047 XC
7047 XC
7087 XC
U69 FWDR
U69 RARAC
Backfilled
320 7123 XC
N 3500 OB

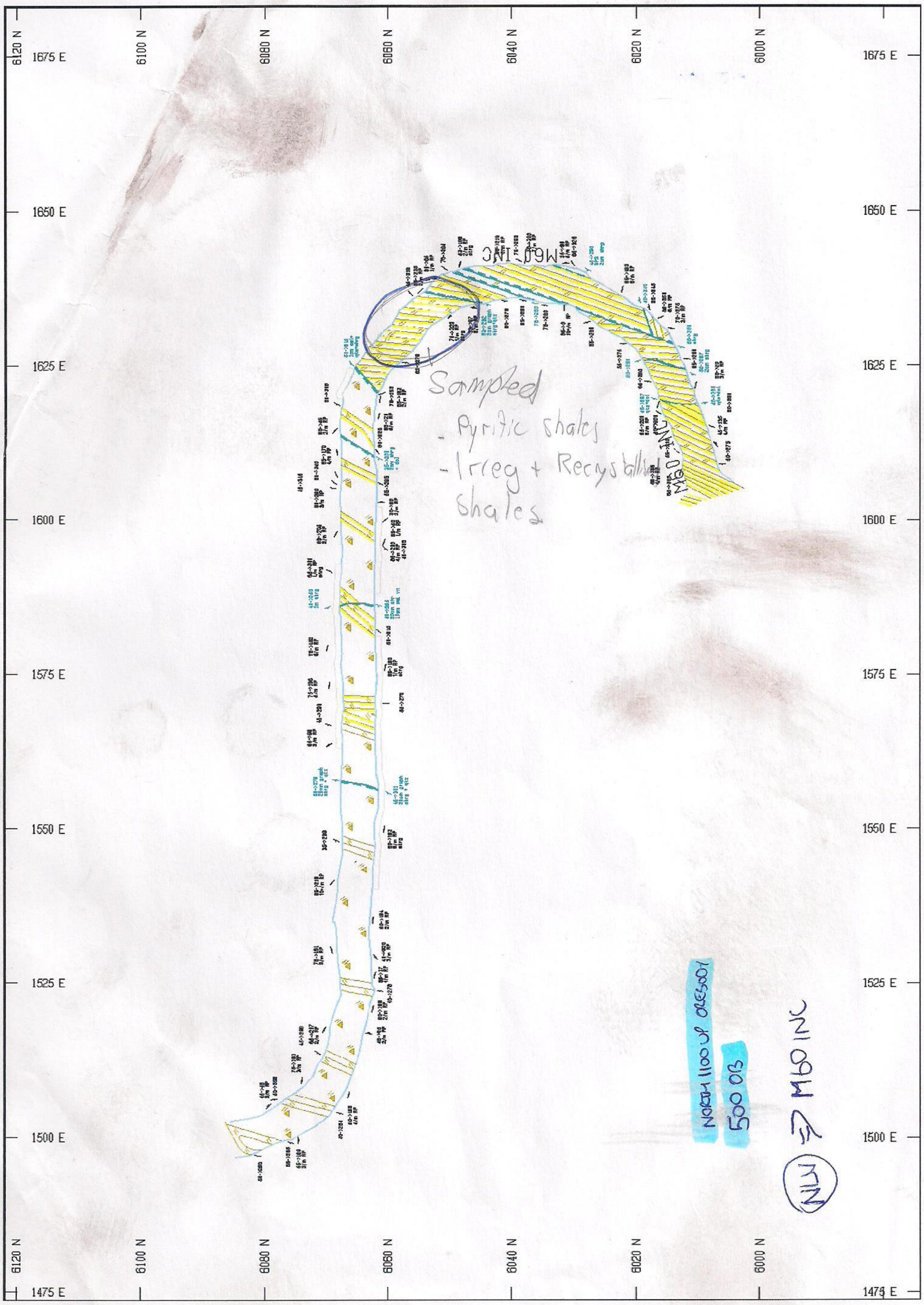

6120 N
6100 N
6080 N
6060 N
6040 N
6020 N
6000 N
1675 E
1650 E
1625 E
1600 E
1575 E
1550 E
1525 E
1500 E
1475 E
M60 INC
Sampled
- Pyritic shales
- Irreg + Recrystallised shales
NORTH 1100 UP ORESOOY
500 OB
NLW ⇒ M60 INC

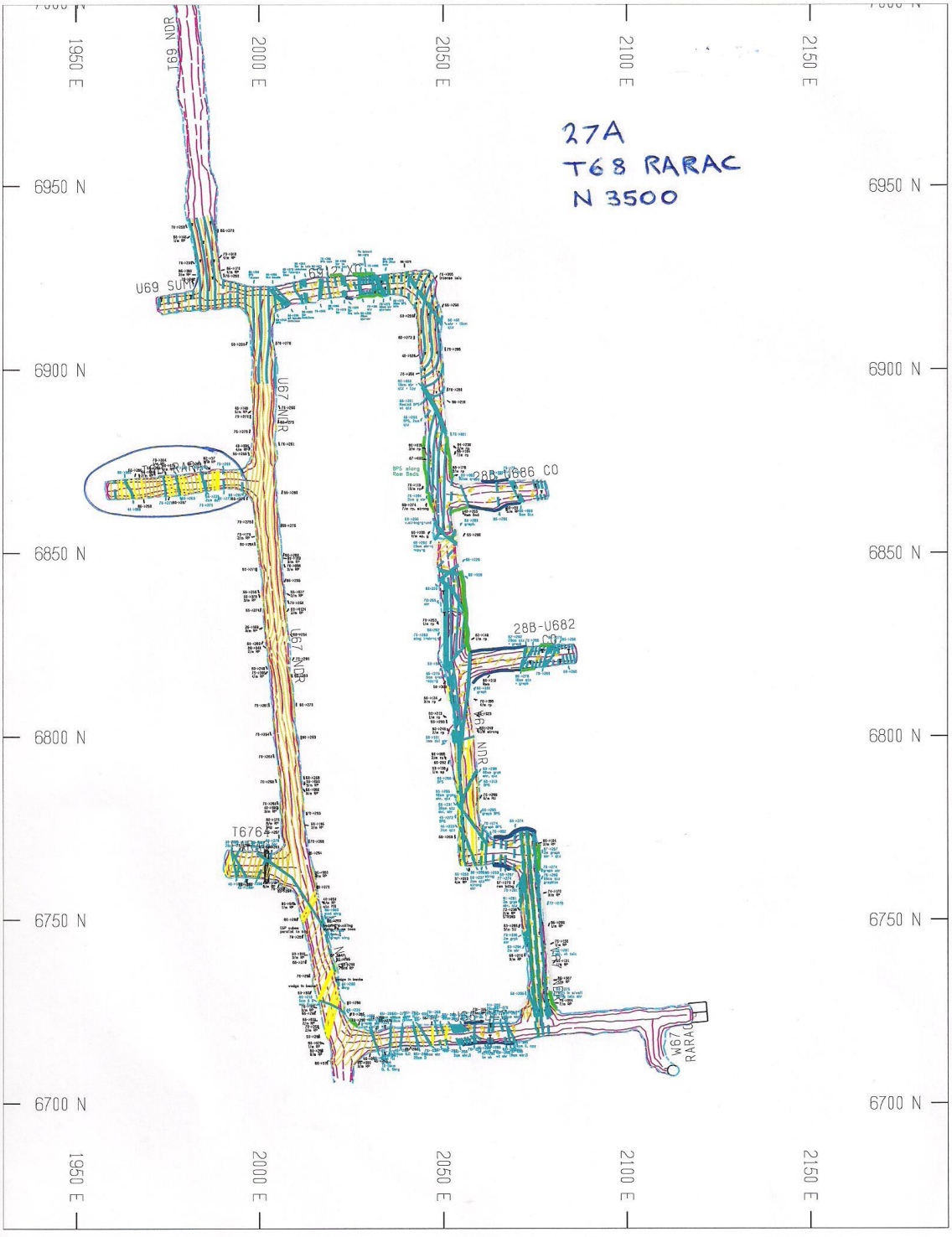
27A
T68 RARAC
N 3500
1950 E
2000 E
2050 E
2100 E
2150 E
6950 N
6900 N
6850 N
6800 N
6750 N
6700 N
T69 NDR
U69 SUMP
U67 NDR
28B-U686 CO
28B-U682 CO
T676
W67 RARAC

Location	Level	Label	Northing	Easting	Elevation
6725 XC	26B	ENTFGo4	6730	2020	2100
L69 FARAC	26B	ENTFG10	6930	1560	2100
M69 SDR	25A	ENTFG09	6860	1630	2160
M67 SEDR	27L	ENTFG11	6040	1640	2030
W61 FWDR	27C	ENTFG03	6550	2125	2055
S65 NDR	29E	ENTFG07	6750	1910	1950
T68 RARAC	27A	ENTFG05	6960	1975	2040
7123 XC	32D	ENTFG05	7120	2040	1765
T67 VCON	26B	ENTFG01	6800	1975	2100
U65 DEC	27A	ENTFG02	6725	2050	2040
K595	18L	ENTFG13-A	6020	1575	2550
P53 FARAC	17C	ENTFG15	5380	1825	2638
M60 INC	17C	X41 FG12	6040	1640	2638
056 INC	15L	X41FG14	5420	1800	2727
R72 SBY	32A	ENTFG08	7200	1800	1735
R63 NDR	25A		6950	1500	2160
R350 DEV	19A		3500	1870	2503.9

Appendix 5

Summary poster on fine-grained pyrite

A study on fine grained pyrite within the Mount Isa Copper System; Geological and Structural Relationships, and association with reactive ground

Samuel Connell

A W.E.S.O.M.E.S. Research Unit, Department of Earth Sciences, University of Adelaide, South Australia

Samuel.connell@student.adelaide.edu.au

Background and Geologic Setting

The project is based on the Mount Isa Copper Deposit, located within the Mount Isa Inlier in North West Queensland. The world class deposit lies within the Western Fold belt of the Inlier, within the Leichhardt river fault trough. Economic mineralisation of Lead-Zinc and Copper occurs within the Urquhart shale, a thinly bedded carbonaceous sedimentary rock. It contains alternating layers of dolomitic siltstone, and shale.

The deposit has undergone multiple stages of deformation and hydrothermal alteration. There are spatially discrete, high grade deposits of lead-zinc, and copper, within the same location. With ongoing debate on how the copper deposit formed, the implications of the abundant fine grained pyrite mineralisation needs re-addressing.

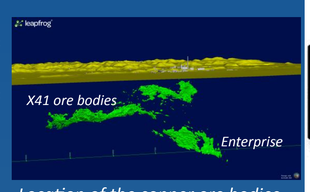

Location of the copper ore bodies below Mount Isa, looking NW

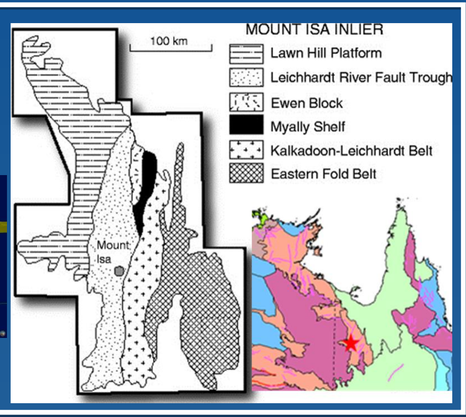

Project Abstract

The Mount Isa Deposit contains abundant strati-form fine grained pyrite mineralisation. Its high concentration within the mine area, and proximity to high grade ore, provokes interest as to what its relationship is to the copper mineralisation, and silica dolomite alteration. The relationships of fine grained pyrite are investigated both on the deposit scale and on the micro-scale. The mineral is also thought to be the primary causal factor for reactive ground, posing a risk to mine operation within the underground environment. My project also aims to test this hypothesis.

Project Aims / Objectives

- **Describe the mineral relationships of fine grained pyrite samples in hand specimen, and on the micro-scale.**
- **Analyse any deposit scale structural relationships between fine grained pyrite, and the copper ore system.**
- **Measure and analyse the relationship between fine grained pyrite and reactive ground.**

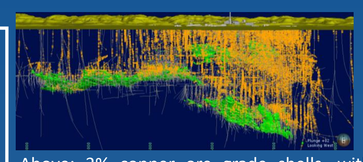

Above: 3% copper ore grade shells, with drilling data showing >5% fine grained pyrite in orange. Pyrite is concentrated within the mining area, proximal to the orebodies.

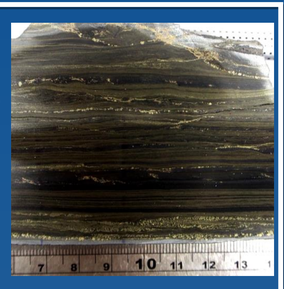

Above: Typical beds of fine grained pyrite amongst black shale. Note its characteristic deep bronze colour.

Hand samples - textures of pyrite rich shale

Important observations:

- Fine grained pyrite had highly ductile and competent nature at time of ore deposition compared to brittle silicified black shales.
- Fine grained pyrite can often act as a ductile barrier for mineralised veins, and potentially concentrating mineralisation to specific areas.
- Lithology's between fine grained pyrite beds often act as preferential channel-ways for ore fluids, and for alteration of existing minerals (dolomite/silica).
- Remnant/deformed fine grained pyrite bands often remain within brecciated rock.

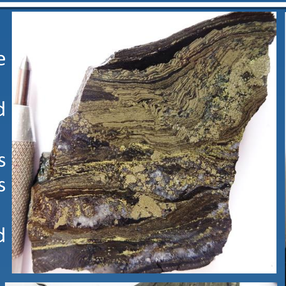

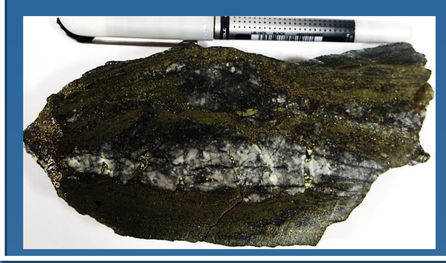

Leapfrog modelling—large scale structural distribution of pyrite

Leapfrog geological modelling of pyritic shales was conducted to assess any large scale patterns. There was an obvious structural distribution of fine grained pyrite on a large scale. This may be related to large carbonaceous rich seams/beds. This is also consistent on the micro-scale. There is an obvious sedimentary control on carbonaceous material both on mine scale and micro-scale.

Pyrite often forms an envelope around copper ore, and brecciated rock, especially evident in the 3500 Ore body. My hypothesis is that fine grained pyrite had an important role in the structural location of ore bodies. It may have facilitated the localisation and formation of high grade ore.

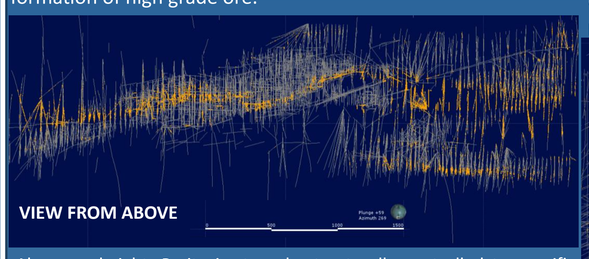

CROSS-SECTION VIEW—LOOKING SOUTH

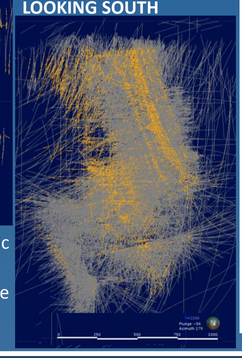

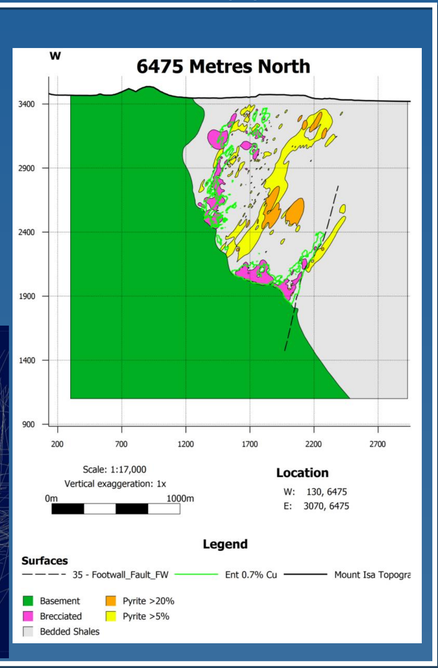

Above and right: Pyrite is strongly structurally controlled to specific lobes on the deposit scale.

Far right: Cross section taken at 6475 metres North showing the relationship between pyrite and brecciated rock.

Petrography Results

- There are three major textural varieties of pyrite. Fine grained pyrite (Pyrite 1), true coarser grained cubic pyrite (Pyrite 2), and a third type (Brassy pyrite) which is a coarser grained form of pyrite 1. Combinations of these interact to give textural variety.
- Fine grained pyrite is lithologically controlled by carbonaceous rich seams within dolomitic and siliceous shale.
- Galena, Sphalerite and Chalcopyrite consistently occur as infill with similar timing relationships when all present. Chalcopyrite and pyrrhotite have a clear timing link.
- Coarse grained pyrite is mainly associated with silica/dolomite veins. It occurs amongst fine grained and brassy pyrite, and may overprint them.
- Fine grained pyrite layers are more able to be folded on micro -scales as opposed to less competent layers. Therefore, they are more likely to form fluid traps.
- Arsenopyrite is a common accessory mineral in the ore system and has similar timing to pyrite 2.

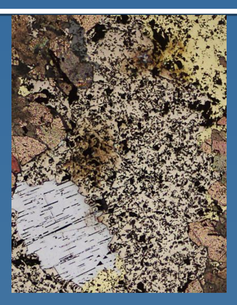

Above: Sulphide grain containing cpy, galena, sphalerite and pyrrhotite.

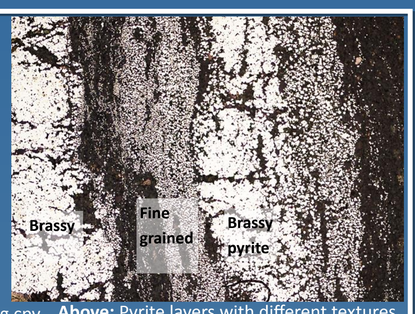

Above: Pyrite layers with different textures. One layer is much coarser grained.

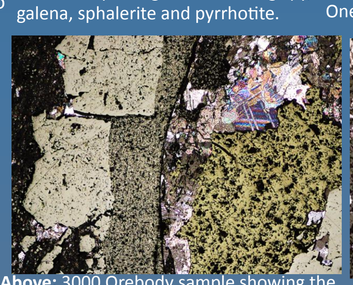

Above: 3000 Orebody sample showing the boundary of fine grained pyrite acting as a weakness for fluid flow and alteration.

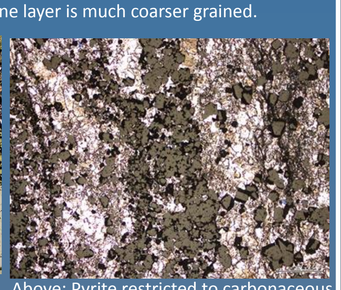

Above: Pyrite restricted to carbonaceous zones within the surrounding dolomitic shale.

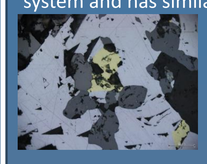

Above: Enterprise samples showing sphalerite, galena and chalcopyrite with similar timing relationships.

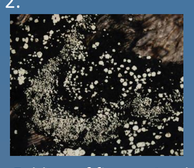

Above: Folding of fine grained pyrite layer. Note the grains themselves do not fold.

Scanning Electron Microscope results on pyritic shales

- Within folded/faulted samples, fine grained pyrite shows a strong orientation parallel to the axial planar cleavage.
- Fine grained pyrite grains display evidence of zonation, and display a variety of shapes and textures.
- Complex mineral relationships are identified in magnetite bearing samples. Related minerals include magnetite, Stilpnomelane, Ba/Mg carbonate, Fe/Mn rich dolomite. Prominent infill of sphalerite, galena and chalcopyrite in strata-bound

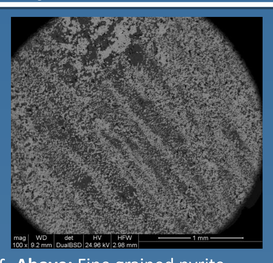

Above: Fine grained pyrite orientated parallel to cleavage.

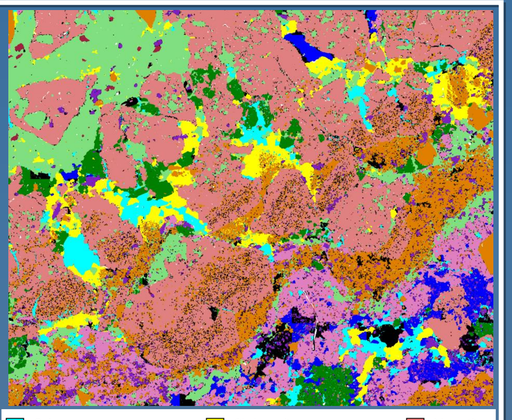

Above: MLA Image generated from a magnetite bearing sample in the Enterprise Orebody. Major minerals present include magnetite, pyrite, sphalerite, galena, chalcopyrite and barium/magnesium carbonate.

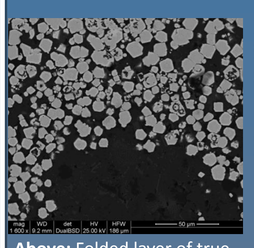

Above: Folded layer of true fine grained pyrite.

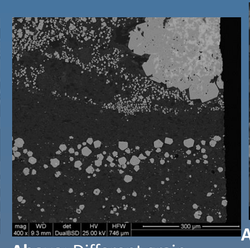

Above: Different grain sizes of fine grained pyrite.

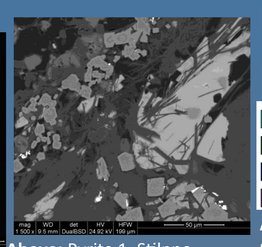

Above: Pyrite 1, Stilpnomelane, and Ba/Mg Carbonate within a magnetite **sample.**

Magnetite; Bedding parallel textures within pyritic shale

Magnetite found within the Enterprise Mine amongst fine grained pyrite.It shows euhedral, bedding parallel textures, and a link with fine grained pyrite and Stilpnomelane mineralisation. Related minerals also include barium/magnesium carbonate, siderite/ankerite and sphalerite.

Para-genesis of minerals in sample

1. Fine grained pyrite (unclear timing with magnetite)
2. Magnetite and iron alteration (Ankerite, Siderite, Stilpnomelane).
3. Ba/Mg Carbonate alteration
4. Coarse grained pyrite
5. Iron rich Sphalerite
6. Galena + Chalcopyrite

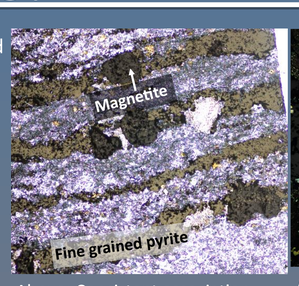

Above: Consistent association between magnetite and fine grained pyrite layers.

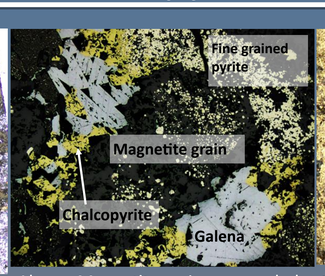

Above: Magnetite grain surrounded by galena, cpy, and FGP. Magnetite also contains inclusions of FGP.

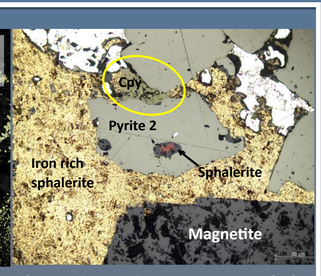

Above: Magnetite grain surrounded by unknown gold coloured mineral, along with pyrite 2 and chalcopyrite.

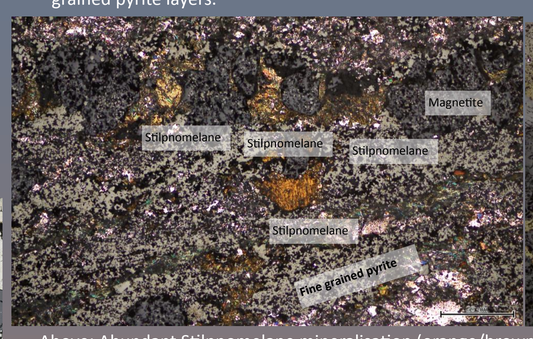

Above: Abundant Stilpnomelane mineralisation (orange/brown) occurring in association with magnetite and Fe alteration.

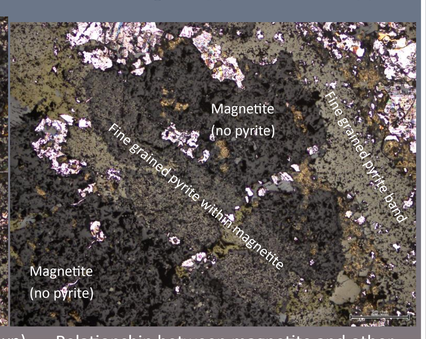

Relationship between magnetite and other sulphide minerals.

Above: Euhedral-magnetite grains.

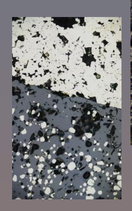

Above: Magnetite grain containing inclusions of pyrite.

Possible hypothesis: Strong Iron alteration caused magnetite, iron carbonate, and stilpnomelane mineralisation. Associated with Ba/Mg carbonate. This was overprinted by economic sulphides.

Fine grained pyrite and safety; reactive ground in the mine environment

Definition: Reactive ground is rock containing abundant sulphide minerals (mainly pyrite) which has the potential to undergo sudden heat releasing reactions, after contact with nitrate explosives. The process is unpredictable, and occurs rapidly, posing a risk when using explosives. Thus, it is important for the safe management of drilling and blasting operations underground.

Project description: Fine grained pyrite abundance is thought to be the causal factor for shale reactivity. In order to test this hypothesis, samples containing variable amounts of fine grained pyrite were collected from locations around the mine (shown in figure on right) and are to undergo lab testing.

Factors thought to cause reactive ground:

- Moisture
- Oxidising conditions
- Thermal properties of host rock.
- Ambient mine temperature
- Smaller grain size of sulphide
- Fine grained pyrite abundance

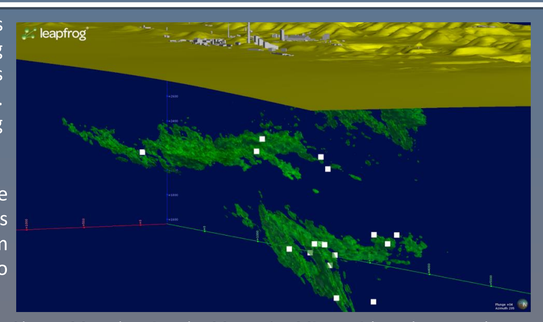

Above: Map showing the Mount Isa Mine, with underground copper ore grades of 3%. The white squares indicate where samples were taken with respect to the orebodies.

Methods for sample collection

- Sampled fresh rock from walls of drives in areas of current mine production.
- Accurately estimate the percentage of fine grained pyrite in the rock samples while underground.
- Validate samples once at surface. Sort into correct groups for lab testing and chemical assaying.
- Currently awaiting results

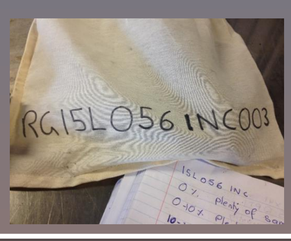

SUMMARY

- ***Pyritic shales seem to help control structures and therefore fluid ingress on a variety of scales. It displays ductile behaviour, acting as barriers to mineralisation, in contrast to more brittle shale layers.***
- ***On deposit and micro-scale ,alteration and fluid pathways are observed between/adjacent to pyritic bands.***
- ***There are multiple generations of fine grained pyrite mineralisation.***
- ***Magnetite mineralisation associated with stilpnomelane, Norsethite (Ba/Mg Carbonate), and Iron/ Manganese rich carbonates. Also significant iron rich sphalerite, chalcopyrite and galena infill.***
- ***Galena, sphalerite and chalcopyrite consistently occur with similar timing relationships as infill within veins.***
- ***Further study and geochemical analysis would be needed to further understand the significance of fine grained pyrite, and its role in the formation of the deposit.***

ACKNOWLEDGEMENTS

Thank-you to my supervisor Richard Lilly for help and support with defining the project structure, and for assisting with sample analysis. Thank-you also to the staff at Adelaide microscopy for their assistance.

Appendix 6.

Reactive ground memorandum submitted to Mount Isa Copper Operations

THE UNIVERSITY of ADELAIDE

Memorandum

To	R. O'Sullivan, D. Taylor (MICO)
From	S. Connell (UofA)
Date	5th Oct, 2016
CC	R. Lilly (UofA)
Subject	Reactive Ground Investigation

EXECUTIVE SUMMARY

Reactive ground refers to any sedimentary rock which has a high risk (high potential) of undergoing exothermic, spontaneous chemical reactions when exposed to reactants such as oxygen, or external chemicals such as nitrates used in explosives. More specifically, it is ground which may pose a risk to drilling and blasting operations involved in the mining of rock. As it is a geological factor, it is the responsibility of the mine geologist team to firstly identify and quantify the risk, and secondly act to minimise this risk. This can only be done effectively if there is sufficient scientific understanding, and geological constraints on the cause of the reactive ground.

- This project aimed to quantify geological and geochemical constraints on the cause of reactive ground by testing the relationship between (fine grained) pyrite abundance (FeS_2; iron sulphide) and reactivity of a rock mass.
- From January – February 2016, 63 fresh rock samples were collected, specifically targeting pyritic shales.
- Results show that very few pyritic shale samples were classified as reactive.
- No statistical relationship could be identified between iron-sulphide abundance and reactivity.
- Results demonstrate that the risk of ground becoming reactive is not directly controlled by the concentration of fine grained pyrite.
- Those samples that were classed as highly reactive, were coated in a limonitic material (possibly microbial in origin), and were abnormally low in dolomitic minerals and alkaline elements.
- Reactivity appears to be a location/area specific occurrence, with the presence of sulphide minerals being a key ingredient.
- Other factors including, but not limited to; host lithology, gangue minerals, base of moderate leaching zone, and presence of bacteria may also be important in generating reactive ground conditions in the underground setting.

PROJECT AIMS

- Investigate the relationship between fine grained pyrite abundance and reactivity of a rock mass.
- Observe and quantify the reactivity response of fresh pyritic shale rock
- Explore the relationship between rock geochemistry and reactive ground

PROJECT OUTLINE:

A reactive ground sampling program commenced in January 2016 and was completed by September 2016. The program investigated the significance of fine grained pyrite abundance and the occurrence of reactive ground. The program involved sampling of fresh rock from the walls of active development drives (rather than rock chips or rock fragments derived from the floor) and locations planned for future stopes. A total of 63 samples were taken throughout the mine (mainly in the Enterprise system) and were tested at 55°C for 48 hours. Only 5 samples returned results indicating that they were potentially reactive, and were therefore sent away to be re-tested at 45°C for 12 days with the results to be confirmed.

There is currently no systematic relationship or geological constraints on what factors contribute to rock becoming reactive, or if the relative abundance of fine grained pyrite directly influences reactivity. A better understanding is important for confidently identifying risk, and for implementing cost-effective safety management practices.

The Q356 incident involved the minor reaction of nitrates within a drill hole, overflowing of a reacting liquid, and raised temperatures. This location was outside the base of moderate leaching zone and so did not meet the criteria for reactive ground at the current time. Pyritic shale was not seen as a hazard for reactive ground and so no reactive ground pre-cautions were taken. Following this incident, the significance of pyritic shale in causing reactive ground required investigating. Less emphasis is now placed on the Base of Moderate leaching zone as a direct indicator of reactive ground and more emphasis is placed on pyritic shale when identifying risk. Factors contributing to this incident included the drill-hole being horizontal, allowing retention of fine particles and water, facilitating oxidation of pyrite particles. The long lag time between drilling and blasting (9 months) also allowed time for oxidation processes to weather the pyritic shale.

In this investigation, the relationship between fine grained pyrite and reactive ground is interpreted using pyritic shale samples collected underground and tested through the Mount Isa Mines testing procedure. I test the hypothesis that fine grained pyrite abundance is directly related to reactivity of a rock mass.

BACKGROUND ON REACTIVE GROUND

Reactive ground is rock containing sulphide minerals (mainly pyrite) which have the potential to undergo spontaneous, exothermic reactions after coming into contact with a reactant or oxidiser (oxygen, water, nitrate chemicals). Because of the sudden release of heat, and potential to pre-detonate explosive products, reactive ground is a significant safety hazard for underground mining operations, operating within sulphide rich sedimentary rock. The reactions occur due to the weathering of iron sulphide. This can occur just through exposure to oxygen in the mine environment. The weathering solutions containing ferrous irons and sulphuric acid, initiate ongoing reactions upon contact with nitrates, which release heat and increase the temperature of the drill-hole.

Drilling and blasting of rock masses using nitrate explosives is a routine process in mining production, and so understanding and managing this risk is necessary for the successful operation of the mine. Currently there is no definitive relationship which describes reactive ground, or a strategy to confidently test for it. Factors thought to contribute to reactive ground include moisture, oxidising conditions, concentration of pyrite (or other sulphides) in the host rock, the poor thermal conductivity of shale (which traps heat within confined areas), and grain size (fine grained pyrite).

It is though that sulphide content alone is not a reliable indicator of degree of reactivity. However, the presence of high amounts of sulphide minerals can generate heat through spontaneous combustion, which can in turn accelerate reactivity reactions. Additionally, high ferrous ion concentrations are known to help accelerate reactions. Partial oxidation of sulphides also increases reactivity because the weathering phase is partially completed. This generates both an acidic environment, and ferrous ions. Common gangue minerals may also interact with the rock to either increase or reduce the reactivity.

Indicators for potential reactive ground include the presence of sulphides in black shale sediments, the presence of white or yellow salts on the rocks, acidic conditions (yellow/red limonitic staining), significant corrosion of rock bolts or mesh (underground infrastructure), fine grain size of sulphides, and if the rock occurs just below the base of moderate leaching zone.

SAMPLING METHODOLOGY

Reactivity sampling and testing is a crucial component of reactive ground management. It must be noted that it is not physically possible, or economically viable to statistically take enough rock samples to characterise the geology, and hence the reactivity of the Mount Isa Mine. Results from this project will only serve as an indication of how pyritic shales react. Testing for reactivity needs to be targeted to analyse the rocks containing sulphides in order to identify the "worst case" reactive rock samples, and hence minimise the degree of risk. Therefore, this study used 63 fresh pyritic shale rock samples (1 – 10kg) taken from *in-situ* locations on the walls of mine drives. Multiple pyritic shale samples were collected from each specific location, with each sample containing different relative abundances of fine grained pyrite. These percentage ranges included 0%, 0-10%, 10-20% and >20%. Sampling was undertaken from a variety of locations across the Mount Isa Copper Mine, but were focussed within the Enterprise system (Figures 1-3), where mine production is currently focussed.

In order to sample from useful locations, a sampling method which was representative of the orebodies was developed. I focussed on areas of current activity/development to increase practicality of the project, and targeted 'worst case scenario' rock types, by sampling rocks with a high abundance of fine grained pyrite. I used drill-core data, geological mapping, development inspections, and underground knowledge from discussions with the Mount Isa geologists, to plan useful sampling locations. Locations contained abundant fine grained pyrite mineralisation, were in active areas of development, and could be readily accessed. Sampling challenges included locations being barricaded, other operations occurring in the area, stockpiles blocking sampling locations, lack of available pyrite to sample, unsafe conditions (heat, dust, no ventilation) and maintaining safe working conditions in areas of limited infrastructure.

The relative percentage of fine grained pyrite in the rock samples was estimated while underground, grouped into sample bags based on this estimate, and labelled. The location was recorded using prepared maps of the mine drives. Once at the surface, the samples were validated for the amount of fine grained pyrite by visual inspection, and were more accurately grouped and labelled for sample testing. Geological descriptions and photographs for each sample were also recorded in order to establish any relationships or correlations. The samples were then stored in sealed bags, and placed in an industrial fridge to limit oxidation processes. Half of each sample was then assayed to derive geochemical data, while the other half was used for reactivity testing.

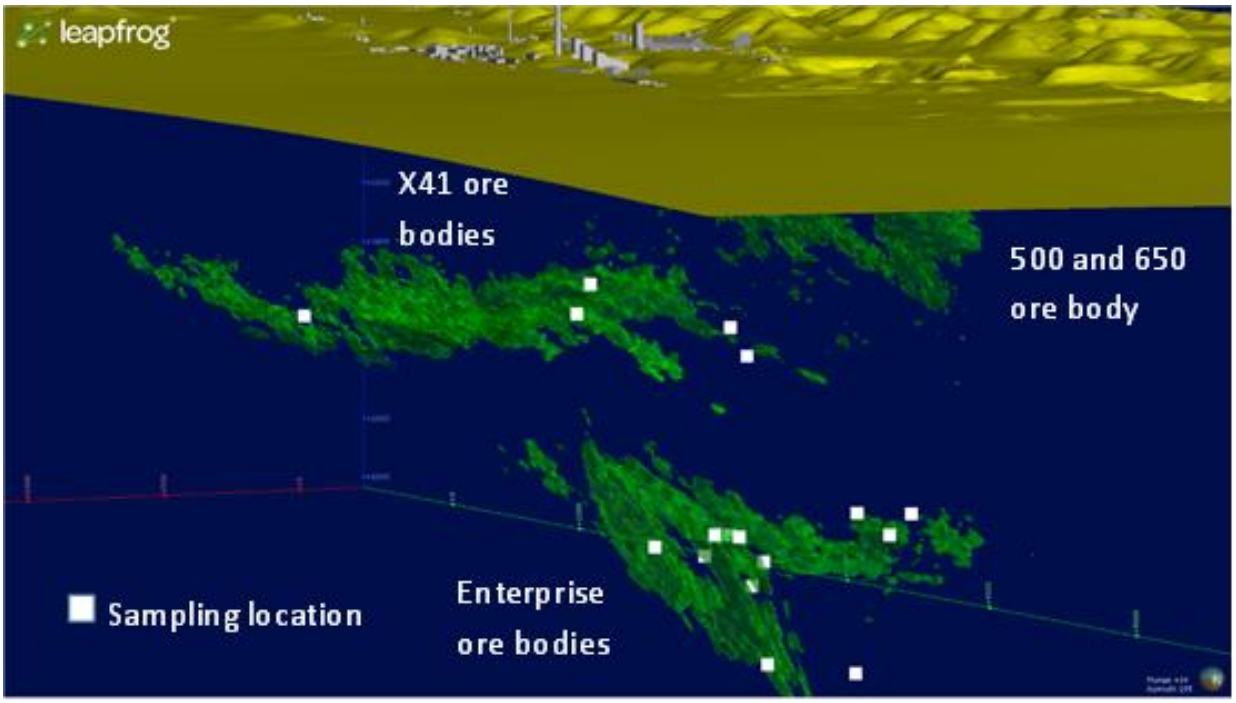

Figure 1: Locations where rock samples were taken from underground. These samples were used for both reactive ground testing and for further research on fine grained pyrite using research techniques.

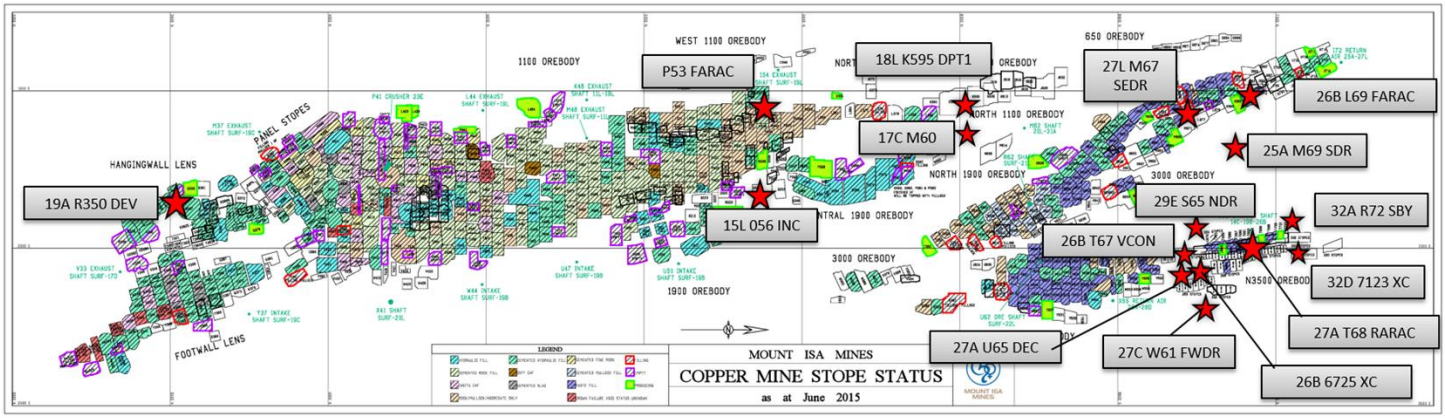

Figure 2: Map of the Mount Isa underground mining stopes, showing the approximate locations of where sampling was conducted. The majority of sampling was done in the Enterprise system; 3000 and 3500 ore bodies.

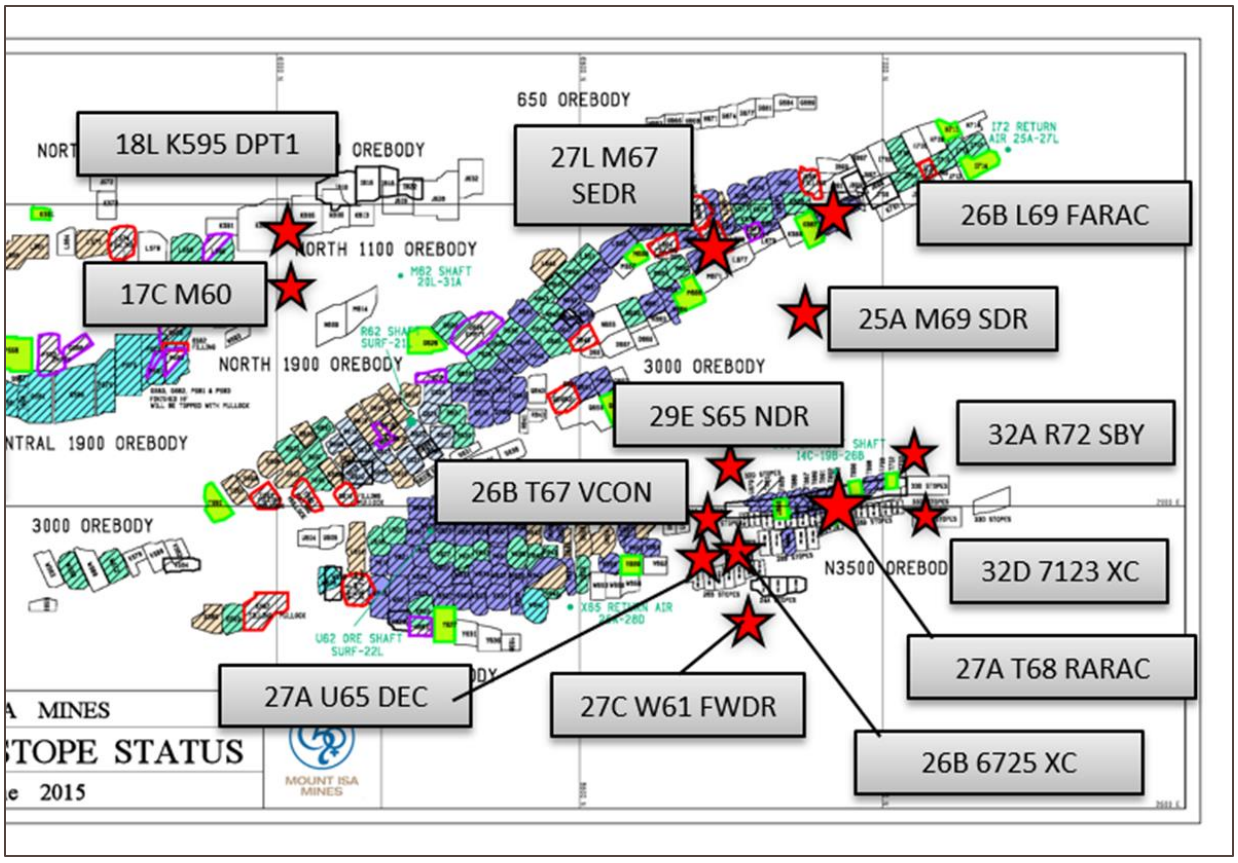

Figure 3: Detailed map of the Mount Isa underground mining stopes, showing the approximate locations of where sampling was conducted on the Enterprise side of the mine. The majority of sampling was done in the Enterprise system, namely the 3000 and 3500 ore bodies.

REACTIVE GROUND RESULTS

Sixty three pyritic shale samples were sampled underground from the Mount Isa mine (mainly in Enterprise), and tested for reactivity using the Mount Isa Mines test method. The results are as follows.

SAMPLE ID	Level	% Fe	% S	% Fe + % S	Estimated FGP	Exotherm (55° for 48 hours)
RG32D7123XC001	32D	5.24	2.67	7.91	0	-0.3
RG32D7123XC002	32D	9.97	8.19	18.16	1-5%	-0.6
RG32D7123XC003	32D				10-15%	-0.5
RG32D7123XC004	32D	18.1	17.3	35.4	>20%	-0.8
RG32AR72SBY001	32A	8.97	4.31	13.28	0	-0.3
RG32AR72SBY002	32A	19.3	17.25	36.55	1-8%	-0.4
RG32AR72SBY004	32A	28.8	32	60.8	>30%	0.7
RG27AU65DEC002	27A				5-10%	0.4
RG27AU65DEC004	27A	29.9	30.7	60.6	20-40%	0.2
RG27AT68RARAC001	27A	11.45	3.97	15.42	<0.5%	0.1
RG27AT68RARAC002	27A	34.3	26.6	60.9	2.5	0.5
RG27AT68RARAC003	27A	32.2	28.6	60.8	0.1	1.4
RG27AT68RARAC004	27A				20-50%	0.6
RG29ES65NDR001	29E	5.95	2.24	8.19	<0.5%	1.7
RG29ES65NDR002	29E	12.05	10.2	22.25	1-6%	1.5
RG29ES65NDR003	29E	19.55	20.3	39.85	10-15%	0.8
RG29ES65NDR004	29E	17.85	18.15	36	20- 40%	-0.3
RG26BT67VCON001	26B				0-1%	0.6
RG26BT67VCON002	26B	7.9	3.67	11.57	1-6%	0.4
RG26BT67VCON003	26B				0.1	0
RG26BT67VCON004	26B				20-40%	0.2
RG27CW61FWDR001	27C	7.61	4.17	11.78	<1% Trace	0.6
RG27CW61FWDR002	27C	22.8	16.4	39.2	5-10%	1.5
RG27CW61FWDR003	27C	18.25	16.65	34.9	0.17	1.1
RG27CW61FWDR004	27C	25.7	16.25	41.95	20-30%	1.6
RG25AM69SDR002	25A				<5%	**25.7**
RG25AM69SDR003	25A				13-15%	1
RG26BL69FARAC001	26B	11.85	9.4	21.25	<0.5%	1.5
RG26BL69FARAC002	26B	20.1	16.65	36.75	1-6%	1.9
RG26BL69FARAC003	26B	27.8	24.5	52.3	10-15%	1.9
RG26BL69FARAC004	26B	27.6	24.8	52.4	0.2	1.6
RG25AR63NDR001	25A	4.15	0.01	4.16	<0.5%	-0.5
RG25AR63NDR002	25A	7.51	2.06	9.57	1-2%	-0.3
RG25AR63NDR003	25A	21.2	5.36	26.56	10-20%	-0.1
RG25AR63NDR004	25A	22.3	19.05	41.35	0.2	0.9
RG27LM67SEDR001	27L				0	-0.4
RG19AR350DEV001	19A	4.65	2.69	7.34	<0.5%	0.3
RG19AR350DEV002	19A	16.6	17.55	34.15	5-10%	0.0
RG19AR350DEV003	19A	16.2	17.3	33.5	0.17	-0.3
RG19AR350DEV004	19A	18.35	18.75	37.1	20 - 50%	-0.3
RG19AR350DEV005	19A	25.1	28.2	53.3	>40%	-0.3

SAMPLE ID	Level	% Fe	% S	% Fe + % S	Estimated FGP	Exotherm (55° for 48 hours)
RG18LK595DEV001	18L	3.99	1.53	5.52	0	1.1
RG18LK595DEV002	18L	6.06	4.11	10.17	0-10%	1
RG18LK595DEV003	18L	9.75	8.71	18.46	0.1	0.6
RG18LK595DEV004	18L	7.99	4.37	12.36	0.3	0.2
RG15LO56INC001	15L	3.33	1.08	4.41	0	0.6
RG15LO56INC002	15L	3.25	0.97	4.22	0-1%	-0.5
RG15LO56INC003	15L	13.6	15.65	29.25	10-20%	-0.2
RG15LO56INC004	15L	18.1	19.8	37.9	20-40%	-0.1
RG15L056INC005	15L	26.6	31	57.6	50-70%	0.3
RG16LM60INC001	NLV	6.49	3.43	9.92	<1%	0.9
RG16LM60INC002	NLV	4.76	1.58	6.34	0-3%	1
RG16LM60INC003	NLV	21.9	20.6	42.5	10-15%	0.8
RG16LM60INC004	NLV	26.1	30.4	56.5	20-30%	0.7
RG17CP53FARAC001	17C	4.6	1.87	6.47	0	0.2
RG17CP53FARAC002	17C	19.15	18.3	37.45	5 - 10%	0
RG17CP53FARAC003	17C	15.05	16.3	31.35	15-20%	-0.2
RG17CP53FARAC004	17C	24.3	35.9	60.2	20-50%	0.2
RG28DJ712001	28D	2.96	1.33	4.29	<0.5%	**28.2**
RG28DJ712002	28D	6.79	5.22	12.01	<0.5%	0.6
RG28DJ712003	28D	6.76	4.85	11.61	1-5%	**4**
RG28DJ712004	28D	8.08	8.5	16.58	5-10%	**51.3**
RG28DJ712005	28D	12.3	13	25.3	5-10%	**37.6**

Table 1: Results of all samples that underwent reactive ground testing. Data includes Fe abundance, S abundance, and estimated fine grained pyrite abundance. The exotherm represents the temperature raised above the background temperature of 55 degrees celcius.

REACTIVE GROUND RESULTS

Reactive samples

Results show that only 5 samples produced a reactive response during the testing procedure. Four of the reactive samples were from the 28D J712 location (figure 4). These samples came back reactive despite low fine grained pyrite abundances (5-10%). Temperatures recorded were up to 50° C above background temperatures (over 100° C) during testing. One of the samples, which reacted 28 degrees above the background temperature, had the ***lowest*** iron content out of all 63 pyritic shale samples, with an iron content of <3%. All samples from this location (J712) were a unique rock type. The rocks were covered in a yellow unidentifiable gritty/clay/limonitic material. Another sample from '25A M69 SDR' also came back highly reactive. It reached 26 degrees above the background temperature. It had an estimated pyrite abundance of around 5% (see figure 6).

Non-reactive samples

Samples from 15L 056 INC (Figure 5) contained 60% iron sulphide (assayed), but only returned reactivity temperatures of 0.3 degrees above background temperature (non-reactive). Another sample from this same location, which had an estimated 0% fine grained pyrite (100% black shale), returned a reactivity temperature of 0.6 degrees above background temperature.

Mineralogy and reactivity

The iron and sulphur content of all samples was plotted against reactivity. This is shown in figures 7 - 9. No statistical relationship has been identified between iron sulphide content and reactivity, or with sulphur or iron content alone. The samples ranged in iron sulphide content from 0% -60%. Reactive samples recorded iron sulphide contents between 1-25%. Evidently, there were many samples with a very high iron sulphide content, which did not produce any reaction.

Chemical data

The trace element geochemistry (bulk rock assay) was recorded for each sample that underwent testing. There was no obvious relationship between any trace element and reactivity. However, highly reactive samples contained elevated levels of phosphorous (up to 500 ppm), copper (up to 2%) and bismuth (80 – 130 ppm). They were also highly depleted in common alkali elements such as calcium, potassium, magnesium and barium.

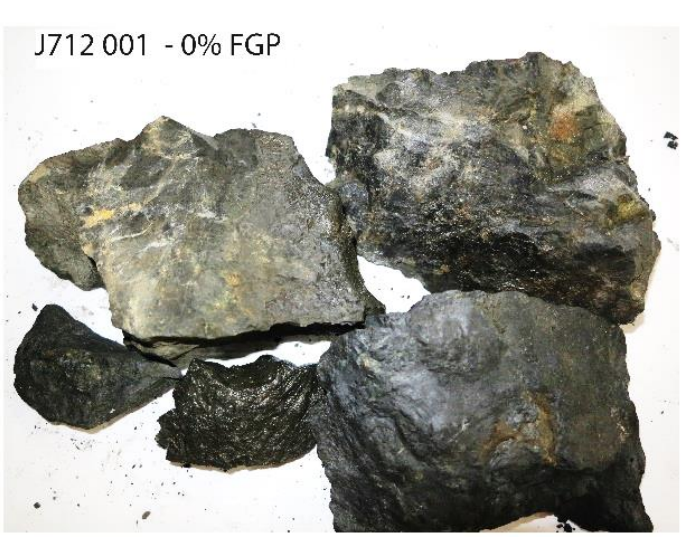

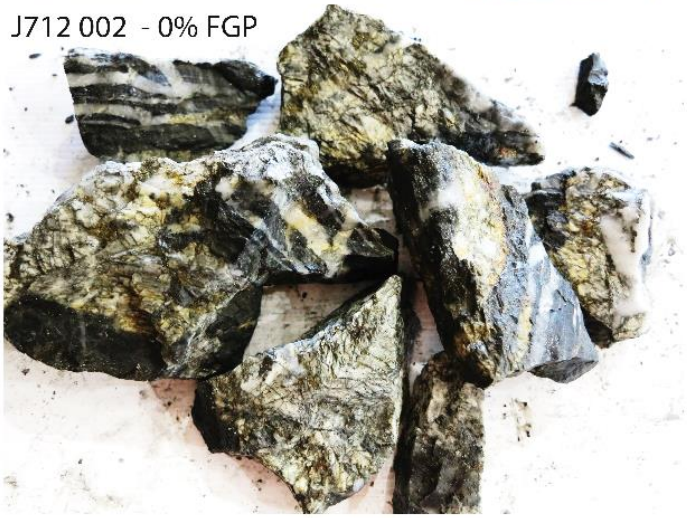

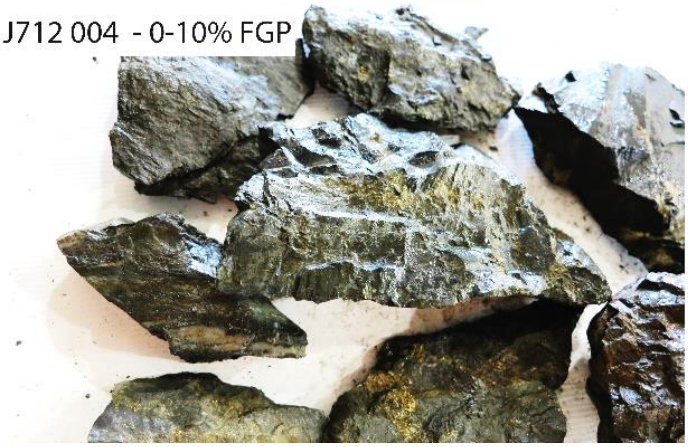

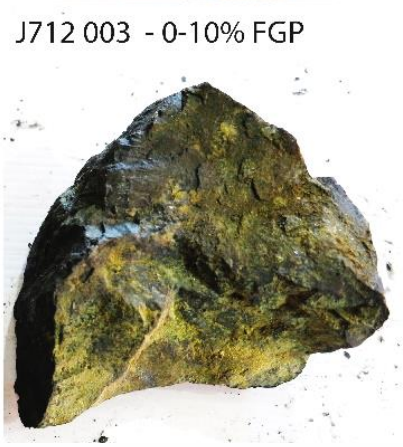

SAMPLE ID	% Fe	%S	%Fe + %S	Estimated FGP amount	Reactivity (degrees)
RG28DJ712001	2.96	1.33	4.29	0	**28.2**
RG28DJ712002	6.79	5.22	12.01	0%	0.6
RG28DJ712003	6.76	4.85	11.61	0-5%	**4**
RG28DJ712004	8.08	8.5	16.58	1-10%	**51.3**
RG28DJ712005	12.3	13	25.3	1- 10%	**37.6**
RG28DJ712006	7.87	8.54	16.41	1-10%	

Figure 4: Reactivity results and samples photos from the 28D J712 sampling location. Data includes iron abundance, sulphur abundance, and estimated fine grained pyrite abundance. Reactivity is measured as the temperature raised above the background temperature of 55 degrees during testing. Several of these samples were highly reactive.

056 INC rock samples that underwent testing

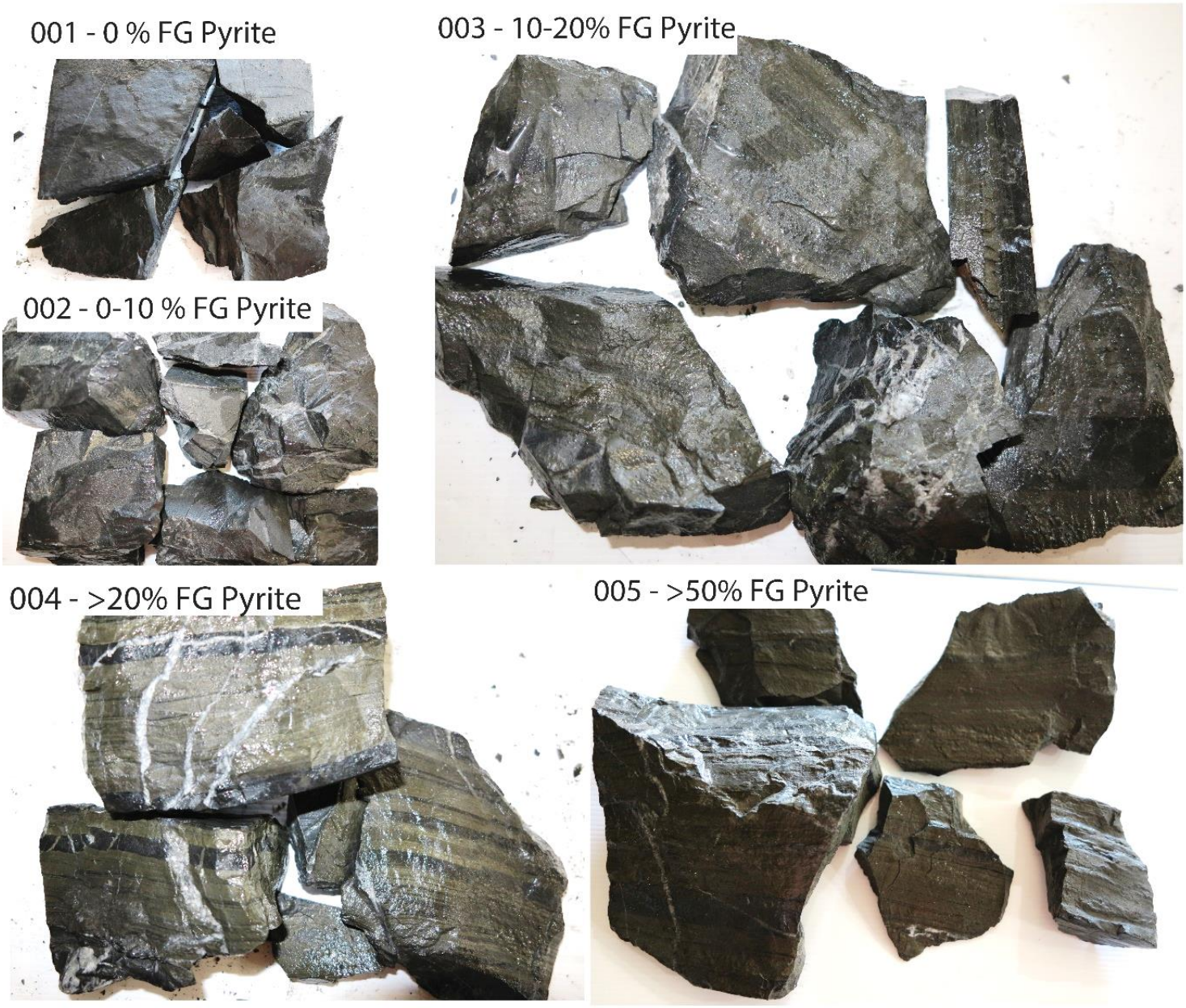

SAMPLE ID	% Fe	%S	%Fe + %S	Estimated FGP amount	Reactivity (degrees)
RG15LO56INC001	3.33	1.08	4.41	0%	0.6
RG15LO56INC002	3.25	0.97	4.22	0-1%	-0.5
RG15LO56INC003	13.6	15.65	29.25	Variable 10-20%	-0.2
RG15LO56INC004	18.1	19.8	37.9	20-40%	-0.1
RG15L056INC005	26.6	31	57.6	>50%	0.3
RG15L056INC006	27.8	32.1	59.9	>50%	

Figure 5: Reactivity results and sample photos from the 15L 056 INC sampling location. Data includes iron abundance, sulphur abundance, and estimated fine grained pyrite abundance. Reactivity is measured as the temperature raised above the background temperature of 55 degrees during testing.

SAMPLE ID	Estimated FGP amount	Reactivity (degrees)
RG25AM69SDR002	5%	**25.7**
RG25AM69SDR003	13-15%	1

Figure 6: Photographs of reactive sample from M69 SDR, and the associated estimations of fine grained pyrite abundance. This sample reacted despite being mostly black shale, with only an estimated 5% pyrite abundance.

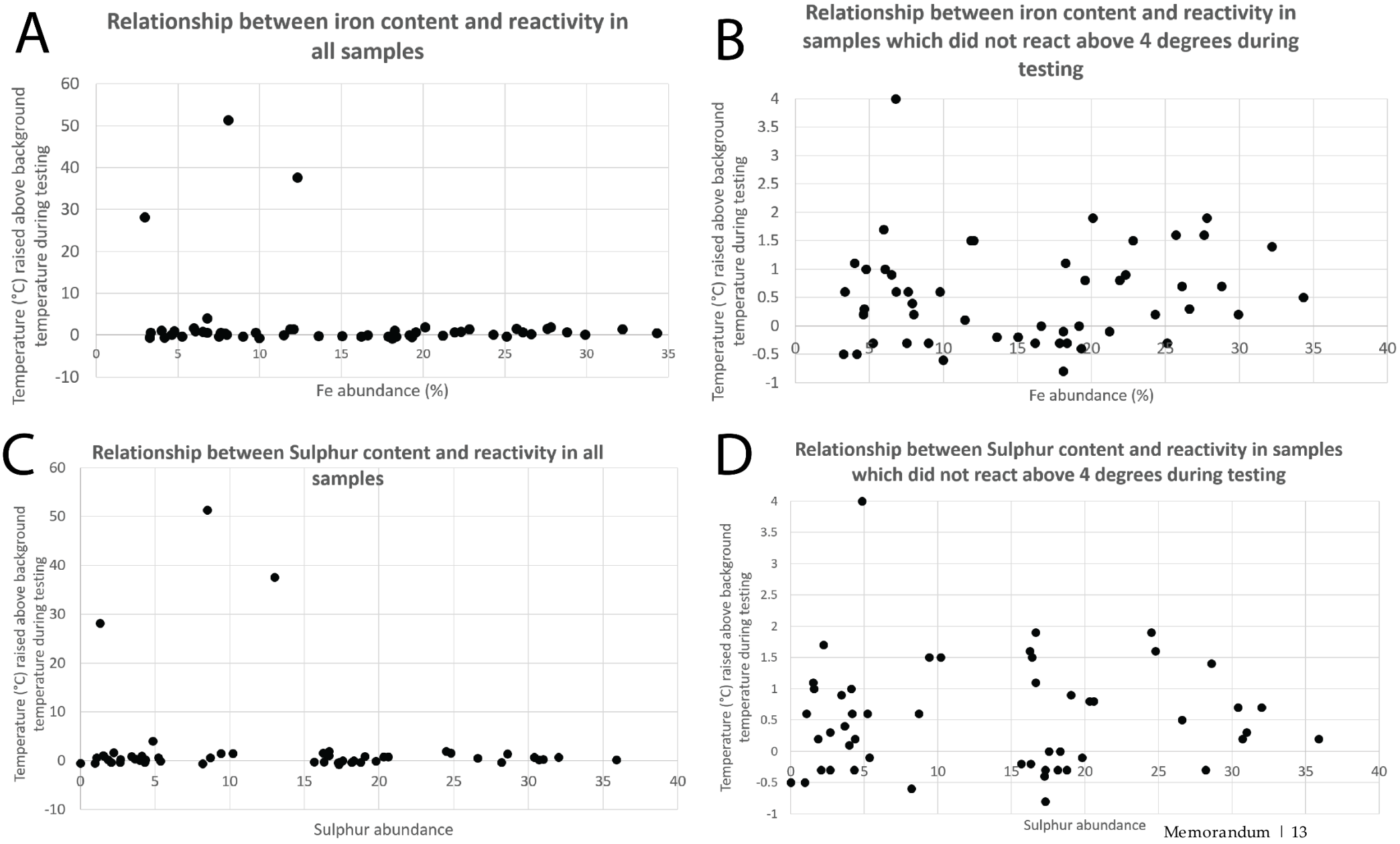

Figure 7: Graphs A and B show the relationship between estimated Iron % and reactivity during testing. Graphs C and D show the relationship between Sulphur %, and reactivity.

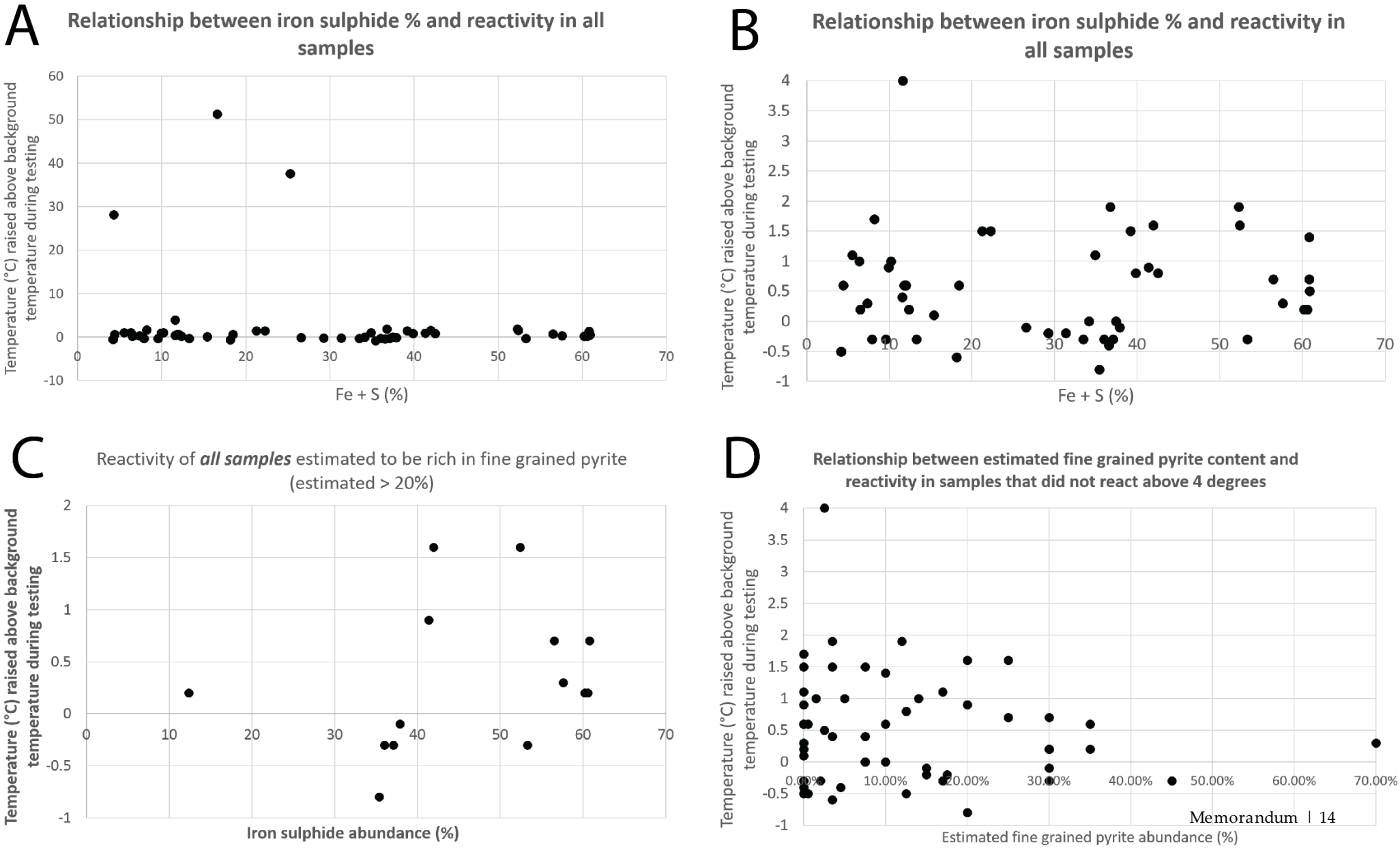

Figure 8: Graphs A and B show the relationship between iron sulphide % and reactivity during testing. Graphs C and D show the relationship between estimated fine grained pyrite %, and reactivity.

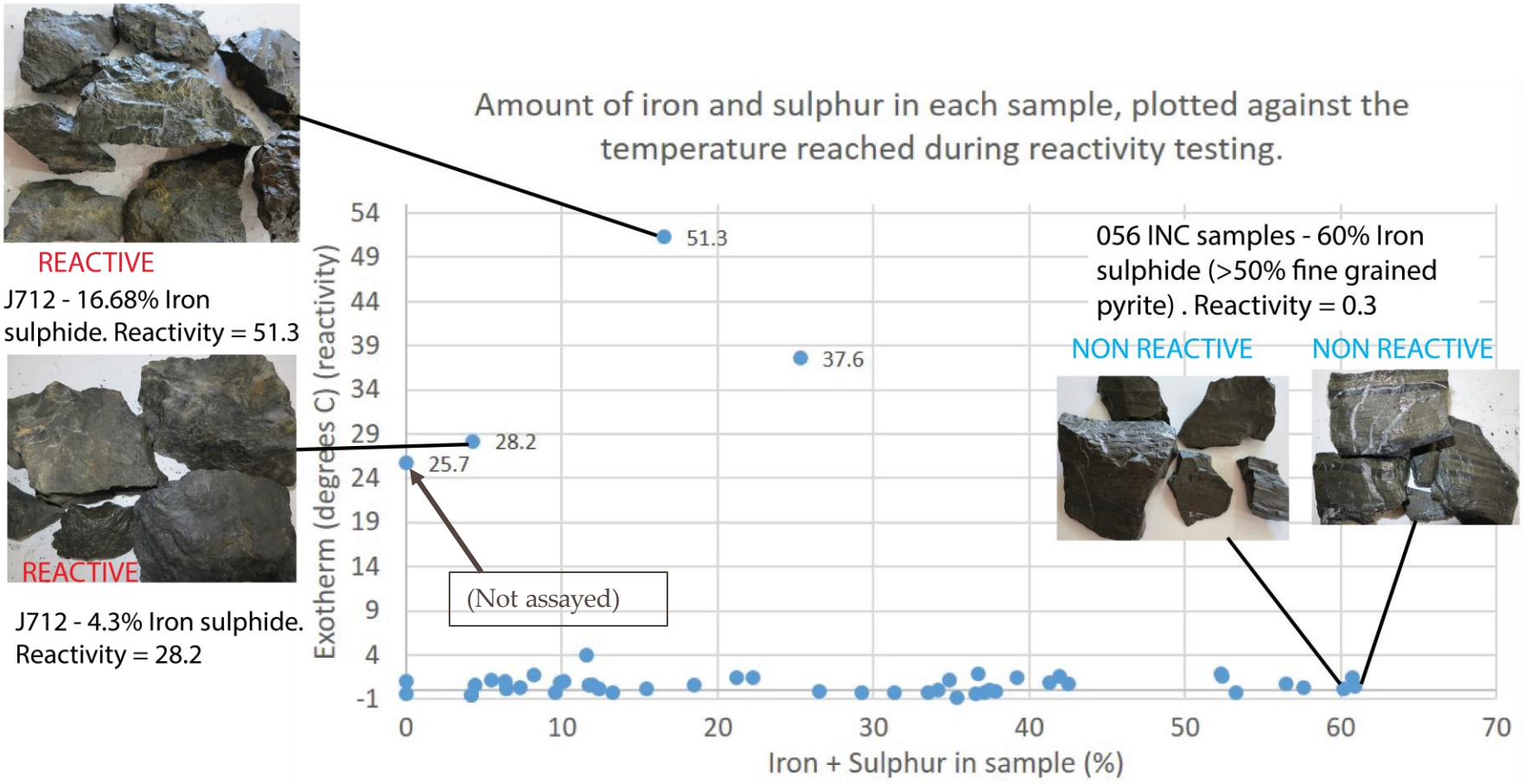

Figure 9: Graph showing the relationship between iron sulphide and reactivity. Pictures of reactive samples and samples rich in fine grained pyrite are included for reference.

Reactive ground sampling regularly conducted by Mount Isa geologists is carried out by not specifically targeting sulphides, but instead systematic sampling over a specified interval, in order to test a specific location or stope. It was noted that in past reactive ground memorandum documents (figures 10-13), when this method is used, there is often a clear pattern relating to the location of reactive samples. Reactive samples appear grouped together in particular zones, or areas of the mine. Examples of this are shown in the following figures, taken from MICO memorandums in late 2015/ early 2016.

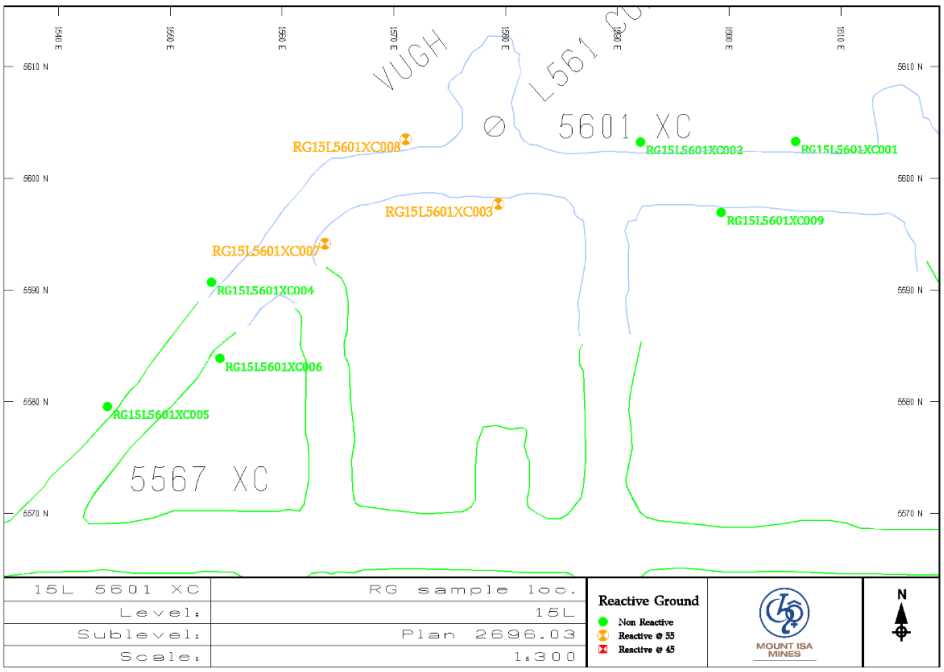

Figure 10: Image showing the distribution of reactive ground results in 15L 5601 XC

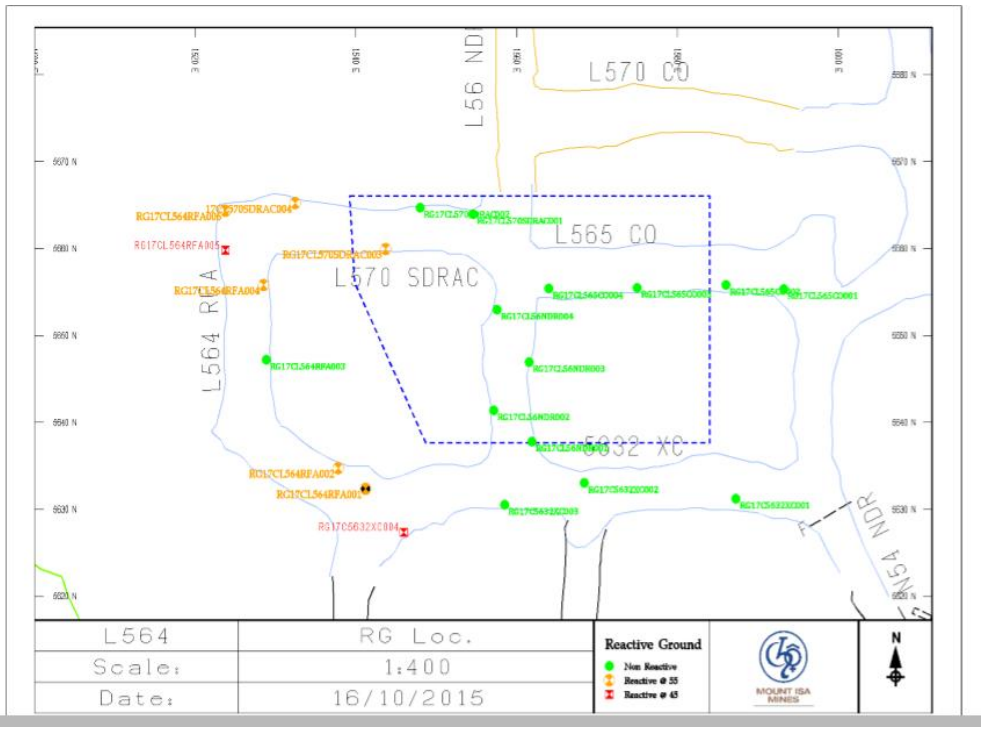

Figure 11: Image showing the distribution of reactive ground results in L564.

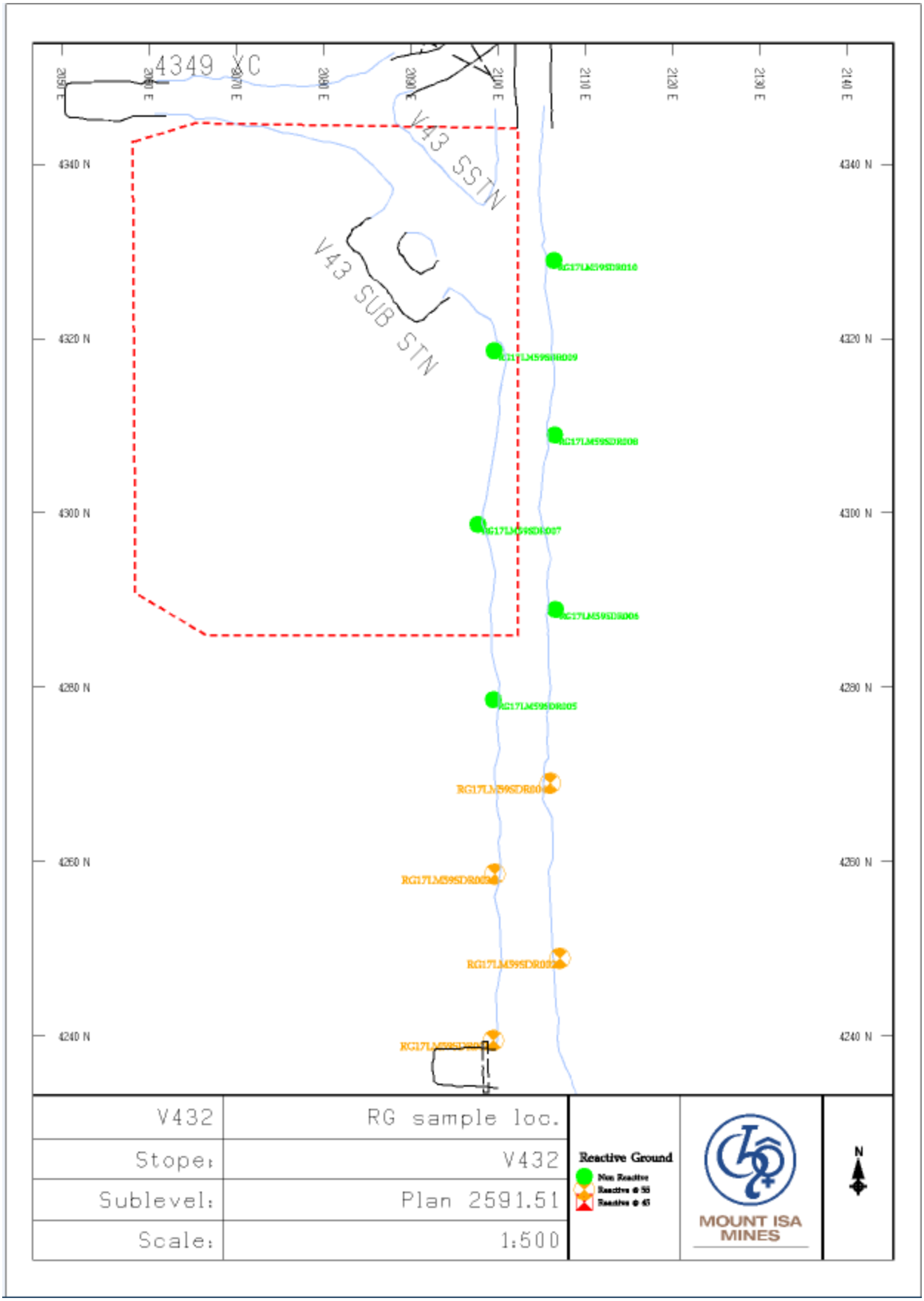

Figure 12: Image showing the distribution of reactive ground results around the V432 stope

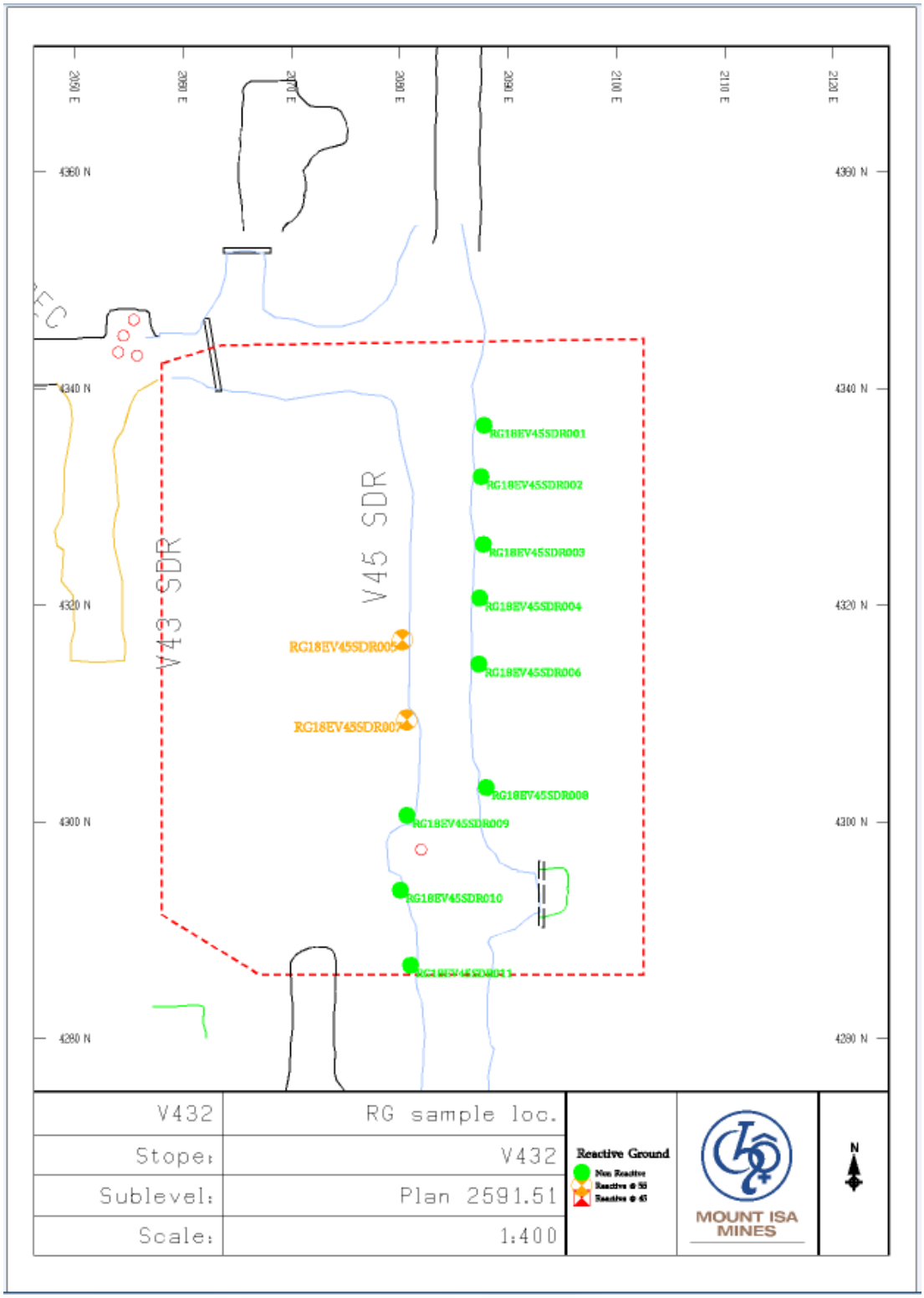

Figure 13: Image showing the distribution of reactive ground results around the V432 stope

INDIVIDUAL LOCATIONS

For individual locations, rocks with a variation in pyrite abundances were deliberately sampled to test the relationship between reactivity and fine grained pyrite. Rocks from the same location were used to eliminate the bias of external variables, which may vary between different locations (see figures 14-16).

- **15L 056 INC (X41)**

As fine grained pyrite abundance increased, reactivity also increased. However, all reactivity values were too small to have any significance. The most reactive sample contained the least amount of fine grained pyrite, and reacted to 0.6 degrees above background temperature.

- **W61 FWDR, T68 RARAC, R63 NDR (Enterprise)**

For these samples, as iron sulphide content increased, so did reactivity. However, there was not enough data for the results to be of statistical significance. Significant variation in reactivity existed for samples with similar amounts of iron sulphide.

- **K595 DEV, M60 INC, R350 DEV (X41)**

As iron sulphide content increased, reactivity appeared to decrease. This is the opposite relationship to what was hypothesised for the results. The samples with the lowest iron sulphide content reacted the highest (reacted to 1.1 degrees above background temperature).

- **P53 FARAC and L69 FARAC (Enterprise)**

These locations displayed unclear results with no systematic relationship observed.

RELATIONSHIP TO TRACE ELEMENT CHEMISTRY

The trace element geochemistry (bulk rock assay) was recorded for each sample that underwent testing (see Appendix). The abundance of each element for all samples was plotted against reactivity of all samples, to test if reactivity was related to any specific trace element (see Appendix for results). There was no obvious relationship between any trace element and reactivity.

Something that was significant to note was that the highly reactive samples (J712) were relatively enriched in phosphorous (up to 500 ppm), copper (up to 2%) and bismuth (80 – 130 ppm). They were also very low in the common alkali elements such as calcium, potassium, magnesium, manganese, and barium. These are common elements (Ca, Mg, Ba, Mn) which make up carbonate/dolomitic minerals at Mount Isa.

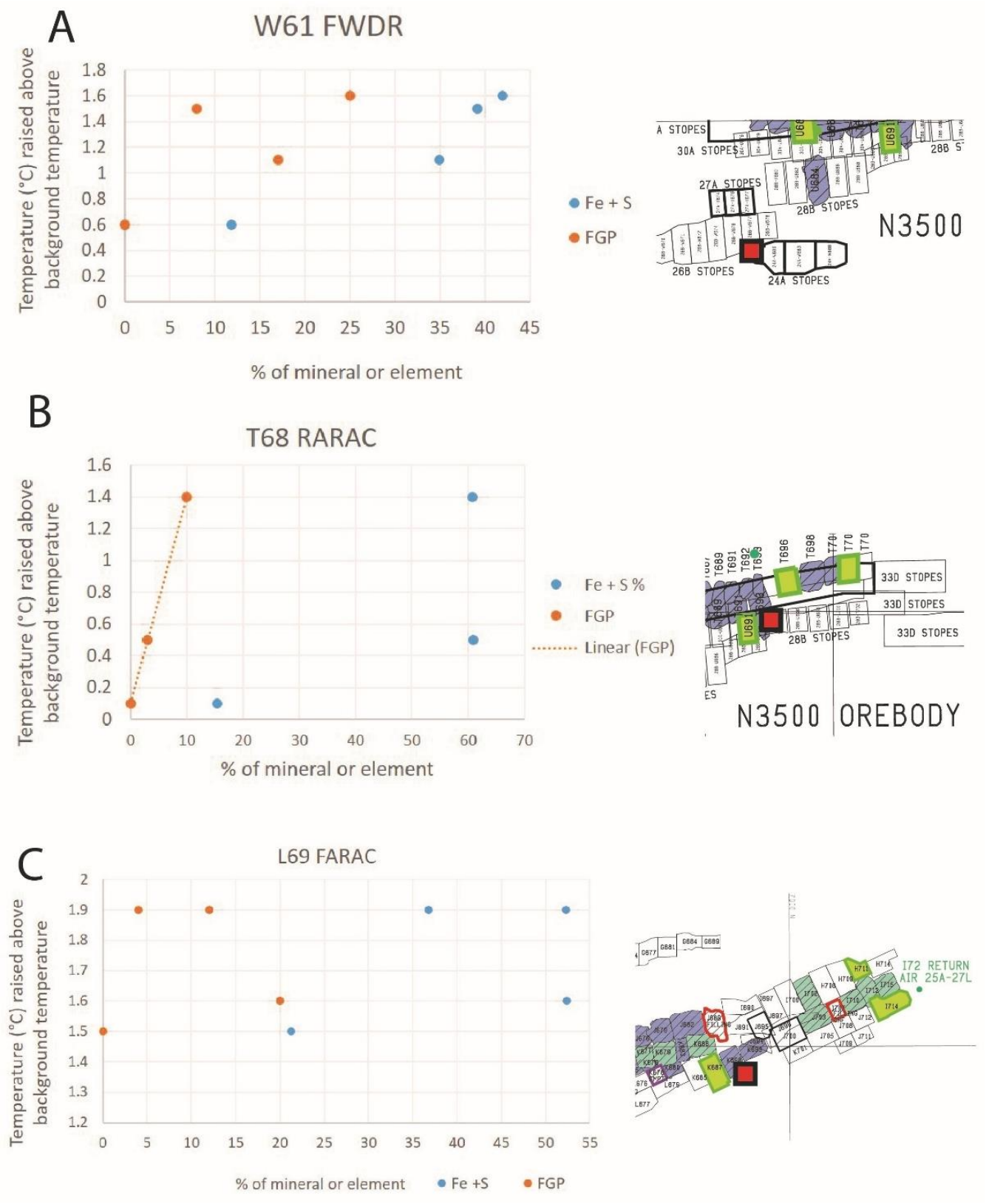

Figure 14: Comparison of samples from each individual location with varying fine grained pyrite abundances. This tests the relationship of fine grained pyrite with reactivity.

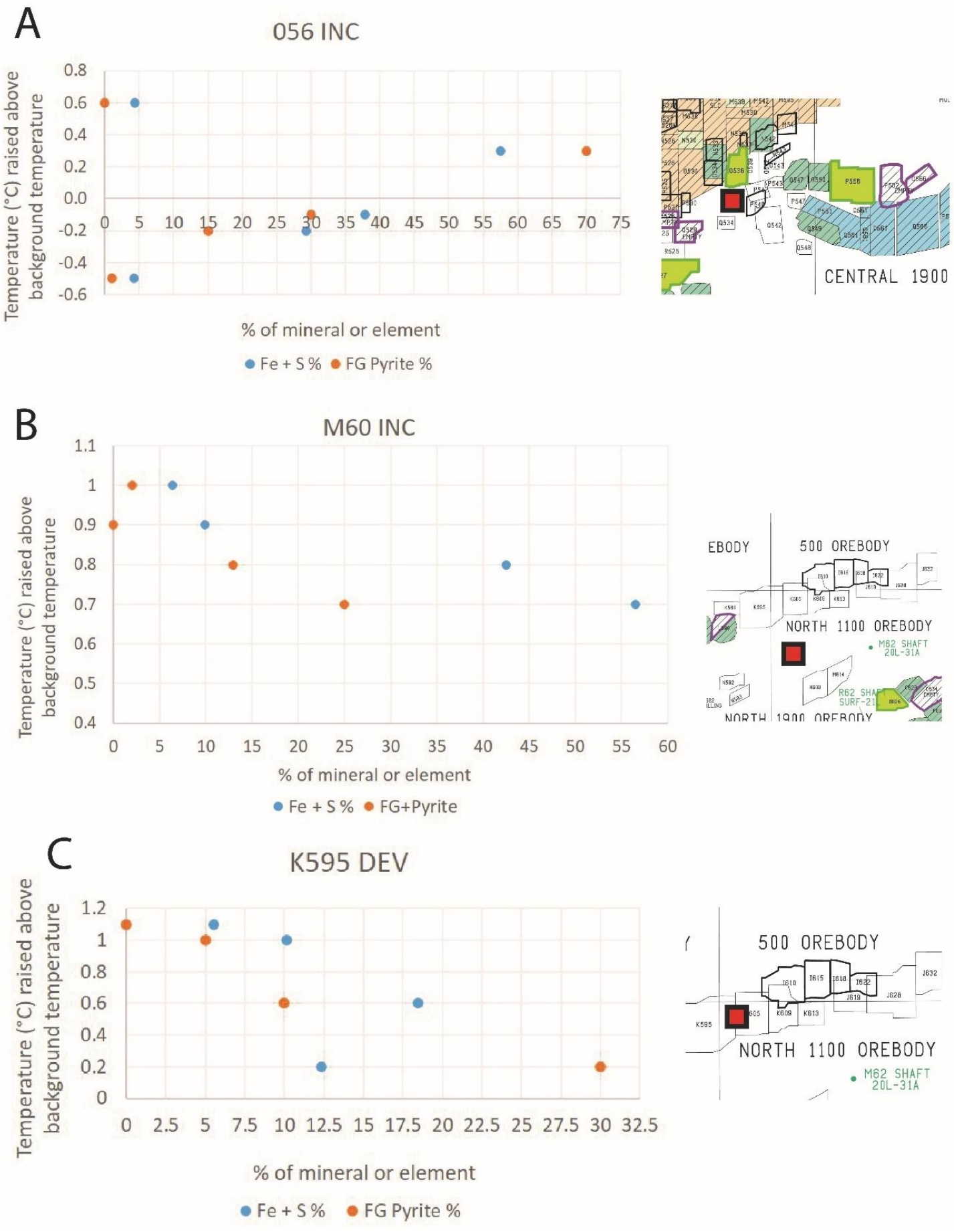

Figure 15: Comparison of samples from each individual location with varying fine grained pyrite abundances. This tests the relationship of fine grained pyrite with reactivity.

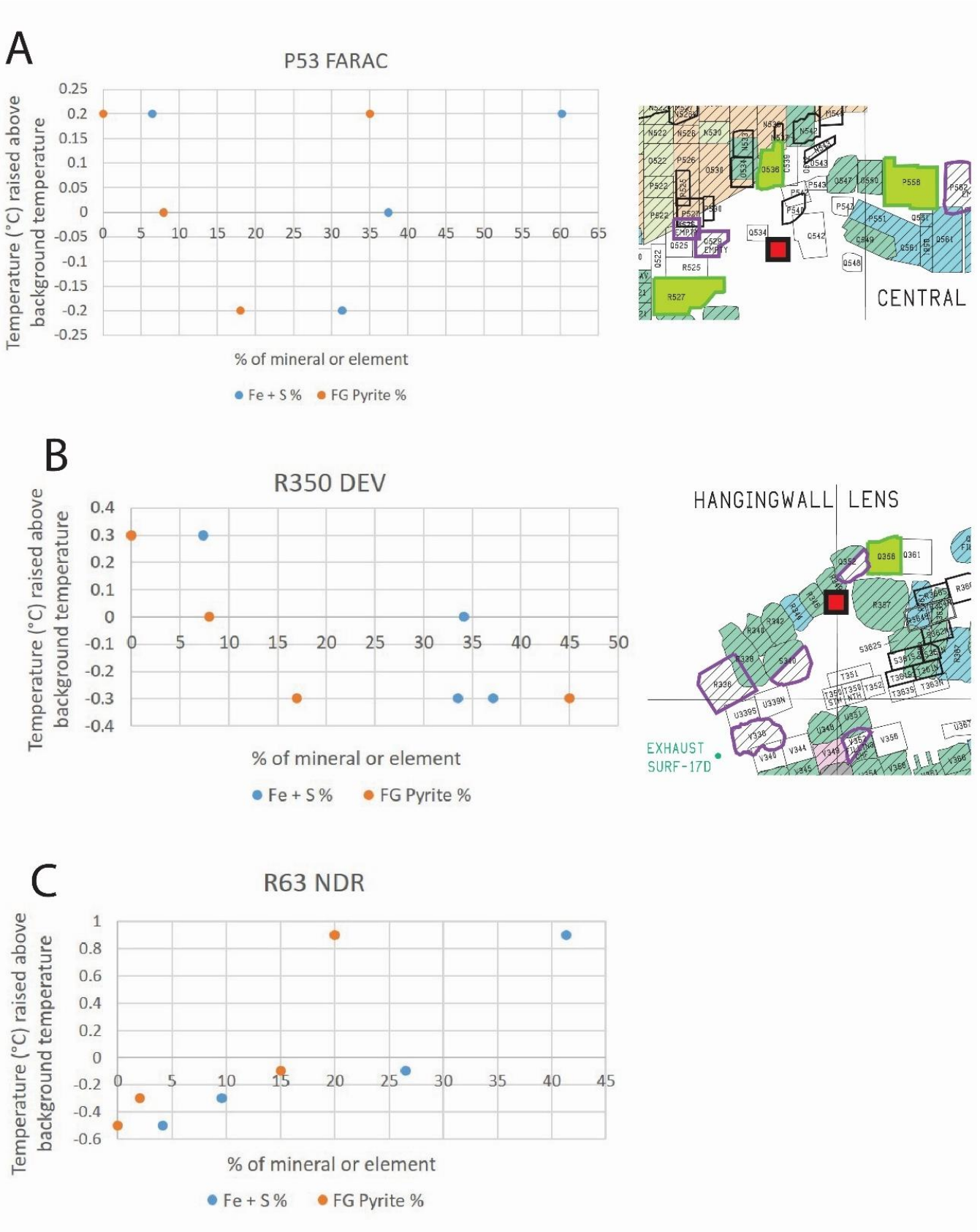

Figure 16: Comparison of samples from each individual location with varying fine grained pyrite abundances. This tests the relationship of fine grained pyrite with reactivity.

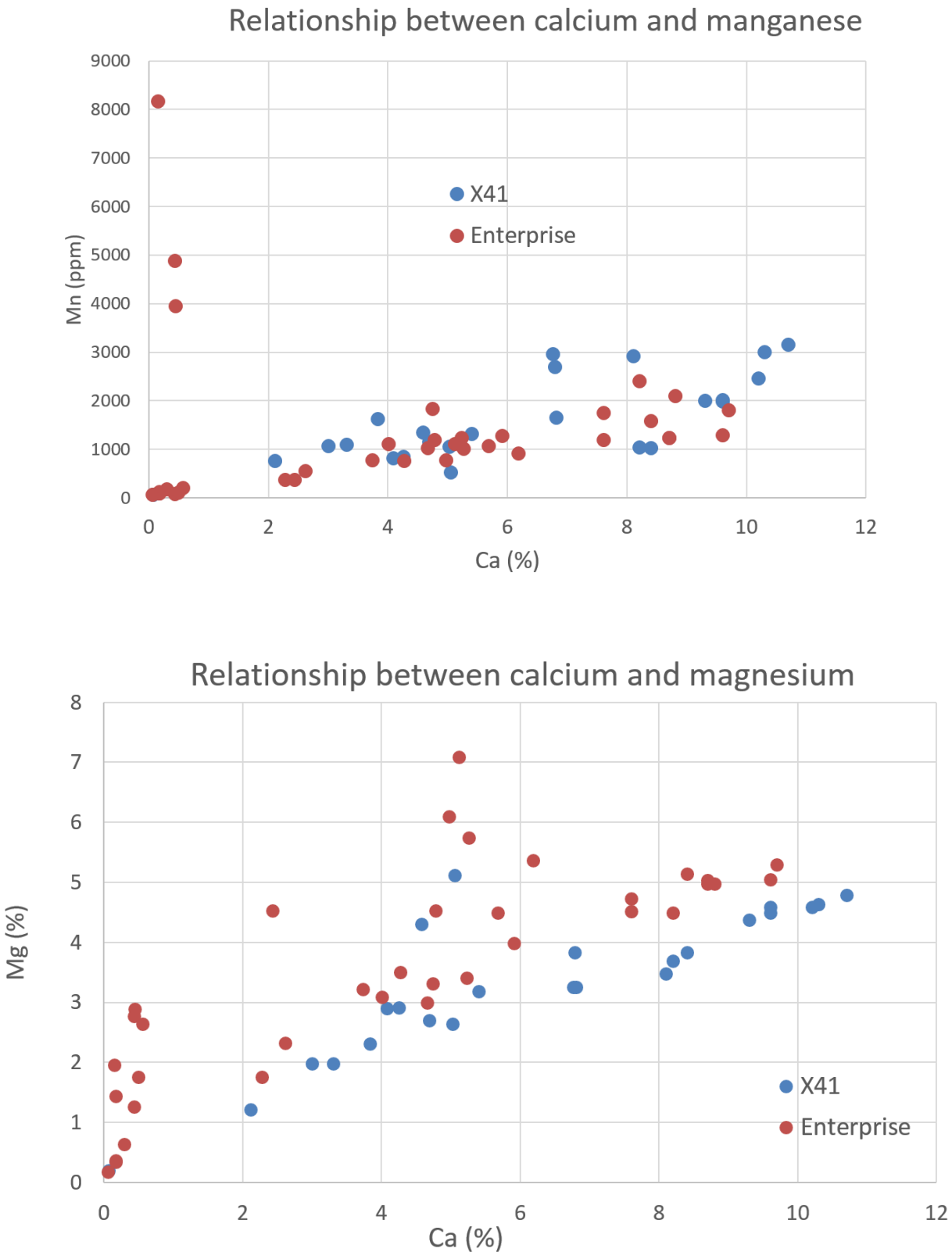

Figure 17: Relationship between alkaline elements found in dolomitic minerals. Magnesium and manganese display linear relationships with calcium, suggesting these elements predominantly occur within a single mineral (dolomite). Therefore, samples low in these elements can be interpreted as being low in dolomitic minerals.

DISCUSSION

The hypothesis for this reactive ground testing project was that fine grained pyrite was directly related to the reactivity of a rock mass, regardless of host lithology or other external variables. In the past, reactive ground has been assumed to be directly related to fine grained pyrite abundance within black shale sedimentary rocks. This is because of the fine grain size, and susceptibility to oxidation in the presence of a reactant (moisture, heat, oxygen, nitrate). Coupled with the Base of Moderate leaching zone, it has been used as an indicator for reactive ground risk within the Mount Isa Mine.

The aim of this project was to determine whether this relationship exists, or whether there are other geological factors involved. This will help implement cost-effective management practices for assessing reactive ground risk. It was expected that when using samples from the same location that location specific factors effecting results would be eliminated, and that reactivity would increase when fine grained pyrite abundance increased.

Primary results obtained by using the Mount Isa Mines testing procedure show a low number of pyritic rock samples (4 out of 63) producing a reactive response. Out of 63 samples containing variable amounts of fine grained pyrite only 4 samples were considered reactive and all contained relatively low amounts of fine grained pyrite. 3 of these highly reactive samples were from the same sampling location (freshly sampled from the wall of mine drives) and were coated by a gritty/yellow/limonitic coloured substance. They were also relatively enriched in phosphorous (common acidic element), copper, bismuth, and presumably silica. Although, iron sulphide concentrations were low, they may have contained enough for reactions to take place. This gives the interpretation that something unique about this location stimulated reactions to take place during testing. This was not solely the concentration of iron sulphide or fine grained pyrite.

Importantly, they contained relatively low abundances of Mg, Ca and Mn. Chemical graphs (figure 17) suggest these elements are strongly related and occur together, most likely as dolomite and/or calcium carbonate. The low relative abundance of these minerals in the reactive samples suggests that these minerals ***may*** play an important role in counteracting reactivity. Apart from these factors, there was no other unusual assay results for these samples. The final reactive sample was not assayed. However it was estimated to contain only 5% fine grained pyrite and offered no visual indication of why it may have reacted compared to other pyritic shale samples.

Additionally, there seem to be no statistical relationships between fine grained pyrite abundance, and reactivity to ammonium nitrate. The low proportion of reactive samples across the sampling program meant that if any relationships were interpreted, they would only be from data measurements taken between exotherms of -1° and 2°, which is classed as unreactive. This is a major limitation on the value of the results. Nonetheless, the results were plotted and data suggested that a wide range of reactivity existed for different abundances of iron-sulphide, and for different estimations of fine grained pyrite abundance.

Initial interpretation of the results is that the reactive ground risk of a particular rock mass is a location specific phenomenon and is not directly related to the abundance of fine grained pyrite. Sulphide mineralogy is proven to be a key ingredient, but results show the abundance of fine grained pyrite does not seem to make it more likely that reactive ground will occur. This is evident in this report with numerous rocks with over 50% iron sulphide being tested without any reaction occurring. The base of moderate leaching zone (BOML), presence of bacteria, and other chemical factors are likely to be involved. The relatively long time between drilling and loading of the hole, followed by further time between loading and blasting, combined with the presence of moisture, orientation of the drill-hole and thermal properties of the host rock, are likely to also be important factors involved in the occurrence of reactive ground.

The current method of sampling over systematic intervals within a mine drive, with specific sampling locations chosen irrespective of fine grained pyrite abundance, seems to be an appropriate pre-caution for risk management when planning future stopes.

If the current testing procedure is considered as a reliable and accurate simulation of chemical reactions of pyritic shale during mining, the operation of drilling and blasting into pyritic shale does not necessarily pose a high risk. If appropriate pre-cautions and protocols are followed, the occurrence of reactive ground should remain well managed.

CONCLUSIONS

- As originally understood prior to the Q356 incident, the ***concentration*** of fine grained pyrite does not seem to be a significant factor in increasing the likelihood of reactive ground occurring.
- Pyrite abundance may not serve as a ***direct indicator*** of reactive ground risk.
- Reactive ground risk seems to be a location specific phenomenon, relating to other factors.
- While reactive samples normally occur grouped together in specific areas, it is also evident that rocks from the same location can also vary significantly in reactivity (25A M69 SDR).
- The ***presence*** of iron sulphide (FeS_2, fine grained pyrite) in shale remains a ***key ingredient***, and an appropriate factor to incorporate into risk identification and assessment.
- The cause of the Q356 incident was likely not due to anomalously high pyrite concentrations, but more likely other factors such as:
    - The drill holes being horizontal; retaining fine sulphide particles from drilling, and water.
    - The drill holes were exposed to oxygen for up to 9 months, allowing weathering and oxidation of the pyrite which was present. This would have generated significant amounts of weathering solution, which could have reacted with nitrates in the ANFO products, when the hole was charged.
- While abundant pyrite can lead to reactive ground, there must be sufficient oxidation and weathering within the rock mass in order to generate weathering solutions which can react with the nitrates.
- There is a ***suggestion*** that a depletion in carbonate minerals (containing Ca, Mg, Mn) may lead to higher risk of reactivity. These elements may assist in counteracting (neutralising) acidic conditions which initiate reactions.
- The influence of carbonaceous gangue minerals is a potential pathway for future study.
- The base of moderate leaching zone, host lithology, presence of iron sulphide, groundwater, presence of sulphate reducing bacteria, and grain size are all factors which remain as potential factors contributing to the occurrence of reactive ground.

Appendix 7

Reactivity testing results for all reactive ground samples

Reactive Ground Test Results

			Date20/06/16
Sample	Run 1 (48HOURS 55°(	Exotherm (°C)	Observations
RG29ES65NDR003	Non Reactive	0.8	No overflow
RG29ES65NDR004	Non Reactive	-0.3	No overflow
RG32D7123XC001	Non Reactive	-0.3	No overflow
RG32D7123XC002	Non Reactive	-0.6	No overflow
RG32D7123XC003	Non Reactive	-0.5	No overflow
RG32AR72SBY004	Non Reactive	0.7	No overflow
RG26BT67VCON001	Non Reactive	0.6	No overflow
RG26BT67VCON002	Non Reactive	0.4	No overflow
RG26BT67VCON003	Non Reactive	0	No overflow
RG26BT67VCON004	Non Reactive	0.2	No overflow
RG27AU65DEC002	Non Reactive	0.4	slight overflow
RG27AU65DEC004	Non Reactive	0.2	slight overflow
BLANK	Non Reactive	0.5	No overflow

Reactive Ground Test Results

Date:11/06/16

Sample	Run 1 (48HOURS 55°(	Exotherm (°C)	Observations
RG18LK595DP1T004	Non Reactive	0.2	No overflow
RG17CP53RARAC001	Non Reactive	0.2	No overflow
RG17CP53RARAC002	Non Reactive	0	No overflow
RG17CP53RARAC003	Non Reactive	-0.2	No overflow
RG17CP53RARAC004	Non Reactive	0.2	No overflow
RG19A350DEV001	Non Reactive	0.3	No overflow
RG19A350DEV002	Non Reactive	0.0	No overflow
BLANK	Non Reactive	-0.2	No overflow

Reactive Ground Test Results

Date:12/06/16

Sample	Run 1 (48HOURS 55°(	Exotherm (°C)	Observations
RG19A350DEV003	Non Reactive	-0.3	No overflow
RG19A350DEV004	Non Reactive	-0.3	No overflow
RG19A350DEV005	Non Reactive	-0.3	No overflow
RG25AR63NDR001	Non Reactive	-0.5	No overflow
RG25AR63NDR002	Non Reactive	-0.3	No overflow
RG25AR63NDR003	Non Reactive	-0.1	No overflow
RG25AR63NDR004	Non Reactive	0.9	No overflow
BLANK	Non Reactive	-0.3	No overflow

Reactive Ground Test Results

Date:12/06/16

Sample	Run 1 (48HOURS 55°(	Exotherm (°C)	Observations
RG26BL69FARAC001	Non Reactive	1.5	No overflow
RG26BL69FARAC002	Non Reactive	1.9	No overflow
RG26BL69FARAC003	Non Reactive	1.9	No overflow
RG26BL69FARAC004	Non Reactive	1.6	No overflow
RG25AM69SDR002	REACTIVE	**25.7**	Small overflow
RG25AM69SDR003	Non Reactive	1	No overflow
RG28DJ712001	REACTIVE	**28.2**	Med overflow
BLANK	Non Reactive	1.2	No overflow

Reactive Ground Test Results

Date:14-6-16

Sample	Run 1 (48HOURS 55°(	Exotherm (°C)	Observations
RG28DJ712002	**REACTIVE**	**4**	No overflow
RG28DJ712003	Non Reactive	0.6	No overflow
RG28DJ712004	**REACTIVE**	**51.3**	Medium overflow
RG28DJ712005	**REACTIVE**	**37.6**	Medium overflow
RG27AT68TATAC001	Non Reactive	0.1	No overflow
RG27AT68TATAC002	Non Reactive	0.5	No overflow
RG27AT68TATAC003	Non Reactive	1.4	No overflow
BLANK	Non Reactive	1.3	No overflow

Reactive Ground Test Results

			Date16/06/16
Sample	Run 1 (48HOURS 55°C	Exotherm (°C)	Observations
RG27AT68RARAC004	Non Reactive	0.6	small overflow
RG27CW61FWDR001	Non Reactive	0.6	small overflow
RG27CW61FWDR002	Non Reactive	1.5	small overflow
RG27CW61FWDR003	Non Reactive	1.1	small overflow
RG27CW61FWDR004	Non Reactive	1.6	small overflow
RG29ES65NDR001	Non Reactive	1.7	No overflow
RG29ES65NDR002	Non Reactive	1.5	small overflow
BLANK	Non Reactive	1.0	No overflow

Reactive Ground Test Results

Date22/06/16

Sample	Run 1 (48HOURS 55°(	Exotherm (°C)	Observations
RG32D7123XC004	Non Reactive	-0.8	No overflow
RG32AR72SBY001	Non Reactive	-0.3	No overflow
RG32AR72SBY002	Non Reactive	-0.4	No overflow
BLANK	Non Reactive	0.6	No overflow
RG27LM67SEDR001	Non Reactive	-0.4	No overflow

Reactive Ground Test Results

Date:08/06/16

Sample	Run 1 (48HOURS 55°(	Exotherm (°C)	Observations
RG17CM60INC001	Non Reactive	0.9	No overflow
RG17CM60INC002	Non Reactive	1	No overflow
RG17CM60INC003	Non Reactive	0.8	No overflow
RG17CM60INC004	Non Reactive	0.7	No overflow
RG18LK595DPIT001	Non Reactive	1.1	No overflow
RG18LK595DPIT002	Non Reactive	1	No overflow
RG18LK595DPIT003	Non Reactive	0.6	No overflow
BLANK	Non Reactive	0.4	No overflow
RG17CL577DDR004	Non Reactive	-0.4	No overflow
RG17CL577DDR005	Non Reactive	-0.2	No overflow
RG15LO56INC001	Non Reactive	0.6	No overflow
RG15LO56INC002	Non Reactive	-0.5	No overflow
RG15LO56INC003	Non Reactive	-0.2	No overflow
RG15LO56INC004	Non Reactive	-0.1	No overflow
3RG15LO56INC005	Non Reactive	0.3	No overflow
BLANK	Non Reactive	-0.6	No overflow

Appendix 8

Informative poster on the occurrence of reactive ground

Reactive Ground

Introduction

Reactive ground has caused several incidents in recent years around Australian Mines. It poses a major safety hazard to the essential mining process of drilling and blasting. It involves the interaction between ammonium nitrate explosives, and sulphide minerals in rock. The degree of severity can range from hot temperatures, ignition/burning, through to premature detonation of blast holes.

What is reactive ground?

Reactive ground is sedimentary rock which contains specific sulphide minerals which can undergo a sudden, heat releasing reaction, given contact with nitrates. The reaction intensifies with time, releasing increasing amounts of energy as heat. It can do this without any input from an outside source. The process is unpredictable, and can occur rapidly, with the potential to cause premature initiation of explosives.

The Q356 Incident

Nitrates in the ANFO within charged holes reacted with the fine grained pyritic shale in the Q356 stope rock mass.

Pyrite was observed and logged in the Q356 diamond drilling core, but the ground was not seen as reactive, as it was outside the **BOML (base of moderate leaching zone)**.

The BOML was linked to the classification of reactive ground. Too much emphasis was placed on the BOML as an indicator of reactive ground. while the impact of pyrite itself was unrecognised. Pyrite was typically considered a secondary explosion hazard, not a reactive ground hazard.

It is now recognised that reactive ground can occur **anywhere** in the presence of pyrite.

The conditions of reactive ground are able to be identified and well managed. Geologists now assess the reactive ground risk for each stope based on the amount of fine grained pyrite, exposure time to oxidation, presence of groundwater and lab reactivity testing.

Severe damage or corrosion of mesh, rock bolts, and other equipment from leaching and oxidation in reactive ground. Oxidation of the actual rock is also visible behind the mesh. These may be used as indicators to reactive ground conditions.

Lab testing for reactivity

Reactive ground samples are taken by geologists for testing with explosive products in laboratories. Sleep times and safe drill-hole temperatures are determined by lab testing from reactive ground sampling.

What you can do to stay safe

Clean out holes thoroughly to ensure there are no fines left in the hole. Finely fragmented material left in the hole could oxidise and react with explosives when charged. Muck the fines off the ground immediately after drilling.

Be sure to monitor down-hole temperatures of drill holes using temperature testing, and report to your supervisor if temperatures exceed the threshold specified in the firing note.

Monitor the column rise, to ensure that no product is being lost into cracks, or void spaces near the blast hole when loading explosives. If material is being lost, it has the potential to react with rock by overcoming the maximum sleep time.

If hot blast holes are identified and are necessary to load, load them last to minimise the sleep time.

Minimising the sleep time in general ensures the risk of explosive reactions is kept to a minimum.

Minimise any hole dislocation. This can allow explosives to be in contact with reactive ground for longer than the maximum sleep time.

Loading in the sequence of firing. Load holes in the sequence that they are to be fired, to reduce the exposure time of nitrates with reactive ground.

Stemming material should never be drill cuttings, as these may contain potentially reactive material.

Avoid overfilling any holes.

In-case a misfire occurs, plans to dig out any misfires within the recommended sleep time of the explosive product should be in place.

What is reactive ground?

All rocks are made up of a variety of minerals, which are all chemical compounds. Although most minerals in rocks are stable and unreactive, some minerals such as fine grained pyrite, are unstable in the presence of oxygen and other chemicals. These minerals alter to different compounds which are reactive.

Reactive ground is a complex process and is difficult to understand. However, there are risk management approaches which keep activity well within safe limits. If successfully adopted, they **will**, and **do prevent incidents occurring**.

The best approach to managing reactive ground is taking the initiative to minimise the recognised risks, rather than responding after an incident occurs.

Factors that triggered the Q356 incident

- Both drill holes were almost horizontal, allowing the retention of water and fine grained sediments which further increased the oxidation of the pyrite.
- The pyrite grain size was small (fine grained pyrite).
- There was a long lag time (~9 months) between drilling and charging, which allowed time for pyrite to oxi-

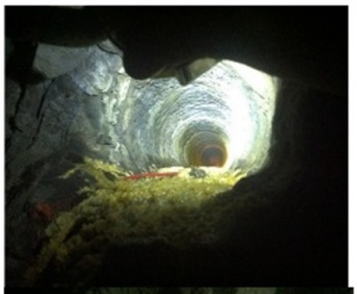

These images show reacting sulphides and explosive leaking from the drill hole during the Q356 incident. It displays a rich yellow colour.

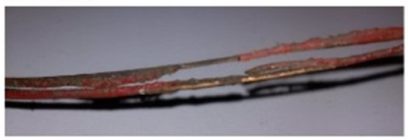

Image showing an I-kon lead which has been melted through by hot temperatures following the Q356 incident. To melt through this lead, temperatures must have exceeded **120 degrees Celsius.**

What can influence the reactivity of sulphides?

- Moisture - Specific ranges of moisture can increase reaction rates (1-5%). Presence of groundwater in an area can increase corrosion/oxidation and therefore reactivity of sulphides.
- Oxidising conditions - presence of air, heat and water.
- Mineralogy - Percentage of fine grained pyrite (or other sulphides) in the host rock.
- Thermal properties of host rock: Shales, sulphides, and ammonium nitrate (AN) are poor conductors of heat away from the source. Confined spaces such as blast holes can act to trap heat into a small area.
- Ambient temperature (surrounding mine temperature) - General hot conditions can increase likelihood of reactions taking place.
- Particle or grain size - Smaller grains (Fine grained pyrite) creates a larger surface area for reactions to take place.

What you need to know and be aware of

Reactive ground indicators

Presence of pyrite + other sulphide minerals (greater than 1%) in black sediments.

White or yellow salts on the rock indicating oxidation.

Acidic conditions (generally resulting from oxidation) as indicated by the colour of run-off water which is usually yellow, red or brown.

Significant corrosion/rust of rock bolts, meshing or equipment.

The combustion of waste rock/ore in dumps as it is exposed to the air (smoking , fuming).

The harsh smell of sulphur dioxide caused by sulphide oxidation.

Elevated blast-hole temperatures + elevated ground temperatures

What causes rock to react with explosive?

When a rock mass is drilled, the hole becomes exposed to oxygen underground. If the rock contains reactive minerals (fine grained pyrite), the addition of explosives increases the chance of reactions taking place. This is because explosives act as powerful oxidising chemicals.

Oxidation/Weathering – Sulphide minerals are unstable in the presence of oxygen, and so will be exposed to oxidation in the mining environment. The oxidation of pyrite (iron sulphides), forms substances which are susceptible to chemical reactions. This happens just by exposure to the air along cracks, in drilled holes, in the muck pile after blasting, and in old stopes. Groundwater can accelerate this process. This is why reactive ground is often linked to leaching and the BOML zone.

Iron Sulphides + Oxygen + Water → Ferrous Ions + Sulphuric Acid

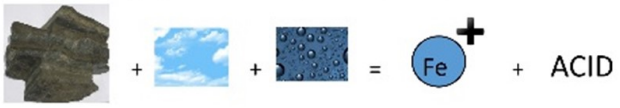

This reaction alone can lead to hot drill hole temperatures for particularly reactive ground.

Upon contact with common explosive products, the weathering solutions cause the breakdown of nitrate, which releases heat.

Nitrates + Iron Sulphides + Ferrous Ions + Sulphuric Acid → Nitric Oxide + Ferric Ions + HEAT

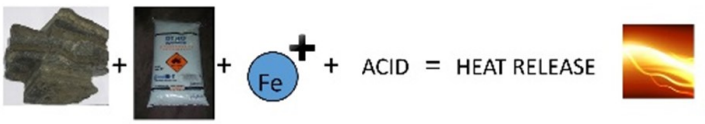

The rate of these reactions is initially slow, and temperature rises may not be easily detected. When the reaction rate increases rapidly, the sudden heat release can cause extreme temperatures.

Nitrates + Fuels (sulphides) + Oxygen + Heat → EXPLOSION

If sufficient fuel is available, the heat can trigger pre-detonation.

Very specific conditions are required for the reaction to progress to dangerous stages. For this reason, mines have been known to operate for years without any incidents using standard explosives. **Years of successful operation, is not a valid argument for the ability to blast safely in reactive ground.**

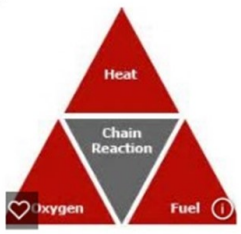

Types of sulphide minerals at Mt Isa

1. Chalcopyrite - This is the main copper bearing mineral of the mine and is the mineral to be mined. Chalcopyrite contains a relatively low amount of sulphur and iron, and so is considered safe for blasting.
2. Pyrrhotite - Mineral containing iron and sulphur. It is present amongst other minerals within the mine . It can contribute to reactive ground..
3. Coarse grained pyrite. Pyrite which occur as coarse crystals which are visible to the eye. The coarse grain size makes it less prone to reaction. .
4. Fine grained pyrite. Very fine grains forming a light bronze coloured mass. This rock type is the one which causes reactive ground.

The surface area principle. Why is the fine grained pyrite (FeS_2) the most reactive?

More surface area allows more surfaces exposed to oxidation reactions , and therefore more likelihood of spontaneous reactions occurring. Fine grains maximise the surface area exposed to reactions compared to coarse grains.

Consider a 2 dimensional situation.

1 coarse pyrite grain.

Diameter of 20 mm.

2D Surface Area = 314 mm^2

Around 50 fine pyrite grains.

Diameters of 2 . 5 mm

2D Surface Area = 1000mm^2

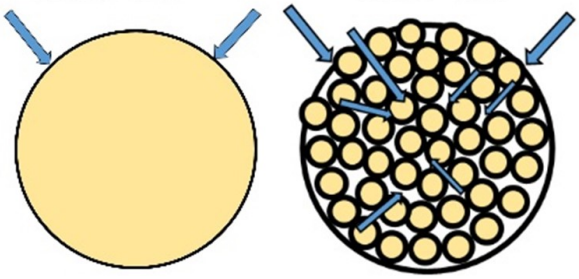

Blue arrows indicate a reaction taking place on a grain surface. Coarser grains have restricted amounts of rock that can be exposed to reaction. Finer grains increase the area where oxygen, fluids and nitrates can react with rock

This image shows fine grained pyrite as It appears in drill core. It can be identified be its deep bronze or light brown colour. Coarse grained pyrite is a much more golden, brighter yellow.

Appendix 9

Investigation into the relationship between trace element geochemistry and reactive ground

Trace element geochemistry and reactive ground

- Assays containing trace element data for 24 different elements was plotted against reactivity for each reactive ground sample.

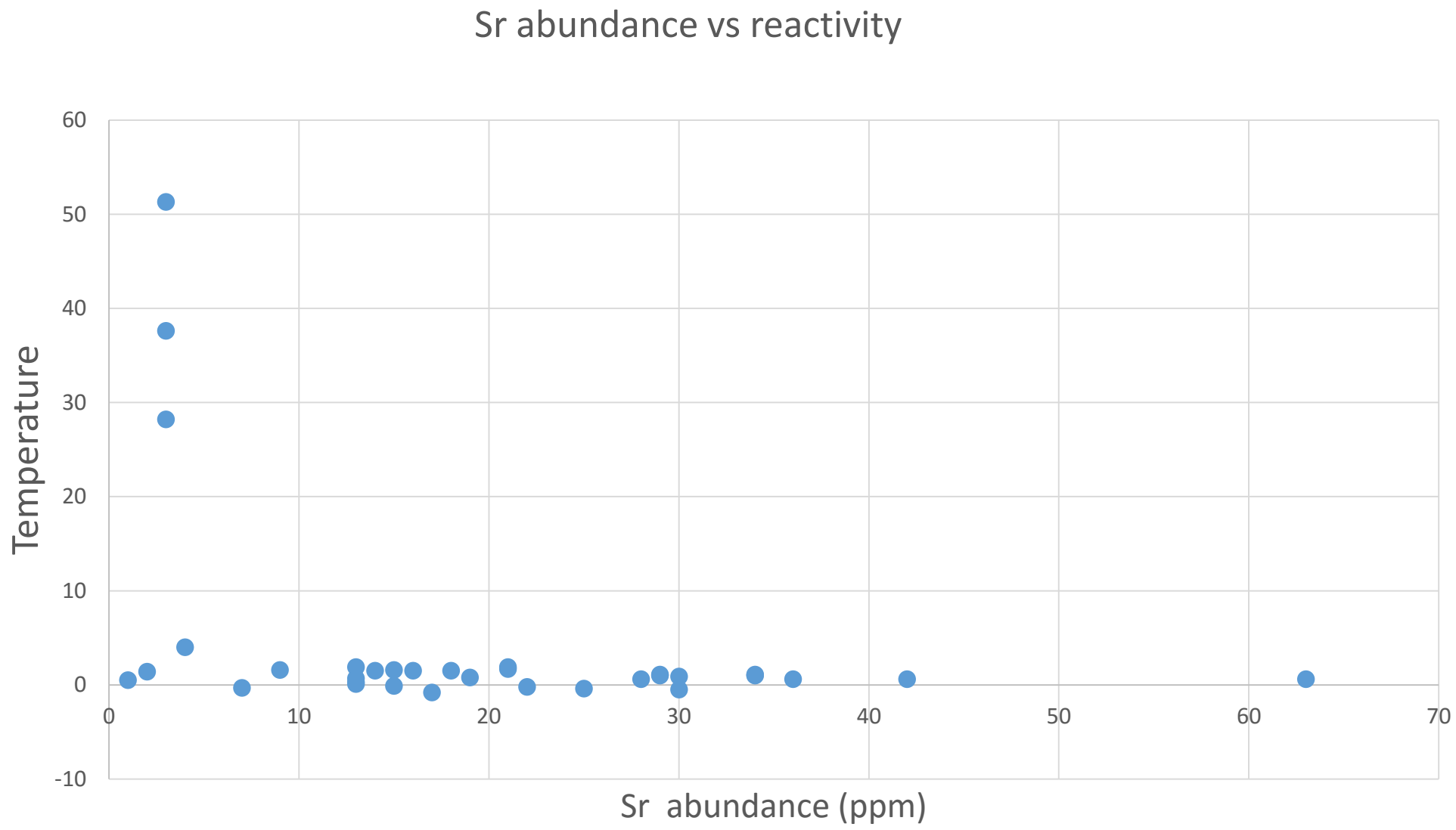
Sr abundance vs reactivity
Temperature
60
50
40
30
20
10
0
-10
0
10
20
30
40
50
60
70
Sr abundance (ppm)

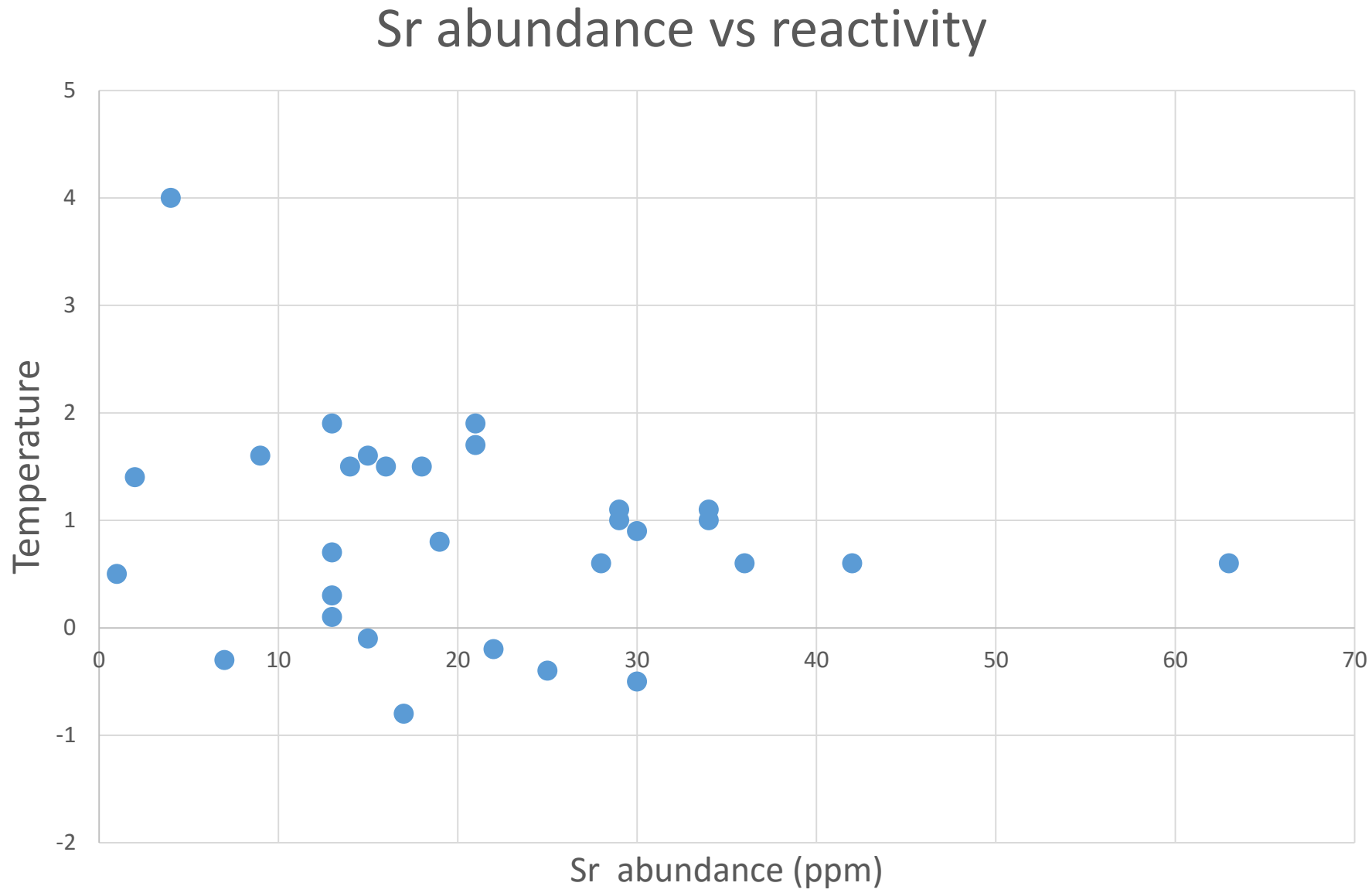
Sr abundance vs reactivity
Temperature
5
4
3
2
1
0
-1
-2
0
10
20
30
40
50
60
70
Sr abundance (ppm)

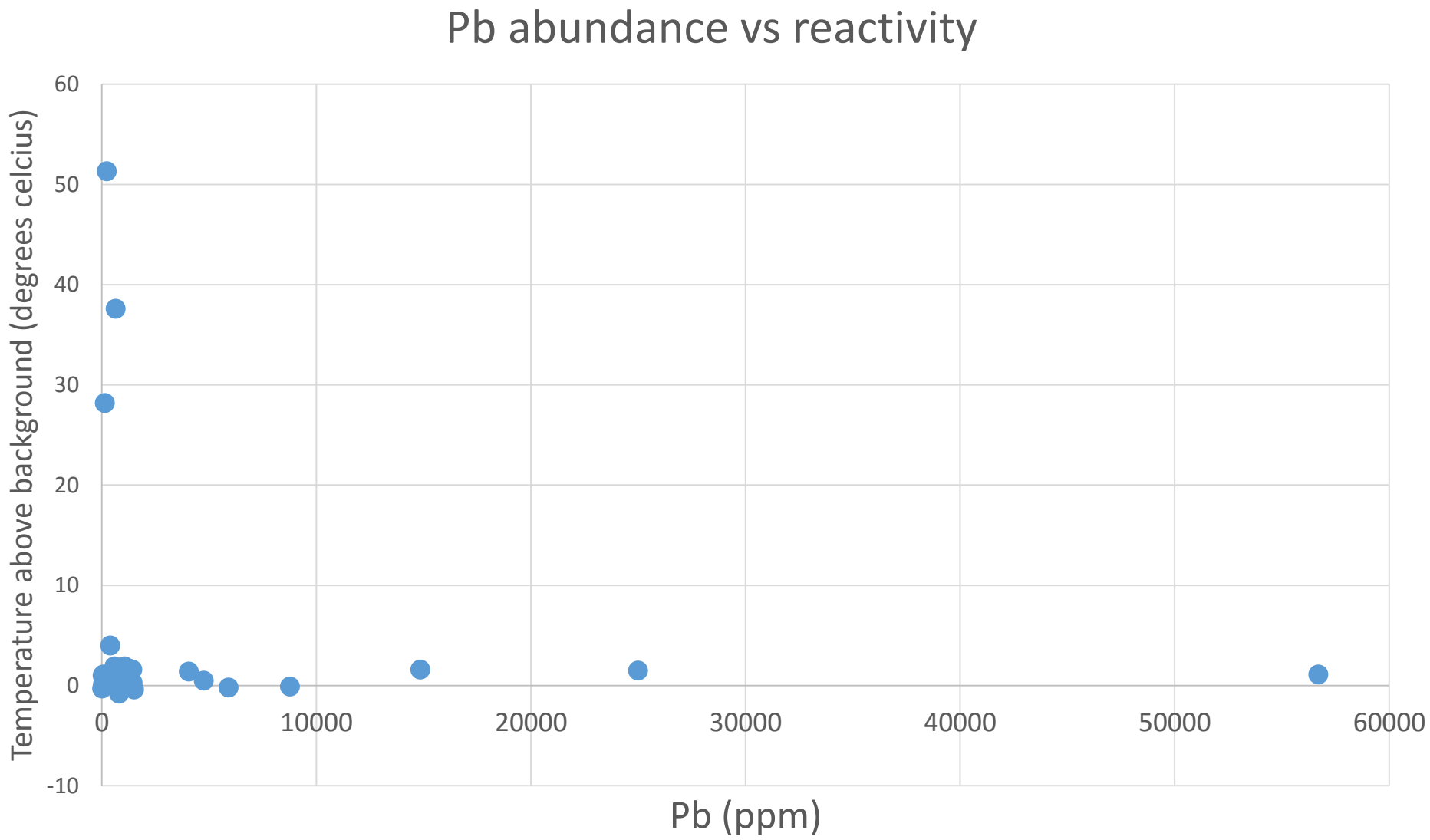
Pb abundance vs reactivity
Temperature above background (degrees celcius)
60
50
40
30
20
10
0
-10
0
10000
20000
30000
40000
50000
60000
Pb (ppm)

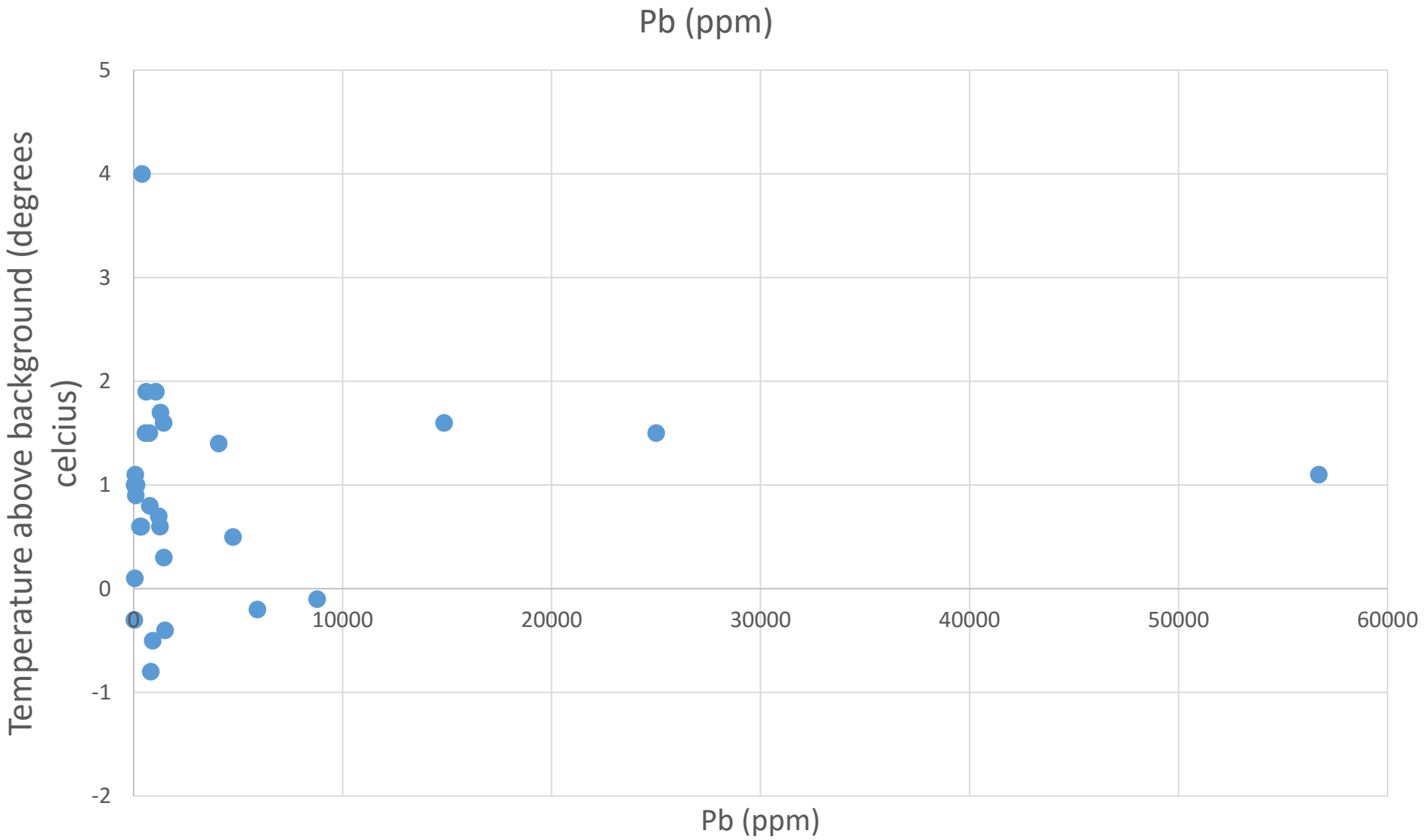
Pb (ppm)
Temperature above background (degrees celcius)
5
4
3
2
1
0
-1
-2
0
10000
20000
30000
40000
50000
60000
Pb (ppm)

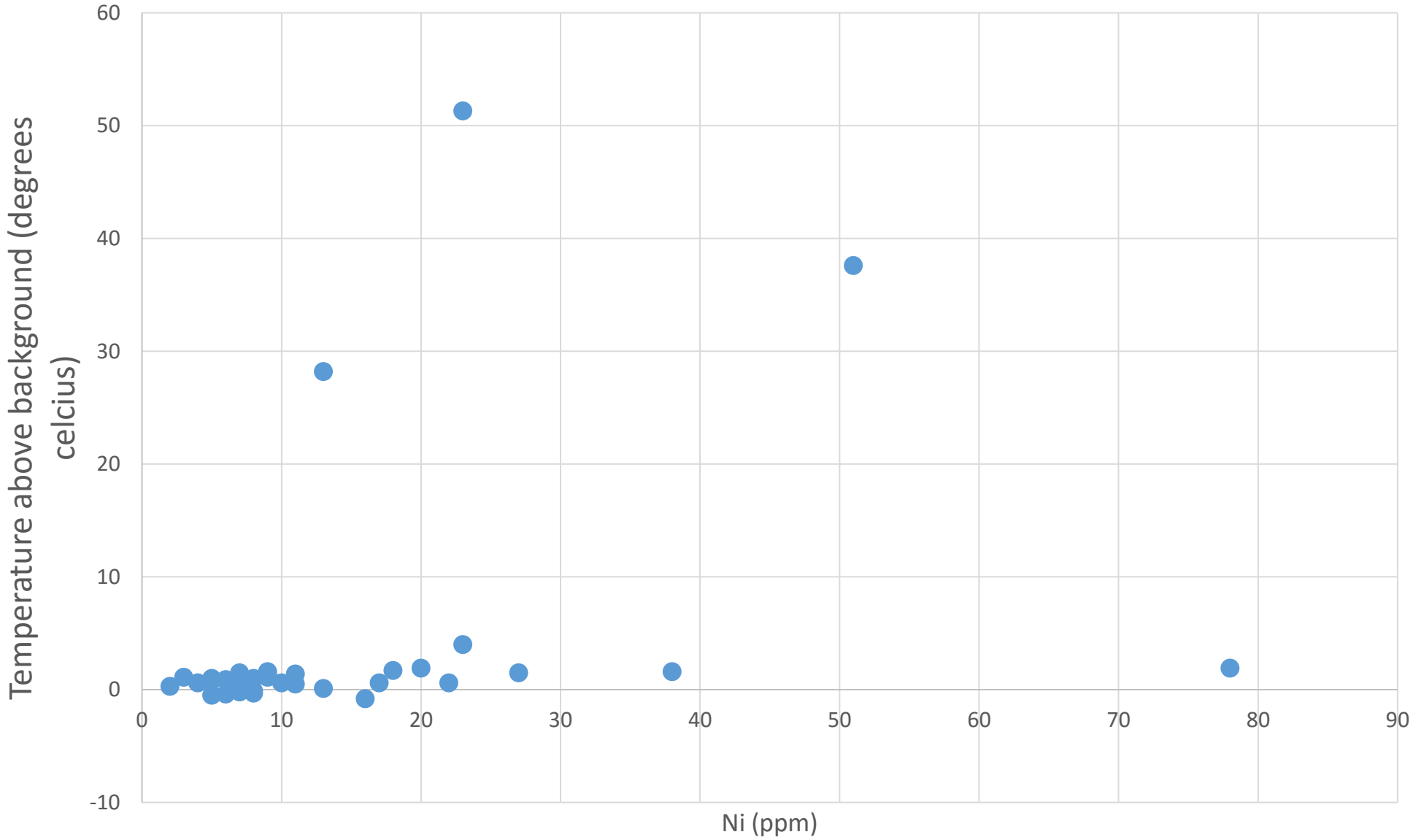
Temperature above background (degrees celcius)
60
50
40
30
20
10
0
-10
0
10
20
30
40
50
60
70
80
90
Ni (ppm)

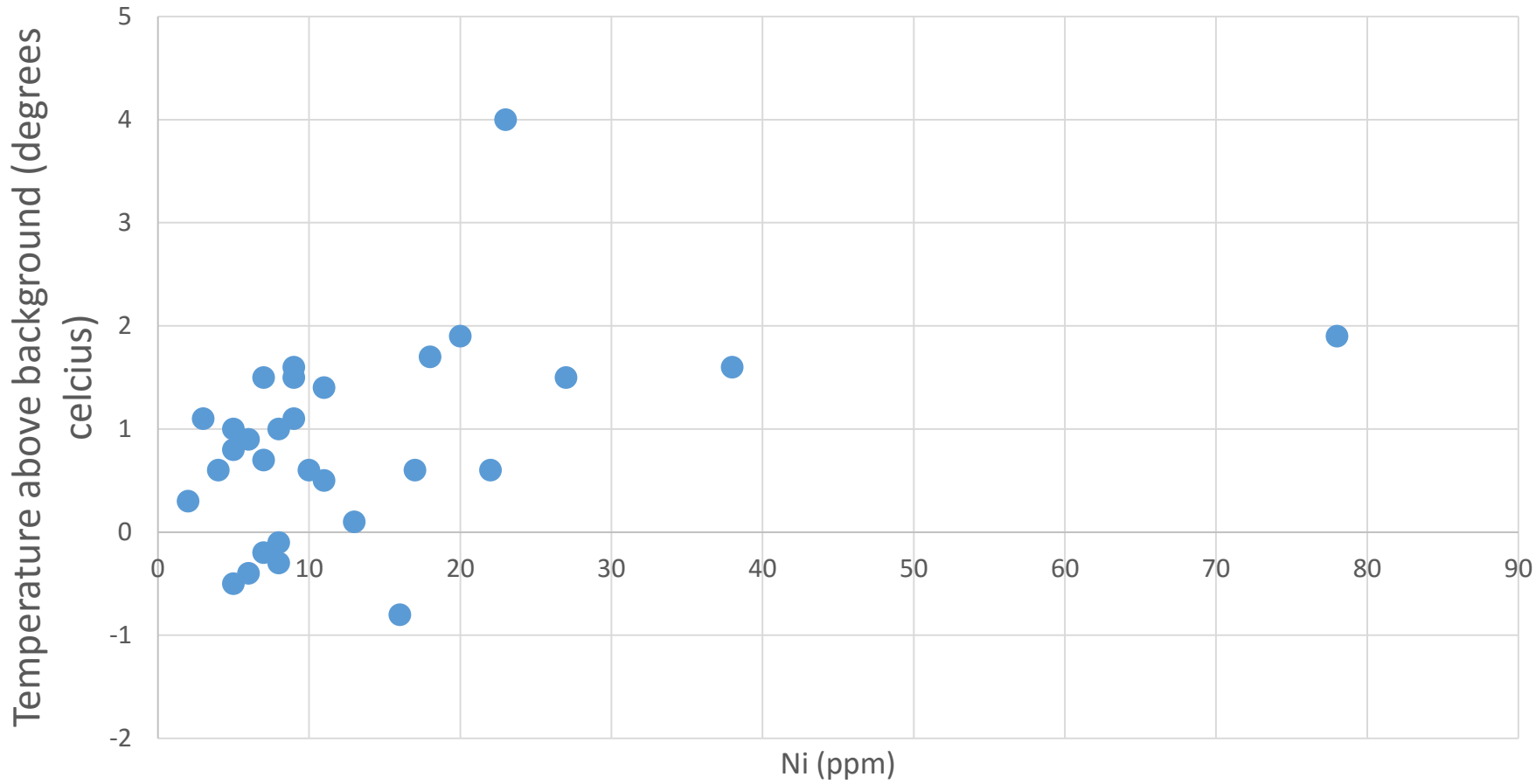
Temperature above background (degrees celcius)
5
4
3
2
1
0
-1
-2
0
10
20
30
40
50
60
70
80
90
Ni (ppm)

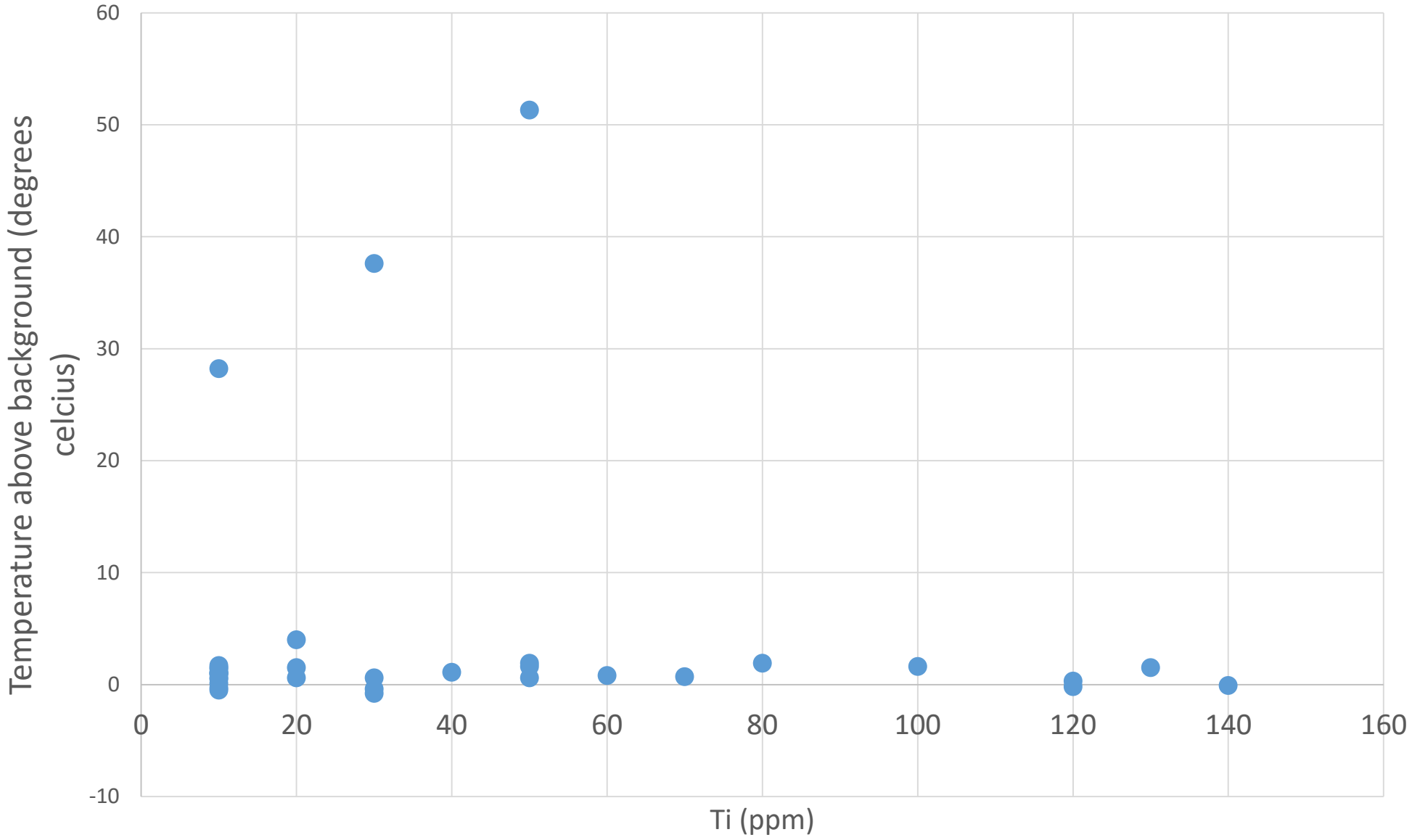
Temperature above background (degrees celcius)
60
50
40
30
20
10
0
-10
0
20
40
60
80
100
120
140
160
Ti (ppm)

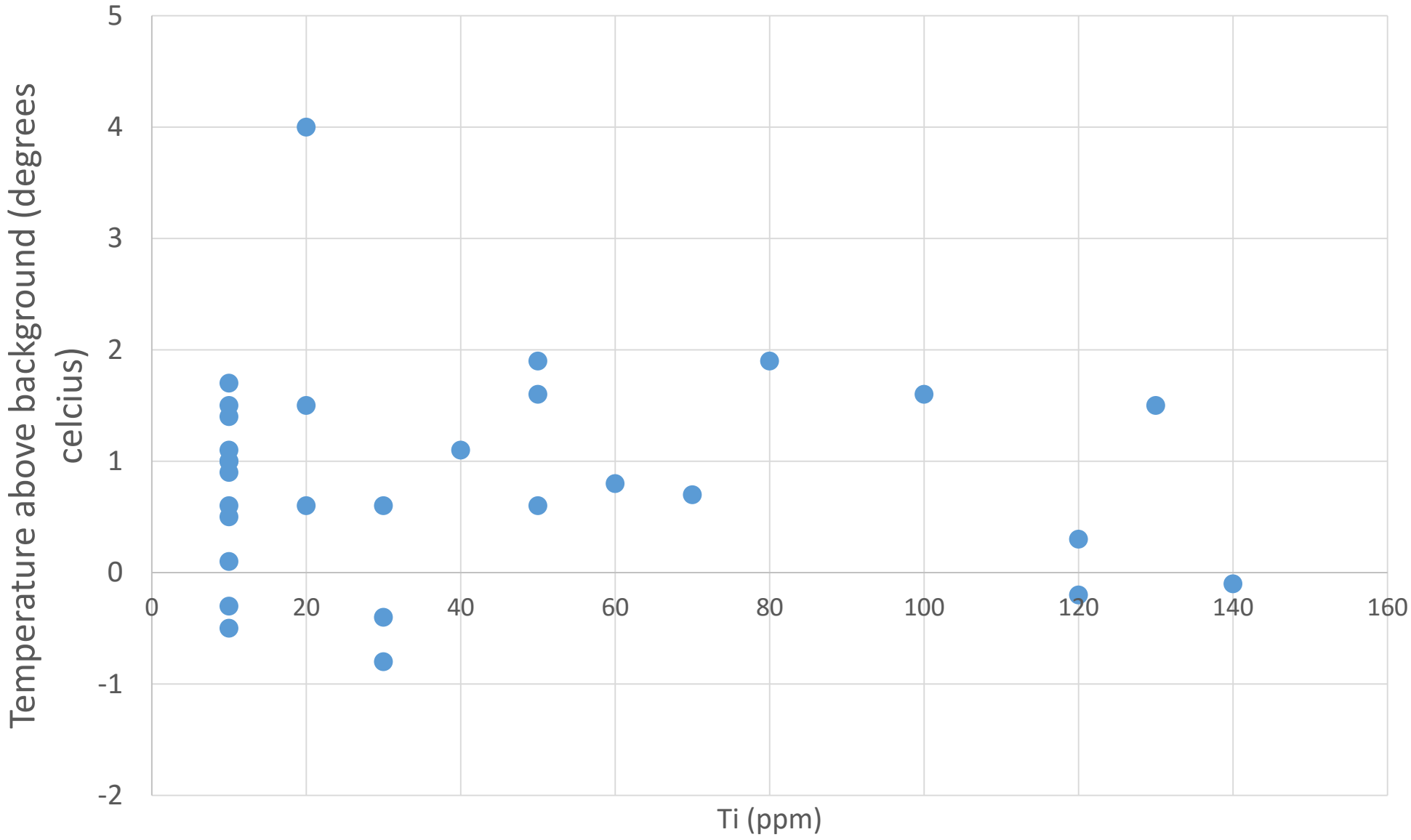
Temperature above background (degrees celcius)
5
4
3
2
1
0
-1
-2
0
20
40
60
80
100
120
140
160
Ti (ppm)

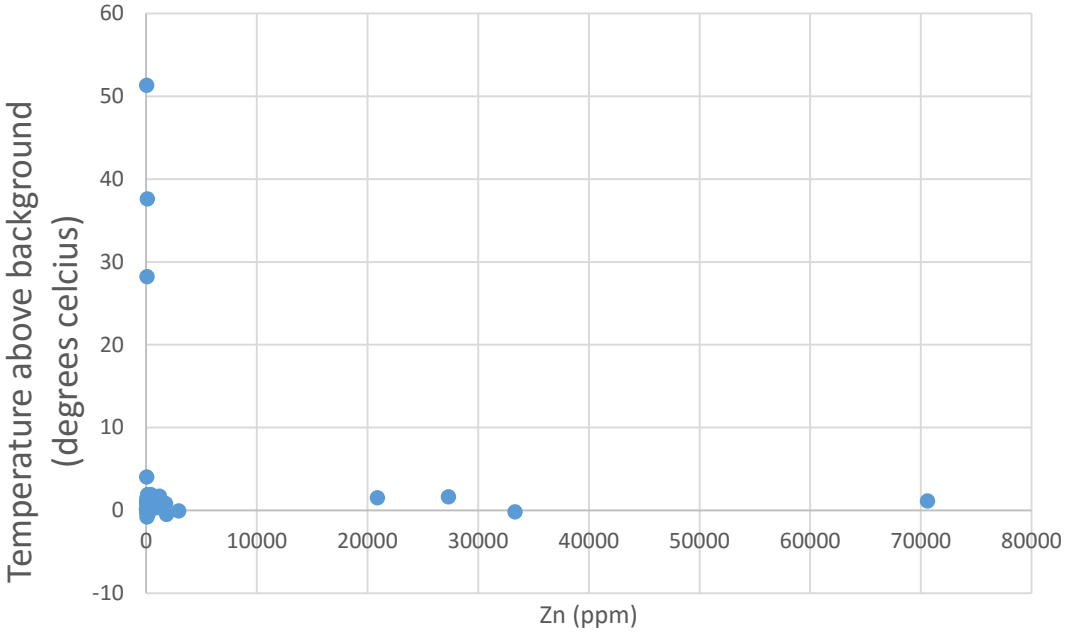
Temperature above background (degrees celcius)
60
50
40
30
20
10
0
-10
0
10000
20000
30000
40000
50000
60000
70000
80000
Zn (ppm)

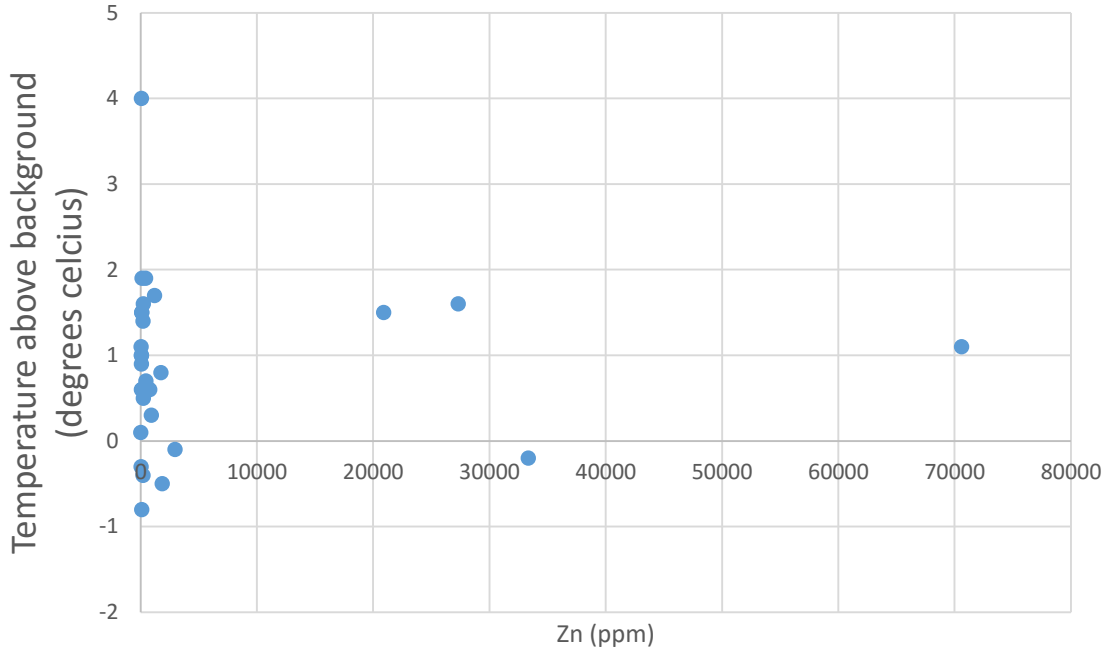
Temperature above background (degrees celcius)
5
4
3
2
1
0
-1
-2
0
10000
20000
30000
40000
50000
60000
70000
80000
Zn (ppm)

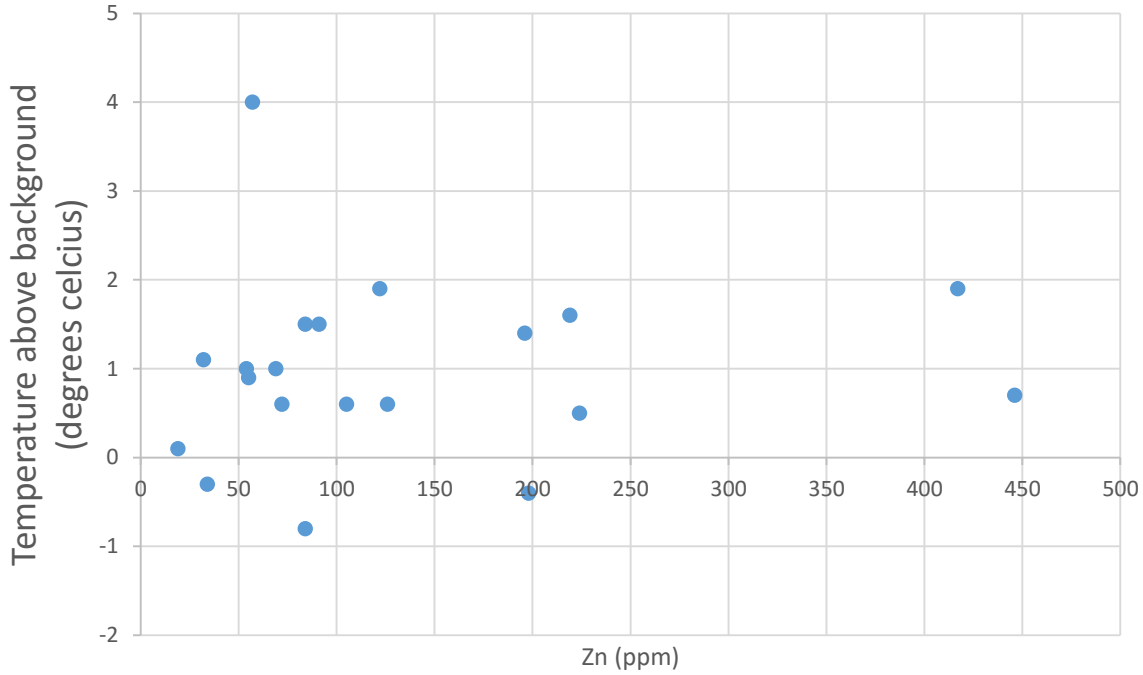
Temperature above background (degrees celcius)
5
4
3
2
1
0
-1
-2
0
50
100
150
200
250
300
350
400
450
500
Zn (ppm)

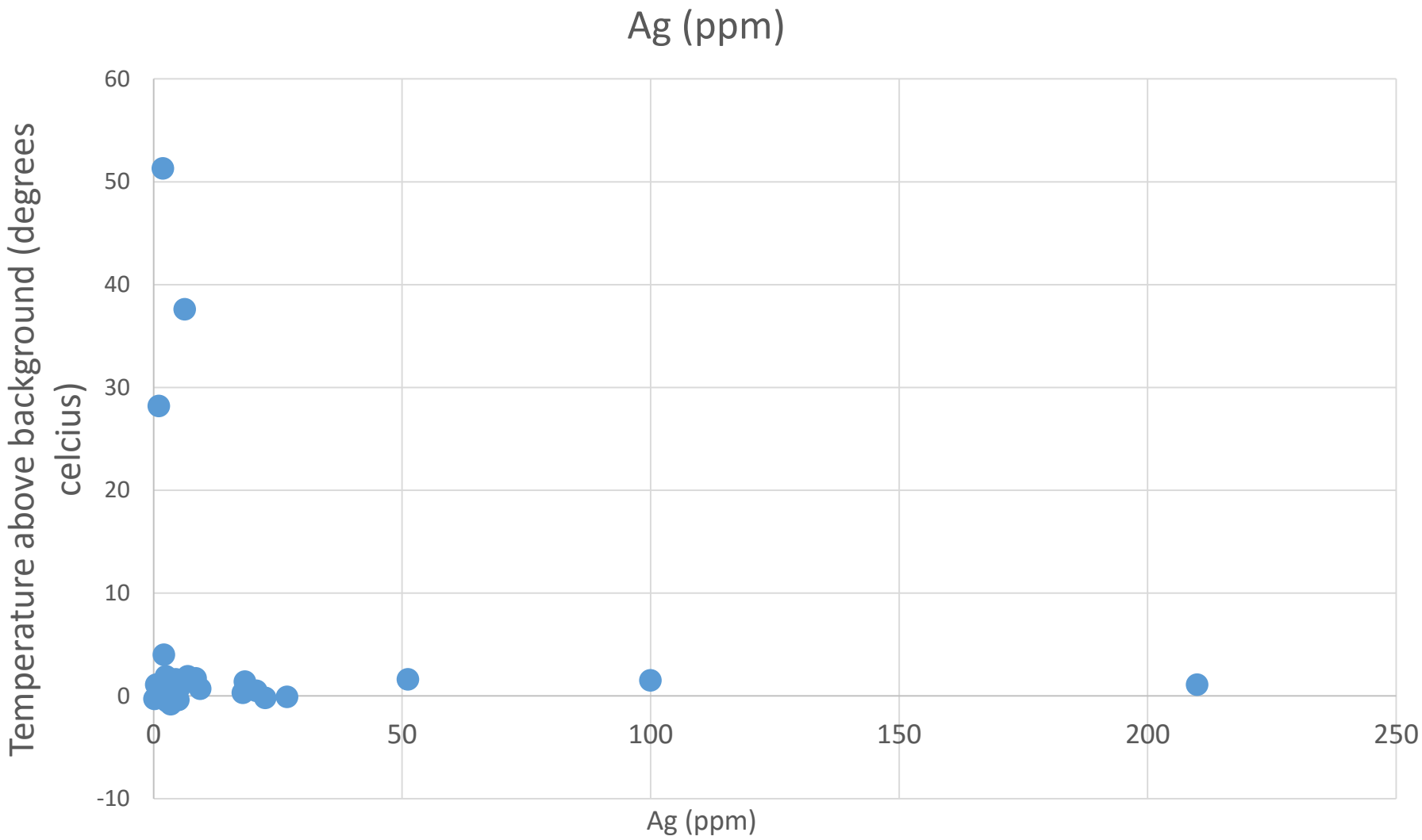
Ag (ppm)
Temperature above background (degrees celcius)
60
50
40
30
20
10
0
-10
0
50
100
150
200
250
Ag (ppm)

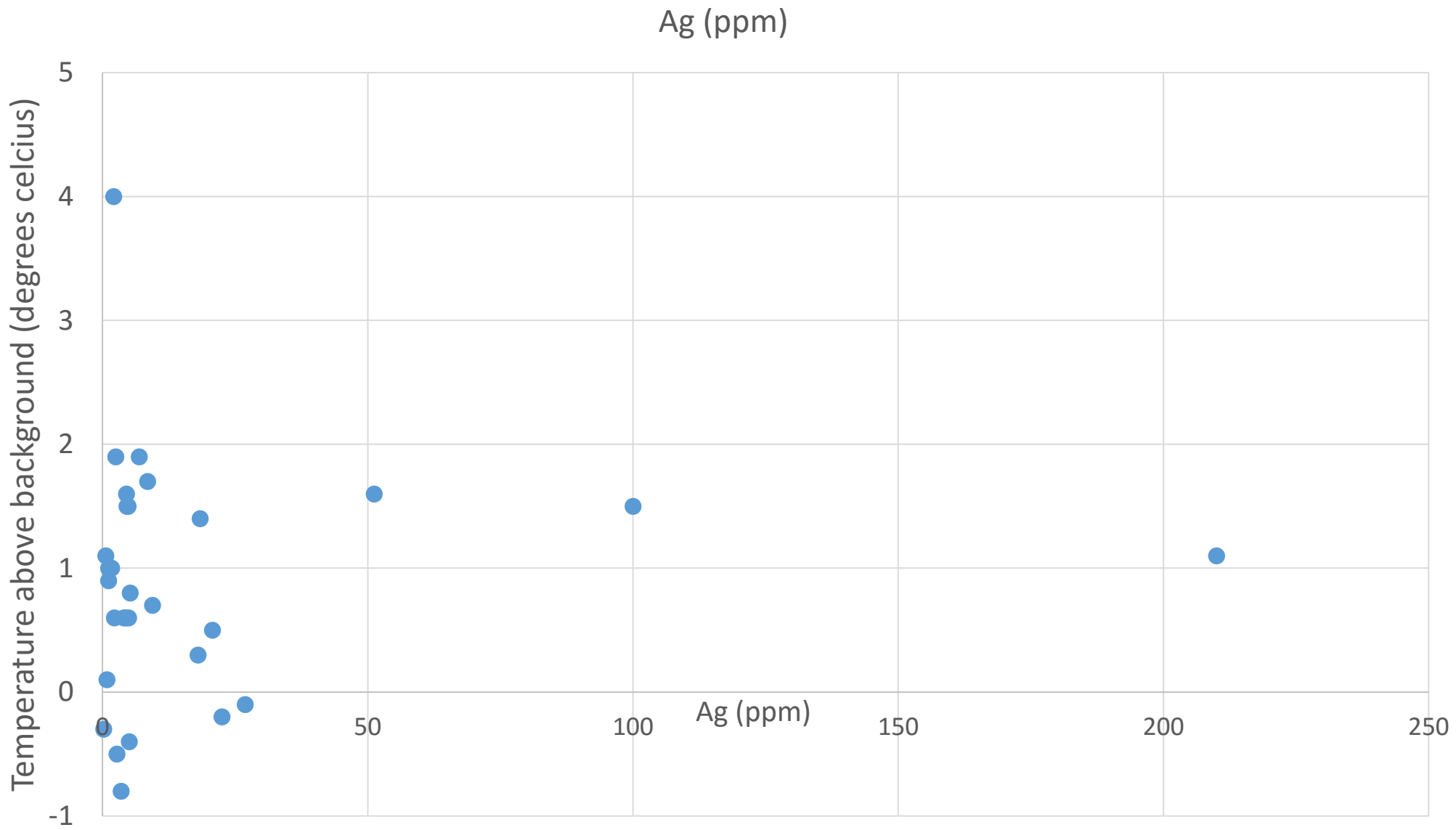
Ag (ppm)
Temperature above background (degrees celcius)
5
4
3
2
1
0
-1
0
50
100
150
200
250
Ag (ppm)

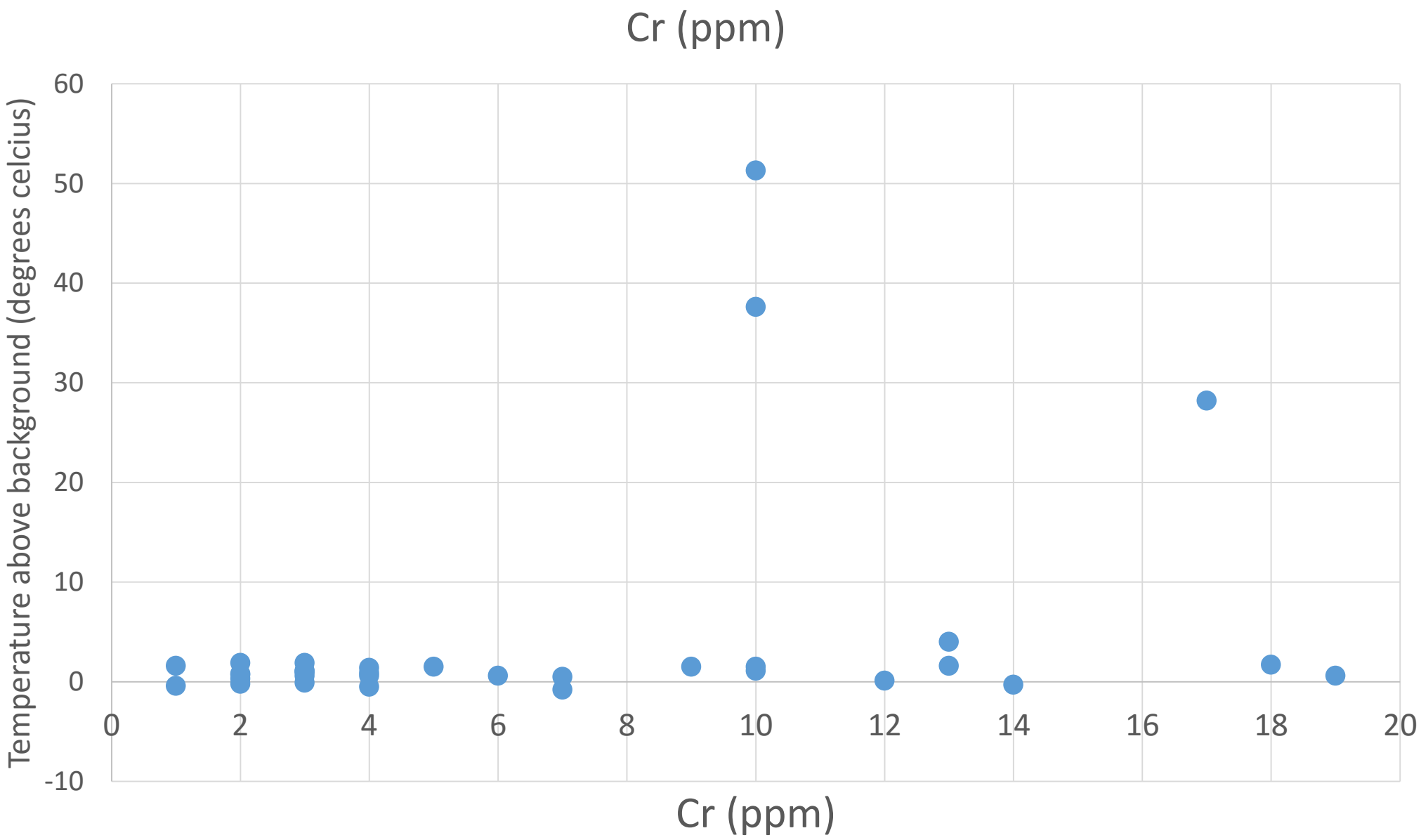
Cr (ppm)
Temperature above background (degrees celcius)
60
50
40
30
20
10
0
-10
0
2
4
6
8
10
12
14
16
18
20
Cr (ppm)

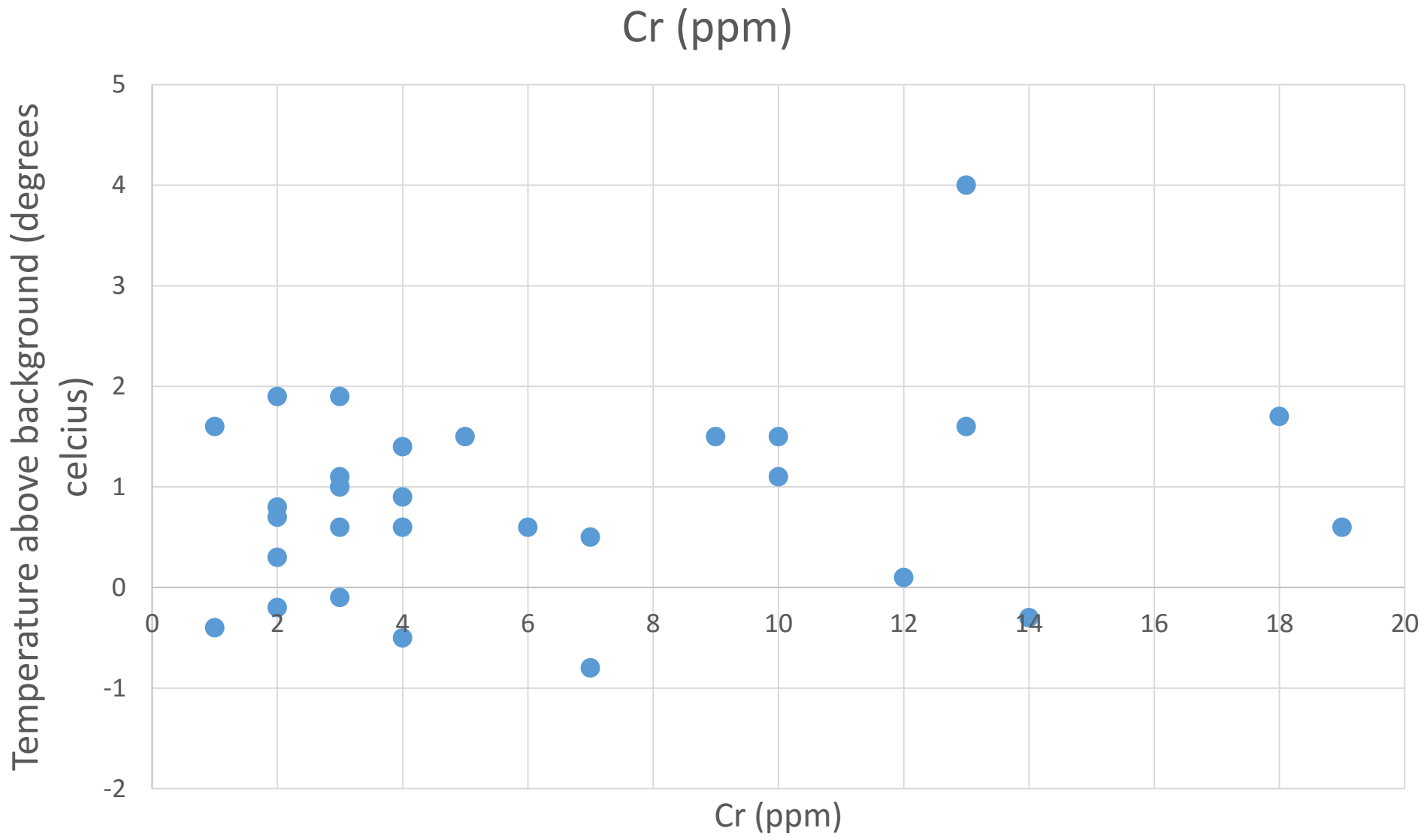
Cr (ppm)
Temperature above background (degrees celcius)
5
4
3
2
1
0
-1
-2
0
2
4
6
8
10
12
14
16
18
20
Cr (ppm)

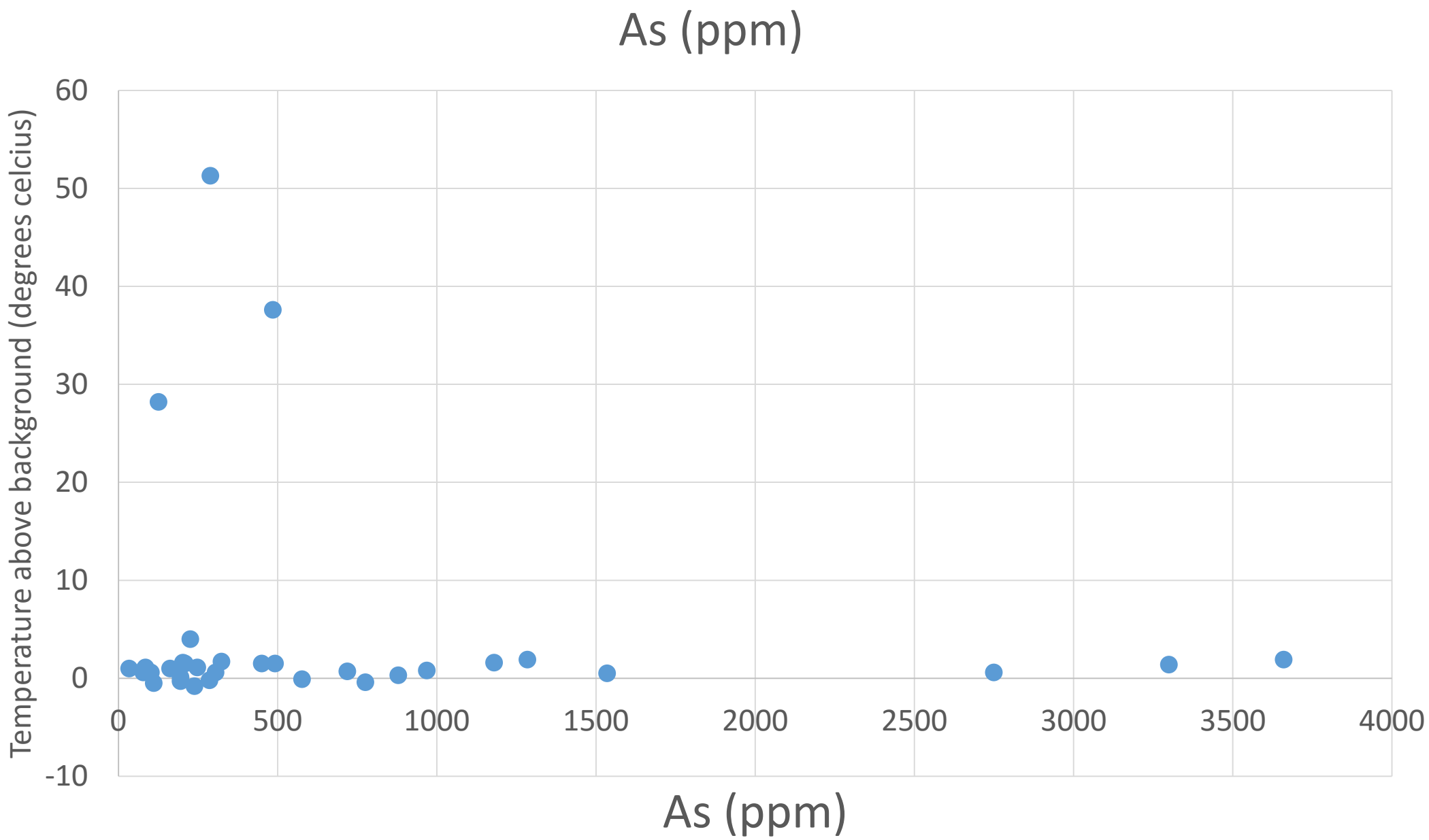
As (ppm)
Temperature above background (degrees celcius)
60
50
40
30
20
10
0
-10
0
500
1000
1500
2000
2500
3000
3500
4000
As (ppm)

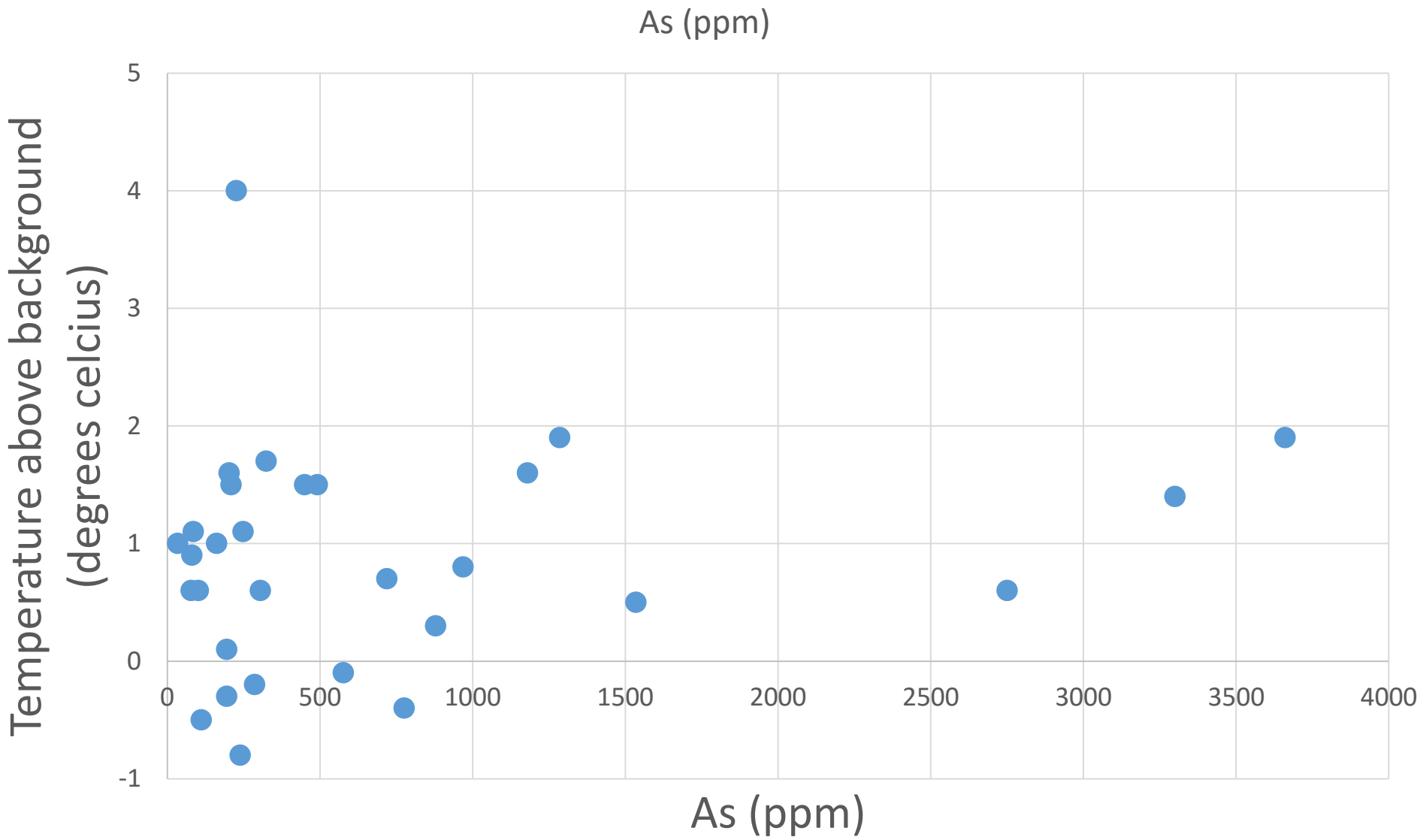
As (ppm)
Temperature above background (degrees celcius)
5
4
3
2
1
0
-1
0
500
1000
1500
2000
2500
3000
3500
4000
As (ppm)

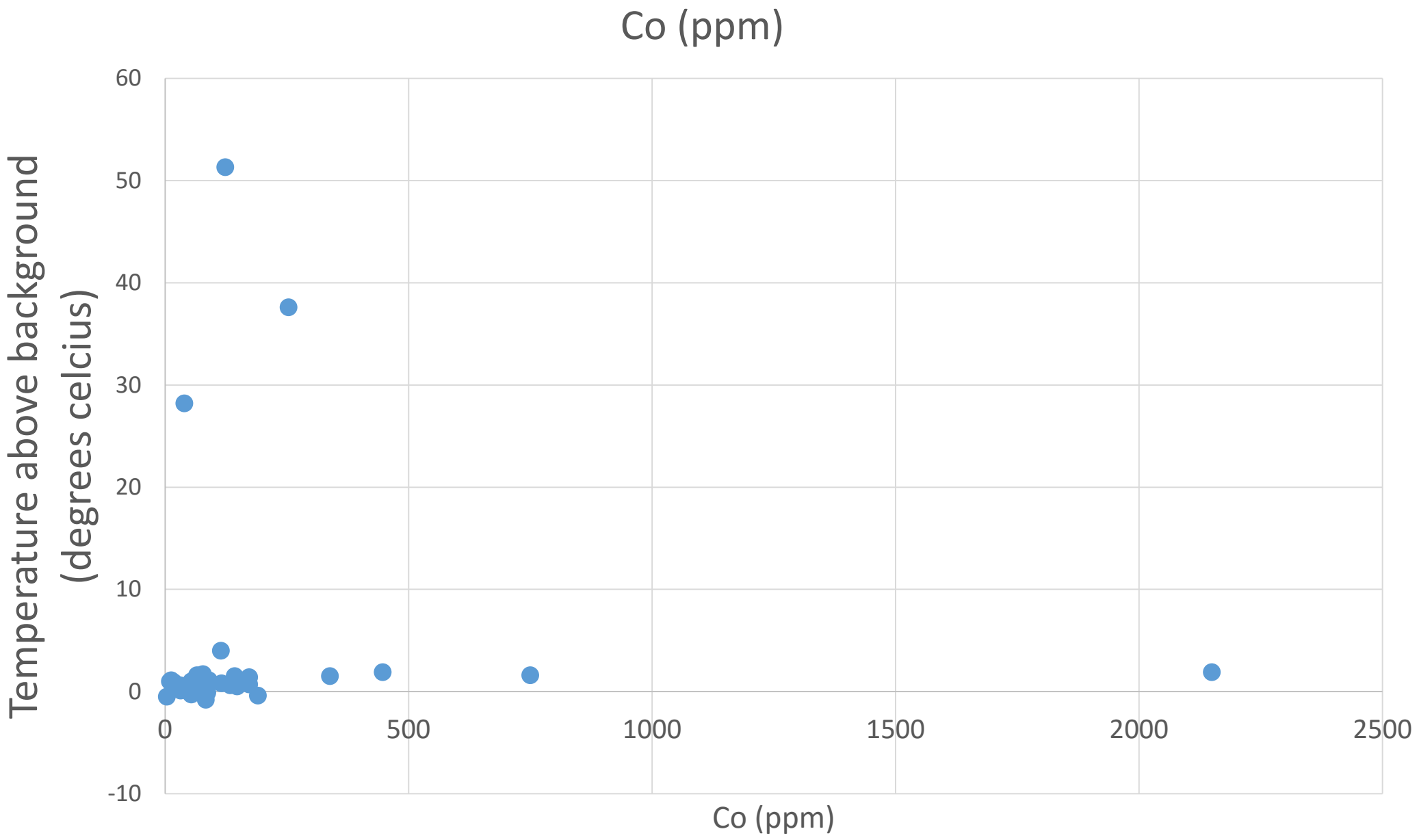
Co (ppm)
Temperature above background (degrees celcius)
60
50
40
30
20
10
0
-10
0
500
1000
1500
2000
2500
Co (ppm)

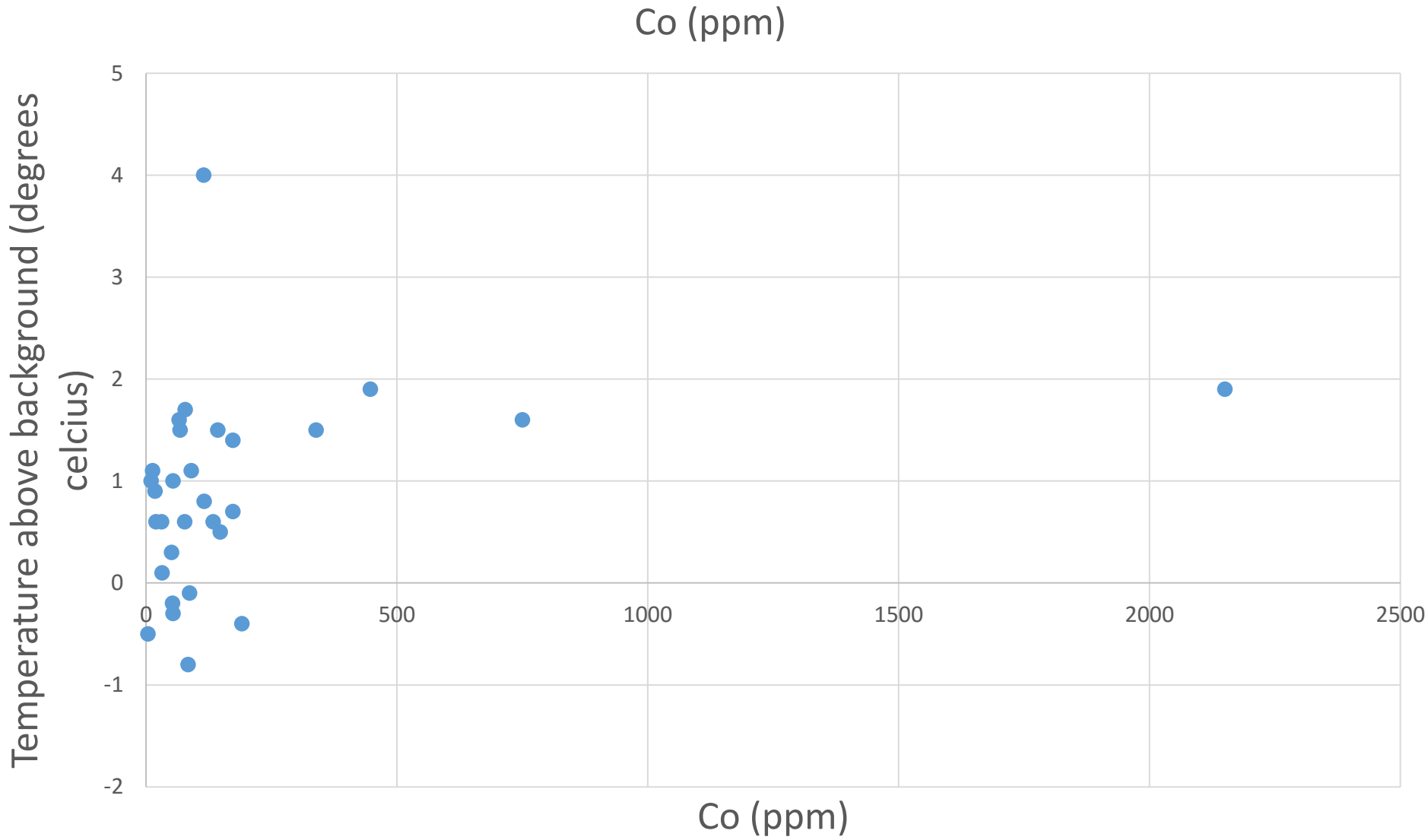
Co (ppm)
Temperature above background (degrees celcius)
5
4
3
2
1
0
-1
-2
0
500
1000
1500
2000
2500
Co (ppm)

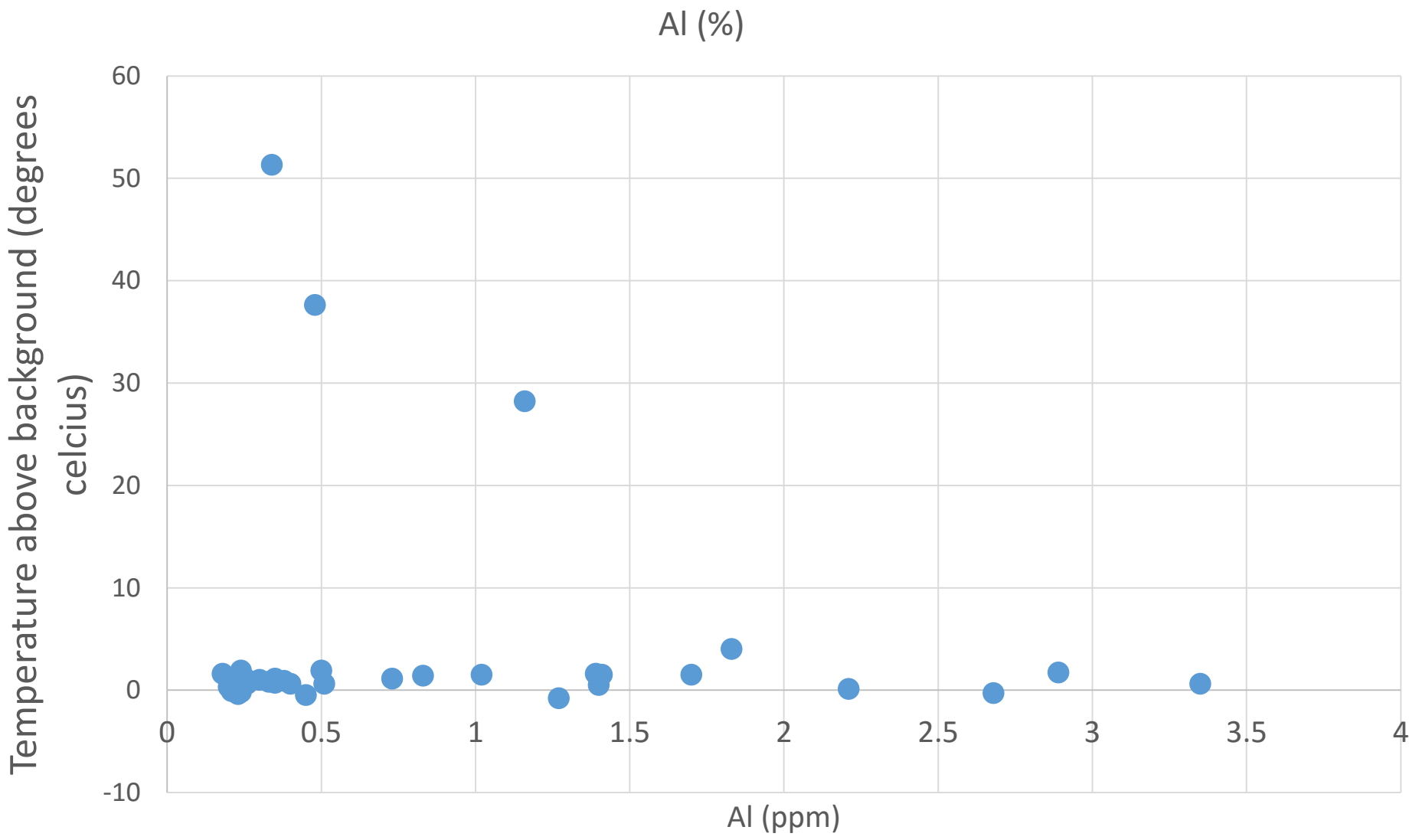
Al (%)
Temperature above background (degrees celcius)
60
50
40
30
20
10
0
-10
0
0.5
1
1.5
2
2.5
3
3.5
4
Al (ppm)

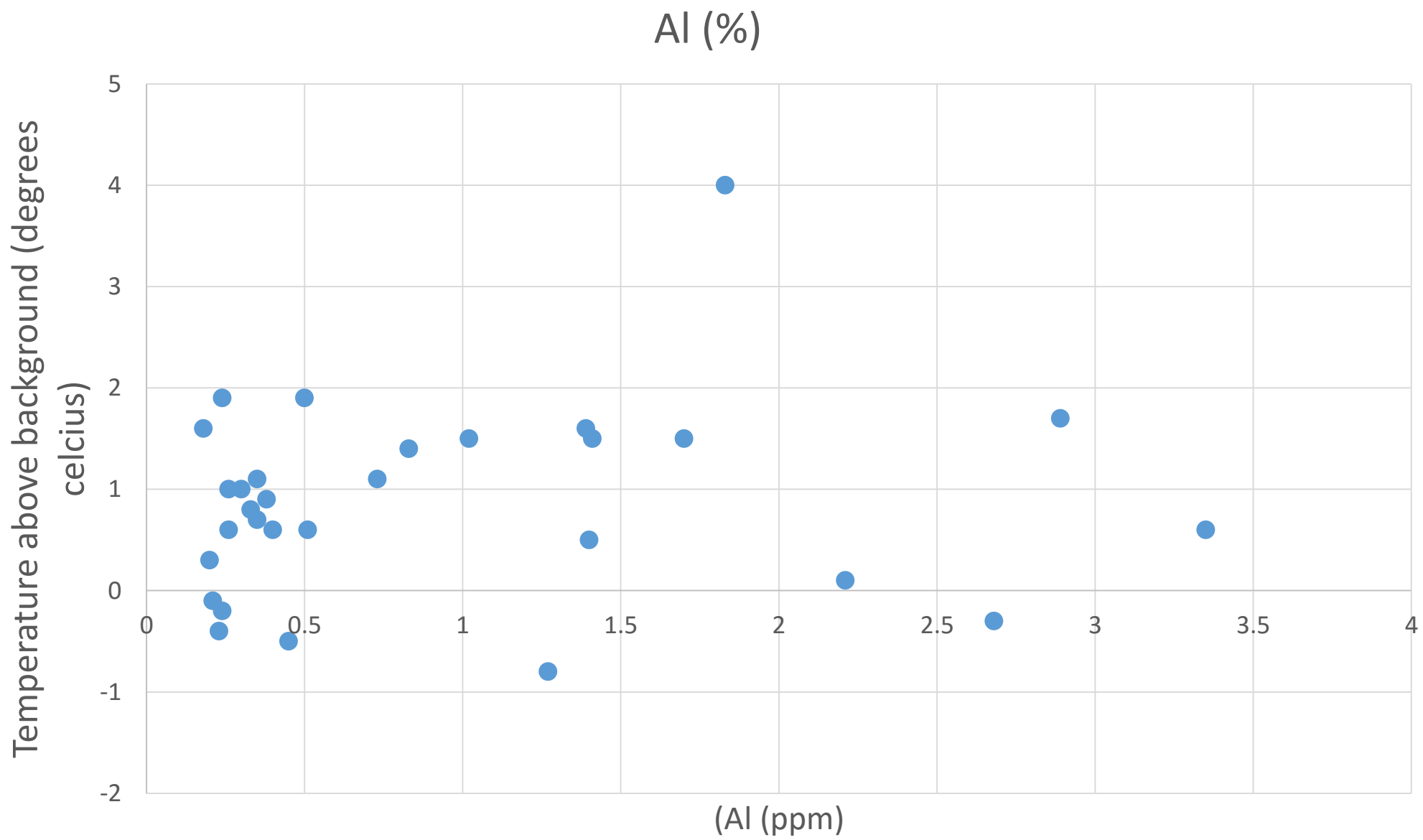
Al (%)
Temperature above background (degrees celcius)
5
4
3
2
1
0
-1
-2
0
0.5
1
1.5
2
2.5
3
3.5
4
(Al (ppm)

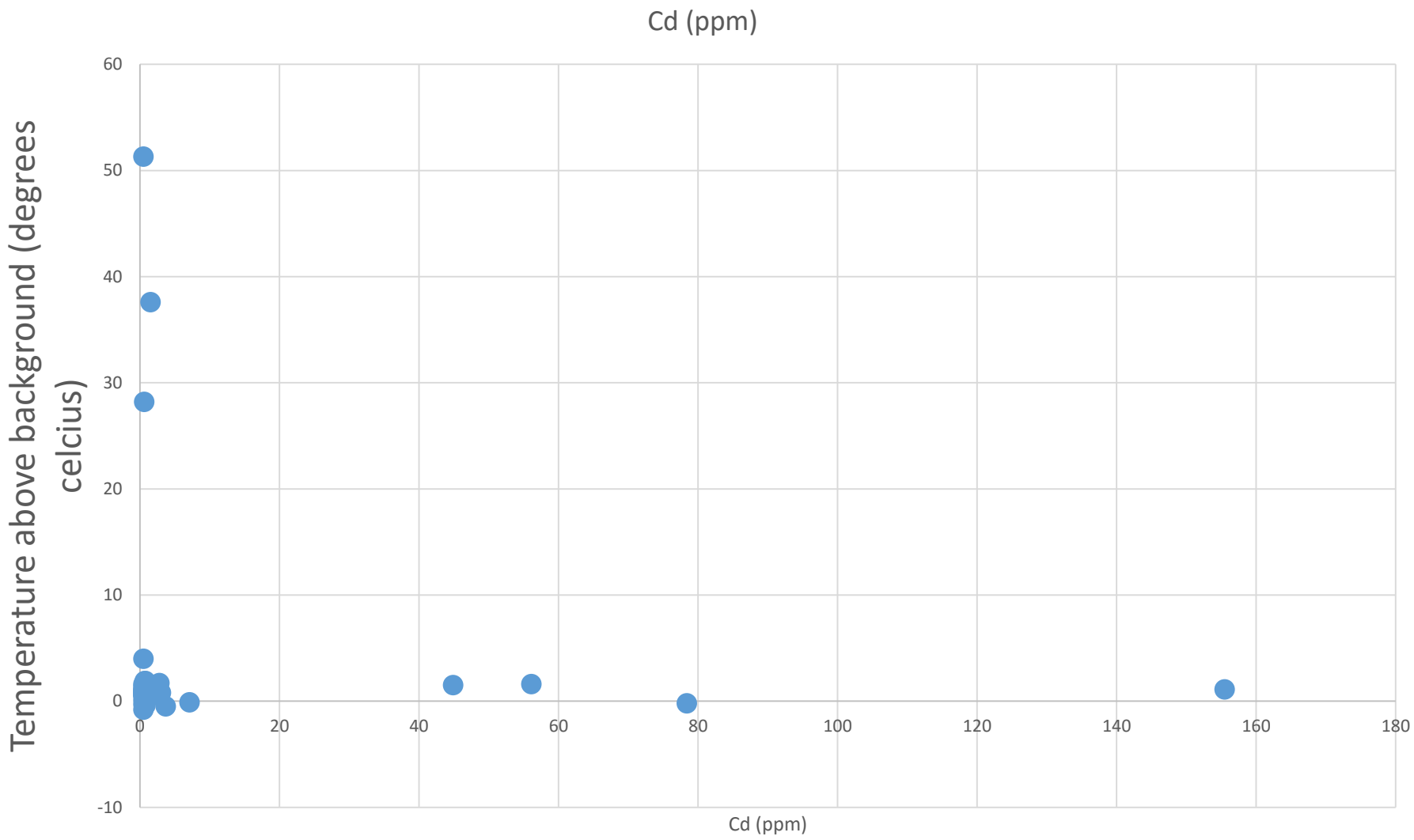
Cd (ppm)
Temperature above background (degrees celcius)
60
50
40
30
20
10
0
-10
0
20
40
60
80
100
120
140
160
180
Cd (ppm)

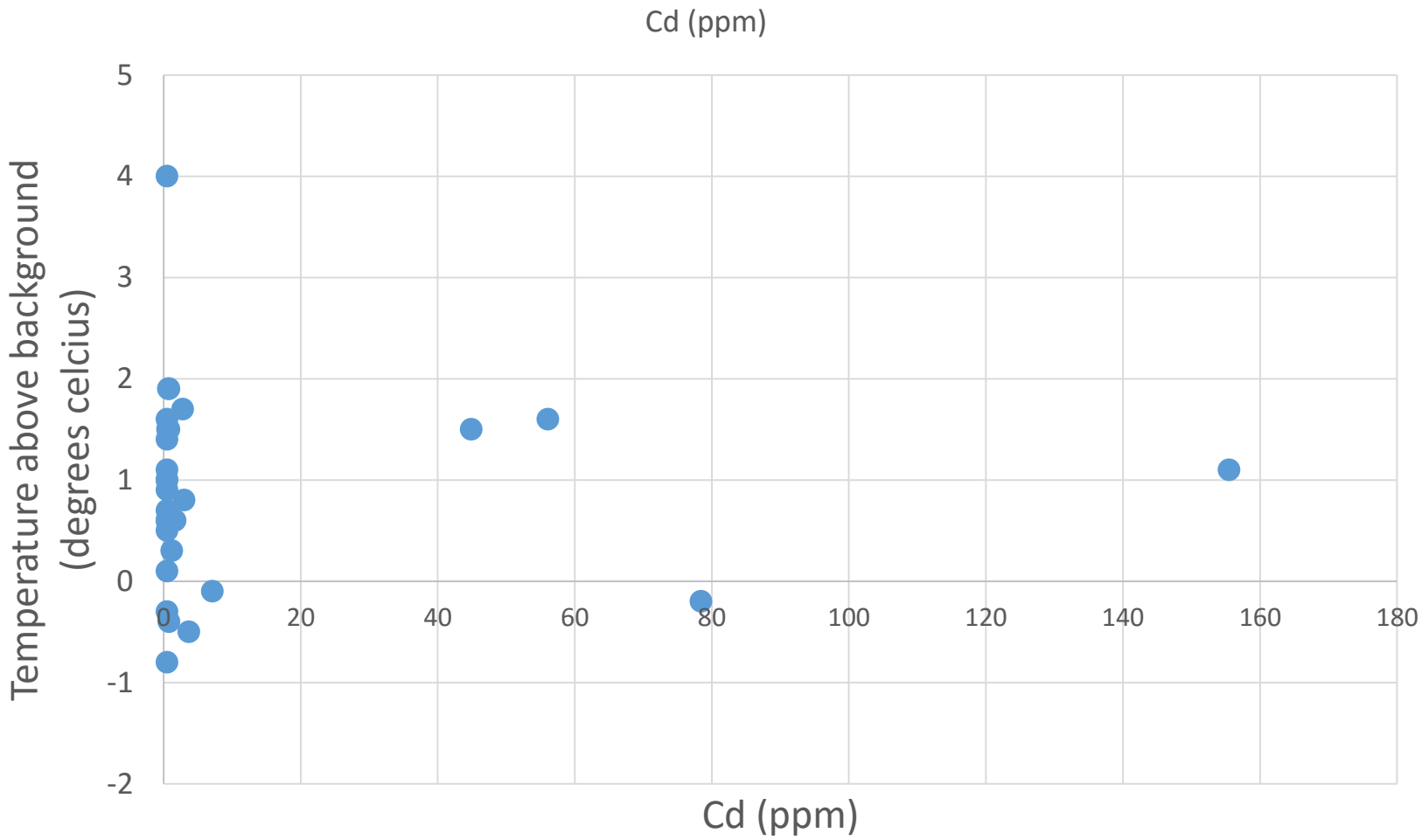
Cd (ppm)
Temperature above background (degrees celcius)
5
4
3
2
1
0
-1
-2
0
20
40
60
80
100
120
140
160
180
Cd (ppm)

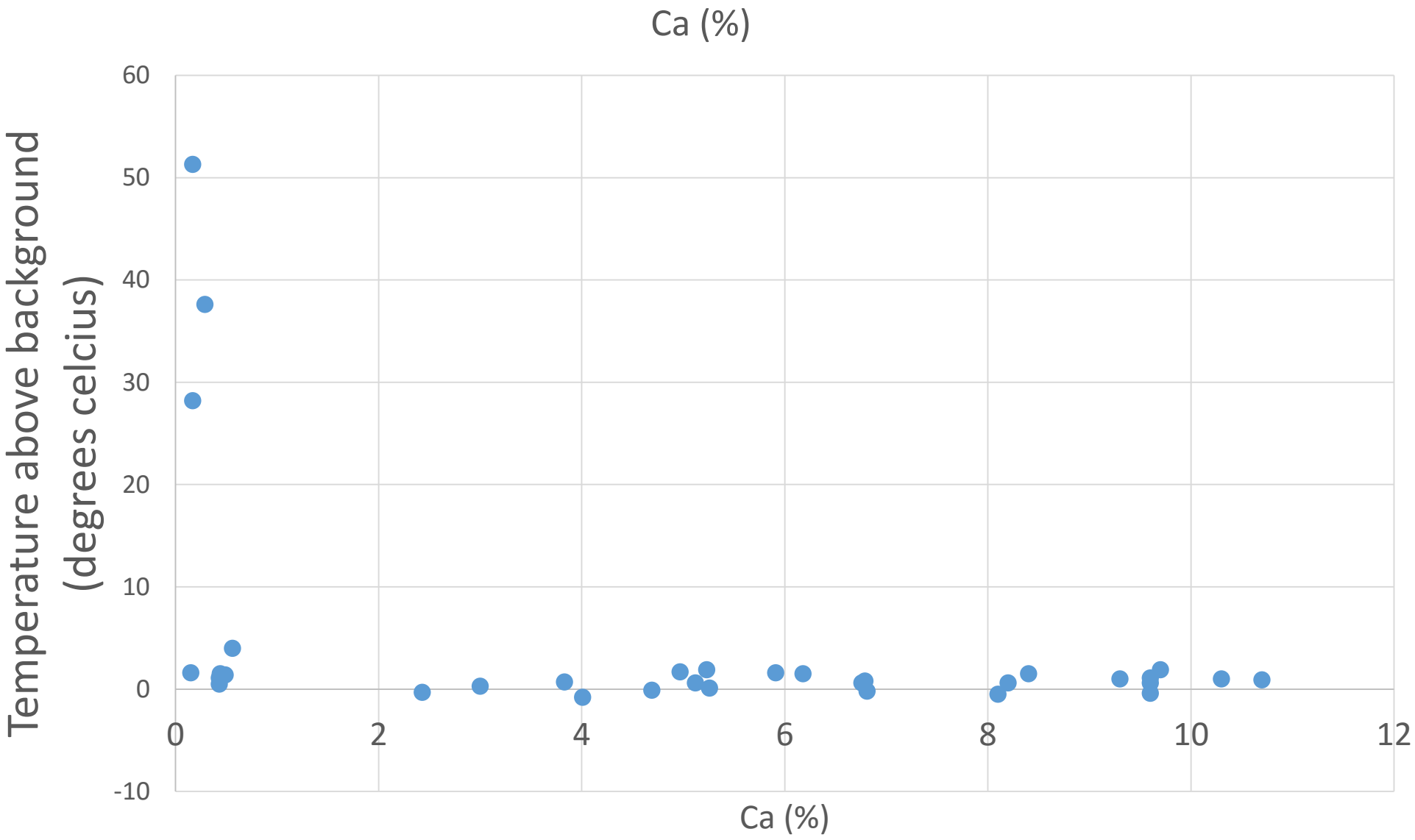
Ca (%)
Temperature above background (degrees celcius)
60
50
40
30
20
10
0
-10
0
2
4
6
8
10
12
Ca (%)

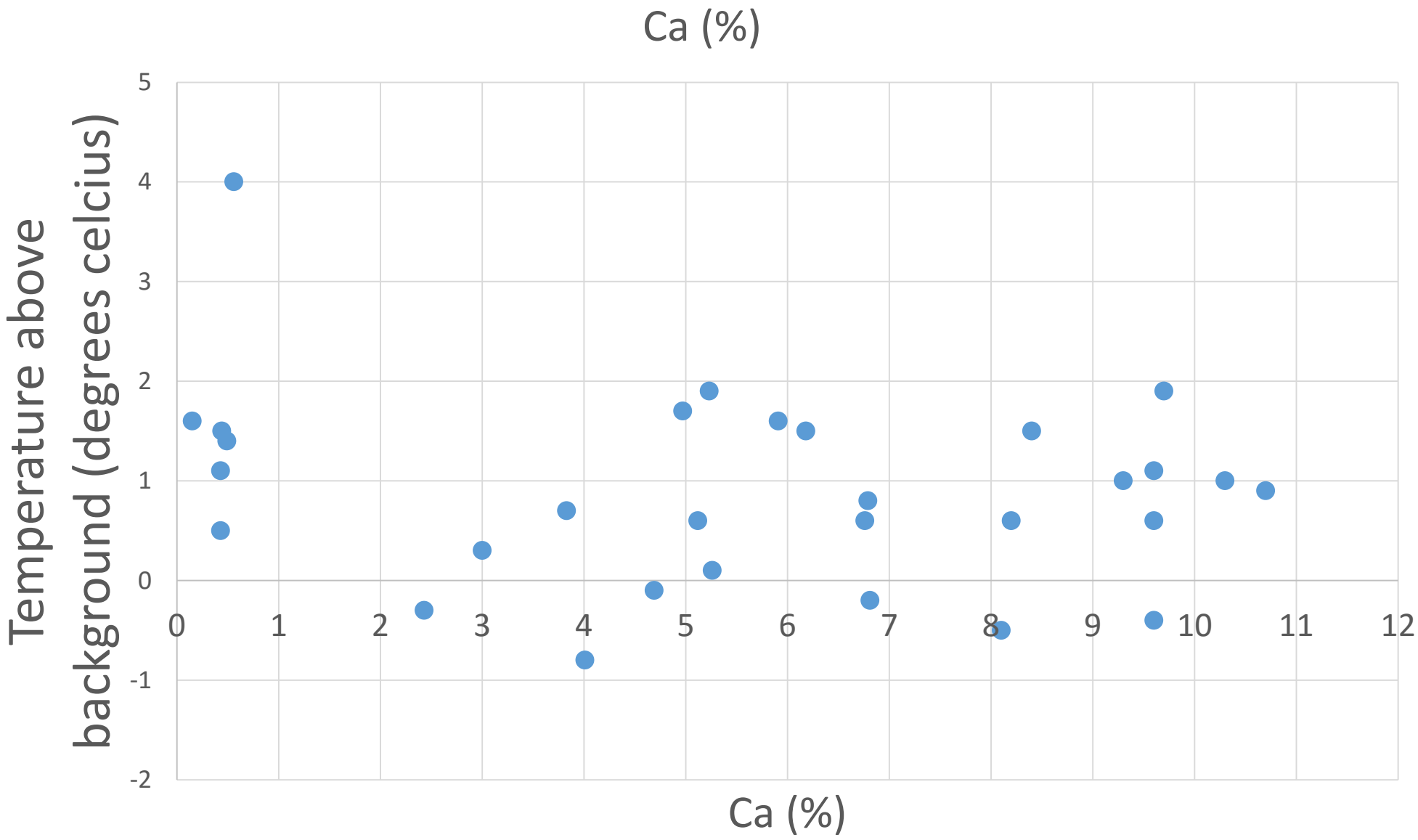
Ca (%)
Temperature above background (degrees celcius)
5
4
3
2
1
0
-1
-2
0
1
2
3
4
5
6
7
8
9
10
11
12
Ca (%)

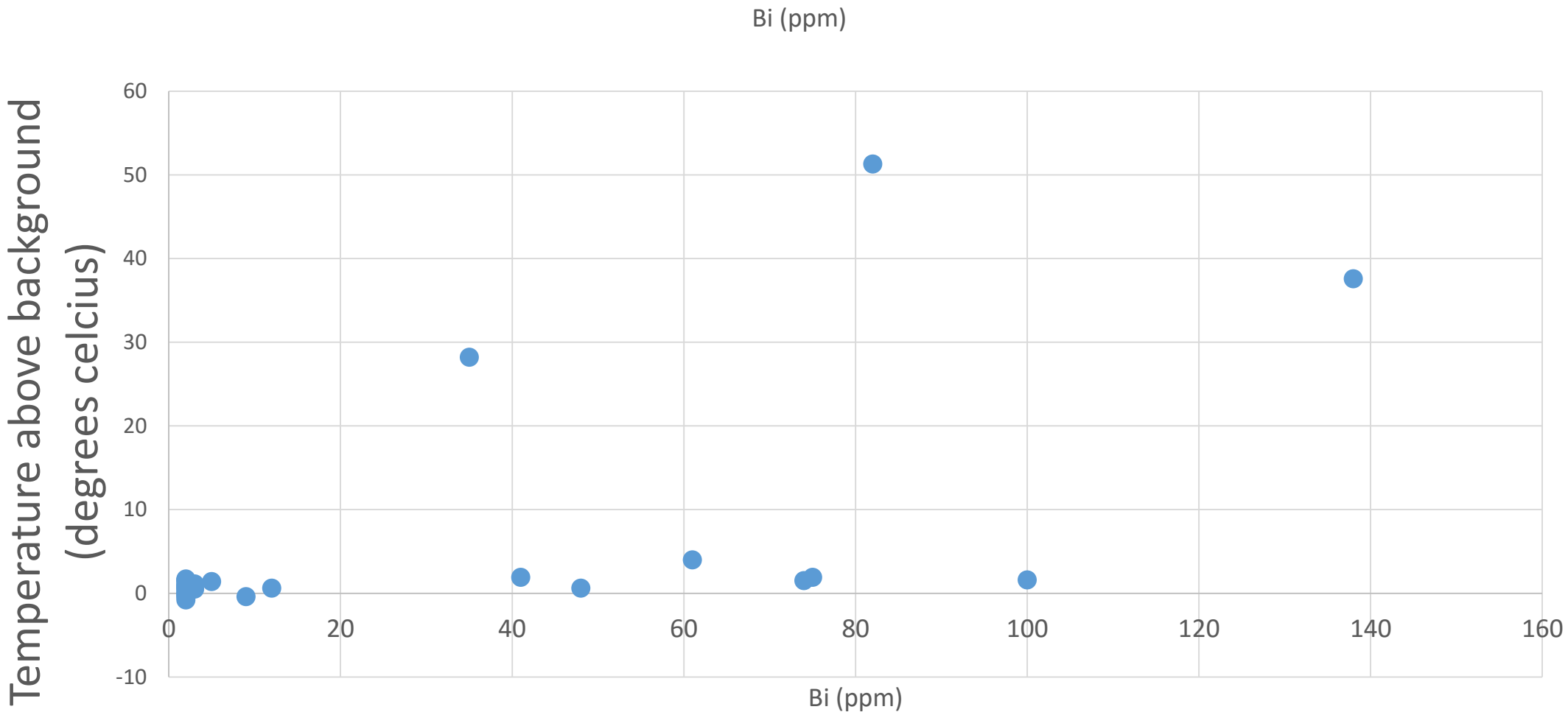
Bi (ppm)
Temperature above background (degrees celcius)
60
50
40
30
20
10
0
-10
0
20
40
60
80
100
120
140
160
Bi (ppm)

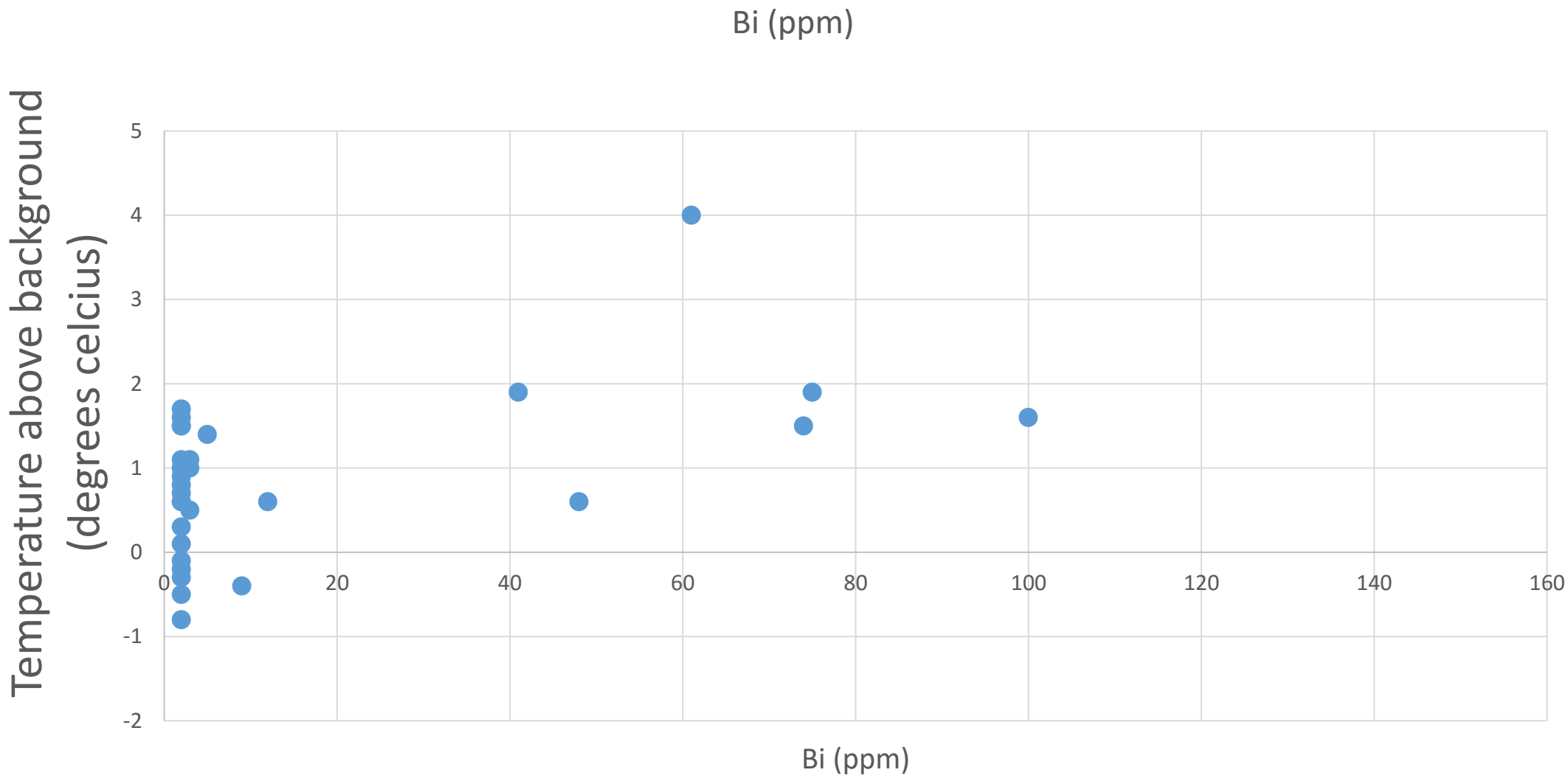
Bi (ppm)
Temperature above background (degrees celcius)
5
4
3
2
1
0
-1
-2
0
20
40
60
80
100
120
140
160
Bi (ppm)

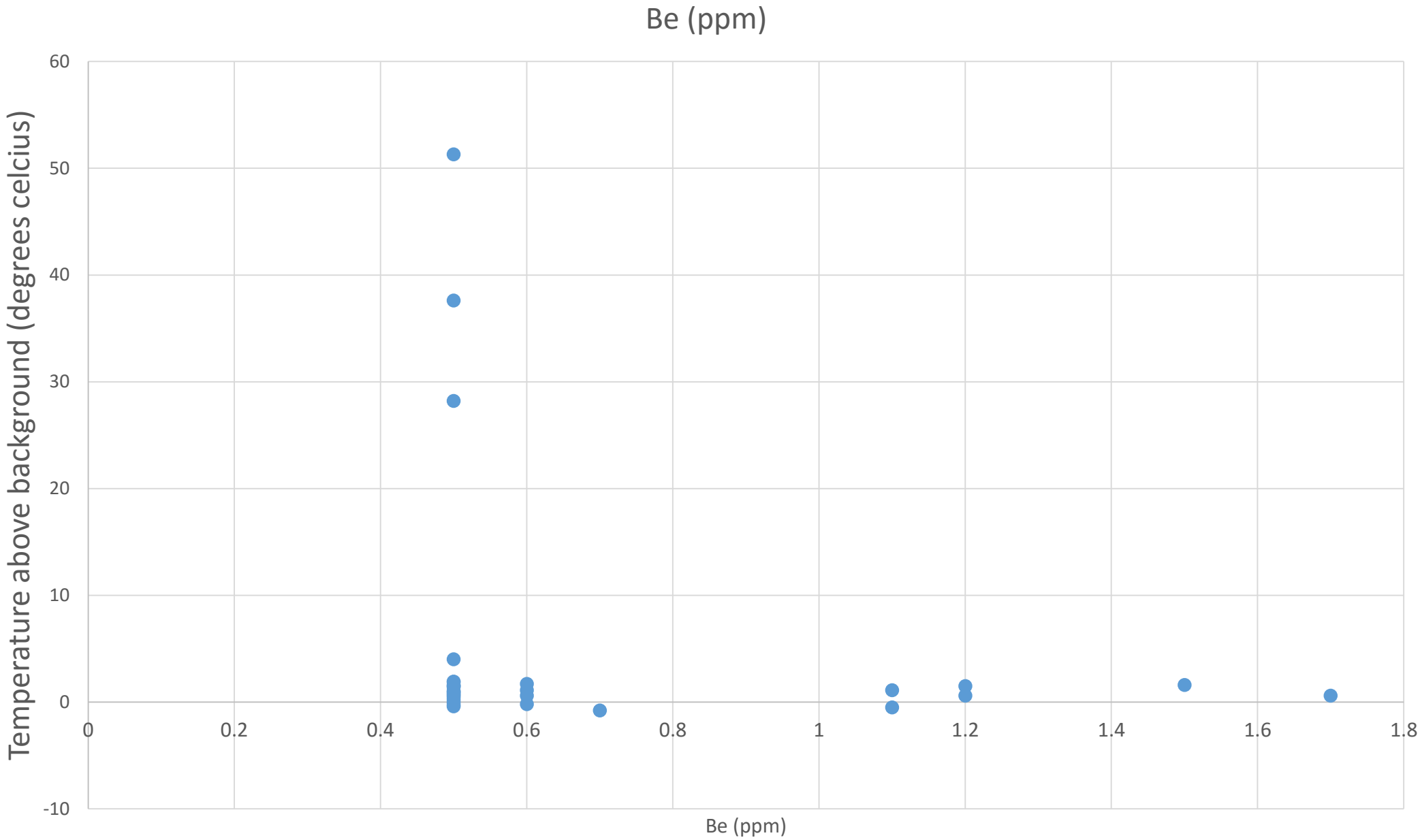
Be (ppm)
Temperature above background (degrees celcius)
60
50
40
30
20
10
0
-10
0
0.2
0.4
0.6
0.8
1
1.2
1.4
1.6
1.8
Be (ppm)

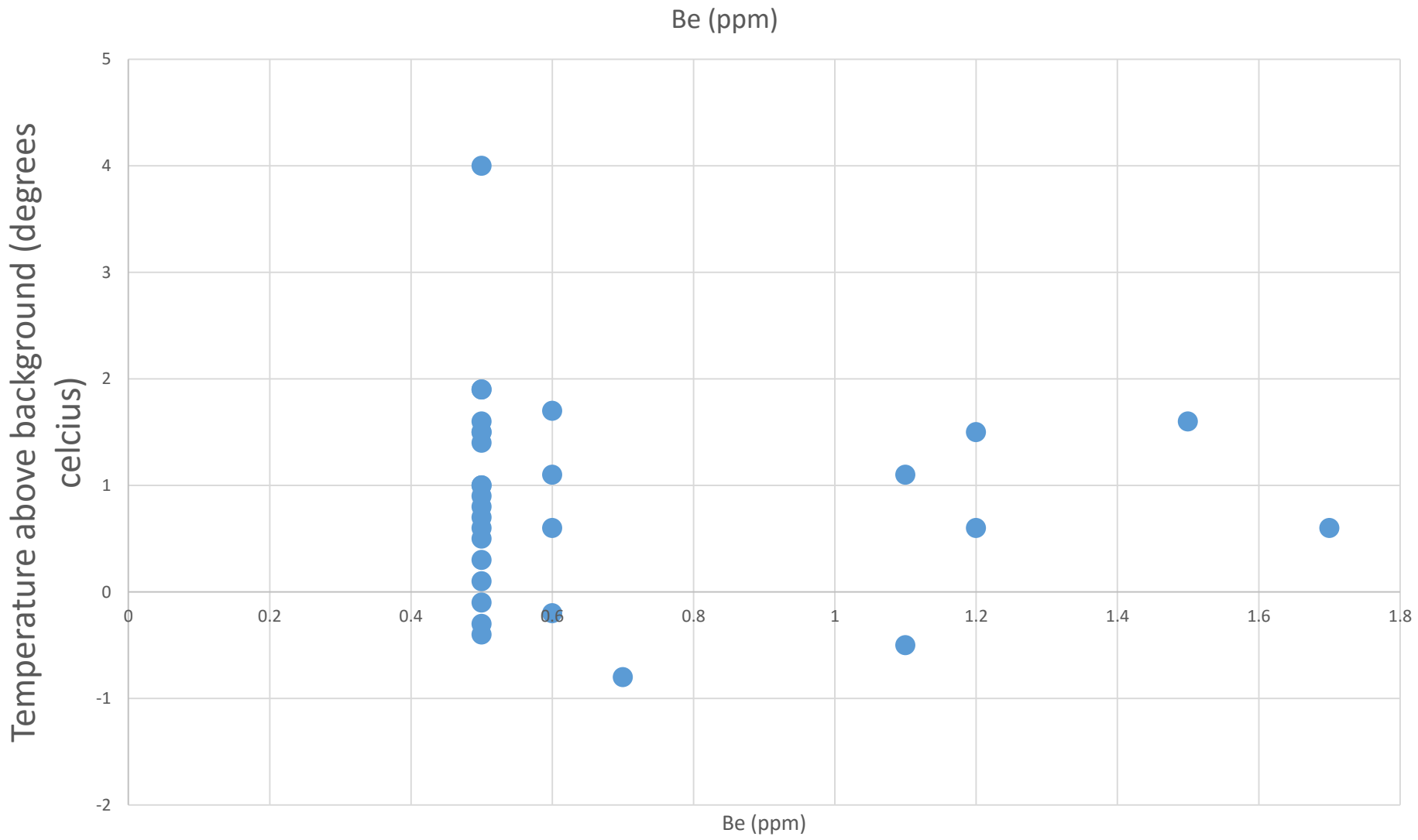
Be (ppm)
Temperature above background (degrees celcius)
5
4
3
2
1
0
-1
-2
0
0.2
0.4
0.6
0.8
1
1.2
1.4
1.6
1.8
Be (ppm)

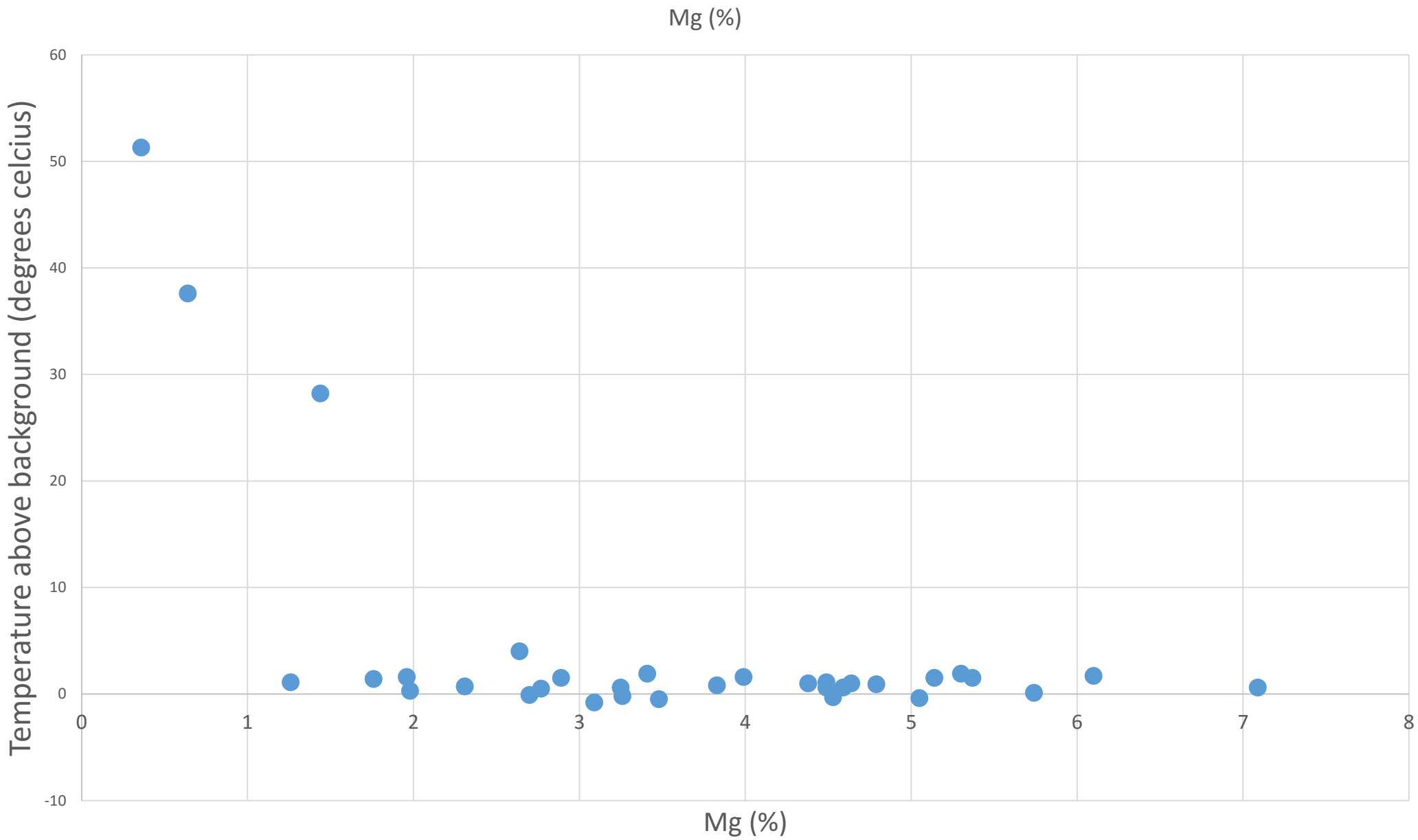
Mg (%)
Temperature above background (degrees celcius)
60
50
40
30
20
10
0
-10
0
1
2
3
4
5
6
7
8
Mg (%)

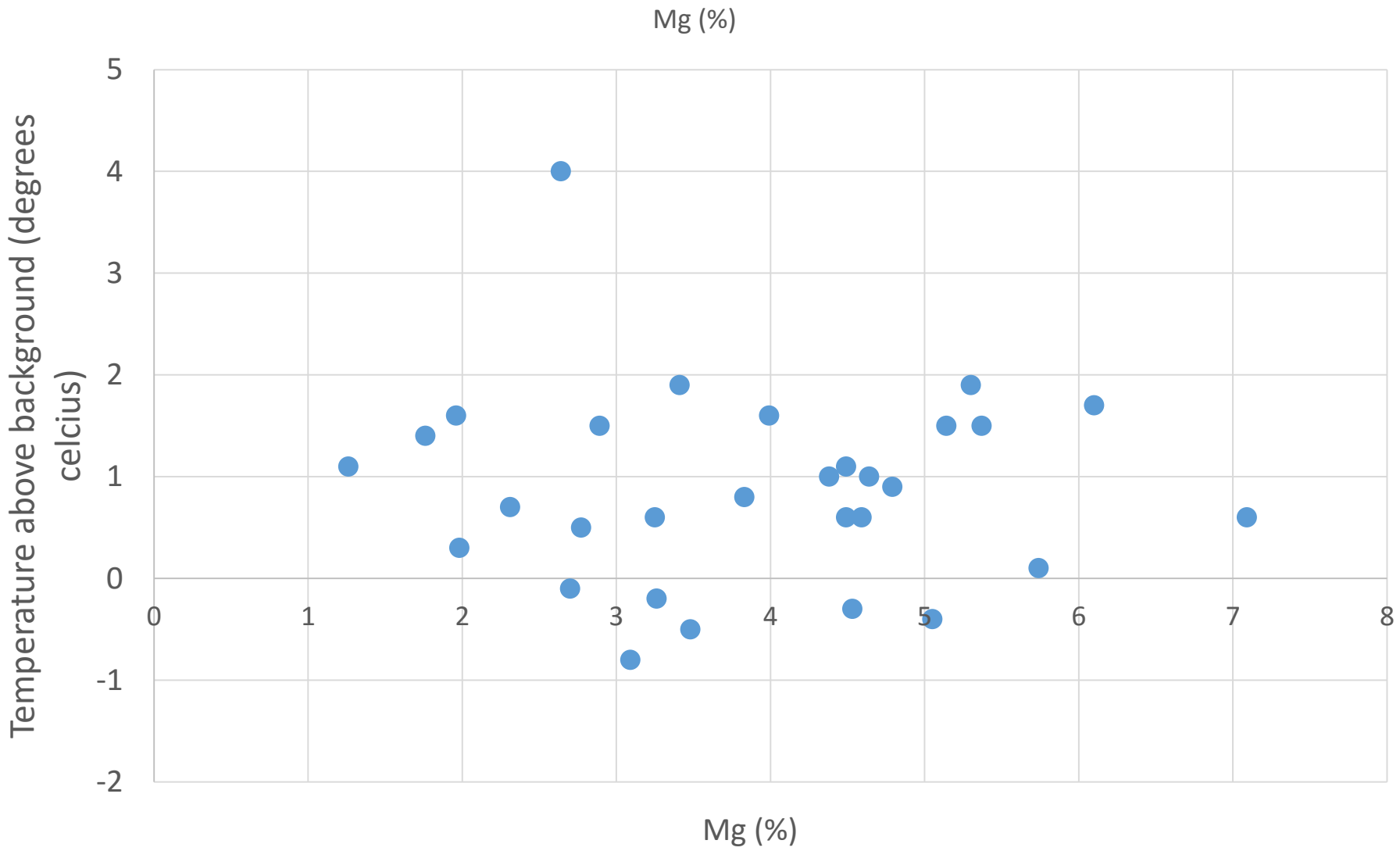
Mg (%)
Temperature above background (degrees celcius)
5
4
3
2
1
0
-1
-2
0
1
2
3
4
5
6
7
8
Mg (%)

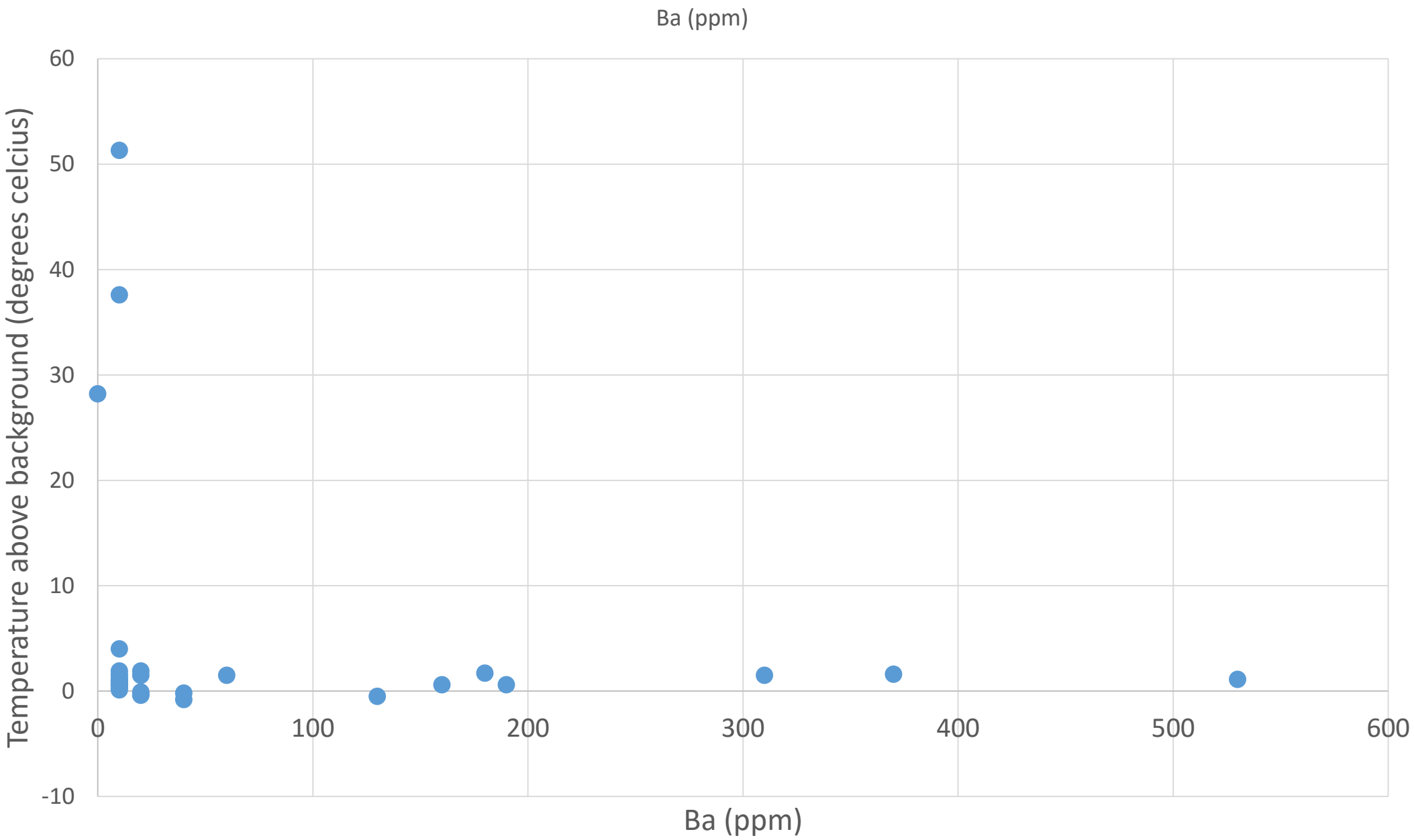
Ba (ppm)
Temperature above background (degrees celcius)
60
50
40
30
20
10
0
-10
0
100
200
300
400
500
600
Ba (ppm)

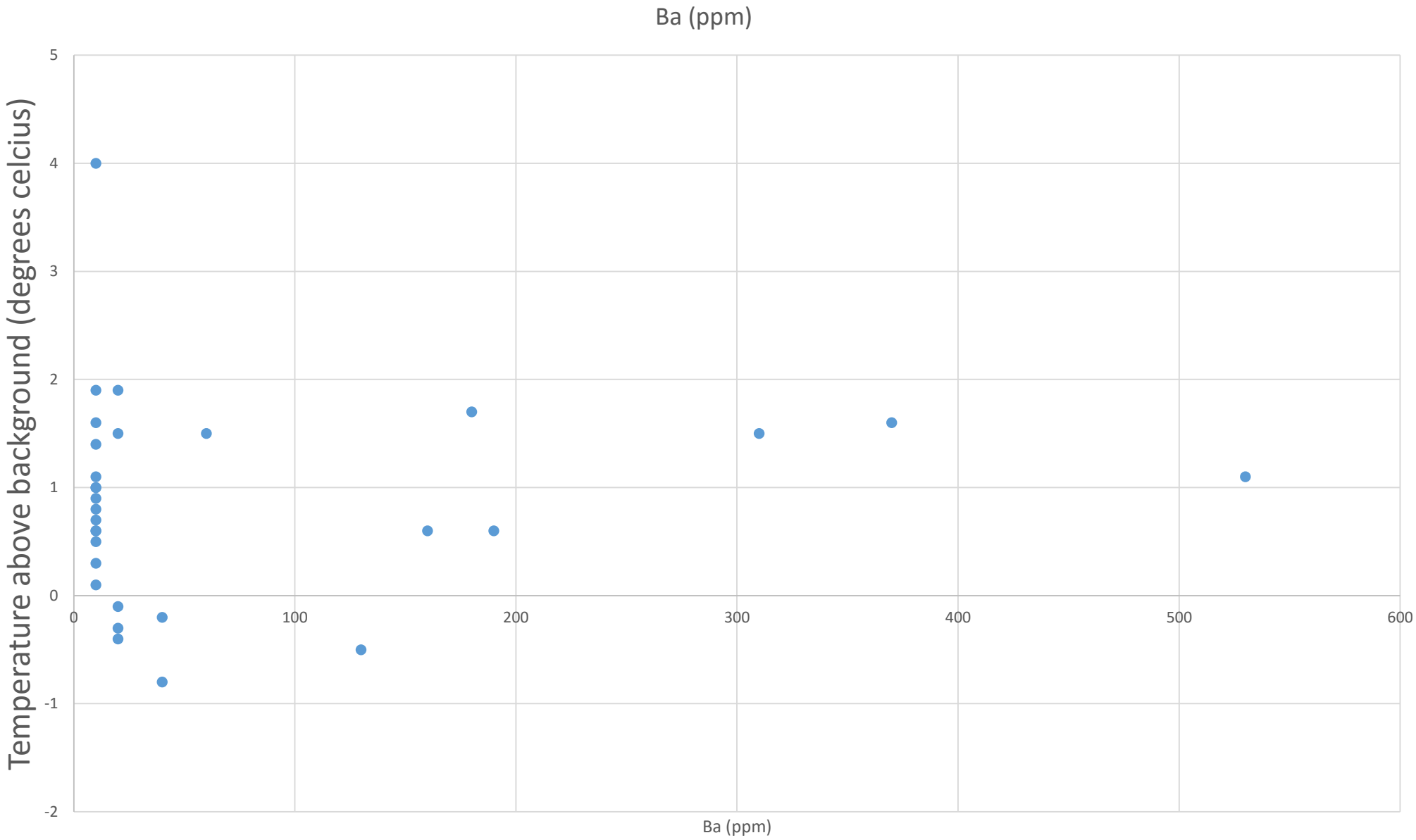
Ba (ppm)
Temperature above background (degrees celcius)
5
4
3
2
1
0
-1
-2
0
100
200
300
400
500
600
Ba (ppm)

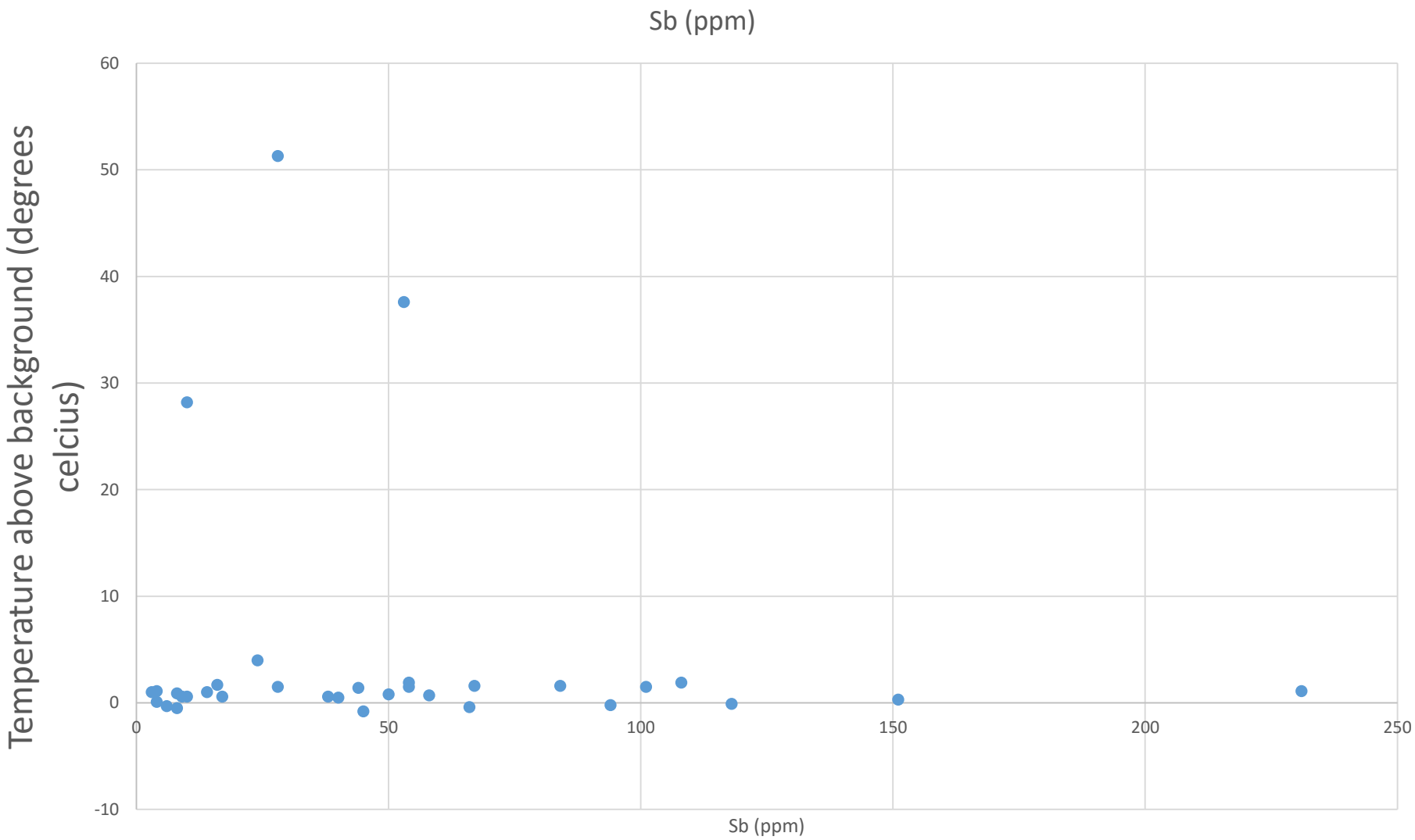
Sb (ppm)
Temperature above background (degrees celcius)
60
50
40
30
20
10
0
-10
0
50
100
150
200
250
Sb (ppm)

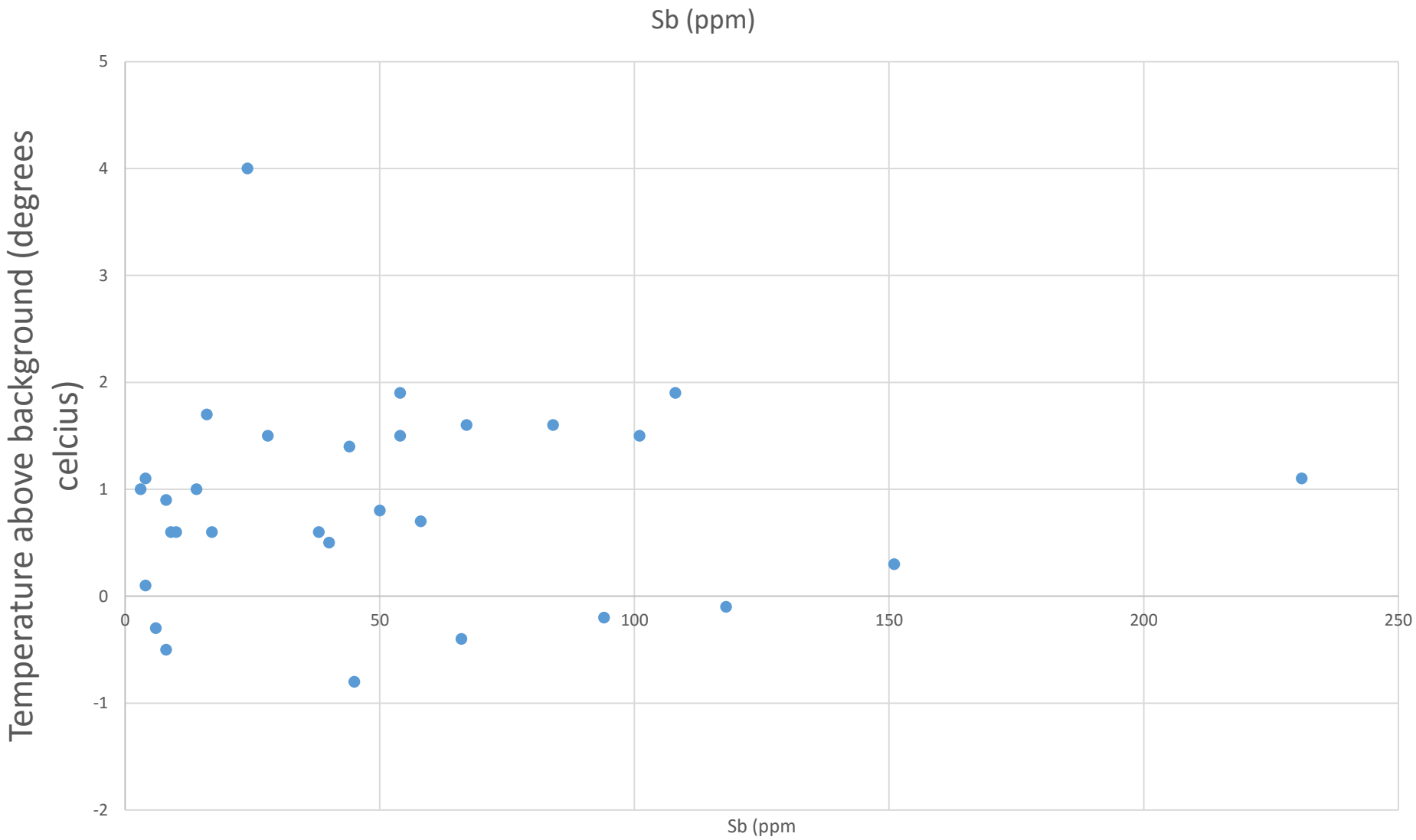
Sb (ppm)
Temperature above background (degrees celcius)
5
4
3
2
1
0
-1
-2
0
50
100
150
200
250
Sb (ppm

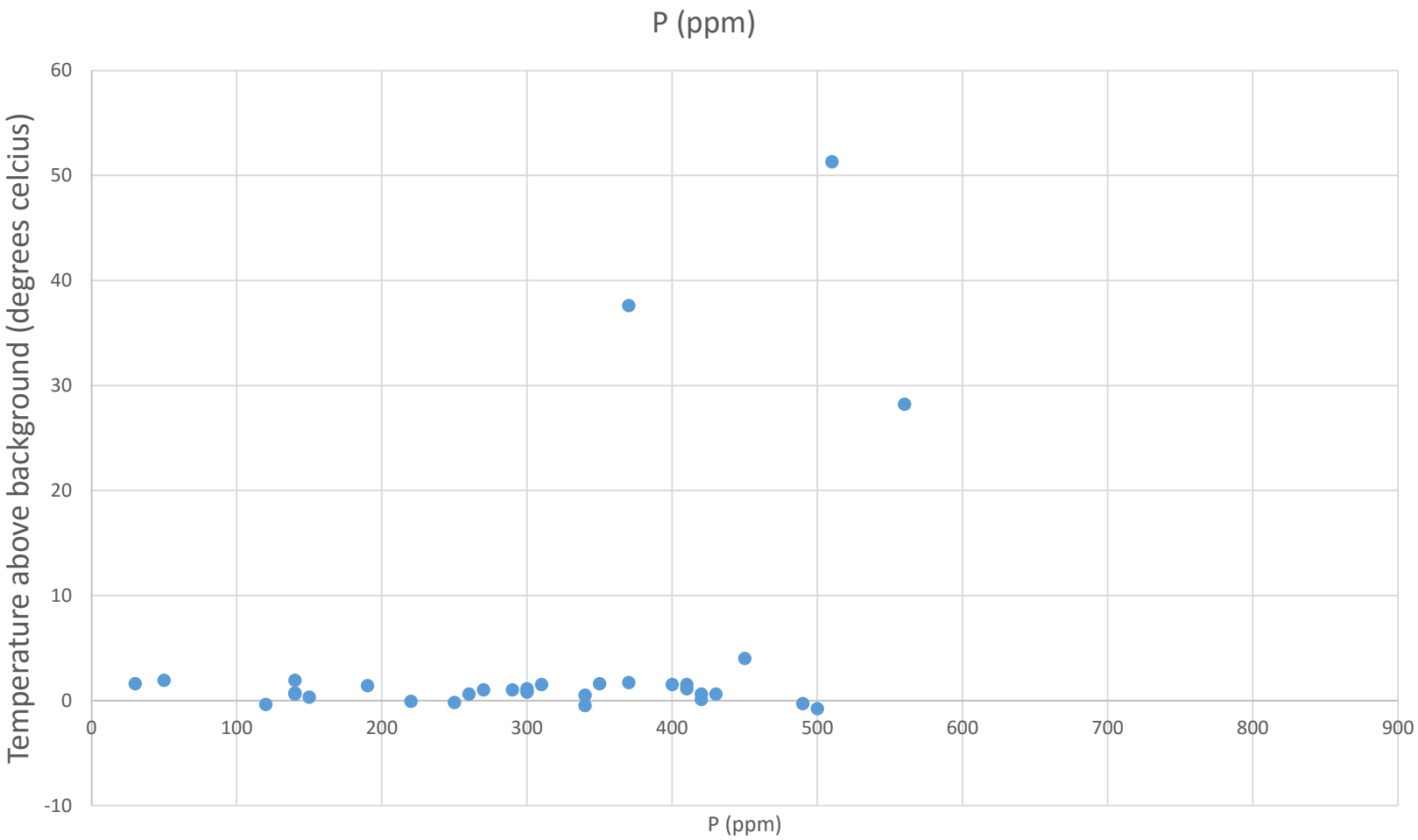
P (ppm)
Temperature above background (degrees celcius)
60
50
40
30
20
10
0
-10
0
100
200
300
400
500
600
700
800
900
P (ppm)

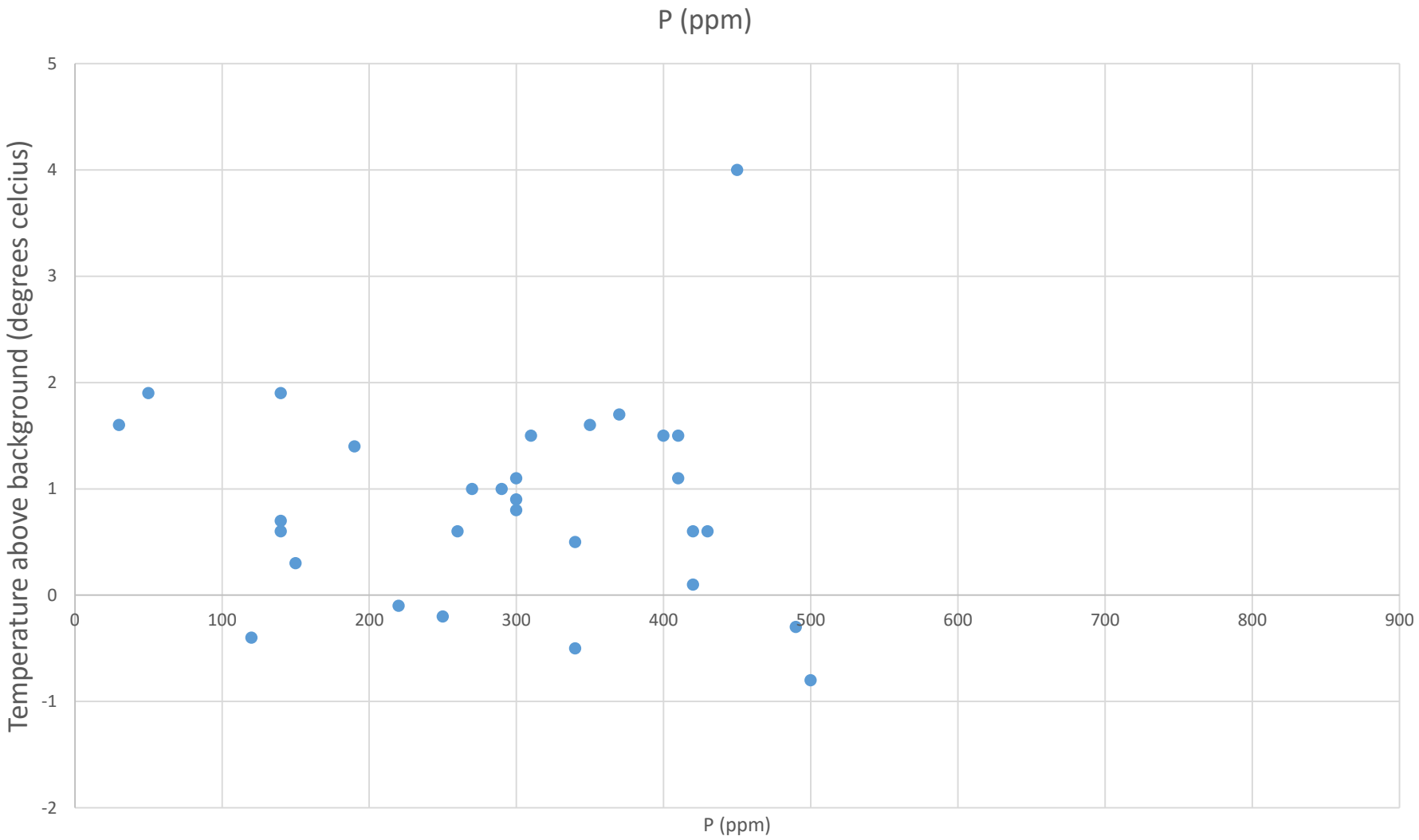
P (ppm)
Temperature above background (degrees celcius)
5
4
3
2
1
0
-1
-2
0
100
200
300
400
500
600
700
800
900
P (ppm)

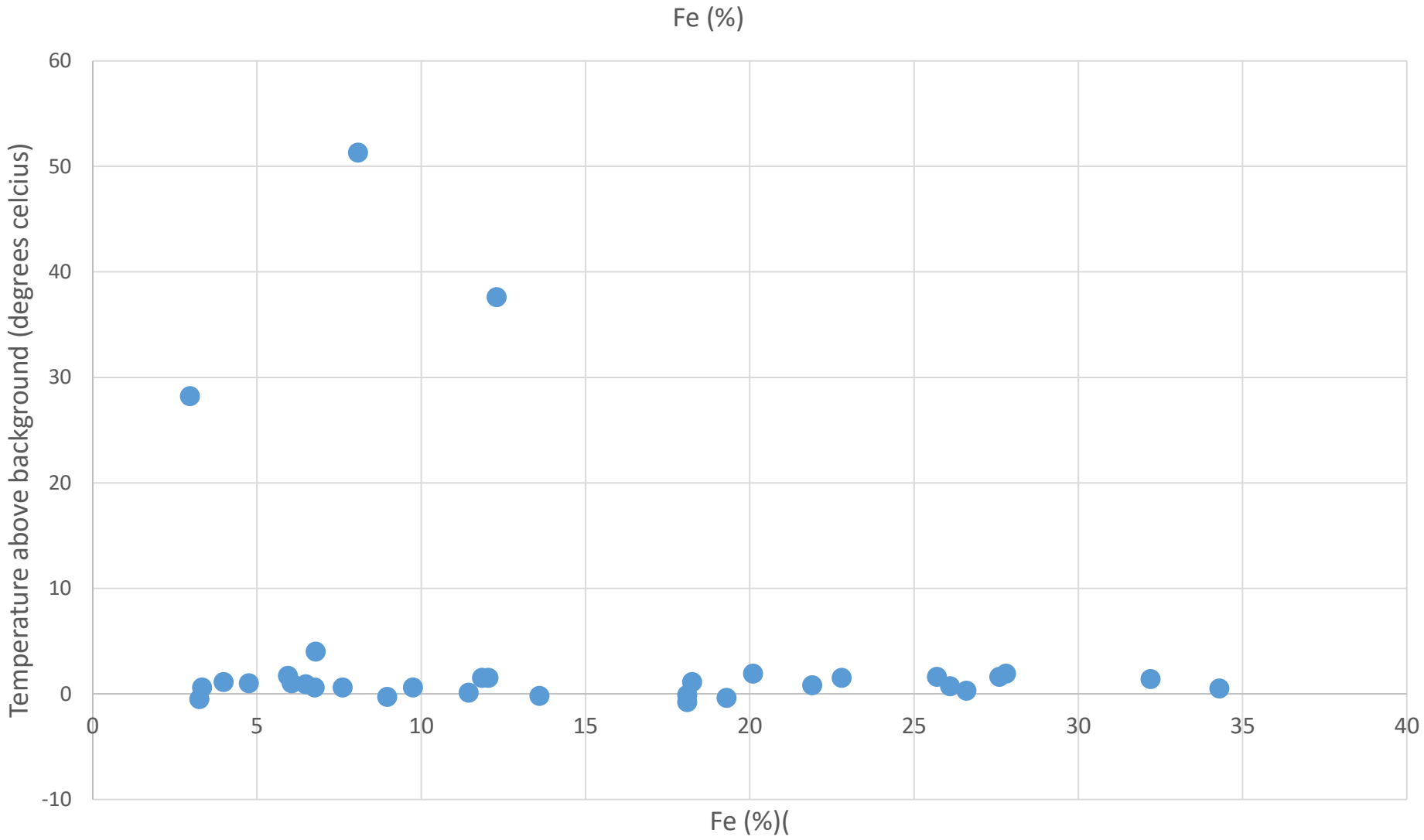
Fe (%)
Temperature above background (degrees celcius)
60
50
40
30
20
10
0
-10
0
5
10
15
20
25
30
35
40
Fe (%)(

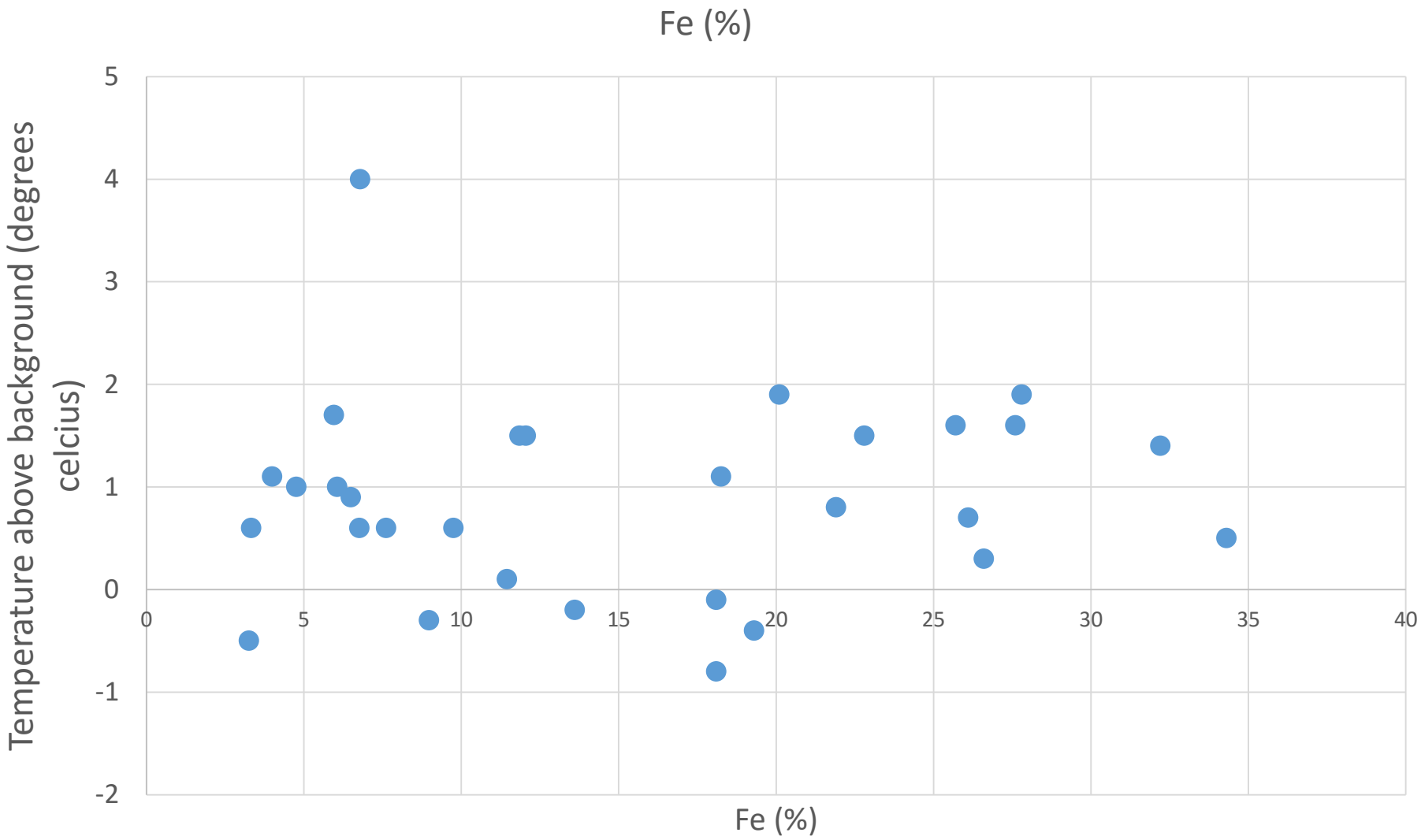
Fe (%)
Temperature above background (degrees celcius)
5
4
3
2
1
0
-1
-2
0
5
10
15
20
25
30
35
40
Fe (%)

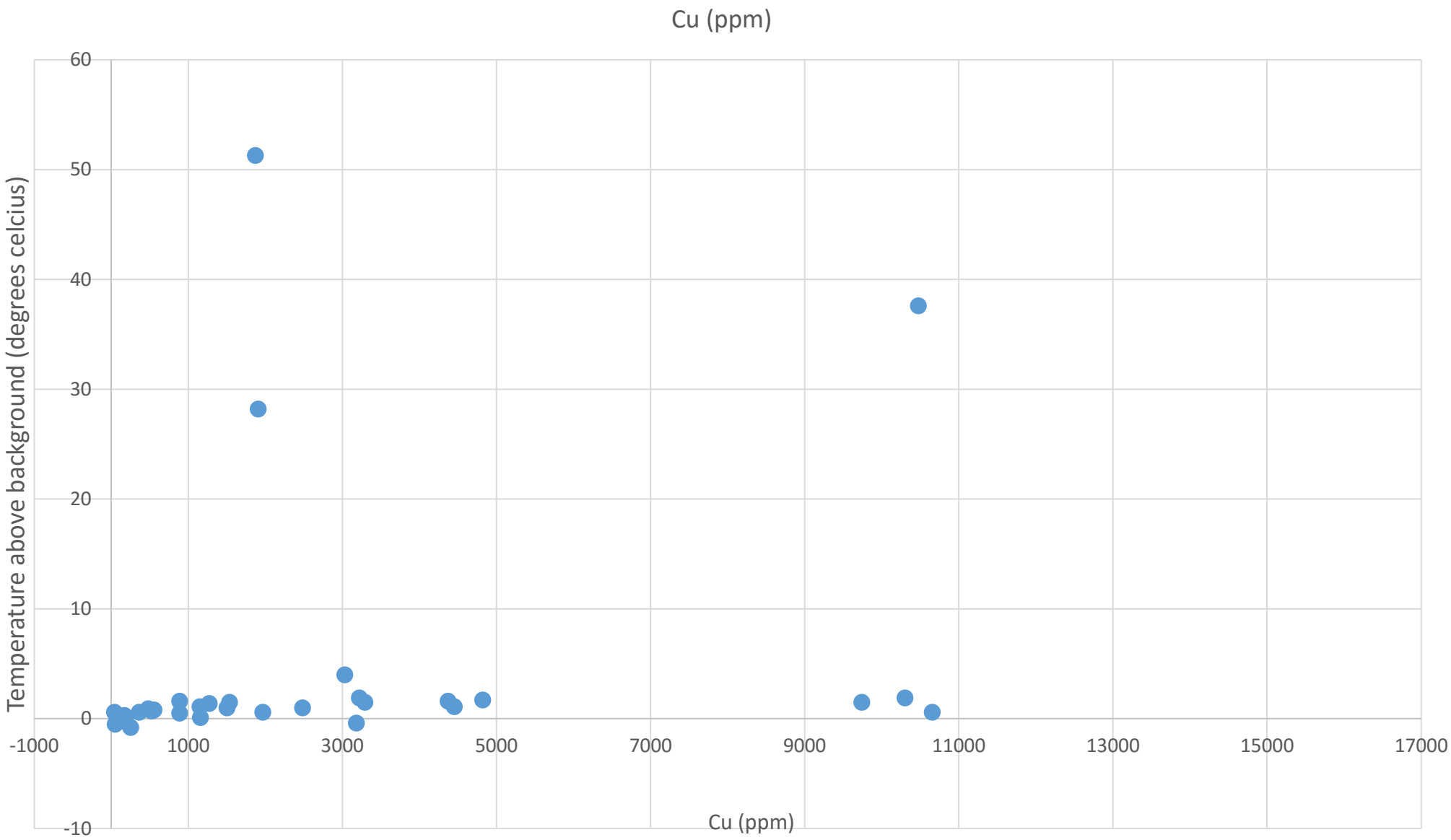
Cu (ppm)
Temperature above background (degrees celcius)
60
50
40
30
20
10
0
-10
-1000
1000
3000
5000
7000
9000
11000
13000
15000
17000
Cu (ppm)

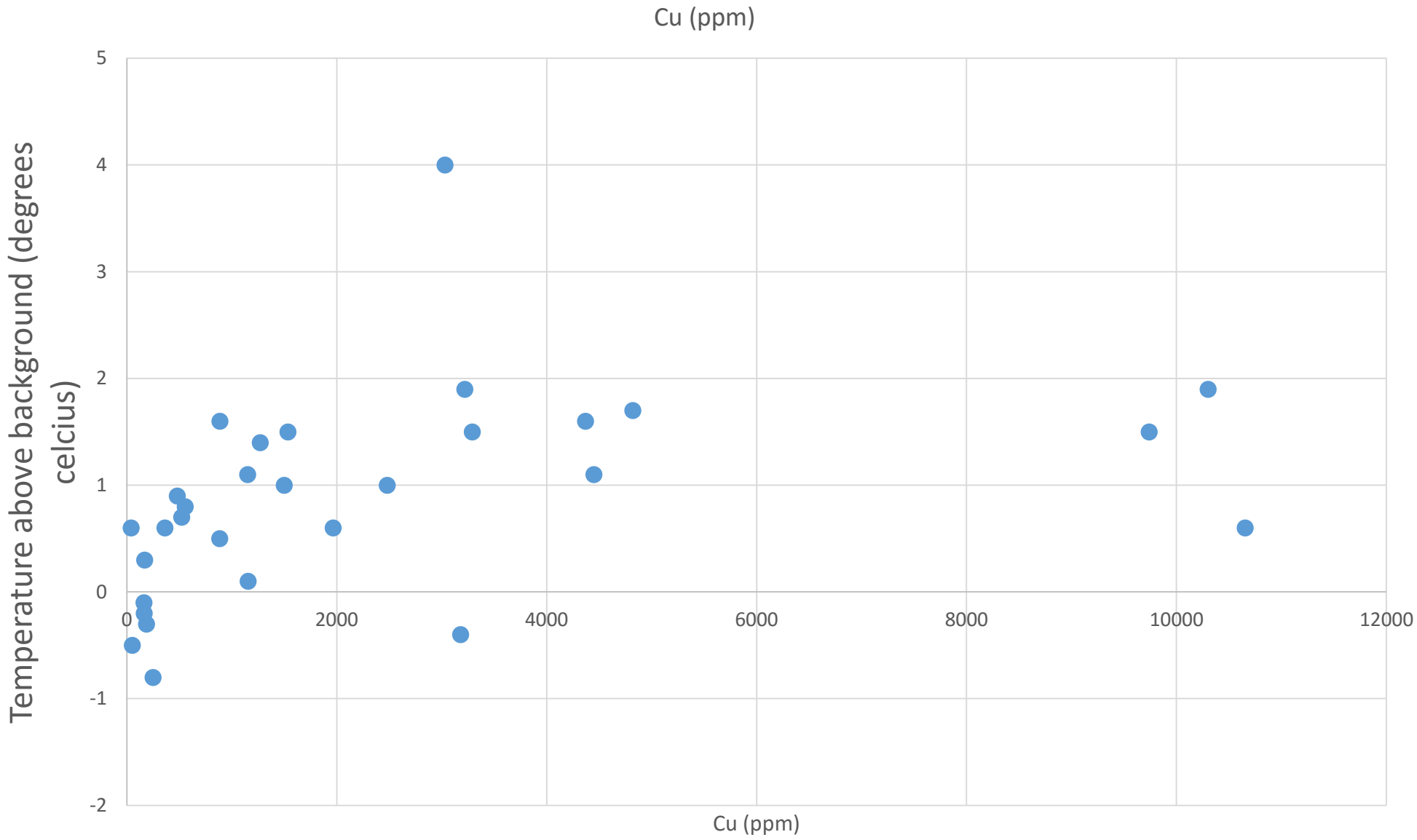
Cu (ppm)
Temperature above background (degrees celcius)
5
4
3
2
1
0
-1
-2
0
2000
4000
6000
8000
10000
12000
Cu (ppm)

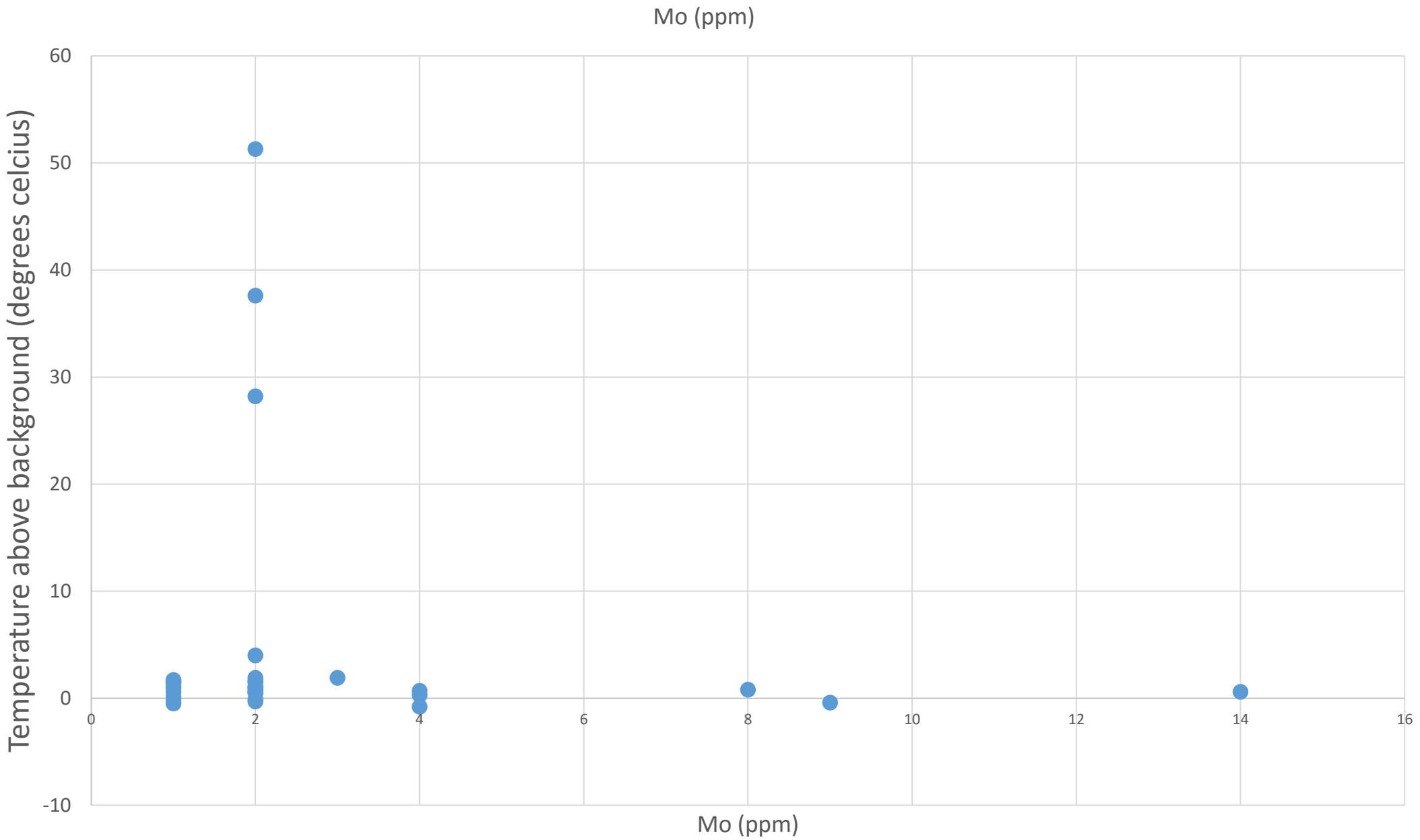
Mo (ppm)
Temperature above background (degrees celcius)
60
50
40
30
20
10
0
-10
0
2
4
6
8
10
12
14
16
Mo (ppm)

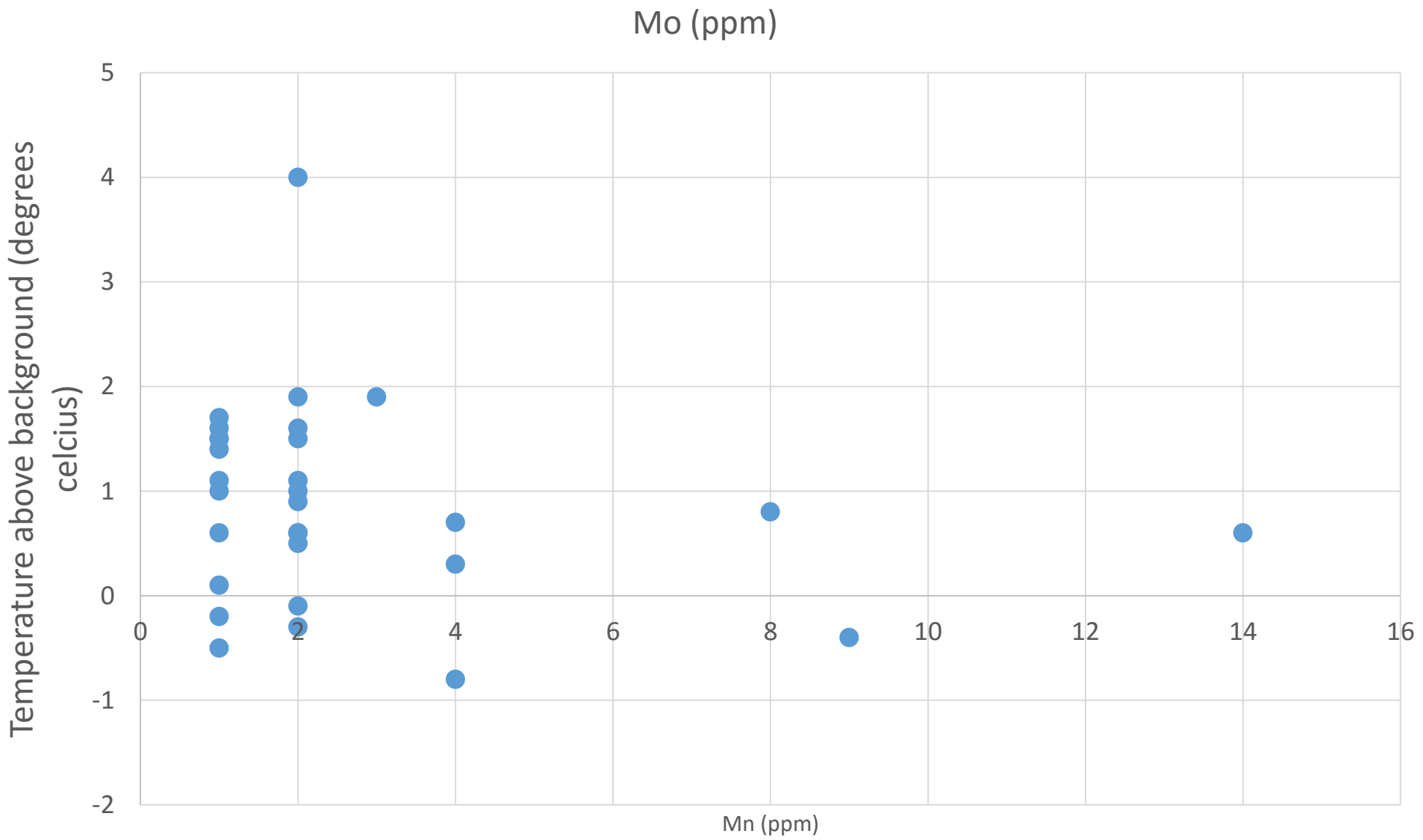
Mo (ppm)
Temperature above background (degrees celcius)
5
4
3
2
1
0
-1
-2
0
2
4
6
8
10
12
14
16
Mn (ppm)

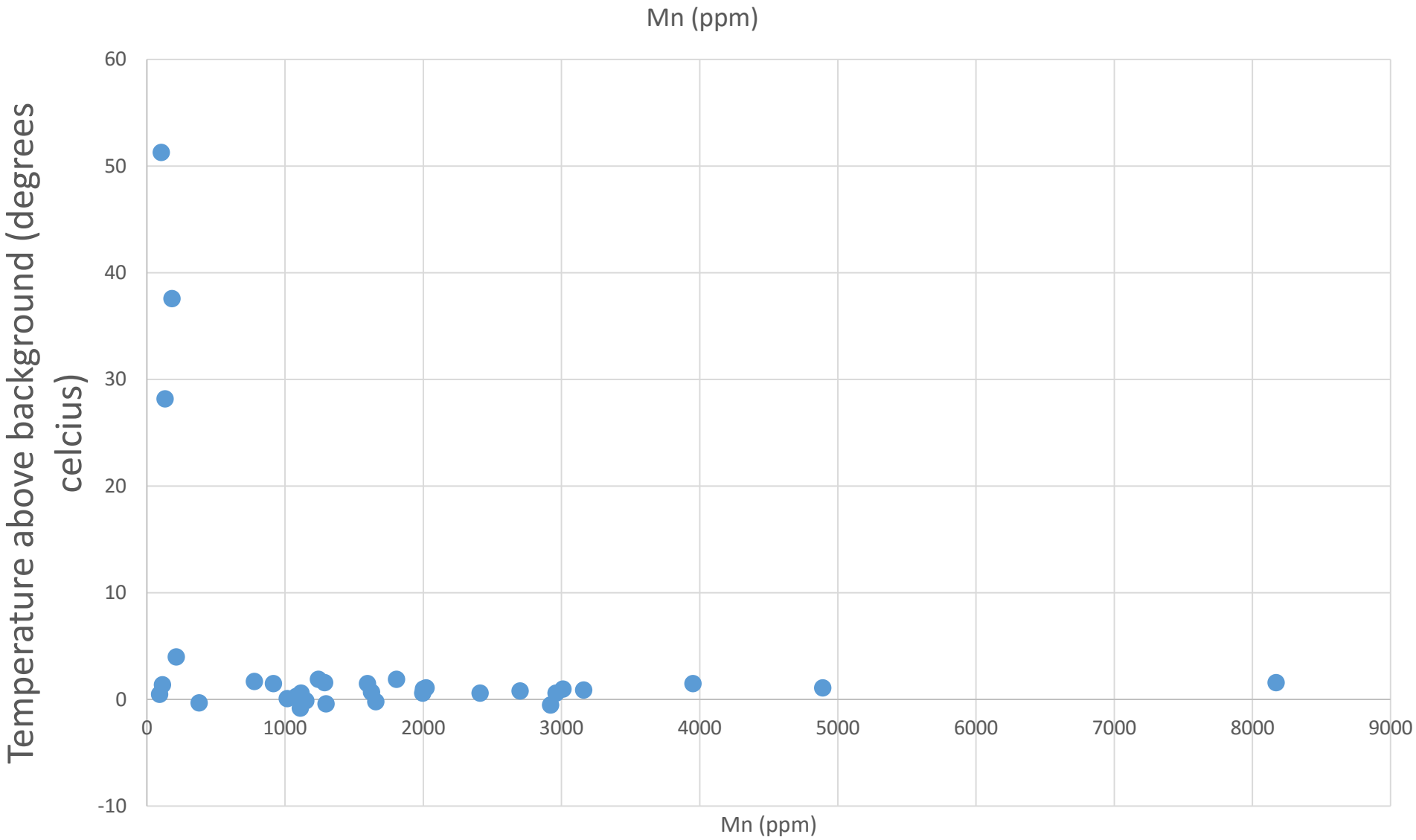
Mn (ppm)
Temperature above background (degrees celcius)
60
50
40
30
20
10
0
-10
0
1000
2000
3000
4000
5000
6000
7000
8000
9000
Mn (ppm)

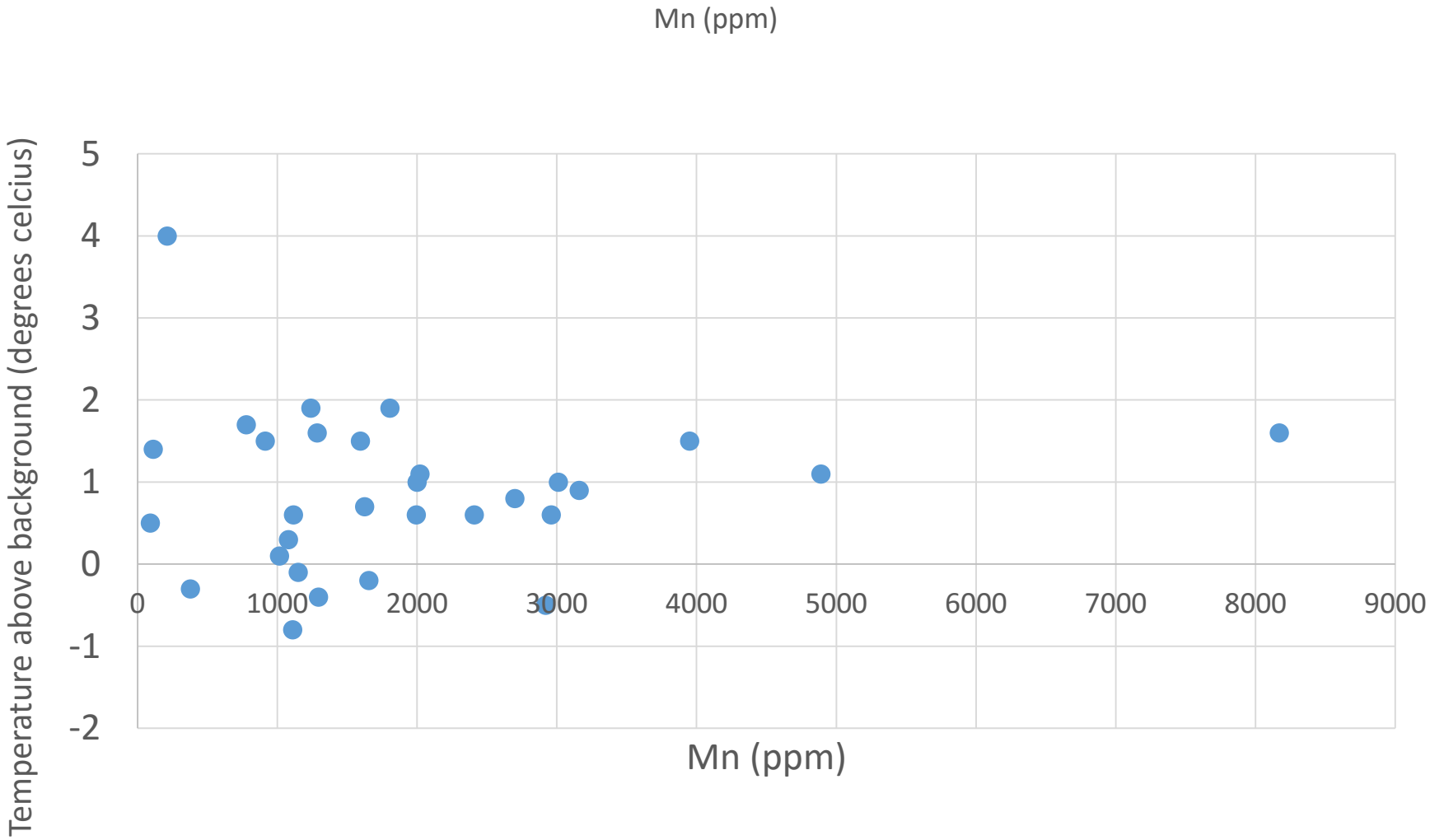
Mn (ppm)
Temperature above background (degrees celcius)
5
4
3
2
1
0
-1
-2
0
1000
2000
3000
4000
5000
6000
7000
8000
9000
Mn (ppm)

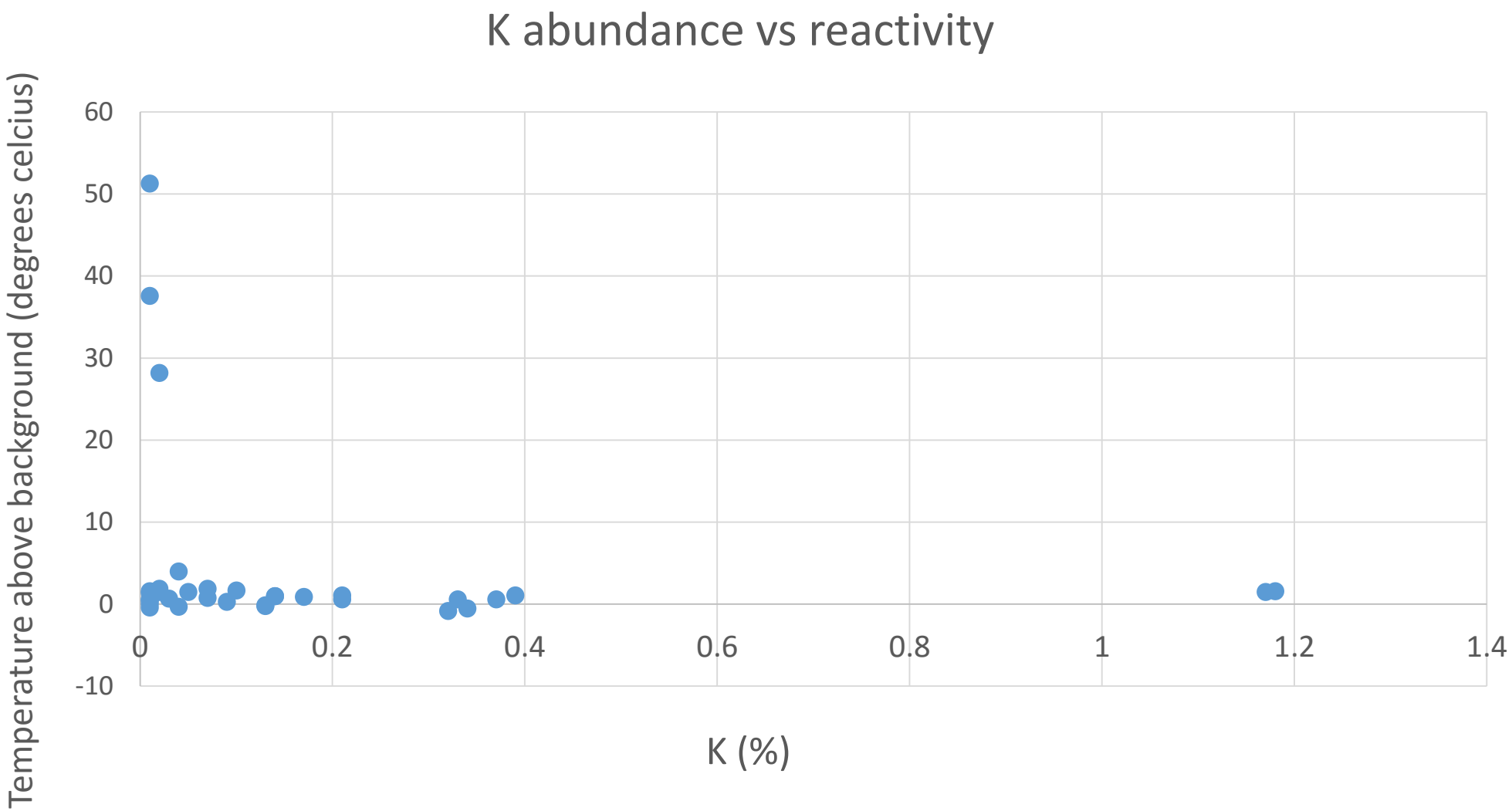
K abundance vs reactivity
Temperature above background (degrees celcius)
60
50
40
30
20
10
0
-10
0
0.2
0.4
0.6
0.8
1
1.2
1.4
K (%)

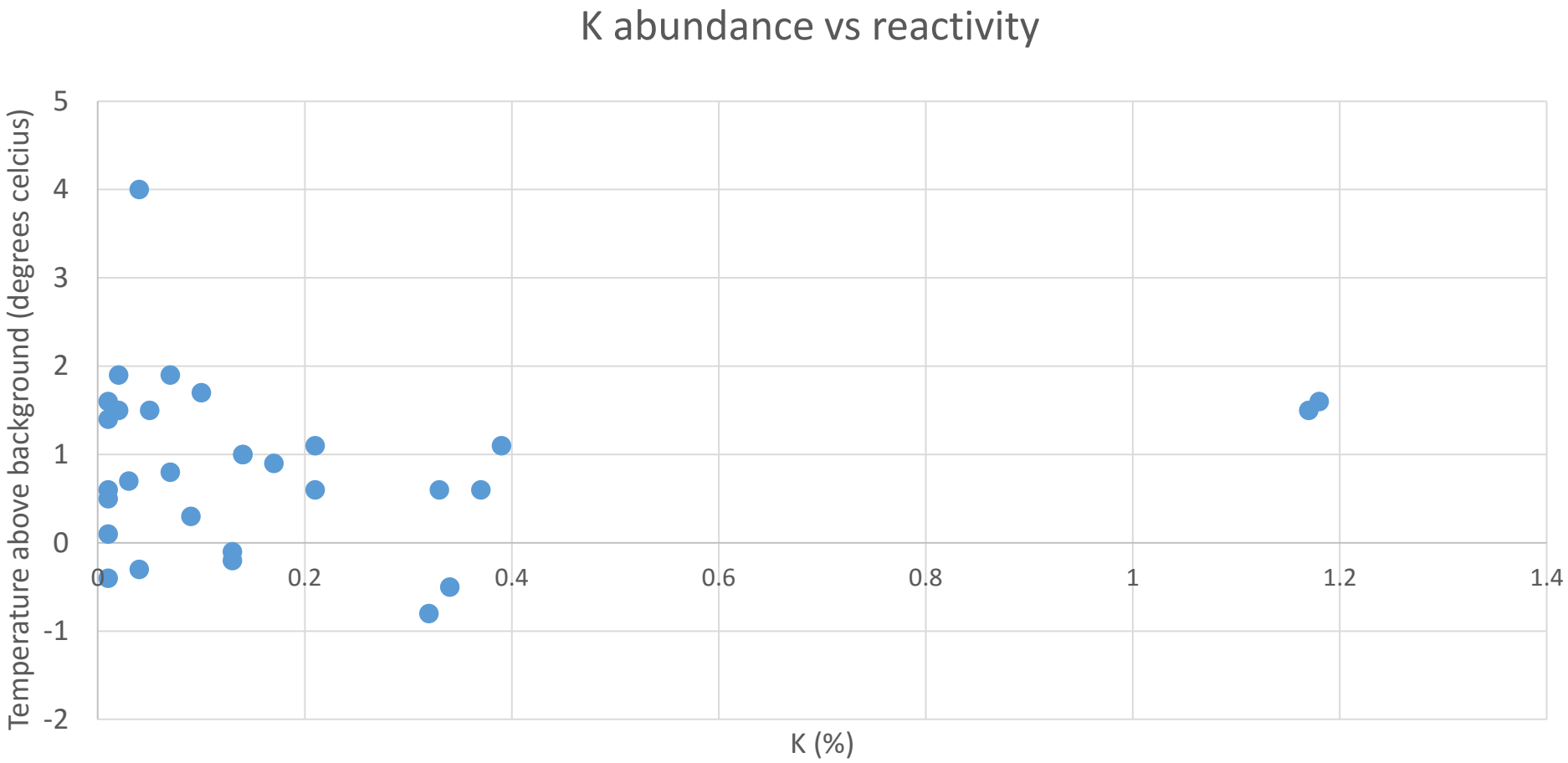
K abundance vs reactivity
Temperature above background (degrees celcius)
5
4
3
2
1
0
-1
-2
0
0.2
0.4
0.6
0.8
1
1.2
1.4
K (%)

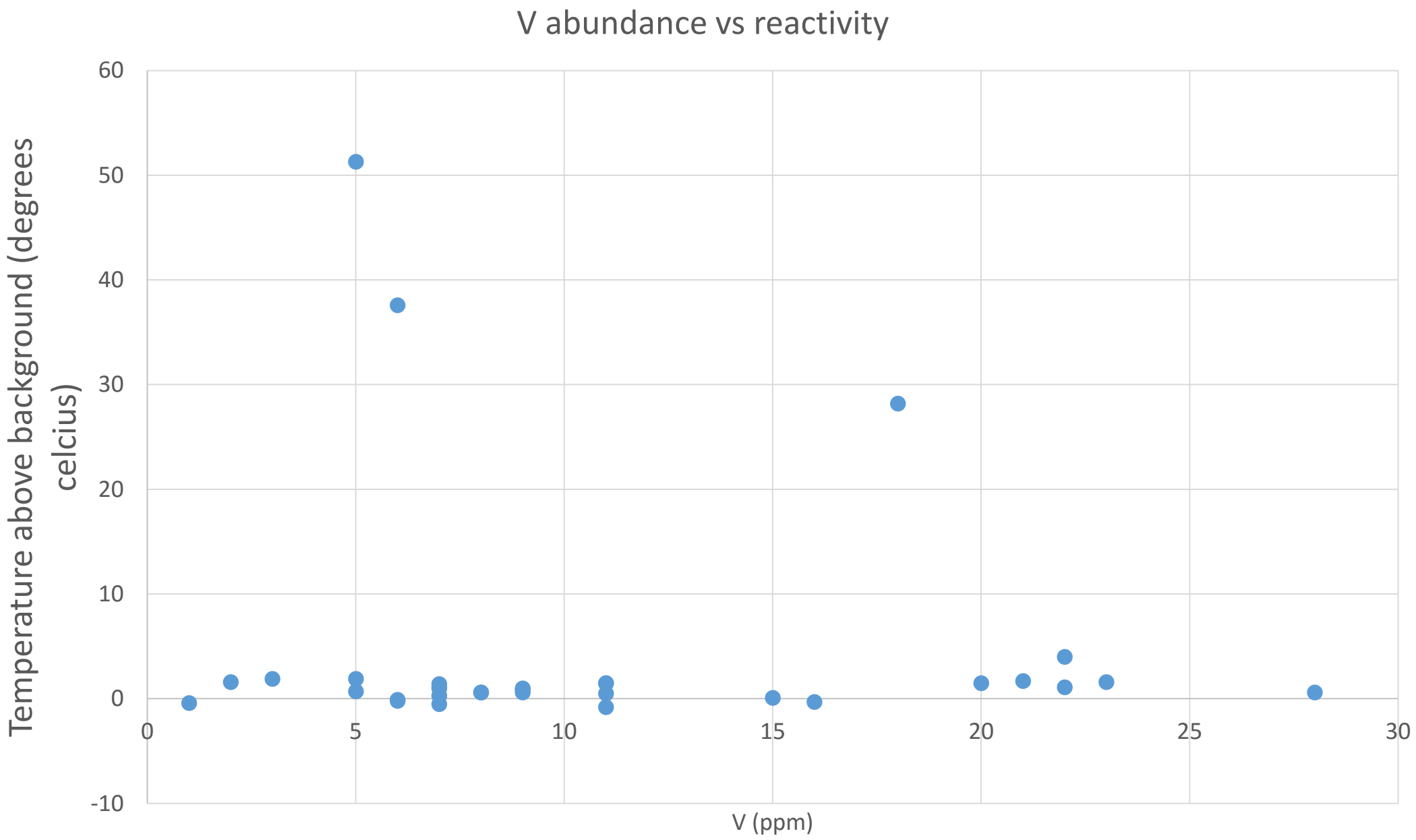
V abundance vs reactivity
Temperature above background (degrees celcius)
60
50
40
30
20
10
0
-10
0
5
10
15
20
25
30
V (ppm)

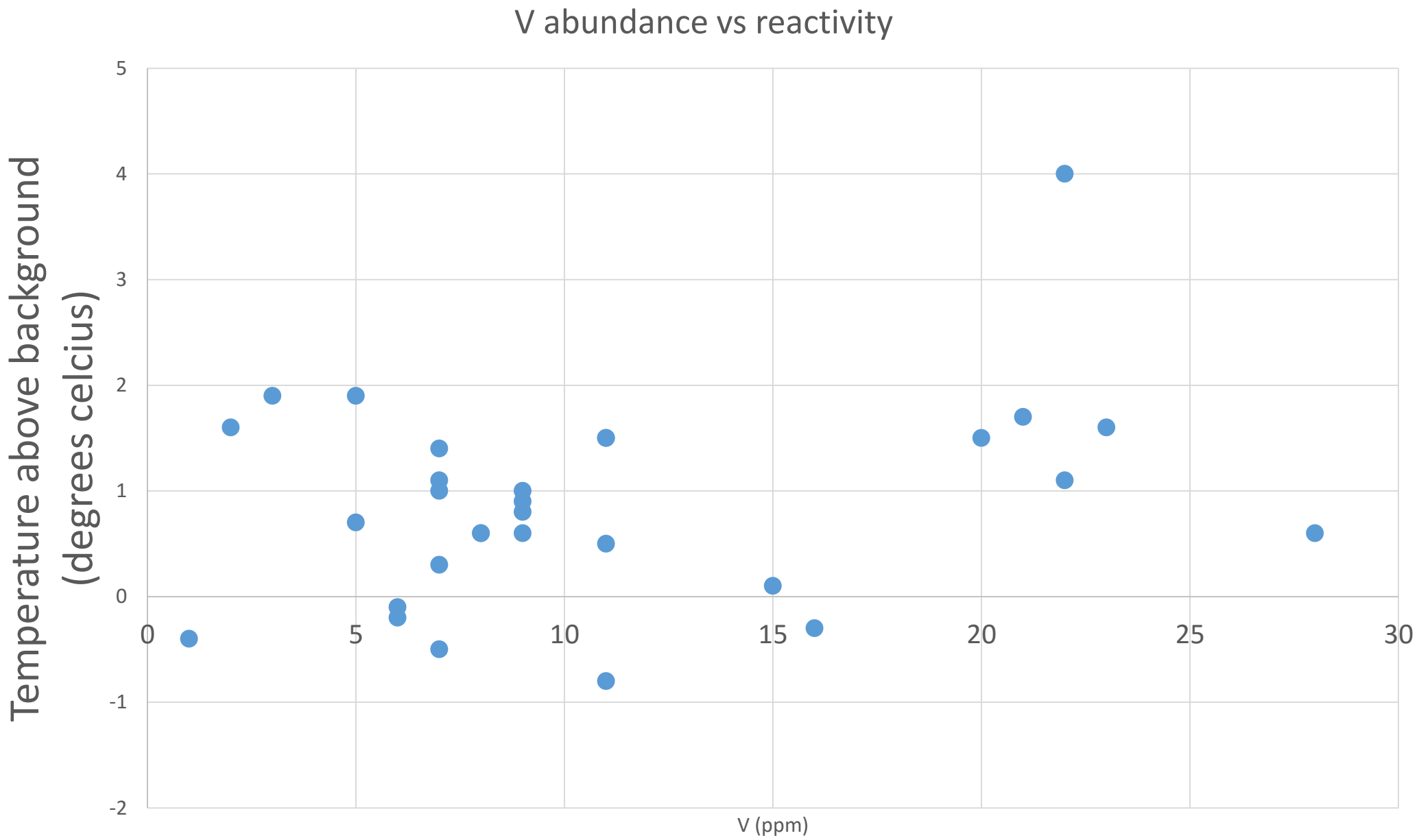
V abundance vs reactivity
Temperature above background (degrees celcius)
5
4
3
2
1
0
-1
-2
0
5
10
15
20
25
30
V (ppm)

Reactive samples – comments

- High in Phosphorous (500 ppm)? But other samples had high P and did not react.
- Relatively high in Copper
- High in Bismuth (low thermal conductivity?)

- Low in Ba
- Very low in Ca
- Low in K
- Very low in Mg
- Low in Mn

Conclusions

- Does not seem to be any obvious relationship between reactivity and trace element geochemistry.
- Reactive ground phenomenon remains complex and is most likely caused by moisture, exposure time, small grain size, fine grained pyrite, and exposure time before contact with explosives, size of drill hole.
- Assuming the current test method is accurate and reliable, it seems drilling operations involving actual fresh fine grained pyrite are safe, providing protocols are followed.
- Unique/weathered (bacteria?) rock types are more likely to react, especially if in a leached zone (Base of Moderate Leaching Zone).
- Incidents may only occur in circumstances when:
  - drill holes are horizontal
  - have long exposure times to moisture and oxidation before exposed to nitrates,
  - There is a long period of time between drilling and blasting
  - have sulphide in the rock
  - the sulphide is of a fine grained size